Driving conformational switching in de novo designed -helical coiled-coils with novel molecular components

ASAHI CANO-MARQUES

Driving conformational switching in *de novo* designed α-helical coiled-coils with novel molecular components

This thesis is submitted for the degree of

Doctor of Philosophy

by

Asahi Cano-Marqués

Department of Physics

University of Durham

England

July 2015

Abstract

This research project is multidisciplinary in nature. It involves the use of biomolecular design –peptide design – and the synthesis of small organic compounds to generate conformational switching in peptide structures.

In this thesis, we demonstrate that we can design and synthesize *de novo* peptide sequences with the necessary information to assemble as α-helical coiled-coil structures when associated with their corresponding peptide partners. In addition, some of the peptide structures are designed to form both α-helical coiled-coils and fibrous systems.

Since we aim to promote conformational changes in the initial folding states of our peptide assemblies, the design of these individual sequences that we refer to as chassis peptides includes tuneable positions which after being modified will help these changes to happen.

We make use of the Negishi reaction to synthesize unnatural amino acids – pyridyl-alanine analogues – for metal-binding investigations. The insertion of these novel amino acids into our self-assembling peptide systems provides different conformational changes depending on the positions in which these amino acids are inserted. These experiments are an attempt to form novel metal-based chiral biocatalysts. They also allow us to investigate to what extent peptide self-assembly can control metal binding and to what extent the metal binding can control peptide self-assembly.

This research project also includes the synthesis of an azobenzene derivative for *trans*-to-*cis* and *cis*-to-*trans* photoisomerization. We successfully attached an azobenzene linker to three different coiled-coil forming peptide structures, exhibiting different switching efficiency in each. By using these *photoswitches* we induce conformational changes in the secondary structure of the peptide structures by the use of light. Some of these are reversible structural changes which makes it a potential power source for protein motors.

Acknowledgements

First of all, I would like to thank Dr Corinna Hess for letting me know about the available PhD position under supervision of Dr Elizabeth Bromley (Beth), and for putting me in contact with her. I would like to acknowledge my sincere appreciation to Beth for her guidance, advice, continuous support during my whole PhD, and for helping me to gain the knowledge and experience needed for a future in this research area. Thanks to the EPSRC for funding my research. I would like to thank my co-supervisor Dr Steven Cobb for his advice and guidance, for letting me use his lab and facilities, and take part in all his group activities.

I would like to thank soon-to-be Dr Lara Small for her support and help during all my years in Durham. Many thanks to all the Cobb group members, past and present, for making my research much more enjoyable: Miriam Everitt, Roderick Dirkzwager, Edward Jones, Guillaume, Dr Neil Colgin, Andy Steer, Maria Czyzewska, Dr Chris Coxon, Dr Gabriella Eggimann, Alex Webster, Zong Jingyi, Nick Robson, Mark Laws, Ambrose Crofton, Caitlin Mooney, Hannah Bolt, Dr Neil O'Connor, Laura Ferreras, Beatriz Martínez, Diana Giménez and Dr Anica Dose. I would like to express special gratitude to Sam Lear, for sharing his scientific opinions, advice and for other discussions, and to Alex Hudson, for all the priceless fun times spent together during my time in Durham, not only in the Chemistry Department, but also in many football matches defending the Ustinov AFC colors.

I would like to thank everyone in CG156 who became very good friends, more than just colleagues; thank you for your delicious chocolate cakes on each of my birthdays: Serena, Brunella, Tatiana, Irina, Paul, Fabian, Dave, Rose, Cat, Pete, Kieran, Ryuma, Gabrielle, Matt, Andy, Russell, Shenghui, Roberto, and of course Dr Davey Cole, who with I shared lots of running sessions. I would also like to acknowledge Dr Mikael Czyzewski and Dr Jose Santos for their wise advice in conversations outside of work, which helped me with some of my chemical reactions.

I would like to thank everyone in the analytical services from the Chemistry Department, in particular thanks to Dr Juan Aguilar for his advice and help. I would also

like to thank Dr Budhika Mendis from the Physics Department for helping me with the preparation of TEM samples and measurements.

As playing football was a really important part of my stay in Durham helping me to overcome difficulties during these years, I would like to extend my acknowledgements and remember everyone who was part of this and made my days more enjoyable in Durham: Alex Hudson, Pete King, Alex Nicholls, Renan Petersen-Wagner, Phil Gill, Juan Duran, D. Williams, D. Hyde, Joonas Lumijarvi, Tan Rueangkul, Enrico Marzano, Jon Worral, Chris James, Akin Taylor, Giannis Sarrigiannis, Bo Han, Kenji Yosihara, Rodrigo Moraga, Marc O. Jones, Josh Düffield, Daniel Conway, Joseph Hardern, Chris Dobson, Scott Sadler, Eddy Walter, Eirik Thune, Bruce Rawlings, Matt Bainbridge, Nury Moreira, Eliud Diaz-Romo, Arm, Tawan, Etienne Lisse and Pete Quinn. I give a special mention to my closest friends Daniel Hölck, Adrián Gutiérrez, Albert Sanz, and Alessio Pastore who have provided unforgettable and priceless moments in the last year of my PhD.

I would like to mention and thank some people from the Thai Boxing Club Society who have become good friends and contributed to some very happy moments: Andrew, Sean, Mark, Guro, Malika, Jakob, Harrison, and Ajay.

I would like to express infinite acknowledgements to the greatest people I have had in my life for many years, my awesome friends from Valencia, who have always been close to me even if we have been physically distant, and who were always able to find time to spend with me whenever I was back home for a break. Thanks to Miguel Del Hoyo, Josemi Gómez, Dr Patricia Cabedo, Alex Alvarez, Mamen Mayo, Carlos Baeza, Edgar Nebot, Alberto Picón, Pablo Tenorio, Daniel Romera, Aurelio Cortés, Patri Ponce, Boni Manguire, Pau Marí, Alejandro Prieto, Mateo Berton, Dr Amparo Sanz and Dr Empar Vengut. Finally, special thanks to Silvia Barato who gave me massive support in countless moments.

To conclude, I would like to dedicate this Doctoral Thesis to my family, who I will never be able to give back all the support they have given to me as it is immeasurable. Thanks to my grandfather, Constantino, my father, Diego, my mother, Loli, my brother, Víctor, and a special mention to my grandmother, Angelita, and my uncle, Antonio, who are now resting in peace.

Abbreviations

3D	three dimensional
Ac	acetyl
Ag	silver
Ala	alanine
Am	amide
Ar	aromatic or argon
Asn	asparagine
Au	gold
BEP	blunt-ended partner
BSBCA	3,3’-bis(sulfonato)-4,4’-bis(chloroacetamido)-azobenzene
Bn	benzyl
Boc	tert-butyloxycarbonyl
Br	bromo
Ca	calcium
Calcd	calculated
CD	circular dichroism
Cd	cadmium
$CDCl_3$	deuterated chloroform
CH_3CN	acetonitrile
Cl	chloro
CL	cross-linked peptide
Co	cobalt
CO	carbonyl
Conc	concentrated
Cu	copper
Cys	cysteine
DCM	dichloromethane

ddH_2O	double distilled water
DIC	*N*,*N*'-Diisopropylcarbodiimide
DIPEA	*N*,*N*-Diisopropylethylamine
DMF	dimethylformamide
DMSO	dimethyl sulfoxide
ε	molar extinction coefficient
e.g.	exempli gratia (for example)
EtOAc	ethyl acetate
ESI	electro-spray ionization
ET	electro-transfer
Et_2O	diethyl ether
eq	equivalent
Fe	iron
Fmoc	fluorenylmethyloxycarbonyl
g	grams
Gd	gadolinium
Gln	glutamine
Glu	glutamic acid
H	proton or hydrophobic
H_2	hydrogen
Hg	mercury
HOBt	Anhydrous 1-hydroxybenzotriazole
HPLC	high performance liquid chromatography
I	isoleucine
I_2	iodine
Ile	isoleucine
IR	infrared
K	lysine or potassium
L	leucine or Ligand
Leu	leucine
Lys	lysine

m/z	mass/charge
M	molecular ion or metal ion
MALDI	matrix assisted laser desorption/ionization
MeOH	methanol
mg	milligram
MBHA	4-Methylbenzhydrylamine
MHz	megahertz
min	minute
ml	millilitre
mM	millimolar
MOPS	4-Morpholinepropanesulfonic acid
MS	mass-spectrometry
mw	molecular weight
MW	microwaves
µm	micrometres or microns
µM	micromolar
n	mol
N	asparagine or nitrogen
Na	sodium
NaOH	sodium hydroxide
Ni	nickel
NMR	nuclear magnetic resonance
nm	nanometer
NMP	1-Methyl-2-pyrrolidinone
O	oxygen
P	polar, phosphorous or protecting group
Pal	pyridylalanine
PBS	phosphate-buffered saline
Pd	palladium
$Pd(dba)_2$	bis(dibenzylideneacetone)palladium(0)
P(*o*-tol)3	tri-(*o*-toluyl)phosphine

PEG	poly(ethylene glycol)
Ph	phenyl
$Ph_3P=O$	triphenylphosphine oxide
ppm	parts per million
Pt	platinum
PTFE	polytetrafluoroethylene
Py	pyridine
PYBOP	(Benzotriazol-1-yloxy)tripyrrolidinophosphonium hexafluorophosphate
r.t.	room temperature
R	side chain or rest of the molecule
Re	renium
RP-HPLC	reverse phase high-performance liquid-chromatography
Ru	ruthenium
SAFs	self-assembling fibres
SDS-PAGE	sodium dodecyl sulfate polyacrylamine gel electrophoresis
Ser	serine
SiO_2	silicon dioxide or silica
SPPS	solid phase peptide synthesis
Sphos	2-Dicyclohexylphosphino-2',6'-dimethoxybiphenyl
*t*Bu	*tert*-butyl
TBTA	*tert*-butyl trichloroacetimidate
TCEP-HCl	Tris(2-carboxyethyl)phosphine hydrochloride
TEM	transmission electron microscopy
TFA	trifluoroacetic acid
TIPS	triisopropylsilane
T_M	melting temperature
TLC	thin layer chromatography
Tris	Tris(hydroxymethyl)aminomethane hydrochloride
TOF	time of flight
Trt	trityl
Tyr	tyrosine

UV	ultraviolet
V	valine
Vis	visible
Xantphos	4,5-Bis(diphenylphosphino)-9,9-dimethylxanthene
Zn	zinc
Zr	zirconium
θ	mean residue ellipticity

Table of contents

Chapter 1

Introduction and background

Proteins are large biomolecules able to perform many different functions within living organisms. They are not only single polypeptide chains but also more complex structures which can bear metal ions able to provide specific functionality depending on the task of the corresponding macromolecule. Nature exhibits a rich variety of proteins which contain self-assembling polypeptide sequences responsible for functionality in the systems they form. The nature of these sequences has been the object of study for many years due to the importance of their functionality. This investigation has covered the nature of the amino acids of each of the polypeptide sequences, their order in the sequence, their structural layout, and the driving forces that allow the sequences to self-assemble.

By investigating why some natural functionalized polypeptides assemble we can mimic what nature offers. The process of mimicking provides an important method for understanding how such assemblies and structures work. After this is achieved there is then a wide range of possibilities for tuning these polypeptidic systems to try either to provide new functionality or improve that which already exists in Nature. However, this is not a simple task as it involves what is known as the "protein-folding problem".[1] This issue is related to the rules followed by a sequence in forming a 3D structure and therefore it is essential to completely understand how different sequences provide different structures, interactions, stability, and functions. To accomplish this goal we need toolkits that help to determine ideally all the necessary aspects for the synthesis of improved sequences. Synthetic biology is the field of science and the tool used for this purpose, for protein engineering, or engineering of biological systems in its broadest sense. In addition, computational approaches can use design algorithms to construct new systems, however, the ability to design *de novo* systems reliably is limited to a small number of specific examples, such as α-helical coiled-coils, zinc

fingers and collagens. Here we focus on *α*-helical coiled-coil systems because *α*-helical secondary structures are the most common polypeptide structures found in Nature and have been investigated for many years as fibrous biomaterials for potential applications in biotechnology. There is, therefore, a wealth of information available to aid the design and synthesis of *de novo α*-helical peptide sequences from the bottom-up.

In the first part of this project, we design and synthesize *de novo* programmed *α*-helical coiled-coil self-assembling peptide sequences, some of which contain information for fibre assembly formation. Once this has been achieved, mutants of these polypeptide sequences are synthesized to provide reactive sites capable of generating conformational switching. These molecular components are synthetic amino acid analogues (pyridylalanine derivatives) for metal-binding and an azobenzene derivative for reversible photoisomerization. By incorporating novel amino acids into self-assembling peptide systems we aim to form both novel chiral metal-based biocatalysts but also to investigate to what extent the self-assembly can control metal-binding and to what extent the metal-binding can control self-assembly. By using azobenzene derivatives, which can be photoswitched between *trans* and *cis* isomers, we can induce conformational changes in the secondary structure of our coiled-coil peptide designs and provide a potential power source for protein motors.

1.1 Hierarchical organization of biomolecular components and the basic units of polypeptides: amino acids

Nature exhibits complexity at a range of different length scales. This spans from *basic units* to *complex functionalized systems* – which emerge from the combination of lower-order units in the hierarchical organization of biomolecular components (**Figure 1.1**).[2] Amino acids, nucleic acids, sugars and lipids are the *basic units* which after self-association or polymerization move up to a higher-order of complexity known as *tectons*. The term *tecton* has been borrowed from supramolecular chemistry to indicate that they contain the information required for further assembly in a programmed mode, e.g. a *tecton* could be programmed tracks of *α*-helices or β-

strands. Thus, combination of *tectons* that adopt defined reproducible structures lead to the next level of complexity in the hierarchy, known as *self-assembled units*. For the examples mentioned, *α*-helices would give way to *α*-helical coiled-coils structures and β-strands would form β-sheets.

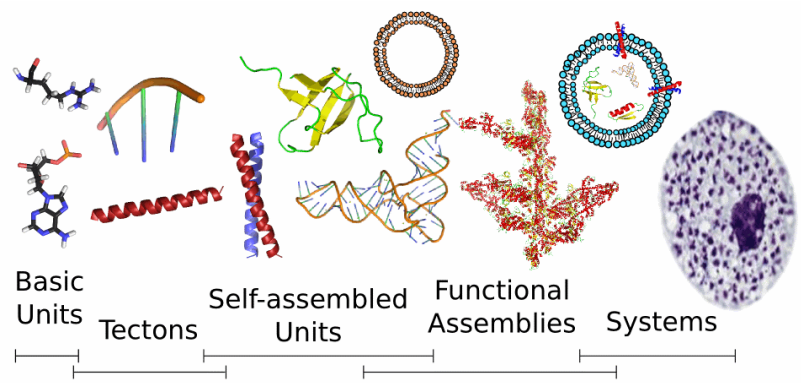

Figure 1.1: Schematic representation of the hierarchical organization of biomolecular components in the synthetic biology space – this space refers to the vast arena where synthetic biologists can operate (adapted picture from reference 2).

Moving up in complexity, *functional assemblies* are described as higher-order associations of *self-assembled units* which provide complex structures and functions, and collections of *functional assemblies* that can perform multiple or complex chemical reactions is what we refer to as *systems*.[3]

Synthetic biology can address each of these levels of complexity by making alterations to each of them in order to achieve different goals. Modified *basic units* can be synthesized and lead to higher-order complexity components that can function as *de novo* designed *tectons*. This can afford building blocks that diverge from Nature, for example, the synthesis of unnatural amino acids could provide programmed self-assembling after insertion in a polypeptide sequence. This would create a new type of *tectons* for synthetic biology. **Figure 1.2** shows an adapted scheme from reference 3 (by E.H.C. Bromley *et al*.) in which different routes of syntheses of more complex systems are placed in the *synthetic-biology space* according to the degree of divergence from Nature within the hierarchical organization of molecular components. In this thesis, we are investigating *de novo* coiled-coil peptide designs. We will therefore primarily discuss amino acids and proteins.

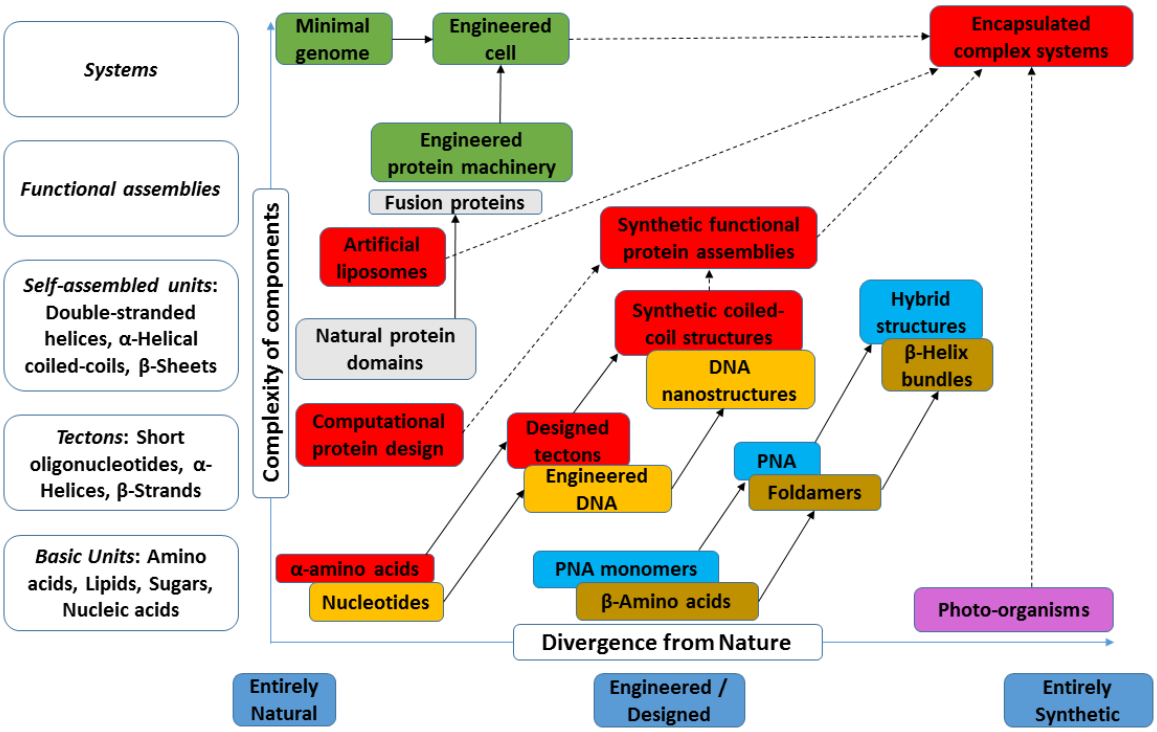

Figure 1.2: Routes for achieving higher-order levels of complexity in the hierarchical organization of molecular components encompassing from natural components to completely synthetic components (adapted picture from reference 3).

α-Amino acids are the fundamental building blocks of polypeptides. They are small biomolecules comprising a central carbon atom, the *α*-carbon, which bears both the amino ($-NH_2$) and the carboxylic groups (-COOH) functionality. The *α*-carbon has a hydrogen and a side chain group referred to as "R" (**Figure 1.3**).

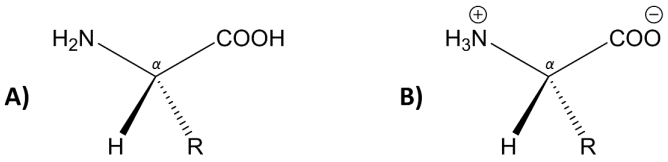

Figure 1.3: A) General structure of a non-ionized α-amino acid; B) Zwitterionic form of an *α*-amino acid when the pH is in the range of 2.2 to 9.4.

There are 20 different "R" groups found in Nature which constitute the 20 essential *α*-amino acids showed in **Figure 1.4**. The term essential means that they can be found in Nature as part of proteins hence the alternative name of *proteinogenic* amino acids. All 20 *proteinogenic* amino acids except Glycine are chiral at the *α*-carbon. The most

common classification of the 20 essential amino acids is carried out according to the functionality of the side chains (**Figure 1.4**). Depending on the pH of the media, either the amine or the carboxylic groups can be found in their ionized forms. At pH lower than 2.2, the amino group is present as ammonia ($^{+}NH_3$) while the carboxylic group is neutral (COOH). At pH higher than 9.4, the carboxylic group is present in its ionized state in the form of carboxylate (COO^{-}) whilst the amino group remains neutral (NH_2). These states have net +1 and -1 charges respectively. When the pH is between 2.2 and 9.4 both groups can ionize at the same time affording a molecular state known as a zwitterion with net zero charge (**Figure 1.3B**).

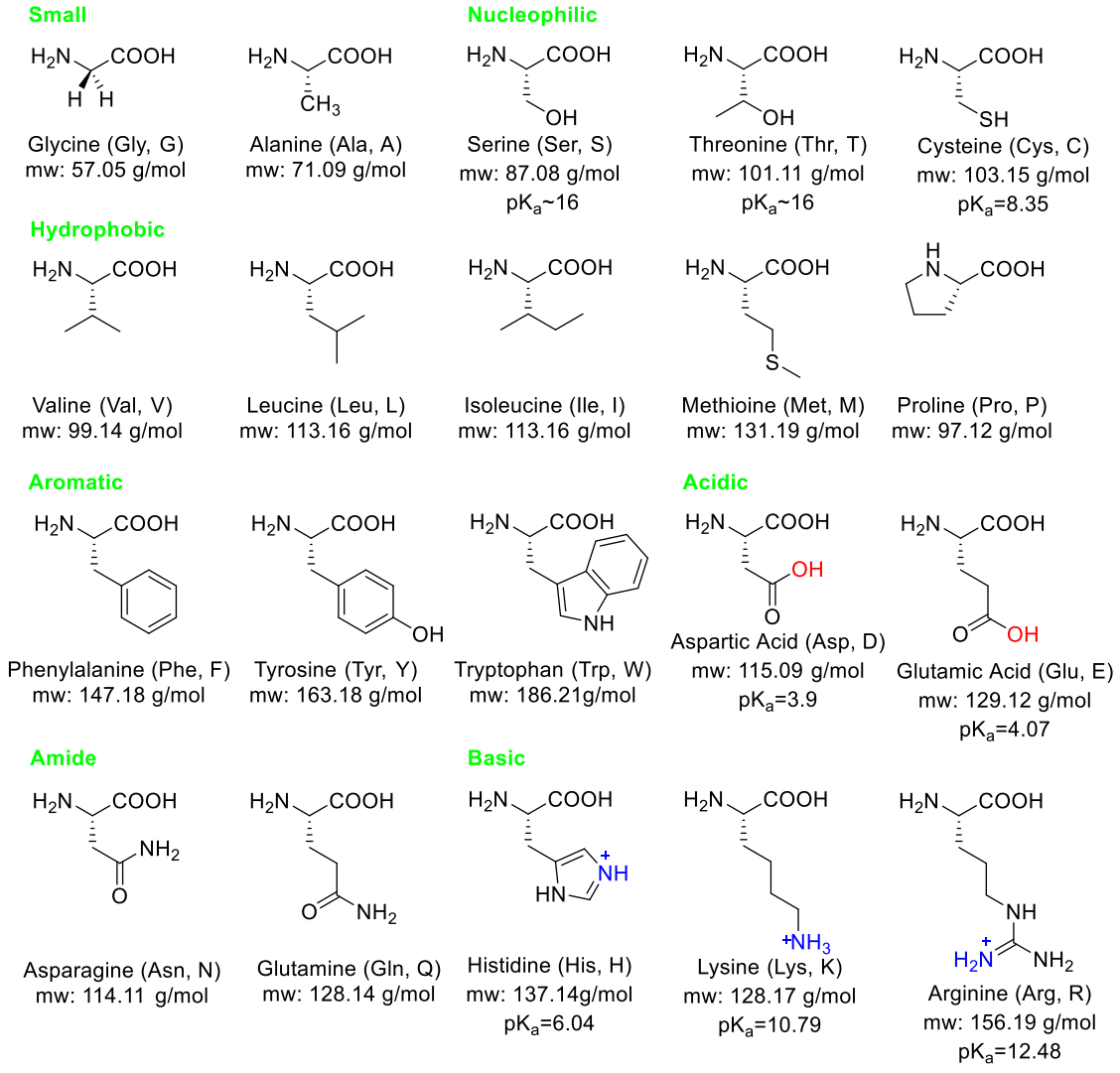

Figure 1.4: Classification of the 20 natural α-L-amino acids according to the properties of their side chains.

When the amino group of one amino acid reacts with the carboxylic group of another amino acid through a condensation reaction we have a dipeptide. Both the N-terminus and C-terminus of the different amino acids condense to create a new *amide bond* or *peptide bond*. The lone par of electrons on the nitrogen atom gives the *peptide bond* a resonant structure with a partial double bond character (**Figure 1.5**). Since double bounds disallow rotation, the *peptide bond* remains in a fixed conformation, being the *trans* conformation the most stable as this allocates both alpha carbons on the opposite corners of the peptide group. The alpha carbons allow rotation, hence, flexibility to the peptide backbone. If several amino acids are joined together, this results in the formation of a polypeptide chain, or a peptide. Consequently, proteins are created when the complexity reaches a higher order and the polymerization of amino acids extends to a higher number of residues.

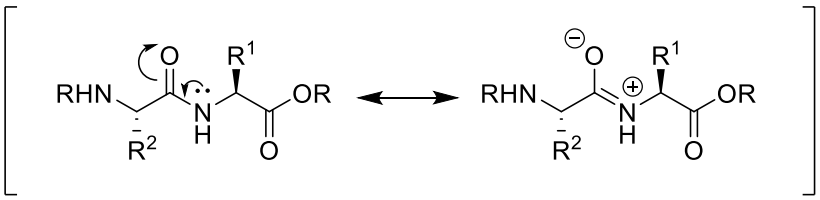

Figure 1.5: Resonant structure of the peptide bond.

The way amino acids are joined together in nature is usually linear and can range from a few to thousands of amino acids in length. This is known as the primary sequence and this contains all the information required for peptide folding, assembly, and function. Once a peptide sequence is long enough, it is possible for a local geometry of the backbone to arise known as the secondary structure of peptides. The two most common secondary structures observed in Nature are the α-helix and the β-strand, and they form the basis of most of the building blocks, or *tectons*, in peptide design.

1.2 Secondary structure of proteins: *α*-helices and β-strands

The secondary structure of proteins refers to the local geometry of the folded state of the polypeptide backbone which is stabilized by the hydrogen bonds between the –CO and –NH groups that are part of the peptide bonds. CO acts as hydrogen acceptor while NH acts as hydrogen donor. This helps the polypeptide sequences to adopt more stable conformations of lower free energy. There are different types of conformational structures that can be distinguished for a protein, including: *α*-helix, 3_{10} helix, π-helix, β-strand (both parallel and antiparallel), β-turn, random coil, and collagen. **Figure 1.6** shows cartoons of some of these secondary structures.

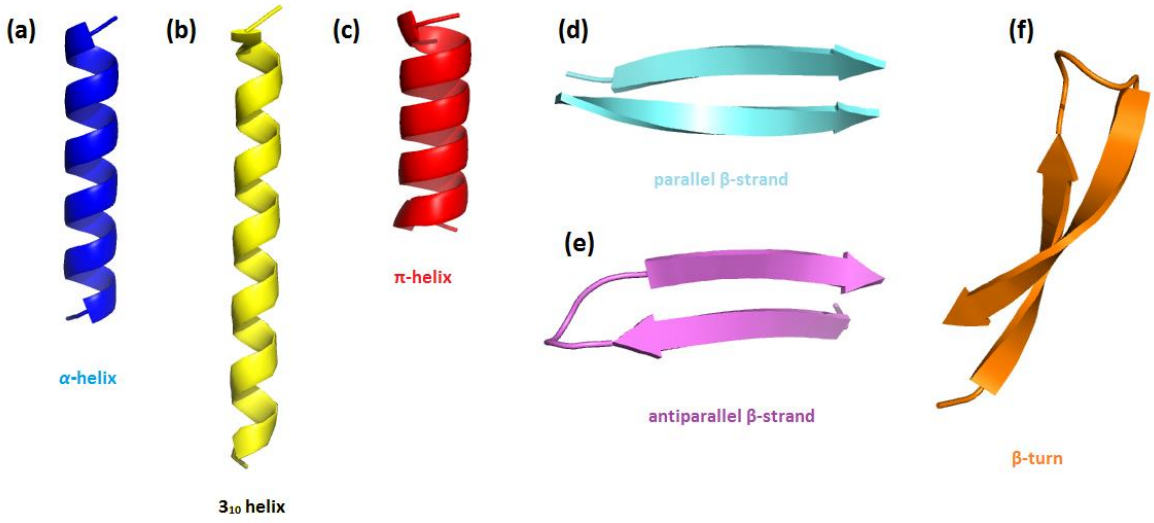

Figure 1.6: Representative cartoons of some of the secondary structures known for proteins. The *α*-helix (in dark blue) contains 3.6 residues per turn whilst the 3_{10} helix (in yellow) contains 3 residues per turn, and the π-helix (in red) contains 4.4 residues per turn; this provokes more or less hindrance along the backbone, hence, differences in length as shown in the picture.

The *α*-helix is a common secondary structure of proteins. It comprises a polypeptide sequence which is wrapped as a right-handed helix where the R groups of the amino acids point outwards from the backbone coil. One stabilizing effect of the *α*-helix is given by the hydrogen bonds formed by NH and CO groups of amino acids placed "*i* + 4" positions away. In other words, amino acids use their NH donating-groups for hydrogen-boding with residues placed four positions earlier in the sequence: "*i* + 4 → *i*" (see **Figure 1.7**). This involves 3.6 residues and 13 atoms per turn, hence the *α*-helix is known as the 3.6^{13}-helix.

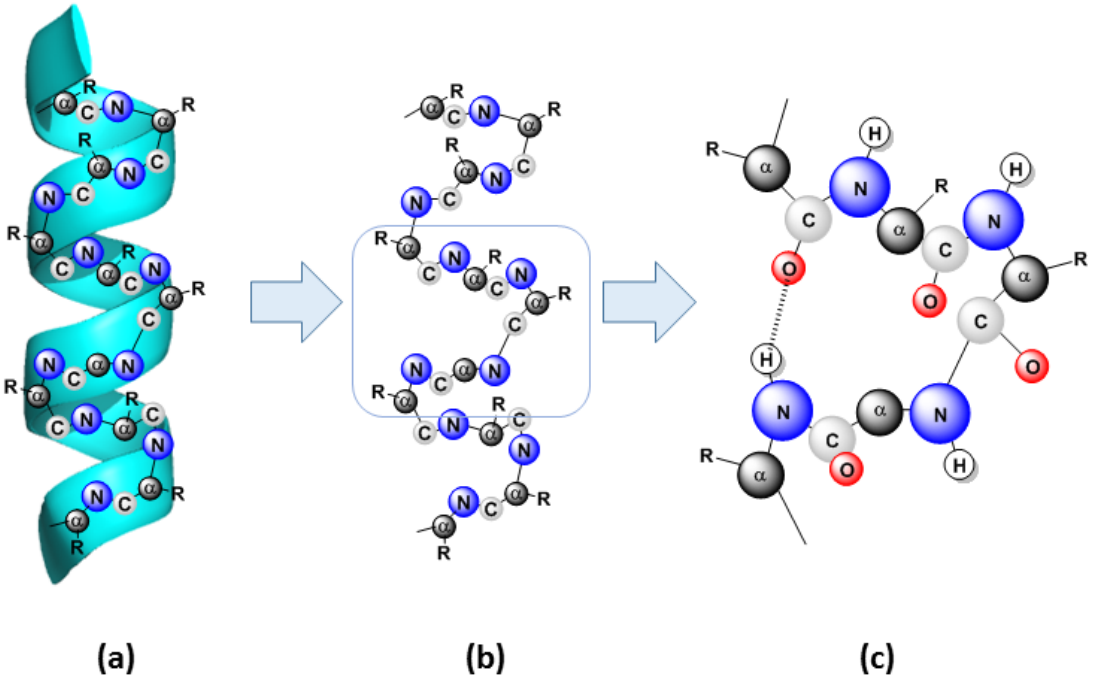

Figure 1.7: Graphical view of (a) the main backbone of a peptide sequence wound up as an α-helix structure with the **R** groups pointing outwards from the central coil; (b) the same backbone of the sequence outside the α-helix cartoon, selecting the 13 atoms of the 3.6 residues of each turn; (c) expanded view of the 13 atoms of one α-helical turn with a hydrogen bond formed between the **NH** group of an amino acid placed at an "*i*" position and the **CO** group of an amino acid placed "*i*+4" positions away.

In addition to the hydrogen bonding pattern, interactions between the side chains of amino acids three and four positions away from each other may favour the formation of an α-helix. This spacing leads to one of the key design principles in the higher-order assembly of the α-helix which will be discussed in the next section. It has been proven that the α-helical structure's stability will depend on the nature of the amino acids forming the peptide sequence. Amino acids such as methionine, alanine, leucine, lysine and uncharged glutamate will generally help the formation of an α-helix, whilst proline and glycine will disrupt its formation.[4-7]

An α-helix has a net charge as a consequence of the aggregate effect of the N- and C-terminus together with all of the individual ionizable groups present in the peptide. The ionizable groups in the peptide are within the side chains of the amino acids, and are either COOH or NH_2 groups. The pK_a of a carboxy-terminal group pK_a(COOH) is

approximately 2.0 and $pK_a(NH_3^+)$ ~ 9.7. This means that at pH 7 both COO^- and NH_3^+ groups will be in their ionized form, and hence, have net charges of -1 and +1, respectively. At a neutral pH, the net charge of a peptide sequence is therefore null without taking into account any other ionizable R groups. To calculate the real net charge of a peptide it is necessary to know what the pK_a of each of the ionizable groups is. In general, at pH < pK_a (acidic) all of the protons will be added onto the COOH and NH_2 groups, and hence they will be in of COOH and NH_3^+ forms. At pH > pK_a (basic) all of the protons will be off the COOH and NH_2 groups, and hence in the COO^- and NH_2 forms. **Figure 1.8** shows the net charges for each end at different pH conditions. There are also the dangling O^- ions at the C-terminus and dangling H^+ ions from the N-terminus which would be making hydrogen bonds if they were not at the end of helices. This means the charge near the N-terminus is greater than +1 and at C-terminus is more negative than -1. In addition, having a neutral pH means that the free end NH_2 is in the NH_3^+ form and COOH in the COO^- form. When interacting two peptide sequences in a parallel arrangement to form a more complex structure, such a coiled-coil, both ends will be either positive or negatively charged. The repulsive interactions produced by the charged groups can affect the peptide structure. Stabilization of the helix can be accomplished by capping the α-helices, either at the N-terminus with a negatively charged group (such as a side chain of glutamate or aspartate, or even a phosphate ion), or at the C-terminus with a positively charged amino acid such as lysine, although this is less effective. Capping the N-terminus with a positive charged group is also possible and can be used to bind negatively charged ligands.

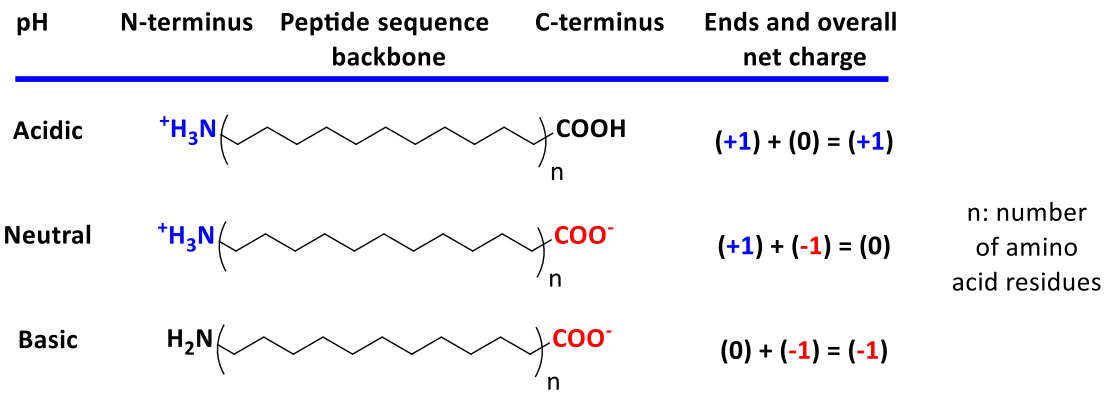

Figure 1.8: Net charge for the N- and C-terminus of a peptide sequence at pH acidic, neutral and basic and their overall net charge without taking into account other ionizable groups as a whole.

1.3 *α*-Helical coiled-coils

Although it can be relatively simple to form peptide sequences which adopt *α*-helical structures, they cannot be considered by themselves as building blocks or *tectons* as they do not include any information about their folding or further assembly with other polypeptides. However, the design of *α*-helical coiled-coils are a starting point to synthesize peptidic *tectons* and self-assembled units.

α-Helical coiled-coils are an example of higher-order assembly of *α*-helices and a quaternary protein structure. Coiled-coil motifs exhibit a surprising richness and diversity in both function and structure of protein-protein interactions in terms of number, orientation, and the nature of the interacting elements. They have been intensively studied for the last two decades, and due to their abundance in nature there are many available and well defined X-ray structures which have been useful to establish a number of rules for the successful design of new coiled-coil structures. These are called *rules-of-thumb* and relate protein sequence and structure in coiled-coil domains.

In terms of sequence and structure, most coiled-coils domains exhibit a heptad sequence repeat pattern, often labelled *abcdefg*, in which the first and fourth residues are hydrophobic (*H*) and the other positions consist of polar (*P*) amino acids, $(HPPHPPP)_n$, being $n = 4$, for most coiled-coils. Their structure is based on the "*knobs-into-holes*" packing-type layout *(KIH)* in which the hydrophobic residues of one helix act as "*knobs*" and can be inserted into the "*holes*" from a different helix (see **Figure 1.9**). Positions *a*, *d* and *e* of one peptide sequence provide the "*holes*" for the "*knobs*" at positions *a*, *d* and *g* of the complementary sequence.

When two or several *α*-helices assemble together as a coiled-coil there is a certain angle between them leading to a left-handed supercoiling of the helices around each other. The angle of assembly is caused by a mismatch between the average spacing of the hydrophobic residues in the heptad repeat (which is 3.5) and the *α*-helix (which is 3.6). Moreover, this type of assembly results in measurements of ~1nm end-to-end length per heptad.

The heptad pattern encodes amphiphatic α-helices which assemble into water to bury the hydrophobic faces, corresponding to positions *a* and *d* of the heptad repeat, hence, leaving the hydrophilic face exposed to water. However, although the hydrophobic effect is the main driving force for the assembly of coiled-coils, there are other effects that can play an important role when defining the structure. Positions *e* and *g* of the heptad are occupied by amino acids able to provide salt-bridging interactions that can help stabilise an α-helical coiled-coil. With respect to the remaining positions of the heptad repeat (*b, c, f*) these are usually kept polar and helix-favoring – this means, combinations of lysine, glutamate, glutamine, and alanine – and aromatic amino acids such as tryptophan or tyrosine are used as to provide a UV chromophore group. Glycine and proline are avoided for disrupting α-helical coiled-coils as mentioned in the previous section.

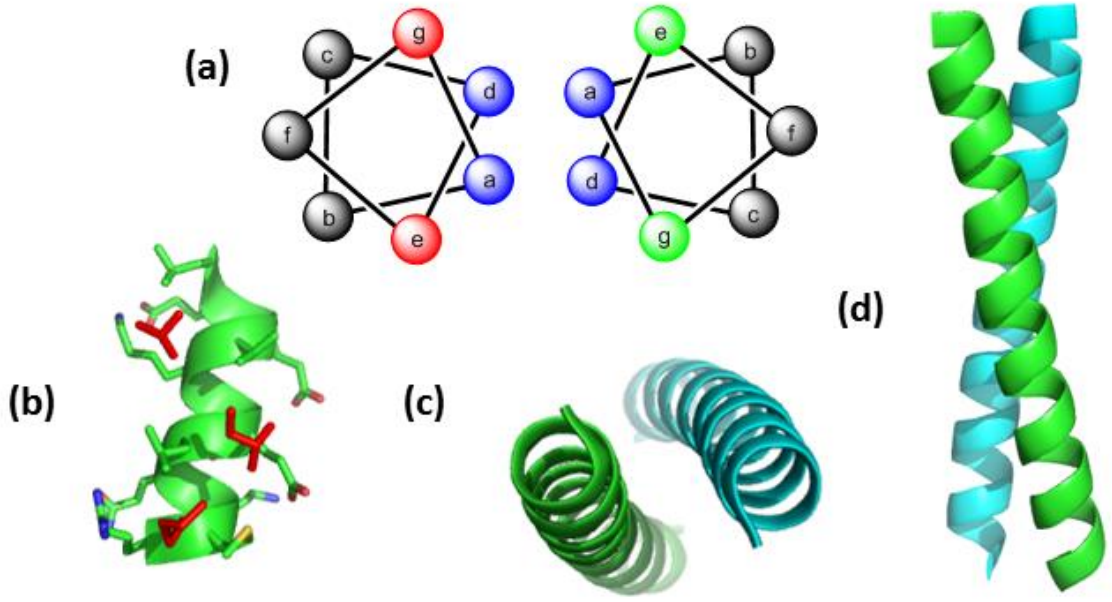

Figure 1.9: Different views of a dimeric α-helical coiled coil. (a) Helical wheel diagram for a parallel dimeric coiled coil: the hydrophobic residues (at *a* and *d*) form the hydrophobic interface, *b*, *c*, and *f* form the solvent exposed face (hydrophilic face), and positions *e* and *g* are for salt-bridged forming residues; (b) *KIH* packing – the residues forming the *hole* are green and the *knob* is occupied by a red residue from the other α-helix; (c) A top-down view of a dimeric coiled coil; (d) A side view of the same, showing the left-handed supercoil (adapted figure from reference 8).

Despite having clear rules for the design of new α-helical coiled-coil systems, there are many important factors to take into consideration. For instance, there are assemblies

in which a peptide assembles with itself – called homotopic assemblies – or assemblies formed by two or more different peptide sequences – called heterotopic assemblies. In addition, different polypeptide sequences can interact to form an *α*-helical coiled-coil structure in an antiparallel arrangement, parallel arrangement, or mixed topologies at the same time when more than two *α*-helices are involved in the assembly. In Nature we find *α*-helical coiled-coil structures with between 2 and 6 helices and these have been investigated for the last decades to discover the reasons certain peptides favour each specific oligomerization state. Having the key for the design of such structures can lead to a new generation of synthetic *tectons* with important applications for bionanotechnology.

An important contribution to the study of the oligomerization state of *α*-helical coiled-coil was first provided by Harbury *et al.* from investigations on the leuzine-zipper peptide (GNC4-p1) from the yeast transcriptional activator.[9] It was found that attempting to place different combinations of isoleucine (*Ile*, I) and leucine (*Leu,* L) in positions *a* and *d* of the heptad repeat, different oligomerization states could be achieved. Thus, when *a* = I and *d* = L the structure turned into a dimer; when *a* = *d* = I it turned into a trimer; and, finally, having *a* = L and *d* = I leaded to a tetramer (**Figure 1.10**).

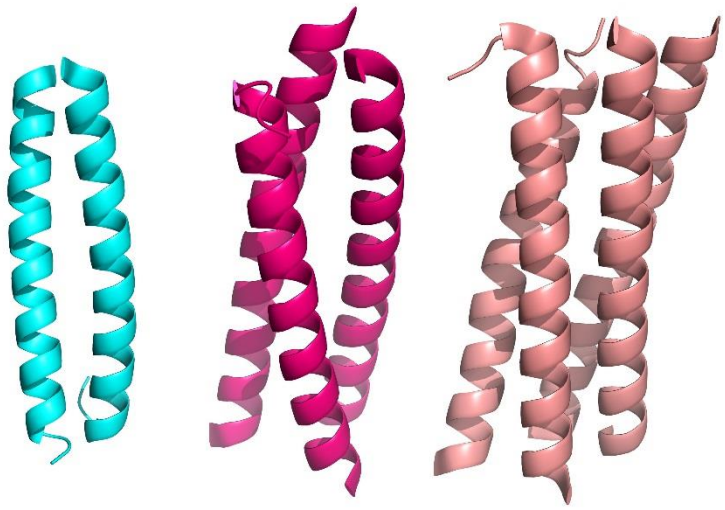

Figure 1.10: Representation of the different oligomerization states for the studies within *α*-helical coiled-coil structures after changing Leu and Ile in between positions *a* and *d* of the heptad repeat: a dimer (light blue), a trimer (light pink) and a tetramer (light brown).

However, these combinations of leucine and isoleucine at positions *a* and *d* was proved not to be completely determining in all cases as demonstrated in *de novo* designs by J.M. Fletcher *et al*. in 2012.[10] An attempt to provide coiled-coil design with a robust set of rules for manipulating and predicting the oligomerization state for *de novo* peptide structures was sought in the Woolfson's lab.[10] The aim was to facilitate understanding of sequence-to-structure relationships within the set. They focused on the most common oligomerization states found in nature – dimers, trimers and tetramers – and used the work of Harbury on the leucine-zipper peptide model as a starting point.[9] Consistent with his results, the trimeric and tetrameric coiled-coil models were afforded when using *a* = *d* = I and *a* = L, *d* = I respectively. However, the dimeric coiled-coil was not reproducible when positions *a* and *d* were occupied by I and L residues respectively. Their further investigations based on *negative design* revealed that having V (valine) and L in position *d* favored trimers hence concluded that for the leuzine-zipper model there are other stronger factors that favor a dimer. Fletcher *et al*. found that incorporating N (*Asn*, asparagine) in position *a*, or K (*Lys*, lysine) in positions *a* or *d* strongly favored dimers.[10] Due to the higher propensity for coiled-coil formation of *Asn* compared with *Lys*, that N occurs more frequently at positions *a* of coiled-coils, that N is empirically associated with dimeric states when placed at *a*, and that *Asn* favors trimers when is placed in position *d*, asparagine was proven to be the most suitable residue to place at position *a* of the heptad, therefore, combinations of *a* = N, *d* = L confirmed the formation of dimeric coiled-coils in solution. In addition, placing the *Asn* residue at the *a* site of the third heptad repeat (that is, in the middle of the whole sequence) was found to be optimal for the formation of the dimeric coiled-coil system, and helped with the rigidity of the structure by means of interhelical hydrogen bonds.

In nature, dimeric and trimeric conformations are predominant, and for the last two decades most of the work in coiled-coil *de novo* design has focused on finding stereoselective partners for heterodimeric coiled-coil interactions. These could be very useful in conducting *de novo* protein-protein interactions within large biosynthetic structures and for applications in nanotechnology, or even in the submicrometre range.

A summary of the work developed by Harbury and Fletcher to investigate the different oligomerization states of *α*-helical coiled-coils depending on the residues placed at *a* and *d* positions can be seen in **Table 1.1**.

Harbury (GNC4-p1)		**Fletcher (*De novo* coiled-coil system)**
a = I, *d* = L	**Dimer**	*a* = N, *d* = L
a = I, *d* = I	**Trimer**	*a* = I, *d* = I, L
a = L, *d* = I	**Tetramer**	*a* = L, *d* = I

Table 1.1: Different oligomerization states of *α*-helical coiled-coils found by Harbury and Fletcher depending on the amino acid residues placed at positions a and d of the heptad repeat.

In conclusion, the process by which *α*-helical coiled-coils are assembled has been reasonably well understood and some rules have been established for the design of new structures. Studies of, first, small sections of the leuzine-zipper peptide model by Harbury,[9] and then, *de novo* designs by Fletcher *et al*.[10] have contributed to our understanding of how selecting residues at each different position of the heptad can be determining as well as the hydrophobic effects that drive the formation of *α*-helical coiled-coils – by means of charged side chains to help salt-bridging formation.[11] Moreover, the remaining heptad positions can be used for the design of new functionalized sequences.

1.4 *α*-Helical based systems: from naturally occurring blunt-ended assembly to programmed self-assembling fibre (SAF) designs

An important aspect to bear in mind when designing *α*-helical coiled-coils is the mode of association or assembly between sequences. The most common conformation of *α*-helical coiled-coil arrangements found in nature is based on the "*flush-ends*", or *"blunt-ends"*, conformation and consists of having both hydrophobic surfaces completely interacting without having any of their residues free of interaction. **Figure 1.11** shows a designed peptide sequence *(***PEP1***)* interacting with another specially designed sequence *(***BEP***)* as in a *blunt-ended* fashion.

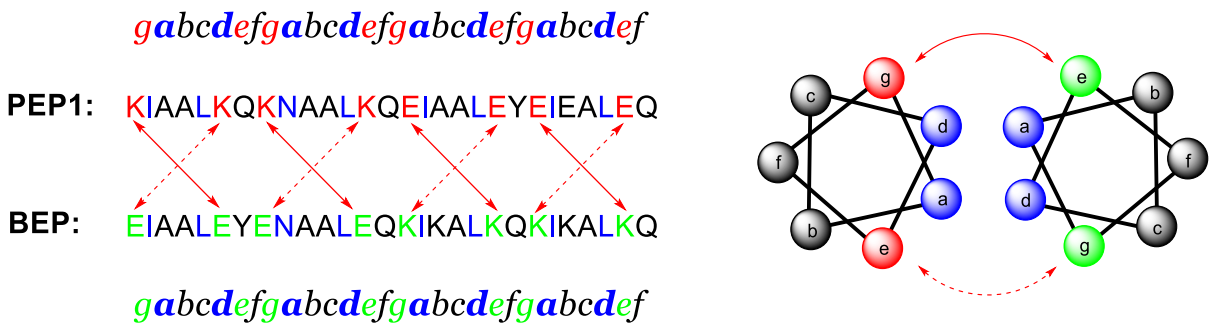

Figure 1.11: Representation of the blunt-ended coiled-coil conformation. At the left-hand side, the heptad repeat pattern is written above the **PEP1** sequence, and also below the **BEP** sequence as to indicate in which position is placed each residue. Ile and Leu are used, as well as Asn, as to favour dimeric coiled-coil formation. Salt-bridging interactions occur between Lys and Glu from positions *g* and *e* of the complementary sequence. At the right-hand side there is a wheel diagram of this same parallel dimeric coiled-coil with the hydrophic residues in blue and the residues for salt-bridging formation in red (from **PEP1**) and in green (from **BEP**). The arrows indicate where these interactions are happening.

However, another approach developed in Woolfson's lab is based on the way self-assembling fibres (SAFs) arrange.[12] These polypeptide sequences interact into an offset parallel coiled-coil dimer in what it is known as a *"sticky-end" tecton* for fibre assembly. The *sticky-ends* present complementary charged residues in positions *e* and *g* of the heptad repeat for salt-bridge formation with their counterparts in the other sequence and promote longitudinal association into extended fibres. **Figure 1.12** represents the concept of a *sticky-end tecton*.

As explained in **Section 1.3**, *α*-helical coiled-coil structures can be either homotopic or heterotopic. In the simplest case where only two polypeptide sequences assemble to form a coiled-coil structure, we call them homodimers or heterodimers. Both have been considered as *tectons* for the formation of extended fibres systems in proteins, with the heterodimeric type being the best to control self-assembly. Kojima *et al*. first reported the synthesis of homodimeric coiled-coils in which a heptad repeated up to three times provided a tetramer that could alter its morphology when the buffer was changed. They found larger assemblies that formed fibrils,[13] though in a later paper the sequence was reversed to render longer fibres which showed an increase in stability and in *α*-helicity.[14] Other research groups such as Potekhin's,[15] Conticello's,[16] or Hartgerink's[17] have also been able to engineer homodimeric coiled-coil systems where fibre assembling systems were formed.

Figure 1.12: Representation of the sticky-ended coiled-coil arrangement. The heptad repeat pattern is written above the **PEP1** sequence, and also below the **SAF** sequence as to indicate in which position is placed each residue. Ile and Leu are used, as well as Asn, as to favour dimeric coiled-coil formation. The arrows indicate the interactions between the residues for salt-bridging formation. They are Lys and Glu residues placed in the *g* and *e* positions of the complementary sequences. Hydrogen bonds formed by Asn residues from complementary sequences are highlighted in yellow.

However, the heterodimeric coiled-coil structures present advantages for fibre formation and control of self-assembling and some examples have been investigated. The best studied example of this type of systems comes from Woolfson's group: the "SAFs".[12] The designed has two complementary peptides in which the hydrophobic residues at positions *a* and *d* promoted parallel dimers, and the charge patterning at positions *e* and *g* was set for staggered assembly. Though, this was helped by the inclusion of offset asparagine residues at positions *a* to promote hydrogen bonding formation between them across the hydrophobic interface. This turned out to be the key design feature for promoting sticky ends and then fibre formation. **Figure 1.13** shows the sequences with their salt-bridging interactions and hydrogen-bonding between both asparagine residues from complementary sequences.

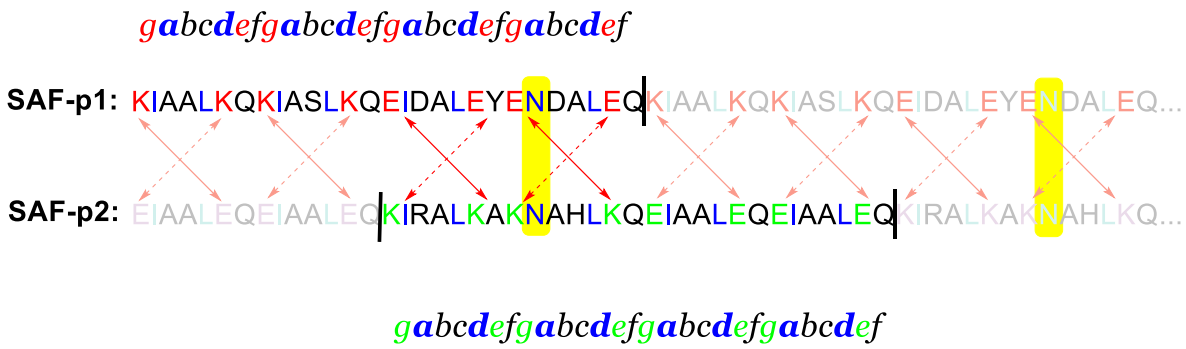

Figure 1.13: Heterodimeric *α*-helices designed by Woolfson's group for coiled-coil fibre formation – *SAFs* (adapted figure from reference 12). The hydrogen bonds formed by the Asn residues from the complementary sequences are highlighted in yellow.

Investigations on this type of fibre-formation systems demonstrated that replacing residues at the polar interface (*b*, *c*, and *f* positions) could promote either interfibre hydrophobic interactions or interfibre hydrogen bonding to produce thinner and more-flexible fibres that form physical hydrogels.[18]

1.4.1 *α*-Helical coiled-coil fibrous systems for bionanotechnology applications

The wide variety of *α*-helical coiled-coil structures inspires the development of new self-organizing biomolecular systems as building blocks for biosupramolecular chemistry. Synthetic biology can use these structures for a wide variety of potential applications in fields such as medicine and biotechnology. Coiled-coil structures can be used, for example, as *hubs* or *spacers* to bring together bioactive components with defined chirality and at set distances with nanometre precision.[19] Arndt *et al*. demonstrated that coiled-coils could be used together as *hubs* to bring together and to increase the efficacy of antibodies.[20] Moreover, coiled-coil structures have been used as linkers to control the aggregation of nanoparticles at set nanometre spacings.[21, 22]

However, nature contains many alternative protein-based fibrous materials, such as collagen, so it is of interest to use synthetic biology as tool for developing new fibrous-based materials at the nanometre scale.[23] Some examples are given by new designed

robust hydrogels by Banwell *et al*. which support mammalian cell growth and differentiation.[18] Other studies have developed scaffolds for tissue engineering,[24] smart biomaterials for nanoelectronic devices,[25] or fibrous assemblies and materials as scaffolds for the adhesion, growth and differentiation of cells.[23] Due to the ability of self-assembled coiled-coils of fibrous systems to form gels upon high peptide concentrations, the applicability as strong fibrous-structures for cell culture and tissue engineering shows promising as well as for wound healing and regenerative medicine, cosmetics, and personal health.[26-29]

1.5 Supramolecular chemistry: self-assembly of complex structures

Bringing two molecules together in space to make a new one implies a chemical reaction in which new bonds are formed. The nature of these bonds may vary. Traditional chemistry has focused on the study of covalent bonds while supramolecular chemistry has tried to investigate other noncovalent forces (which tend to have lower energies and may break) that also participate in the process, such as hydrogen bonds, metal coordination, van der Waals and hydrophobic forces, π–π interactions, and electrostatic effects.

Supramolecular chemistry started to emerge as an important field of chemistry when Latimer and Rodebush gave a better description of how the hydrogen bond must be understood – this was useful to demonstrate the real double helical structure of DNA.[30] However, it is after the Nobel Prize for developing selective "*host-guest*" complexes, awarded to Donald J. Cram, Jean-Marie Lehn, and Charles J. Pedersen in 1987, when supramolecular chemistry starts to play a more important role in the design of new complex structures. After seeing that it was possible to design molecules which would only be recognized selectively by a specific partner, new and more ambitious complex systems were proposed and achieved. Thus, for example, James Fraser Stoddart developed molecular machinery and self-assembled structures,[31] as well as other researchers contributing other models.

Since we aim to use molecular components for both generating and controlling conformational switching in *de novo* coiled-coil peptide systems, it is important to

understand the way some sequences encode two or more folded states. One protein can show activity in one of their conformational states whilst can remain inactive in another one. In some cases, this conformational switch may be induced by a noncovalent interaction,[32] by changes in the pH,[33] by different responses to heat,[34, 35] or by other effects such as disulphide-bond reduction.[36] Here we focus on metal-binding and azobenzene photoswitching as modes to control the self-assembling of *de novo* designed peptide systems, and they are discussed next.

1.5.1 Self-assembling systems regulated by metal-binding

Due to the richness in the properties of the metal ions, supramolecular chemistry makes use of coordination chemistry to design novel structures in order to develop new functionalized materials for technological applications. Most biological systems contain proteins which rely on the effect and properties given by the metal ion to which they are bound. The ability of transition metals to form coordination complexes can provide us with new systems with well-defined coordination geometries which could be used to investigate the relationship between sequence, structure and function, but also to control the self-assembly of higher ordered molecular structures. The goal is to mimic these natural processes and also to design new metallo-proteins which function as building blocks in which different metal ions could favour the formation of new functionalized structures.

It has also been found that metal ions can coordinate ligands, and in such cases the affinity of this metal-binding could be enhanced. It is also possible that the production of unnatural metal-binding motifs could provide medicinal applications for peptides, as well as other different roles in imaging, catalysis, or metal-ion detection.[37-43]

An important feature is to select the appropriate ligand to coordinate the metal ion. As reported by Imperiali and co-workers,[44] there are a limited number of natural amino acids capable of binding metals in aqueous media. For this reason, the design of synthetic ligands to enhance metal ion selectivities as well as to widen the range of metal-binding is an interesting target.

Pyridine is one of the most used ligands in coordination chemistry due to the chemical nature of nitrogen as electron-donor for bond formation. Pyridylalanine, which is the substituted analogue of pyridine is commonly used as part of bioactive compounds and as chiral building blocks. These properties make this type of ligands very interesting when coordinated to metal ions as the interaction could affect some of their physical or chemical properties such as binding angle, coordination geometry, and electron donating effects. Moreover, they can be used as part of components of antitumour[45] and anti-inflammatory[46] agents, as well as in pharmaceutical applications.[47, 48] On this pathway, Imperiali *et al*. stereoselectively synthesized several bipyridine amino acids[44, 49, 50] capable of being inserted into polypeptides and studied their effects when coordinating to some metal ions such as Co(II), Cd(II), Cu(II), Ni(II) and Zn(II).[44] When changing the ratio of this amino acid in the presence of a constant concentration of the metal ions, the spectroscopic studies showed differences and hence the geometry of association could then be examined.

Kwong and co-workers developed the synthesis of a type of chiral bipyridine ligands sensitive to the nature of the coordinated metal ion.[51] These bipyridine ligands had an axially unfixed bridge that was able to rotate. They complexed the ligand with Ag(I) and Cu(I), and ammonium ions and observed different behaviours and geometries of association, concluding that these ligands had switchable properties (**Figure 1.14**).

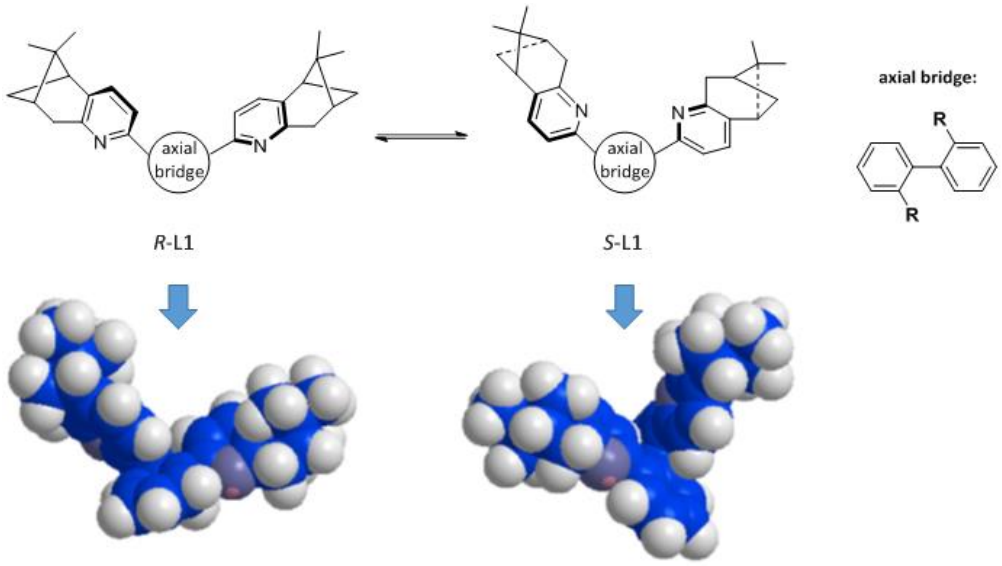

Figure 1.14: Chemical structure of the rotational conformers of the biphenyl ligand **L1** in equilibrium (top) and their space filling model (below) developed by Kwong and co-workers (adapted picture from reference 51) The structure of the axially unfixed bridge is shown.

To date, other examples of polypeptides with novel ligands inserted into their sequences by modified amino acids have been reported. There are both examples in which the insertion of these novel amino acids takes place in the middle of polypeptidic chains or attached in their terminal amino groups.[52] Kaiser and Sasaki designed the "helichrome" based on a coproporphyrin as a template to control the folding of four peptides in a helical-like bundle (**Figure 1.15**).[53]

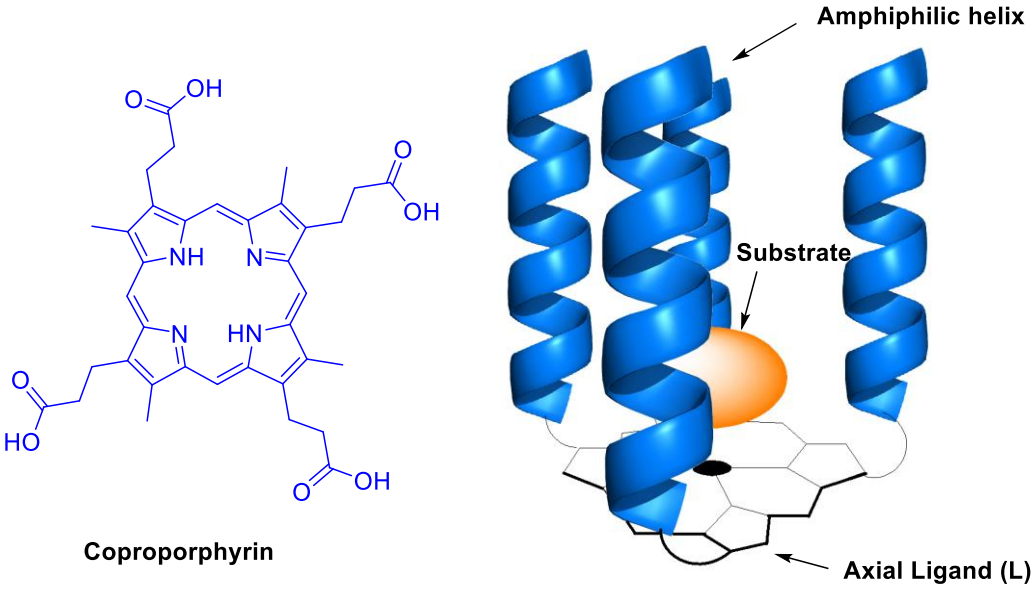

Figure 1.15: Structure of coproporphyrin, and the proposed structure of the helicrome when folding the α-helices (adapted figure from reference 53).

Sasaki and Hopkins were also able to achieve metal-binding to peptides by inserting unnatural aminodiacetic acid residues in their sequences (**Figure 1.16**).[54, 55] Moreover, in order to prove the ability to form a stable bond for the helix, some metal ions were tested: Cd(II), Co(II), Cu(II), Ni(II), and Zn(II). Ghadiri's group designed a peptide in which the N-terminus had a pyridyl motif attached.[56] The result after complexation with Ru(II) was the formation of a four-helix bundle structure which was found to be soluble in water (**Figure 1.17**).

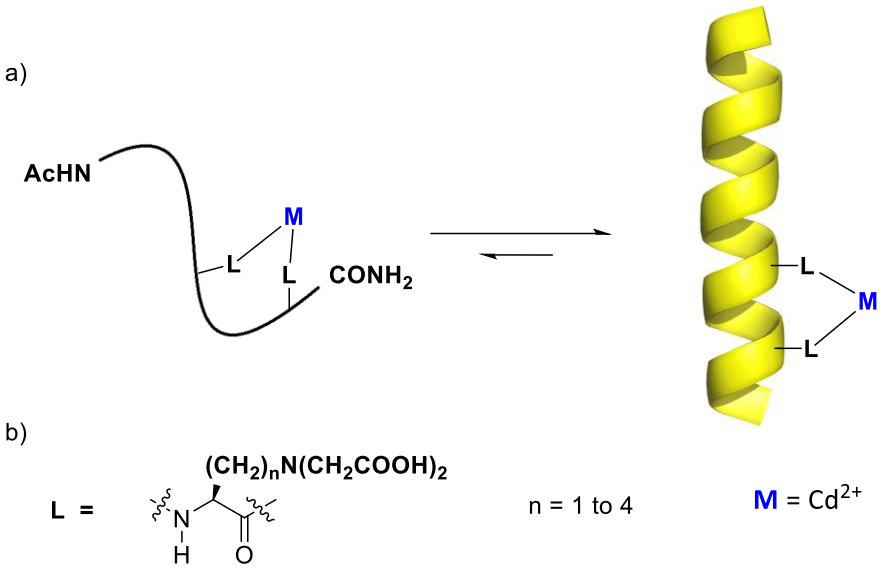

Figure 1.16: (a) Structure of the cross-linked peptide in aqueous solution (adapted figure from reference 55); (b) Chemical structure of the aminodiacetic acid residue responsible for metal binding (adapted figure from reference 52).

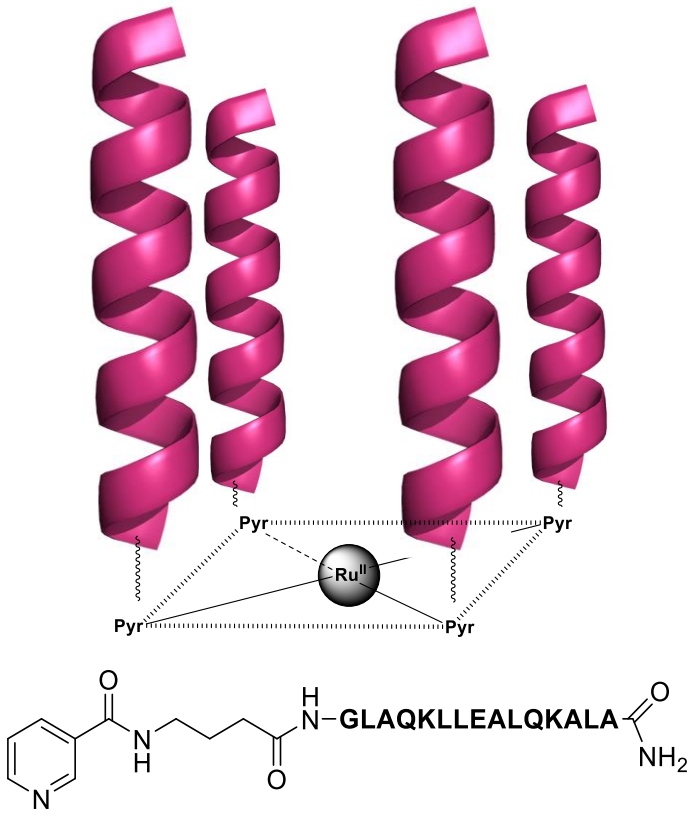

Figure 1.17: Four-helix bundle structure produced after coordination of Ru(II) to the pyridyl motifs of a pyridyl-functionalized peptide. The functionalized peptide sequence is shown at the bottom of the picture (adapted picture from reference 52).

Functionalization in the N-terminus with bipyridyl motifs was studied and developed at the same time but separately by the research groups of Sasaki and Ghadiri.[57, 58] Sasaki demonstrated that Fe(II) was able to induce a three-bundle folding when coordinated to this bipyridyl motif inserted in a peptide. Ghadiri showed the same folding effect for different metal ions such as Ru(II), Co(II) and Ni(II) when coordinated to a peptide sequence which included another bipyridyl motif. The two different bipyridyl-ligands and the three-bundle structure provided are shown in **Figure 1.18**.

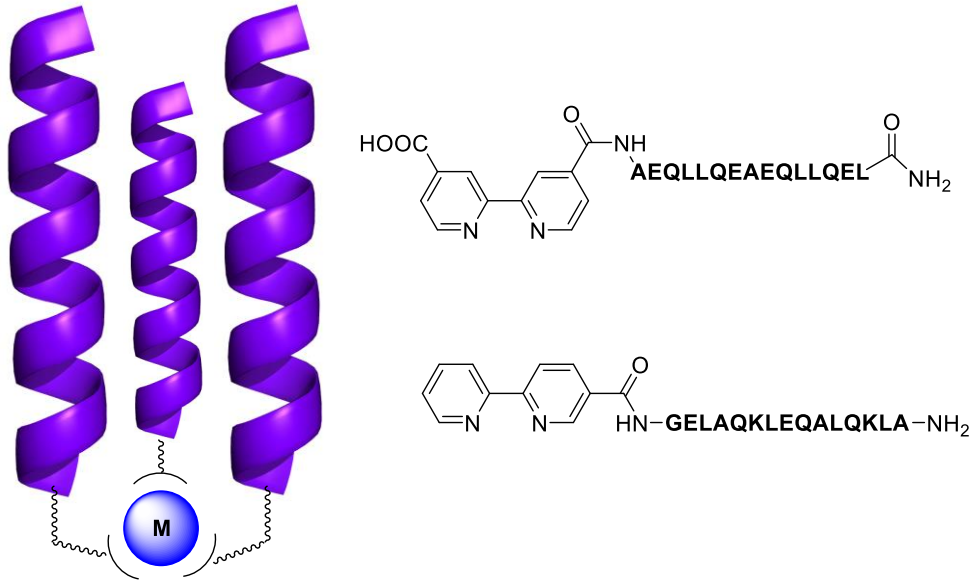

Figure 1.18: Three-bundle structure produced by the folding of the peptide sequences functionalized with the bipyridine ligands developed in Sasaki's group (represented at the top right), and in Ghadiri's group (represented at the bottom right) after metal-binding (adapted pictures from reference 52).

Ghadiri further incorporated a histidine residue into the bipyridyl-sequences but right on the other side of the helix so as to allow an extra metal-binding ligand to coordinate from both edges of the helices.[59] This new type of metal-binding complexes was designed due to some reports which showed the ability of copper to coordinate histidine residues in natural proteins.[60] The peptide sequence and the folding system are shown in **Figure 1.19**.

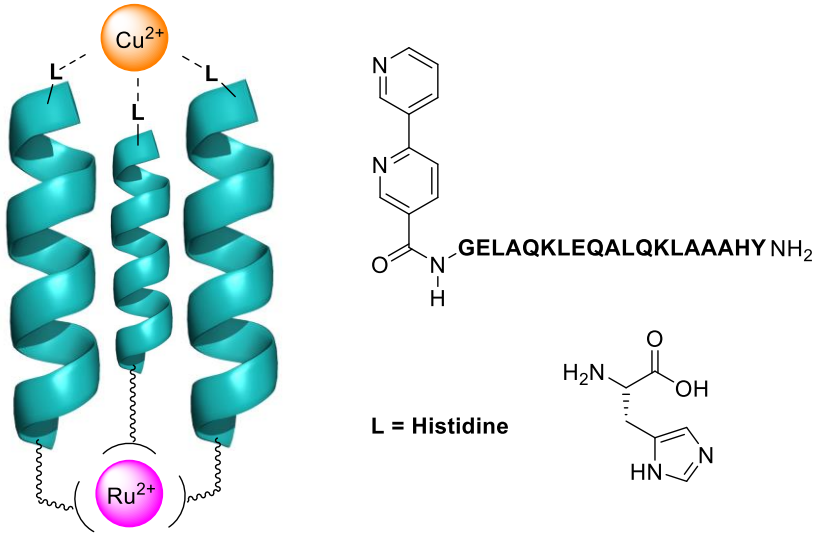

Figure 1.19: The peptide sequence is shown at the left and the three-helix bundle structure at the right (adapted picture from reference 52).

Metal binding not only can provide new functionality but it can also improve the activity of the fastest known metalloenzymes, as in the case of the human carbonic anhydrase.[61] **Figure 1.20** shows a ribbon diagram of an artificial metallohydrase that Zastrow *et al*. designed and successfully synthesized. This contained two separate metal binding sites able to coordinate both Zn(II), enhancing the nitrogenous catalytic activity for either pNPA hydrolysis or CO_2 hydration, and Hg(II), which provided structural stability.

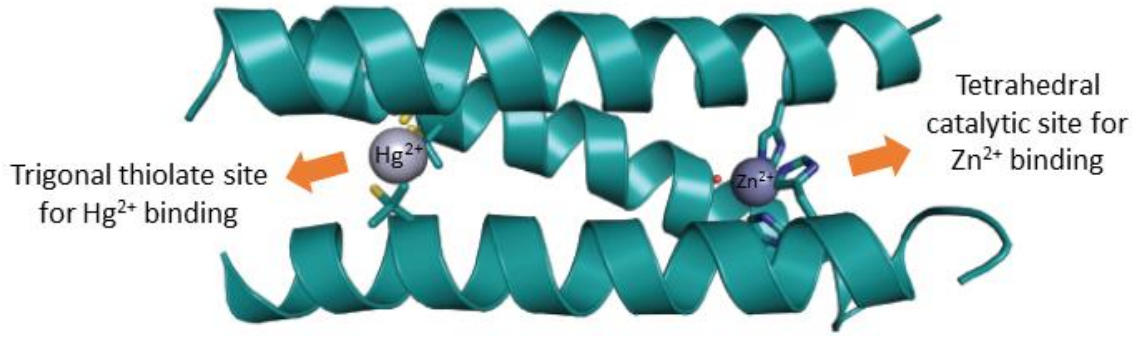

Figure 1.20: Ribbon diagram of the metalloenzyme synthesized in Pecoraro's group (adapted picture from reference 61).

Anna Peacock and co-workers designed a *de novo* peptide sequence of 30 residues capable of binding a therapeutic gold(I) phosphine complex into aqueous solution.[62] Analysis by *UV*/Vis confirmed metal-binding of Au(I) to the peptide and the CD spectrum showed that the coiled coil structure was retained upon coordination with the metal ion. A potential application of this type of compound would be to generate a new class of gold(I) phosphine peptide therapeutics. In 2014, Peacock's group designed artificial peptide dimers, to which polypyridine switching units were incorporated, to demonstrate that biomolecular recognition, and specifically sequence-selective DNA binding could be controlled by metal-ion coordination, Cu(II) and Zn(II).[63] Their aim was to develop a base for a wide range of applications in the future.

In summary, there is an increasing interest in this field and there are a few examples that inspire not only the design of new metal-binding structures to control the assembly and folding of polypeptidic structures but also to bring both improved and new functionality into these biochemical systems.

1.5.2 Photo-switching molecules to control peptide-assembling

Nature shows biological systems which are able to control their assembly or conformational state through many alternative ways. Photoresponsive systems work by irradiating light into a photosensitive element embedded into their matrix which after capturing the optical signal transforms it into a physicochemical stimulus. This stimulus causes a conformational change in the structure of the biomolecule and may provide it with new functionality. These photosensitive elements are called chromophores and are responsible for absorbing light to activate the photoswitching process which in some cases can be reversibly controlled.

Using azobenzene derivatives as chromophores is one utilized strategy to photoreversibly control the secondary structure of polypeptide sequences or proteins. Irradiating light on the azobenzene derivatives at the right wavelength when they are attached to peptide sequences may induce a conformational change in the peptides secondary structure. The ability to photo-control helical content also offers the possibility of photo-controlling protein activity, and hence, protein function.

Azobenzene derivatives may vary in their structure and size but the main and common feature of these type of molecules is that two phenyl rings are linked by an *"azo"* N=N bond. **Figure 1.21** shows the general structure of a *trans* isomer of an azobenzene derivative, having the simplest of them at the left-hand side, and showing the different positions for substituents at the right-hand side.

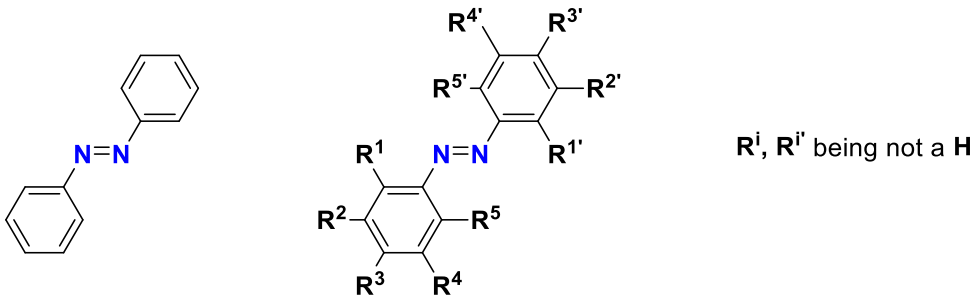

Figure 1.21: General structure of a *trans* isomer of an azobenzene derivative. At the left-hand side we can see the simplest example of these type of compounds at where all the R groups are hydrogens. The degree of substitution in the different positions will provide a wide class of this type of molecules.

Azobenzene derivatives can be interconverted from the *trans,* and most stable isomer, to the *cis* isomer by irradiating with light at the right wavelength (**Figure 1.22**). Thus, *UV* light will be used for the *trans*-to-*cis* isomerization and visible light can be used for the *cis*-to-*trans* isomerization. Because the *cis* isomer is thermally disfavored it will return to *trans* slowly by thermal activation.

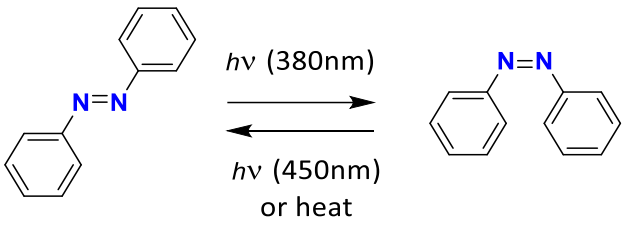

Figure 1.22: Photoisomerization of an azobenzene by light irradiation.

In general, it has been demonstrated that the *trans* isomer of an azobenzene derivative represents a >99% when the molecule is in the dark, while the percentage of *cis* isomer that can be achieved after irradiation may vary from 70-90% depending on the structure of such derivative, as well as the barrier energy to interconvert both isomers. The mechanism through which this isomerization happens is still an object of

study and may vary depending on the substituents on the rings, however, there are a few proposed mechanisms which are showed in **Figure 1.23** adapted from Dhammika Bandara's paper in 2011.[64] The characteristic bands of absorption are in the visible and *UV* region, hence, can be monitored by *UV*/visible absorption spectroscopy. There are low lying ***n*** → **π*** bands between 380 and 520 nm, while the **π** → **π*** bands appear at around 330 nm for the *trans* isomer and at around 275 nm for the *cis* isomer.

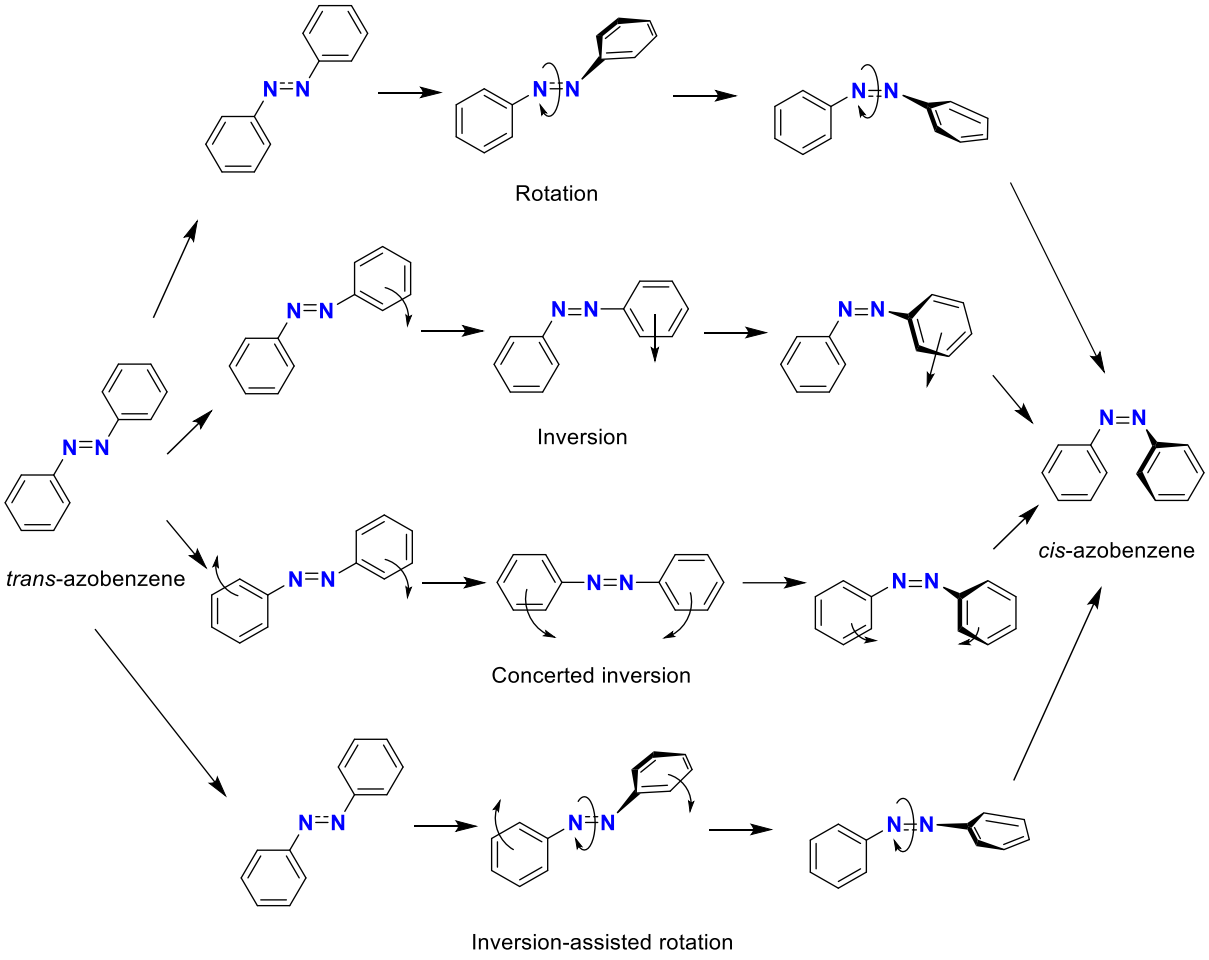

Figure 1.23: Proposed mechanisms for the *trans*-to-*cis* photoisomerization of an azobenzene molecule. The arrows do not indicate electron movement but the movement of the phenyl rings (adapted figure from reference 644).

When azobenzene derivatives are incorporated into polypeptide sequences they act as the photoswitching element to interconvert the secondary structure of these peptides by the effect of light irradiation at the right wavelength. Attachment of azobenzenes to polypeptides is done via the reaction of halo-substituted azobenzenes with *thiols* that are part of the peptide sequences. Since the amino acid Cys contains a terminal *thiol*

group, having Cys as part of a polypeptide chain may provide a reactive site to incorporate azobenzene derivatives. *Thiols*, or more specific their conjugate bases, *thiolates*, are readily alkylated to give *thioethers* when using an adequate base. As an azobenzene derivative is attached at two sites, this means that two Cys residues are needed within the peptide sequence. However, these *thiols* can react together to form a disulfide bond, -S-S-, and this reaction would block the incorporation of the azobenzenes. The way to avoid this unwanted reaction is to control the pH of the media. Since pK_a(Cys) = 8.35, a pH near 8 is needed to maintain the Cys residues in their reduced states and to make possible the reaction with the azobenzene derivatives in both reactive sites of these molecules. In addition, as we wish to allow the photo-control of the secondary structure of our designed peptide sequences, we are interested in the design of simple systems which can operate in water. Therefore, having azobenzene derivatives which can be easily dissolved in water will enhance the process.

Woolley *et al*. have been investigating the distance at which the Cys residues must be spaced within the polypeptide sequence so as to be readily cross-linked by the azobenzene moiety. In Woolley's group they designed a few model sequences in which the spacing in between Cys residues was: $i \rightarrow i$+4, $i \rightarrow i$+7, and $i \rightarrow i$+11, and used the same azobenzene derivative as to find out which spacing could maximize the photo-switching in the dark-adapted, or inactive, state of the system. They saw that having the Cys residues in a spacing at $i \rightarrow i$+4 in the dark-adapted state the *trans* conformation leaded to a distorted helicity content.[65] However, after photo-irradiation to get the *cis* conformation the helical content increased. For the model at a spacing at $i \rightarrow i$+7 they found that the azobenzene in its *trans* conformational state was too long to adopt an α-helix conformation, but when the cross-linker was excited with light and photo-isomerized to its *cis* conformation, its length matched the spacing and favored an ideal α-helix.[66] In contrast with these two models, the spaced at $i \rightarrow i$+11 favored the formation of an α-helix in the dark-adapted and distorted the α-helix in a high degree when the azobenzene moiety was photo-irradiated (**Figure 1.24**).[65]

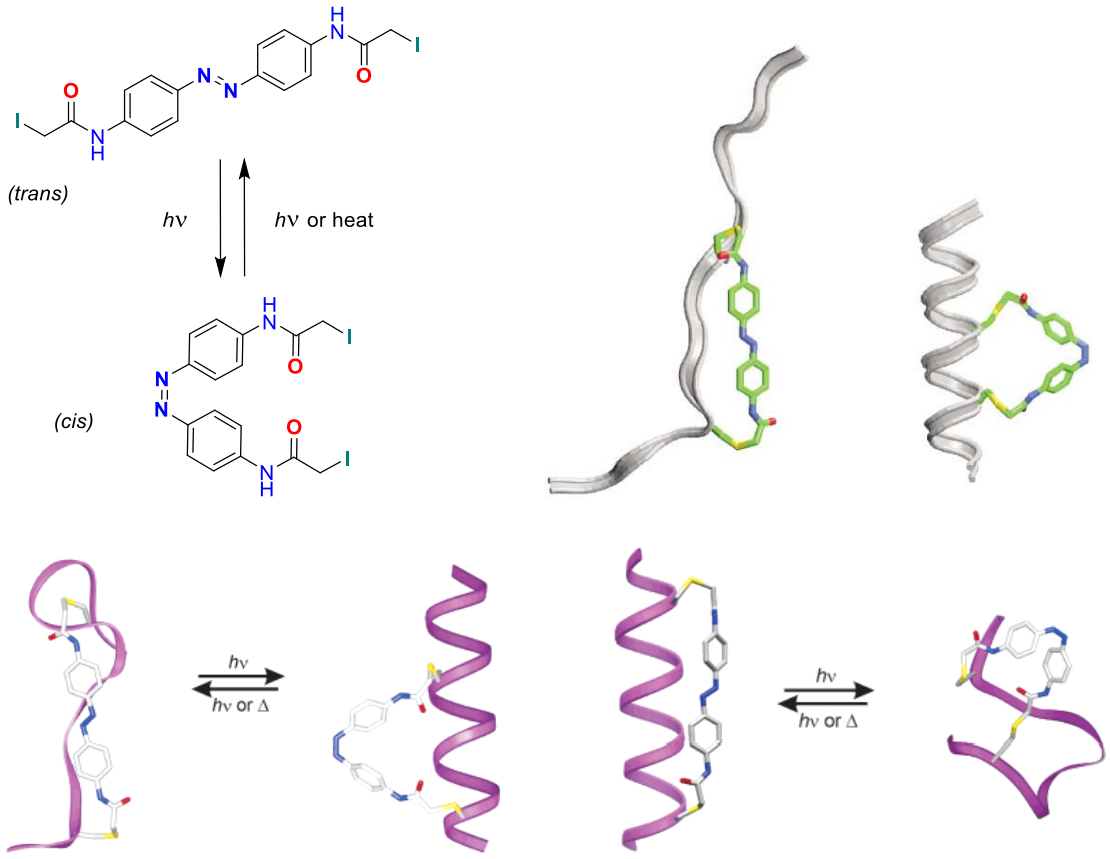

Figure 1.24: At the top left, the photo-isomerization of the azobenzene derivative used in reference 65; FK-4-X model (*i* → *i*+4) at the top right (*trans* and *cis* isomers respectively); at the bottom left, JRK peptide at a spacing at *i* → *i*+7 (*trans* and *cis* isomers respectively) and FK-11-X model (*i* → *i*+11) at the bottom right (*trans* and *cis* isomer respectively) (adapted pictures from reference 65).

Once the azobenzene moiety has been incorporated into the polypeptide sequence, circular dichroism (CD) is used to demonstrate whether the helix content of such peptide can be reversibly photo-controlled when irradiating with the appropriate wavelength. **Figure 1.25** at the left-hand side shows the typical CD spectra for each of the possible conformational structures and, at the right-hand side, an example of the spectrum of a polypeptide attached to an azobenzene derivative before and after irradiation with light.

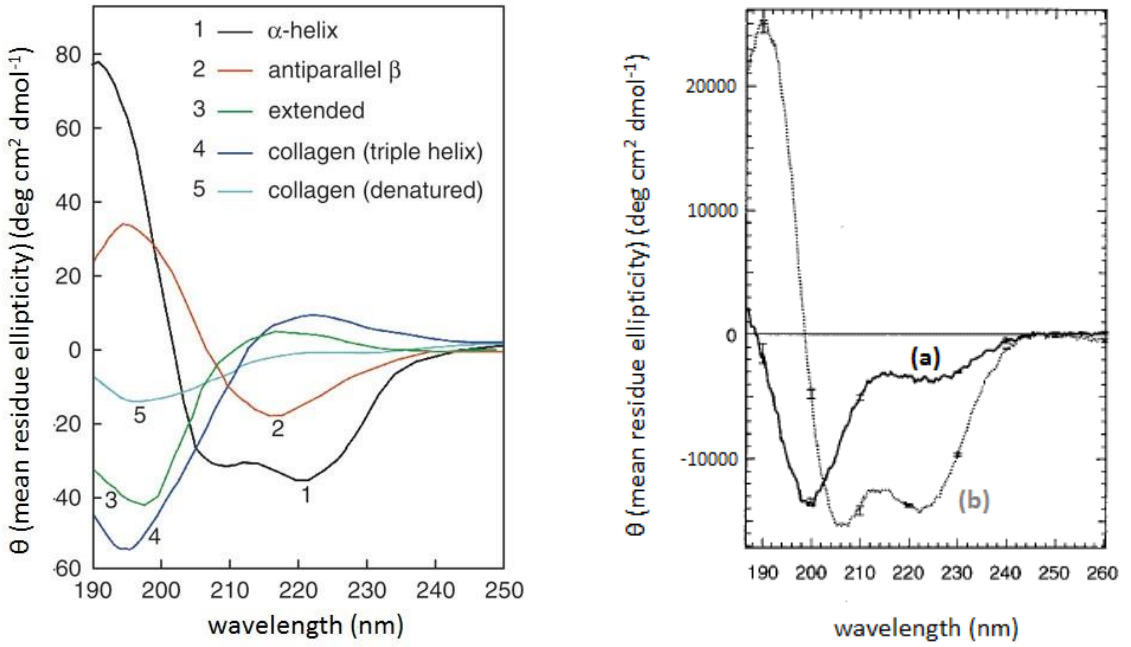

Figure 1.25: At the left, CD spectra for different conformational structures. This picture was adapted from *Nature Protocols* **2007**, 1, 2527 – 2535. At the right, the CD spectra of both *trans* and *cis* conformational states of a polypeptide sequence when contains an azobenzene moiety attached to it. This picture was adapted from *PNAS* **2000**, 97, 3803 – 3808. In this case, the curve **a** represents the CD spectrum of the dark adapted peptide, whereas curve **b** represents the spectrum obtained after exposure of the solution to 380 nm light. Therefore, for this given example, the *trans* conformation will orientate the structure of the peptide in a non-helical conformation while the *cis* conformation will favour an *α*-helical content.

As seen in **Figure 1.25** at the right hand side, for that given example, the *trans* conformational state (curve a) has a lower *α*-helical content than the peptide structure at the *cis* conformational state (curve b). Since the *trans* isomer of the azobenzene molecule is the most stable, it would be of interest to have the azobenzenes in their *trans* conformational state able to favor an *α*-helical conformation of the polypeptide sequence.

Depending on the azobenzene derivative and the R^i substituents the cross-linked state may couple either the *trans* or the *cis* conformation to *α*-helical content (**Figure 1.26**).[67] The conformational states of these different linkers can be monitored by *UV*/visible absorption spectroscopy.[68] As well as the R groups in an azobenzene derivative can affect the conformational state to photo-control polypeptide sequences, the position in which these chromophores are placed within the sequences can show different effects and efficiency in the photo-regulation of the structures. This was

demonstrated in Woolley's group by synthesizing a polypeptide of 32 residues with a determined core structure and inserted their *BSBCA* derivative at a spacing of $i \rightarrow i + 7$ and, also, at different positions along the helix. Analysis by CD indicated that photo-control of helix folding or unfolding by *BSBCA* was most effective when this was located in the middle of the sequence, causing the best propagation effect along the helix.[69]

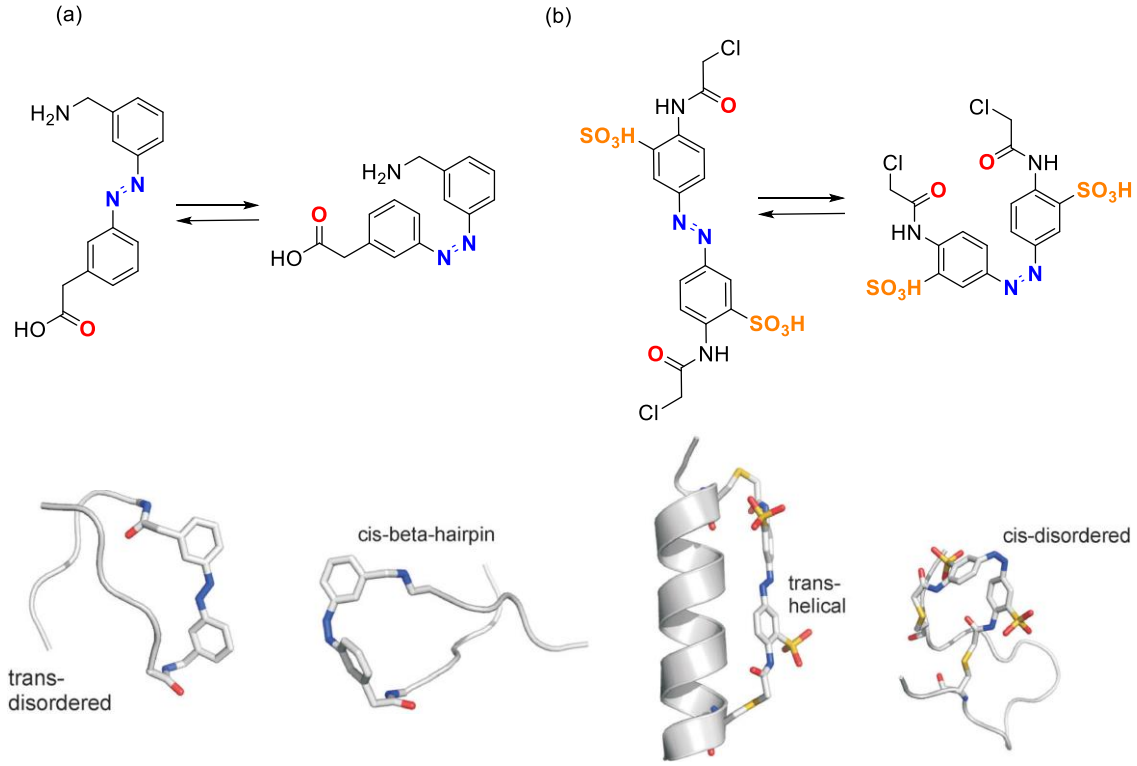

Figure 1.26: (a) Structure of an azobenzene cross-linker where the *cis*-β-isomer shows stabilized and when switching to *trans* is disordered. (b) An azobenzene derivative which stabilizes the *trans* isomer for an *α*-helix sequence and shows a disordered structure when switches to *cis* (adapted pictures from reference 67).

There are many examples of azobenzene derivatives photo-regulating polypeptidic structures within proteins. For example, Rudolf K. Allemann *et al.* used azobenzene cross-linkers to control *α*-helical peptides within MyoD.[70] MyoD is a human protein with a key role in regulating muscle differentiation. When an azobenzene unit binds the DNA-recognition helix of MyoD, this protein shows photo-control of its activity (**Figure 1.27**).

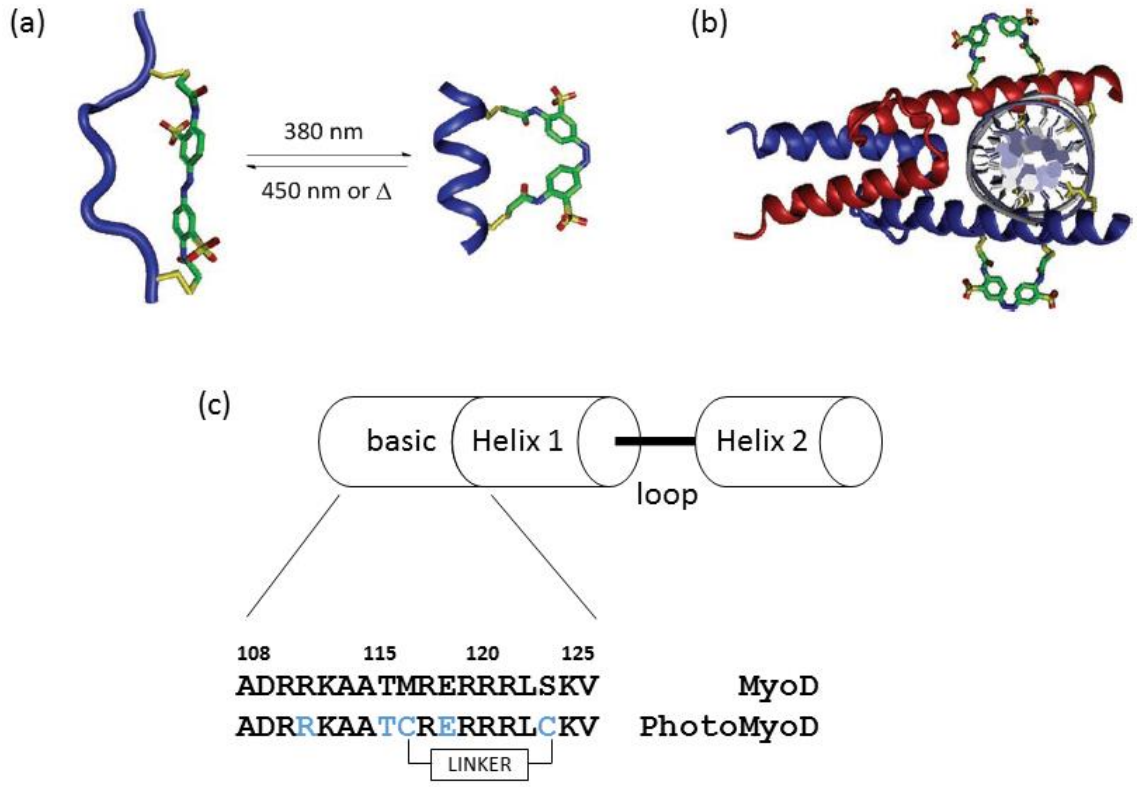

Figure 1.27: (a) Photo-isomerization of photoMyoD; (b) schematic representation of the MyoD and photoMyoD structures showing the primary peptide sequence of their basic regions; (c) model of the DNA complex of photoMyoD with the cross-linker in its cis configuration complexed by recognition helices of two bHLH subunits of the dimeric protein (adapted figure from reference 70).

Although azobenzene derivatives have the ability to photoisomerize from *trans*-to-*cis* and *viceversa*, some of the experiments with polypeptides that were investigated showed incomplete reversibility due to the fact that the chromophore became trapped in one photo-isomeric state. Woolley and co-workers designed a modified GCN4-bZIP protein which utilizes an azobenzene motif to enhance the DNA-binding ability in a fully thermally reversible process.[71]

Wanting to show the versatility of the azobenzene derivatives, Woolley's group designed longer azobenzene cross-linkers to allow photo-isomerization of peptides when the Cys residues were located in a spacing of 12, 15 and 16 residues away.[72] The azobenzene derivative which they used for this purpose is shown in **Figure 1.28a**. However, in an attempt to expand this scope they designed a bis-azobenzene derivative **Figure 1.28b** which showed to stabilize structures at much longer spaced relationships.[73]

(a)

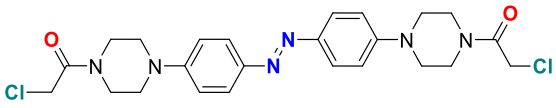

(b)

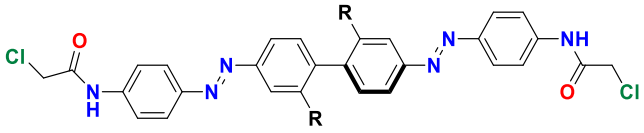

BPDB (4,4'-bis[4-(2-chloroacetamido)phenyl]diazenylbiphenyl) : **R**=H
BPBDS (4,4'-bis[4-(2-chloroacetamido)phenyl]diazenylbiphenyl)-2,2'-disulfonate): **R**=SO_3H

Figure 1.28: Structure of longer azobenzene-like chromophores to photo-control peptide folding at a higher spacing relationship.

Rener and Moroder also described azobenzenes as chromophores able to photo-regulate the structures in which peptides were folded.[74] Schultz *et al*. incorporated an azobenzene into proteins in *E. coli* in order to control enzyme activity.[75] Woolley also tested azobenzenes as photoregulators of the activity in ion channels.[76] In 2010, the work developed by Woolley's group shown that coiled-coils of proteins within living cells could also been controlled by light irradiation.[77] Again, in 2011, Woolley *et* al. attached a fluorescent dye near the azobenzene in order to test whether the intensity in fluorescence emission changed when conformational isomerization occurred (**Figure 1.29**).[78]

Woolley's group have also found an alternative to switching by UV, using visible light (red-shifted) in biological systems. They find successful results with new synthesized azobenzene derivatives in which their four *ortho* positions to the azo group were substituted with bulky, polar and electron-rich substituents, such as methoxy (or even with chloro),[79] *S*-ethyl groups,[80] and also using a longer bisazobenzene cross-linker which contained a central piperazine unit linking both azobenzene chromophores in *para* position.[81]

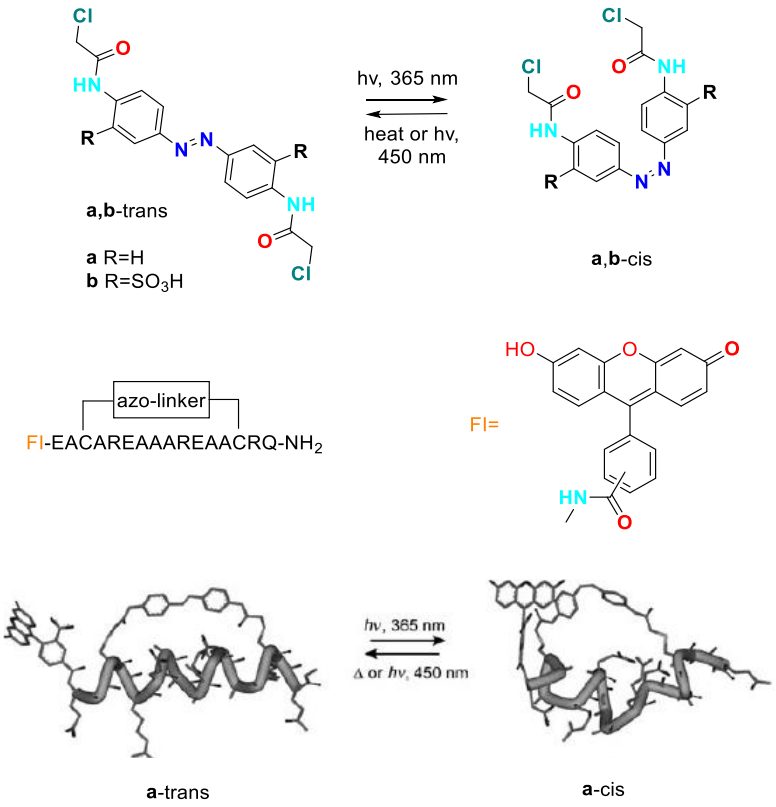

Figure 1.29: Above, the representation of the photo-isomerization of the azobenzene motif. Below this, the peptide sequence is shown as well as the dye, or fluorescent reporter. The structure when the cross-linker is attached to the peptide and its photo-isomerization is shown below (Adapted picture from reference 78).

Since azobenzene derivatives have a wide range of applicability, there is a growing interest in designing new types of azo-switches to develop new enhanced applications such as molecular motors[82, 83] and molecular electronic devices,[84] smart polymers for optical data storage,[85] conformational switches in cyclic peptides,[86] design of light-activated proteins within complex biochemical systems,[71] chromopeptide[74] and carbohydrate applications,[87] molecular sensors of plasmonic nanoantennas,[88] regulation of porous hybrid materials,[89] for energy-storage of solar thermal fuels with functionalized carbon nanotubes,[90] as potential substitute for conventional metallic paints,[91] enhance gene delivery and contributing to more exposure of genes for transcription,[92] and as pH indicators,[93] in between some of them. In this project we aim to use an azobenzene derivatives as molecular switch to reversibly photo-control and trigger peptide assembly and folding.

1.6 Project aims

Having a clear concept of what an amino acid is, how amino acids are brought together to form peptide sequences through amide bonds, and how these peptide sequences can interact and assemble with other peptide sequences to form higher order structures is the starting point of this research project. Here we focus on *α*-helical coiled-coils as the elements of higher order peptide structures.

We can say that peptide chemistry is the base of this thesis and we use solid-phase peptide-synthesis (SPPS) strategies to synthesize the designed self-assembling peptide systems. However, this project is described as interdisciplinary due to the use of both organic chemistry (that we make use to synthesize small organic molecules) and inorganic chemistry (through the use of metal-binding), but also spectroscopy (that we use for analysis).

As seen in Nature, biomolecules containing a metal ion within their structure provide different functionality within living organisms (structural, electron transfer, catalytic functionality, etc.). It has also been demonstrated that *de novo* metalloproteins can be built from scratch and can also be competitive with known natural metalloenzymes.[94]

Therefore, we aim to use novel molecular components to generate conformational switching in *de novo* coiled-coil peptide designs. This includes both the synthesis of synthetic amino acids analogues for metal-binding and the synthesis of azobenzene derivatives for photoisomerization.

By incorporating synthesized novel amino acids into self-assembling peptide system we aim to form both novel chiral metal-based biocatalysts but also to investigate to what extent the self-assembly can control metal-binding and to what extent the metal-binding can control self-assembly. Moreover, the geometry of association between polypeptides and metal ion may vary depending on the metal ion (size, oxidation state, reactivity properties). In this case we say that metal binding is a tool to trigger or suppress assembling.

By using azobenzene derivatives, which can be photoswitched between *cis* and *trans* isomers, we can induce conformational changes in the secondary structure of coiled-

coil peptide designs. The success of this effect in simple systems could encourage to test it in larger systems which would add a whole extra layer of complexity to the assemblies. The use of azobenzene derivatives for photo-regulation of peptide sequences may provide a potential power source for protein motors, e.g. in a motor hub to influence the direction and efficiency of stepping.[95, 96]

[1] A.L. Boyle, and D.N. Woolfson, *Chem. Soc. Rev.* **2011**, 40, 4295-4306.

[2] K. Channon, E.H.C. Bromley, and D.N. Woolfson, *Curr. Opin. Struct. Biol.*, **2008**, 18, 491-498.

[3] E.H.C Bromley, K. Channon, E. Moutevelis, and D.N. Woolfson, *ACS Chem. Biol.*, **2008**, 3, 38-50.

[4] P.Y. Chou, and G.D. Fasman, *Biochemistry* **1974**, 13, 211-222.

[5] C.B. Anfinsen, and H.A. Scheraga, *Adv. In Prot. Chem.* **1975**, 29, 205-300.

[6] B. Robson, and E. Suzuki, *J. Mol. Biol.* **1976**, 107, 327-356.

[7] S.S. Zimmerman, and H.A. Scheraga, *Biopolymers* **1977**, 16, 811-843.

[8] A.L. Boyle, and D.N. Woolfson, *Supramolecular Chemistry: From molecules to nanomaterials* **2012** "Rational Design of Peptide-Based biosupramolecular systems".

[9] P.B. Harbury, T. Zhang, P.S. Kim, and T. Alber, *Science* **1993**, 262, 1401-1407.

[10] J.M. Fletcher, A.L. Boyle, M. Bruning, G.J. Barlett, T.L. Vincent, N.R. Zaccai, C.T. Armstrong, E.H.C. Bromley, P.J. Booth, R.L. Brady, A.R. Thomson, and D.N. Woolfson, *ACS Synth. Biol.* **2012**, 1, 240-250.

[11] W.D. Kohn, C.D. Kay, and R.S. Hodges, *J. Mol. Biol.* **1998**, 283, 993-1012.

[12] M.J. Pandya, G.M. Spooner, M. Sunde, J.R. Thorpe, A. Rodger, and D.N. Woolfson, *Biochemistry* **2000**, 39, 8728-8734.

[13] S. Kojima, Y. Yuriki, T. Yoshida, K. Yazaki, and K. Miura, *Proc. Jpn. Acad., Ser. B, Phys. Biol. Sci.*, **1997**, 73, 7-11.

[14] S. Kojima, Y. Yuriki, K. Yazaki, and K. Miura, *Biochem. Biophys. Res. Commun.*, **2005**, 331, 577-582.

[15] S.A. Potekhin, T.N. Melnik, V. Popov, N.F. Lanina, A.A. Vazina, P. Rigler, A.S. Verdini, G. Corradin and A.V. Kajava, *Chem*. *Biol.,* **2001**, 8, 1025-1032.

[16] Y. Zimenkov, V.P. Conticello, L. Guo, and P. Thiyagarajan, *Tetrahedron*, **2004**, 60, 7237- 7246.

[17] H. Dong, S.E. Paramonov, and J.D. Hartgerink, *J. Am. Chem. Soc.*, **2008**, 130, 13691-13695.

[18] E.F. Banwell, E.S. Abelardo, D.J. Adams, M.A. Birchall, A. Corrigan, A.M. Donald, M. Kirkland, L.C. Serpell, M.F. Butler, and D.N. Woolfson, *Nat. Mater.*, **2009**, 8, 596-600.

[19] S. Nautiyal, D.N. Woolfson, D.S. King, and T. Alber, *Biochemistry* **1995**, 34, 11645-11651.

[20] K.M. Arndt, K.M. Muller, and A. Pluckthun, *J. Mol. Biol.* **2001**, 312, 221-228.

[21] M.G. Ryadnov, B. Ceyhan, C.M. Niemeyer, and D.N. Woolfson, *J. Am. Chem. Soc.* **2003**, 125, 9388-9394.

[22] M.M. Stevens, N.T. Flynn, C. Wang, D.A. Tirrell, and R. Langer, *Adv. Mater.* **2004**, 16, 915-918.

[23] D.N. Woolfson, and M.G. Ryadnov, *Curr. Opin. Chem. Biol.* **2006**, 10, 559-567.

[24] C.E. MacPhee, and D.N. Woolfson, *Curr. Opin. Solid State Mat. Sci.*, **2004**, 8, 141-149.

[25] R. Fairman, and K.S. Akerfeldt, *Curr. Opin. Struct. Biol.* **2005**, 15, 453-463.

[26] A.Y. Wang, X. Mo, C.S. Chen, and S.M. Yu, *J. Am. Chem. Soc.* **2005**, 127, 4130-4131.

[27] S.G. Zhang, F. Gelain, and X.J. Zhao, *Semin. Cancer Biol.* **2005**, 15, 413-420.

[28] V. Jayawarma, M. Ali, T.A. Jowitt, A.F. Miller, A. Saiani, J.E. Gough, and R.V. Ulijn, *Adv. Mater.* **2006**, 18, 611-614.

[29] M. Reches, and E. Gazit, *Phys. Biol.* **2006**, 3, S10-S19.

[30] W.M. Latimer and W. H. Rodebush, *J. Am. Chem. Soc*. **1920**, 42, 1419-1433.

[31] T. Ikeda, and J.F. Stoddart, *Sci. Technol. Adv. Mater.*, **2008**, 9, 1-7.

[32] Q. Lin, C.F. Barbas, and P.G. Schultz, *J. Am. Chem. Soc.* **2003**, 125, 612-613.

[33] M.M. Stevens, N.T. Flynn, C.Wang, D.A. Tirrel, and R. Langer, *Adv. Mater.* **2004**, 16, 915-918.

[34] B. Ciani, E.G. Hutchinson, R.B. Sessions, and D.N. Woolfson, *J. Biol. Chem.* **2002**, 277, 10150-1-155.

[35] R.A. Kammerer, D. Kostrewa, J. Zurdo, A. Detken, C. Garcia-Echeverria, J.D. Green, S.A. Muller, B.H. Meier, F.K. Winkler, C.M. Dobson, and M.O. Steinmetz, *Proc. Natl.Acad. Sci. USA* **2004**, 101, 4435-4440.

[36] M.J. Pandya, E. Cerasoli, A.Joseph, R.G. Stoneman, E. Waite, and D.N. Woolfson, *J. Am. Chem. Soc.* **2004**, 126, 17016-17024.

[37] G. Dirscherl, and B. Koenig, *Eur. J. Org. Chem*. **2008**, 597-634.

[38] K.A. Stephenson, S.R. Banerjee, T. Besanger, O.O. Sogbein, M.K. Levadala, N. McFarlane, J.A. Lemon, D.R. Boreham, K.P. Maresca, J.D. Brennan, J.W. Babich, J. Zubieta, and J.F. Valliant, *J. Am. Chem. Soc*. **2004**, 126, 8598-8599.

[39] S.M. Okarvi, *Cancer Treat. Rev*. **2008**, 34, 13-26.

[40] S.I. Kirin, I. Ott, R. Gust, W. Mier, T. Weyhermueller, and N. Metzler-Nolte, *Angew. Chem., Int. Ed*. **2008**, 47, 955-959.

[41] R.P. Cheng, S.L. Fisher, and B. Imperiali, *J. Am. Chem. Soc*. **1996**, 118, 11349-11356.

[42] C.T. Choma, E.P. Schudde, R.M. Kellogg, G.T. Robillard, and B.L. Feringa, *J. Am. Chem. Soc., Perkin Trans. 1* **1998**, 769-774.

[43] Z. Kovacs, and L.M. De Leon-Rodriguez, *Mini-Rev. Org. Chem*. **2007**, 4, 281-291.

[44] S.L. Fisher, and B. Imperiali, *J. Org. Chem*. **1992**, 57, 757-759.

[45] J.E. Rivier, J. Porter, C.L. Rivier, M. Perrin, A. Corrigan, W.A. Hook, R.P. Siraganian and W.W. Vale, *J. Med. Chem*. **1986**, 29, 1846.

[46] H. Shimeno, S. Soeda and S.H. Nagamatsu, *Chem. Pharm. Bull*. **1977**, 2983.

[47] E.C. Jorgensen and K. Hsiek, *J. Med. Chem*. **1979**, 22, 1199.

[48] P.T. Sullivan, M. Kester and S.J. Norton, *J. Med. Chem*. **1968**, 11, 1172.

[49] S.L. Fisher and B. Imperiali, *J. Am. Chem. Soc*. **1991**, 113, 8527-8528.

[50] T.J. Prins, S.L. Fisher and B. Imperiali, *J. Org. Chem.* **1993**, 58, 1613-1616.

[51] K.C. Sham, C.S. Lee, K.Y. Chan, S.M. Yiu, W.T. Wong, and H.L. Kwong, *Polyhedron* **2011**, 30, 1149-1156.

[52] J.P. Schneider and J.W. Kelly, *Chem. Rev*. **1995**, 95, 2169-2187.

[53] T. Sasaki and E.T. Kaiser, *J. Am. Chem. Soc*. **1989**, 111, 380.

[54] F. Ruan, Y. Chen, and P.B. Hopkins, *J. Am. Chem. Soc*. **1990**, 112, 9403-9404.

[55] F. Ruan, Y. Chen, K. Itoh, T. Sasaki, and P.B. Hopkins, *J. Org. Chem*. **1991**, 56, 4347-4354.

[56] C. Soares, C. Choi and M.R. Ghadiri, *J. Am. Chem. Soc*. **1992**, 114, 4000-4002.

[57] M. Lieberman, and T. Sasaki, *J. Am. Chem. Soc*. **1991**, 113, 1470-1471.

[58] C. Soares, C. Choi and M.R. Ghadiri, *J. Am. Chem. Soc*. **1992**, 114, 825-831.

[59] M.A. Case, and M.R. Ghadiri, *Angew. Chem. Int. Ed. Engl*. **1993**, 32, 1594-1597.

[60] E.I. Solomon, H.B. Gray, *Met. Ions Biol. Syst.* **1981**, 3, 1.

[61] M.L. Zastrow, A.F.A. Peacock, J.A. Stuckey, and V.L. Pecoraro, *Nature Chemistry*, **2012**, 4, 118-123.

[62] A.F.A. Peacock, G.A. Bullen, L.A. Gethings, J.P. Williams, F.H. Kriel, and J. Coates, *J. Inorg. Biochem*., **2012**, 117, 298-305.

[63] E. Oheix, and A.F.A. Peacock, *Chem. Eur. J.*, **2014**, 20, 2829-2839.

[64] H.M.D. Bandara, and S.C. Burdette, *Chem*. *Soc*. *Rev*. **2012**, 41, 1809-1825.

[65] D.G. Flint, J.R. Kumita, O.S. Smart, and G.A. Woolley, *Chemistry & Biology* **2002**, 9, 391-397.

[66] G.A. Woolley, *Acc. Chem. Res.* **2005**, 38, 486-493.

[67] A.A. Beharry, and A.G. Woolley, *Chem. Soc. Rev*. **2011**, 40, 4422-4437.

[68] J.R. Kumita, O.S. Smart, and G.A. Woolley, *Proc. Natl. Acad. Sci. USA* **2000**, 97, 3803-3808.

[69] A.M. Ali, and G.A. Woolley, *Org. Biomol. Chem.* **2013**, 11, 5325-5331.

[70] L. Guerrero, O.S. Smart, C.J. Weston, D.C. Burns, G.A. Wolley, and R.K. Allemann, *Angew. Chem. Int. Ed*. **2005**, 44, 7778-7782.

[71] M. Berezovski, J.P. Calarco, S.N. Krylov, O.S. Smart, J.R. Kumita, A.S.I. Jaikaran, and G.A. Woolley, *Biochemistry* **2006**, 45, 6075-6084.

[72] A.A. Beharry, O. Sadovski, and G.A. Wooley, *Org. Biomol. Chem*. **2008**, 6, 4323-4332.

[73] S. Samanta, and G.A. Woolley, *Chem. Bio. Chem*. **2011**, 12, 1712-1723.

[74] C. Renner and L. Modorer, *Chem. Bio. Chem*. **2006**, 7, 868-878.

[75] M. Bose, D. Groff, J. Xie, E. Brustad, and P.G. Schultz, *J. Am. Chem. Soc*. **2006**, 128, 388-389.

[76] L. Lien, D.C.J. Jaikaran, Z. Zhang, and G.A. Woolley, *J. Am. Chem. Soc*. **1996**, 118, 12222-12223.

[77] F. Zhang, K.A. Timm, K.M. Arndt, and G.A. Woolley, *Angew. Chem. Int. Ed*. **2010**, 49, 3943-3946.

[78] A.A. Beharry, L. Wong, V. Tropepe, and G.A. Woolley, *Angew. Chem. Int. Ed*. **2011**, 50, 1325-1327.

[79] S. Samanta, A.A. Beharry, O. Sadovski, T.M. McCormick, A. Babalhavaeji, V. Tropepe, and A.G. Woolley, *J. Am. Chem. Soc*., **2013**, 135, 9777-9784.

[80] S. Samanta, T.M. McCormick, S.K. Schmidt, D.S. Seferos, and A.G. Woolley, *J. Am. Chem. Soc*., **2013**, 135, 9777-9784.

[81] S. Samanta, H.I. Qureshi, and G.A. Woolley, *Beilstein J. Org. Chem.*, **2012**, 8, 2184-2190.

[82] J.F. Morin, Y. Shirai, and J.M. Tour, *Org. Lett*., **2008**, 8, 1713-1716.

[83] T. Sasaki, and J.M Tour, *Org*. *Lett*., **2008**, 10, 897-900.

[84] B.C. Yu, Y. Shirai, and J.M. Tour, *Tetrahedron*, **2006**, 62, 10303-10310.

[85] R. Hagen, and T. Bieringer, *Adv*. *Mater*., **2001**, 13, 1805-1810.

[86] C. Renner, U. Kusebauch, M. Loweneck, A.G. Milbradt, and L. Modorer, *J*. *Pept*. *Res*., **2005**, 65, 4-14.

[87] F. Hamon, F. Djedaini-Pilard, F. Barbot, and C. Len, *Tetrahedron*, **2009**, 65, 10105-10123.

[88] G.K. Joshi, K.N. Blodgett, B.B. Muhoberac, M.A. Johnson, K.A. Smith, and R. Sardar, *Nano Lett*., **2014**, 14, 532-540.

[89] R.D. Mukhopadhyay, V.K. Praveen, and A. Ajayagosh, *Mater. Horiz*., **2014**, 1, 572-576.

[90] T. J. Kucharski, N. Ferralis, A.M. Kolpak, J.O. Zheng, D.G. Nocera, and J.C. Grossmat, *Nature Chemistry*, **2014**, 6, 441-447.

[91] Y. Kondo, A. Matsumoto, K. Fukuyasu, K. Nakajima, and Y. Takahashi, *Langmuir*, **2014**, 30, 4422-4426.

[92] Y. Li, J. Yang, L. Sun, W. Wang and W. Liu, *J. Materials Chemistry B*, **2014**, 2, 3868-3878.

[93] M.A. Cardona, and D.C. Magri, *Tetrahedron Letters*, **2014**, 55, 4559-4563.

[94] M.L. Zastrow, A.F.A. Peacock, J.A. Stuckey and V.L. Pecoraro, *Nature Chemistry* **2012**, 4, 118-123.

[95] E.C.H. Bromley, N.J. Kuwada, M.J. Zuckermann, R. Donadini, L. Samii, G.A. Blab, G.J. Gemmen, B.J. Lopez, P.M.G. Curmi, N.R. Forde, D.N. Woolfson, and H. Linke, *HFSP Journal* **2009**, 3, 204-212.

[96] E.C.H. Bromley, N.J. Kuwada, M.J. Zuckermann, R.B. Sessions, P.M.G. Curmi, N.R. Forde, D.N. Woolfson, and H. Linke, *Physical Review*, **2011**, 84, 031922.

Chapter 2

Synthesis of molecular components to generate conformational switching in coiled-coil structures

2.1 Background

As previously discussed in **Section 1.5**, it is possible to control the self-assembly of polypeptide sequences that encode two or more folded states in different ways.[1-4] However, here we focus on metal-binding and azobenzene-photoswitching as tools to reversibly control the different conformational states of *de novo* designed *α*-coiled-coil and fibrous systems. We aim to design synthetic amino acids which can act as ligands for metal-binding. Incorporating these unnatural amino acids into our peptide designs should allow a reasonable degree of control of both peptide folding and self-assembly leading to a generation of protein nanostructures that have a highly defined 3D architecture. On the other hand, azobenzene linkers have been proven to act as photoswitches to reversibly control protein functions by means of their *trans*-to-*cis* photoisomerization effect when attached to them.[5, 6] We aim to design an azobenzene moiety which after cross-linking two side chains in our peptide sequences will represent a potential alternative to metal-binding as method to control the self-assembly as well as for applications in protein motors.

2.1.1 Metal-binding

Metal-binding has been extensively used from the late 80's as a tool to control the self-assembly of relatively small peptides[7] and, more recently, to control the folding of proteins.[8] Binding a metal ion to a polypeptide sequence can either enhance or provide metalloproteins with different functionality and/or activity. Some of these are related to fundamental biological processes such as respiration, metabolism, nitrogen fixation, and signal transduction.[9] Moreover, new types of metalloprotein-based therapeutics, and medical biosensors or screening agents can be developed.[10]

To achieve metal-binding with polypeptides we need to have an amino acid within the sequence capable of offering a binding site to the metal ion. Ogawa and co-workers designed and synthesized a 30-residue polypeptide in which a histidine residue was placed in position 21 (H21). The peptide self-assembled in a two-stranded coiled-coil (**Figure 2.1.a**). Upon complexation with Ru(II), the metalloprotein serves as a scaffold to incorporate electron-transfer (ET) functionality (**Figure 2.1.b**).[11] With the same aim of incorporating ET functionality into synthetic metalloproteins, Ogawa's group synthesized a polypeptide sequence in which two Cys residues were placed at positions 16 and 19 (allocated within the hydrophobic core) capable to bind both Cd(II) and Cu(I) ions providing the polypeptide with different conformational changes, being a two-stranded coiled-coil when Cd(II) was bound (**Figure 2.1.c**) and a four-stranded coiled-coil with Cu(I) (**Figure 2.1.d**).[12]

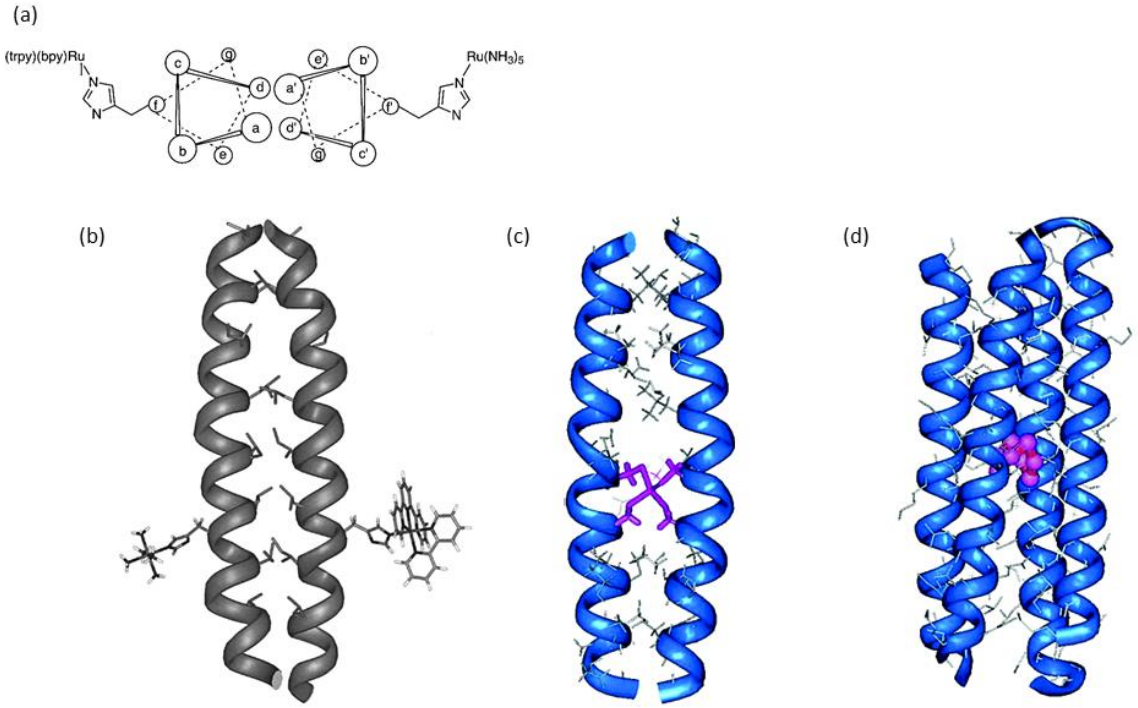

Figure 2.1: (a) Schematic representation of the third heptad repeat of the ET metalloheterodimer; (b) Computer-generated model of the heterodimer ET metalloprotein; (c) Energy-minimized computer model of the Cd-bridged C16C19 peptide dimer in which Cys residues located at positions 16 and 19 of each peptide chain bind the Cd center in a tetrahedral geometry; and (d) Computer-generated model of the tetrameric Cu^{I}-C16C19-GGY metalloprotein. (Pictures taken and described as in references 11 and 12)

Although there are a few examples where histidine or cysteine have been used for this aim, we are interested in the design and synthesis of polypeptide sequences bearing unnatural amino acids with metal-binding properties. Incorporation of either one or several of these unnatural amino acids within the sequences could make the peptides adopt a previously designed and desired conformation. As mentioned in **Section 1.5.1**, ligands including nitrogen atoms are ideal for coordinating amino acids with metal ions due to the chemical nature of nitrogen in coordination chemistry. **Section 1.5.1** showed a few examples where pyridine- and bipyridine-based derivatives were used to control the conformation of *α*-helical peptide sequences. Hence, pyridylalanine derivatives represent our target amino acids for this project.

Mikhail V. Tsurkan and Michael Y. Ogawa combined the principles of supramolecular coordination chemistry with those of *de novo* protein design to lead to a new class of metal-peptide nanoassemblies.[13-15] We looked into their work as the unnatural amino

acid for metal-binding that they were using was a 4-pyridylalanine derivative (Pal, **38**), the same type of ligand that we decided to use for incorporation in our designs. Tsurkan and Ogawa started these type of experiments by turning one of their previous sequences used for generating *α*-helical coiled-coils into a metal binding sequence. This consisted of a 30-residue polypeptide sequence (containing 4 heptads) in which the unnatural amino acid Pal was placed in position *f* of the third heptad, which is the most solvent exposed, and a Cys was placed in position *d* of the second heptad, that is in the hydrophobic face (**Figure 2.2.a**). Upon oxidation of the Cys residues, a disulphide covalent bond was internally formed to help the construction of dimeric coiled-coils and the Pal residue coordinated a Re(III) complex to form short metal-peptide oligomers (**Figure 2.2.a**).[13] Modification of the initial peptide sequence again, this time inserting two metal-binding Pal residues at positions *f* of the second and third heptads, favored the formation of a stable two-stranded *α*-helical coiled-coil structure which after complexation with a Pt(II) complex, discrete four-helix bundles were observed (**Figure 2.2.b**).[14] In an attempt to form a more conformationally flexible peptide than before and to compare the conformational properties of the assemblies, a new modification to the initial sequence was made. This time only one Pal unnatural amino acid was inserted at position *f* of the third-heptad (without that Cys residue which favored an internal covalent disulphide bond in the previous model). The result was the formation of nanospheres and fibrils upon coordination with a Pt(II) complex (**Figure 2.2.c**).[15] Further investigations on this last system showed that the oligomerization state was buffer-dependent and could afford either nanometer-scale globular materials or millimiter-scale rod-like materials depending on the conditions used, suggesting that different driving forces dictated the final structures, such as the structure of the peptide sequence and/or the ligand-ions interactions when the metal-peptide complex is formed.[16] This matches with our idea of investigating to what extent our ligands can determine the oligomerization state or assembly of the peptide sequences, and the way our peptide designs may have bigger influence than metal-binding on self-assembly.

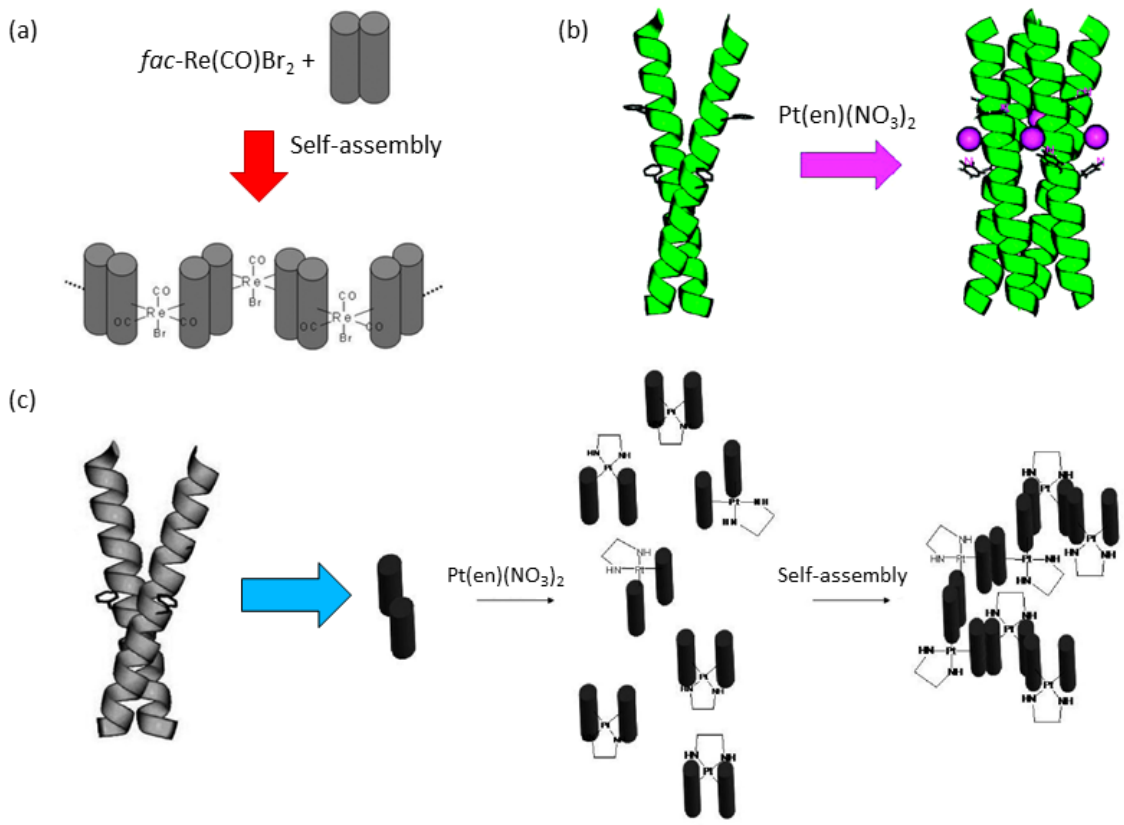

Figure 2.2: Schematic representation of (a) the short metal-peptide oligomers formed when coordinated to a Re(III) complex; (b) two-stranded α-helical coiled-coil of AQ-PAL14PAL21 coordinating to a Pt(II) complex to form discrete four-helix bundles; and (c) two-stranded α-helical coiled-coil of AQ-PAL14 that coordinates to a Pt(II) complex to form nanospheres and fibrils (adapted pictures from references 13, 15 and 16).

2.2 Synthesis of pyridylalanine (Pal) derivatives.

The initial target amino acids of our study were the 2- and 3-pyridylalanine derivatives and they were synthesized in the form of Fmoc- and Boc-protected pyridylalanine amino acids **1** to **4** (**Figure 2.3**).

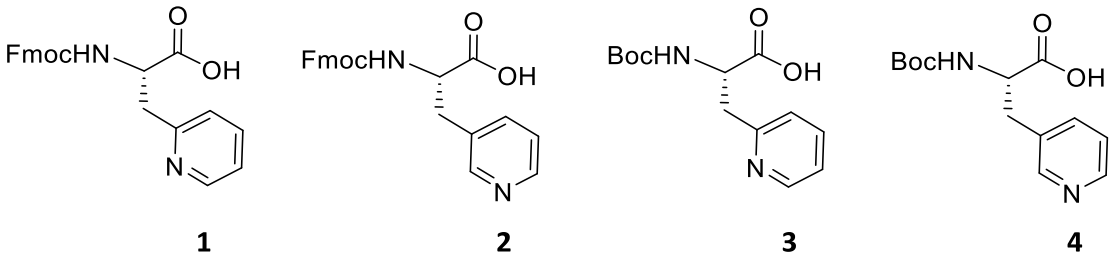

Figure 2.3: Structures of the initial target ligands pyridylalanine amino acids **1** to **4**.

The retrosynthetic analysis to make **1** and **2** (Fmoc-protected amino acids), and **3** and **4** (Boc-protected amino acids) are given in **Scheme 2.1** and **Scheme 2.2** respectively. In both synthetic routes the key intermediates were the orthogonally protected iodoalanine derivatives **7** and **10**. The iodoalanine compounds were reacted with different halopyridines via a palladium-catalysed Negishi cross-coupling reaction to access the corresponding orthogonally protected pyridylalanine amino acids.[17] The Negishi methodology had already been used in the Cobb group to synthesize a library of novel phenylalanine and tyrosine analogues.[18] Finally, removal of the protecting groups at the carboxylic groups afforded the target compounds **1** to **4**. Acid-labile protecting groups (-*t*Bu) were used in the case of the Fmoc-protected amino acids and benzyl-groups in the Boc-protected derivatives, which could be removed by H_2/Pd in a weak acidic media.

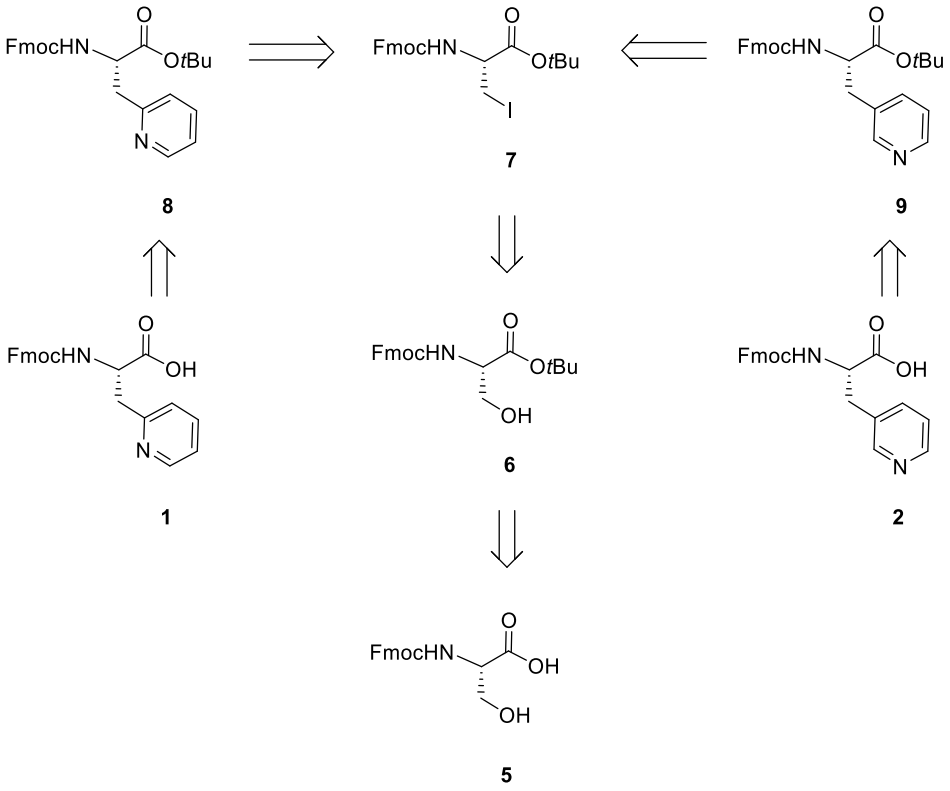

Scheme 2.1: Retrosynthetic pathway for the synthesis of the Fmoc-protected pyridylalanine amino acids **1** and **2**.

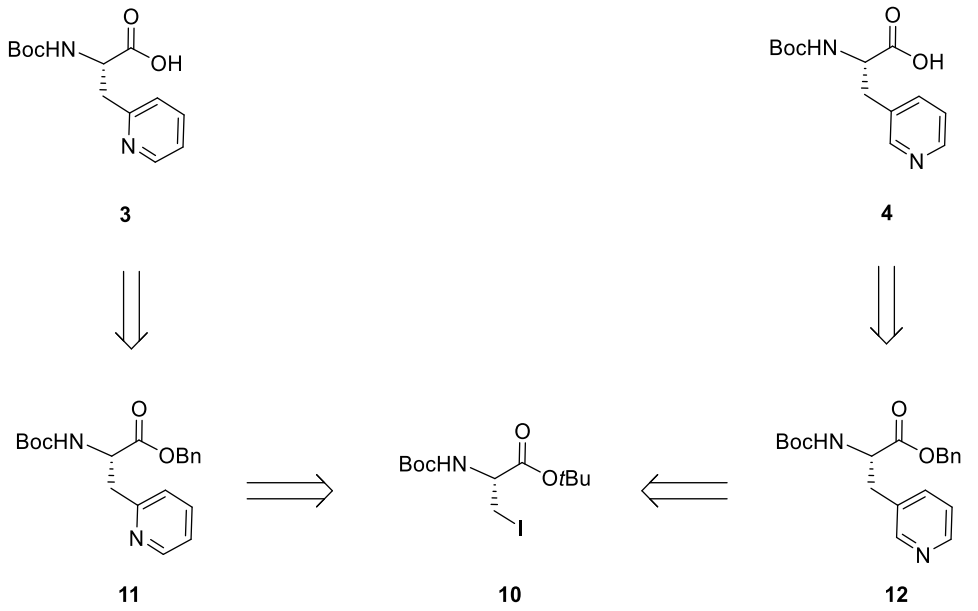

Scheme 2.2: Retrosynthetic pathway for the synthesis of the Boc-protected pyridylalanine amino acids **3** and **4**. The Boc-protected iodoalanine benzyl ester **10** is already available in our research group.

As outlined in **Scheme 2.1**, the first step in the synthesis of the unnatural Fmoc-protected pyridylalanine amino acid derivatives **1** and **2** consisted of a reaction to prepare an orthogonally-protected serine derivative, Fmoc-Ser-O*t*Bu (**6**). As the amino terminus was protected with an Fmoc group (required for SPPS), which could be cleaved under basic conditions, we used an acid-labile protecting group for the carboxylic terminus. The reagent *tert*-butyl trichloroacetimidate (TBTA) could be used as a protecting group for a carboxylic acid in the presence of an alcohol,[19] and this was used as shown in **Scheme 2.3**. Fmoc-Ser (**5**) was reacted with TBTA in EtOAc to give **6** in a 65% yield.

Although 65% is a good yield, different reaction conditions were used in an attempt to try to increase it, but also to minimise unwanted side products. When EtOAc was the solvent of reaction, we found higher yields when working at higher scales of reagents. Thus, the lowest yield (53%) was achieved when starting from 3.05 mmol of **5**, and the highest (94%) when starting from 15.27 mmol of **5**. A different solvent system for this same reaction consisting of a mixture of ethyl acetate and cyclohexane was found in the literature to afford a 90% yield.[20] However, we were not able to reproduce the

same results and only achieved a maximum yield of 46% under those conditions. A summary of the conditions used are given in **Table 2.1**.

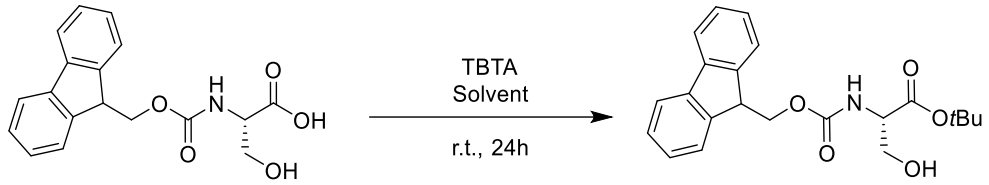

5 **6**

Scheme 2.3: Synthesis of Fmoc-Ser-O*t*Bu **6**. See **Table 2.1** for reagents and conditions.

Solvent system	eq. of amino acid (**5**)	eq. of TBTA	Yield (%) (**6**)
EtOAc	1.0	1.5	53 - 94
EtOAc/cycloexane	1.0	4.0	46

Table 2.1: Effect of solvent for the synthesis of compound **6**.

After purification by column chromatography of the crude of reaction, compound **6** was not the only product of this reaction but a by-product (**13**) was observed to form in all these set of reactions. The ^{1}H NMR signals of **6** (in black) and **13** (in red) showed great similarities (**Figure 2.4**): the shifts of both their Fmoc-aromatic and aliphatic protons remained the same and so did the corresponding signals of the NH protons next to the Fmoc-group. However, a few differences in the shifts of the proton signals were observed: this was the case of the signal of the α-H in **13** which got mixed with the signals of the CH_2-Fmoc protons whilst these two different group of signals could be seen individually in the ^{1}H NMR spectrum of **6**; the β-protons of the CH_2 group next to the OH in **6** that were seen as a singlet, split into two different double doublets in the spectrum of **13** and shifted to a higher field. This indicated that a chiral component had attached to the oxygen next to this CH_2 group, hence removing the alcoholic functionality. In addition, the new singlet observed in the spectrum of **13** at 1.06 ppm integrating at 9 protons – that matched the number of protons of a *tert*-butyl group – was indicative of the formation of a terminal *tert*-butyl ester group. As this *tert*-butyl group was linked to an aliphatic CH_2 and this is less electro-releasing than a C=O group, it showed a shift to a lower frequency than the existing *tert*-butyl group directly

attached to the carbonyl group. The mass analysis by ESI-MS of compound **13** confirmed the formation of the double *tert*-butyl protected amino ester: (ES^+) *m/z* 462.4 $[M+Na]^+$. ESI-MS analysis of compound **6** showed (ES^+) *m/z* 407.2 $[M+Na]^+$ as expected.

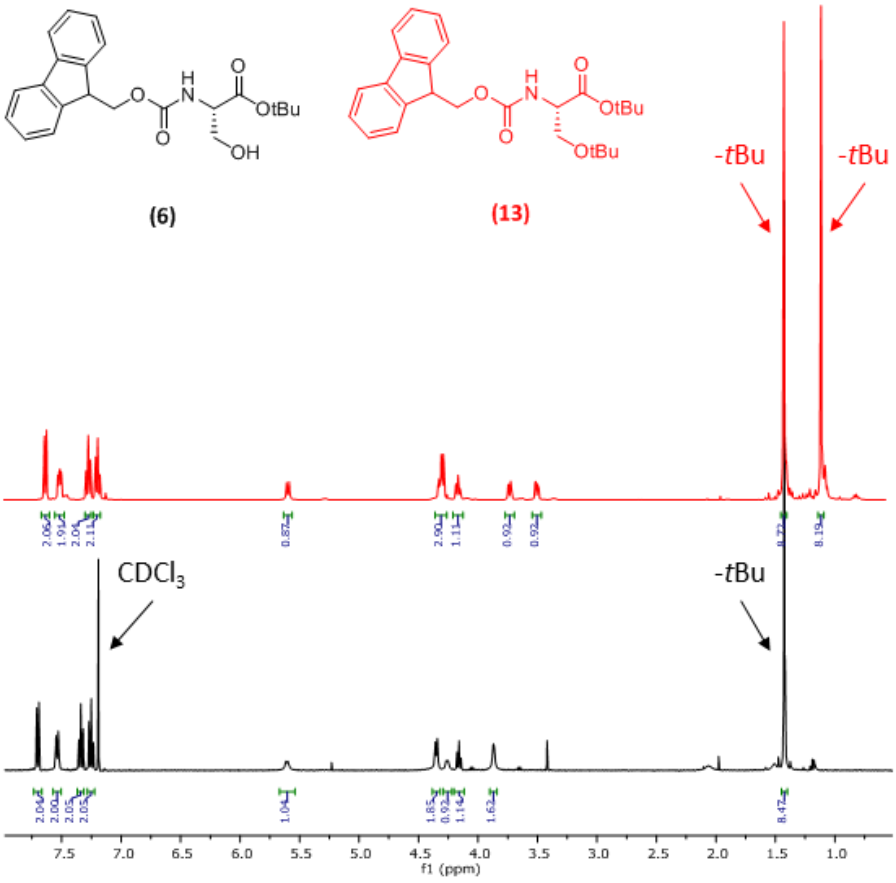

Figure 2.4: ^1H NMR spectra of compounds **6** (in black) and **13** (in red). The two peaks integrating near 9 protons and the slight shift in the other proton signals suggest the formation of a di-*tert*-butyl protected amino ester (**13**).

As previously reported in our research group, easily accessible N-protected iodoalanine derivatives as starting materials for the coupling reaction with haloaromatic reagents were needed for the synthesis of novel amino acids containing both homo- and heteroaromatic molecules of interest, such as pyridylalanines. The iodoalanine protected amino ester could be achieved by following the known methodology to form alkyl iodides.[21] The alkyl-iodide compound was prepared by a first reaction of triphenylphosphine and elemental iodine *in situ*. The alcohol **6** and the weak organic

base, imidazole, were then added. The overall result was the conversion of the alcohol into Fmoc-Ala(I)-O*t*Bu (**7**) (**Scheme 2.4**).

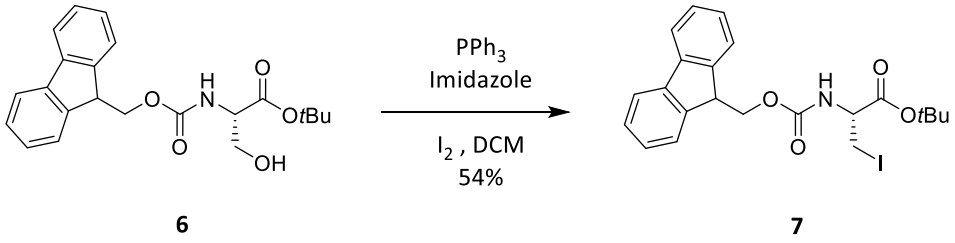

6 **7**

Scheme 2.4: Synthesis of Fmoc-Ala(I)-OtBu (**7**).

The β-OH group of **6** was substituted and an alkyl-iodide compound **7** was formed. ESI-MS analysis of the crude showed: (ES^+) *m/z* 516.2 $[M+Na]^+$, as expected for the formation of compound **7**. The ^1H NMR spectrum of the crude of reaction supported this information by showing a shift in the signal of the CH_2 protons next to the OH group, indicating the conversion of -CH_2-OH (at 3.87 ppm) into -CH_2-I (at 3.60 ppm) (**Figure 2.5**). Due to the lower electronegativity of iodine compared to that of the OH group, this CH_2 signal was shifted to a lower frequency. As seen in the previous stage where the yield of compound **6** was higher when working at higher scale, a set of reactions to make **7** were also prepared at different scales from 3.5 to 13.5 mmol, however, similar yields were obtained in all cases with the best recorded yield being 54%. All reactions were carried out at room temperature and, after 24 hours, the crude product was purified *via* column chromatography on SiO_2. Compound **7** was achieved as a sticky yellow oil that became a solid at low temperature. The reason for the low yield could be due to the formation of side products such as $Ph_3P=O$ species which were difficult to remove from the products during purification.

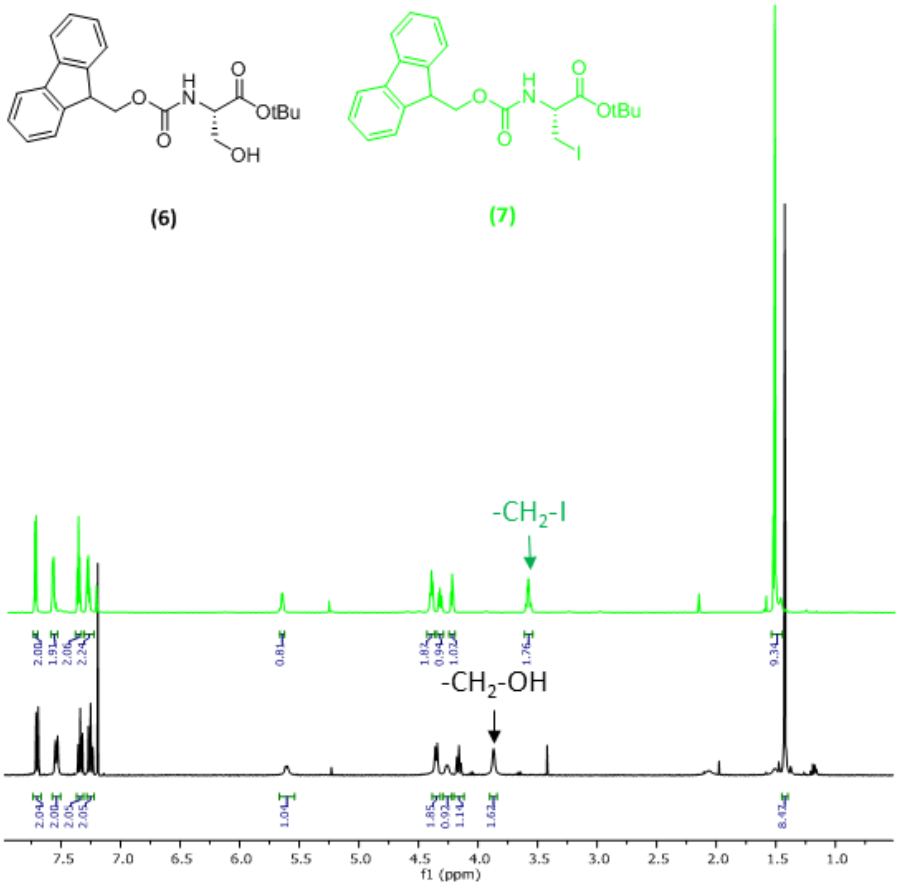

Figure 2.5: ^{1}H NMR spectra of compounds **6** (in black) and **7** (in green). The shift in the CH_2 signals corresponding to the groups where OH and I exchange indicate the formation of compound **7**.

The syntheses of both Fmoc- and Boc-protected pyridylalanine amino acids **1** to **4** (**Figure 2.4**) were achieved by following the general procedure of protecting groups cleavage in SPPS (by either acid or basic wash depending on the protecting groups) of the amino esters **8**, **9**, **11**, and **12** (see **Scheme 2.1** and **2.2**). We then carried out synthesis of the Fmoc- and Boc-protected amino esters **8, 9, 11** and **12** using palladium-catalysed cross-coupling reactions.

There exist several types of cross-coupling reactions. These involve reactions between two different reagents aided by a metal catalyst to make a new bond that "couples" them. Initially, the use of Ni, Cu or Fe as metal catalysts was generalized for this type of reactions, however, the palladium-catalysed cross-coupling of an organometallic compound with an organic electrophile appeared to be superior when stereo-, regio-, and chemoselectivities were required.[22] Many examples of the advantages of Pd over

Ni had been reported, e.g., superior stereospecificity.[23] Most palladium catalysed reactions are believed to follow a similar catalytic cycle. The concept of double metal catalysis and the favourable effects of additives on the Pd-catalysed cross-coupling reactions were first demonstrated by Negishi in 1978.[24] Negishi chemistry can make use of Zn, Al and Zr as the second metal catalyst, however, we used Zn due to the favourable results achieved in our group in previous work.[18] Moreover, there are several advantages to using supported catalysis in organic synthesis and these include reagent stability, suitability for automation, ease of work-up, recyclability, and lower Pd contamination in the final product.

Thus, amongst all the Pd-catalysed cross-coupling methodologies, we chose the Negishi reaction to synthesize the Fmoc- and Boc-protected amino esters **8**, **9**, **11** and **12** as this has been proven to lead to the direct formation of new C-C single bonds and it has shown extremely robust for couplings when using aryl iodide derivatives. In addition, Negishi chemistry is tolerant to a wide variety of functional groups such as aldehydes, esters, alcohols, amines and phosphonates,[25,26,27] and enables the integrity of the α-carbon to be unaffected by the coupling conditions so that the enantiomeric excess of the final product is only dependent on the initial starting material.

Zinc was acid washed since a proper activation of zinc dust was essential for good zinc insertion. Although two procedures had been reported for the activation of zinc dust, the methodology using a catalytic amount of elemental iodine was found to be favoured over the Knochel procedure.[28] . Anhydrous DMF was used as solvent due to the sensitivity of organozincs to both moisture and air. Therefore, the Negishi coupling must be performed in an oxygen and water free environment. Despite a wide range of Pd(0) and Pd(II) catalysts being used in this type of reaction, we used the commercially available $Pd(dba)_2$ since this had been previously tested in our group and had achieved good results. With respect to the ligand and co-ligands, their choice determined the mechanism by which the oxidative addition occurred.[29] The elimination step was accelerated by the use of bulky ligands.[30]

In order to investigate which co-ligand produced a more reactive specie of Pd(0), both tri-(*o*-tolyl)phosphine and Sphos were tried and compared in the coupling reactions of the Fmoc-protected amino esters, whilst Sphos and Xantphos were used and compared in the synthesis of Boc-protected amino esters. As coupling reagents, different halo-pyridines were used in order to investigate the effects of the leaving groups. For a given **R** group, the normal order of reactivity of halogens should be I > Br > Cl. Unfortunately, the least expensive, and hence most desirable, Cl-containing pyridine was the least reactive. The different halo-pyridines tested in our set of experiments were: 2-bromopyridine, 3-bromopyridine, 2-iodopyridine and 3-iodopyridine, and the results are discussed.

The general coupling conditions used for the Negishi methodology used to synthesize compounds **8**, **9**, **11**, and **12** are shown in **Scheme 2.5** and consisted of several steps: firstly, Zn dust (acid wash) (4.00 eq.) was placed in the reaction vessel under vacuum at 100 °C and for 30 min; secondly, I_2 in DMF under argon was added dropwise at 70 °C; after decreasing the temperature to 50 °C, the protected iodo-alanine reagent P^1HN-Ala(I)-OP^2 (1.00 eq.) together with the catalyst $Pd(dba)_2$ (0.03 eq.) and the corresponding co-ligand (0.09 eq.) dissolved in DMF were added under argon. The coupling reagent (1.00 eq.) was then added and the reaction mixture stirred for 6 h. The mixture was cooled down to room temperature and stirred overnight (for a minimum of 15 hours) before purification by column chromatography.

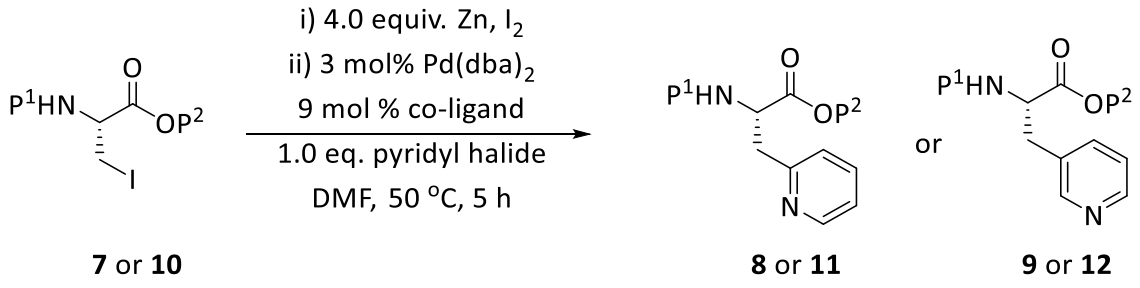

7 or **10** **8** or **11** **9** or **12**

Scheme 2.5: General conditions for the cross-coupling reactions between the protected iodoalanine amino esters **7** and **10** and the pyridyl halides using the Negishi methodology. Co-ligands can be: $P(o\text{-}tol)_3$, Sphos and Xantphos; pyridyl halides can be: 2- and 3-bromopyridine, and 2- and 3-iodopyridine; P^1 can be Fmoc- and Boc-; and P^2 can be *t*Bu and Bn respectively.

The proposed mechanism for the Negishi cross-coupling reaction of this set of experiments is shown in **Figure 2.6**. The first step consists of an oxidative addition of the Pd(0) catalyst. The addition of the halopyridine to the Pd atom increases the number of ligands changing its oxidation state to Pd(II). The second step is the transmetallation step. An alkylzinc specie, formed by the insertion of the activated Zn into the side chain and the iodine atom of the protected amino ester, proceeds to exchange the ligands with the palladium centre. Finally, the last step of the reaction consists of an eliminative reduction. This proceeds with the elimination of the cross-coupled product and the regeneration of the Pd(0) catalyst.

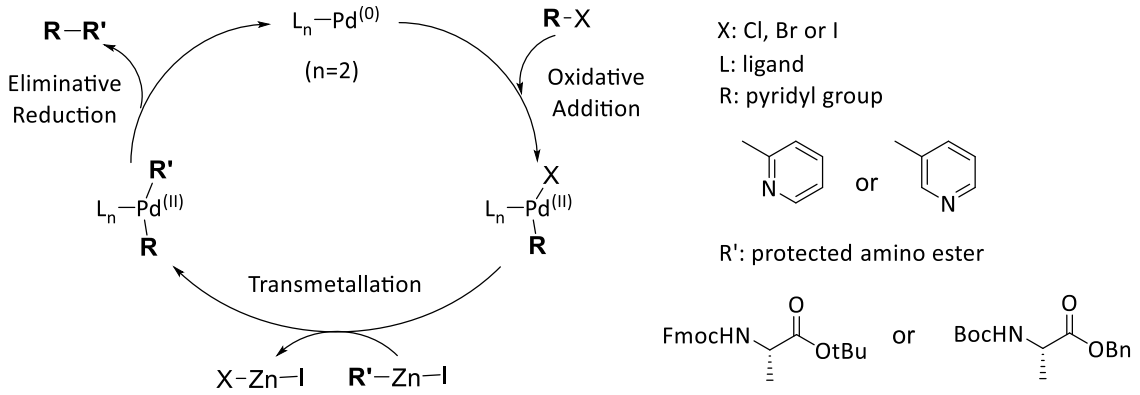

Figure 2.6: Mechanism for the Negishi cross-coupling reaction.

Scheme 2.6 shows the general scheme for the Negishi cross-coupling reactions to synthesize the Fmoc/*tert*-butyl protected amino esters **8** and **9**.

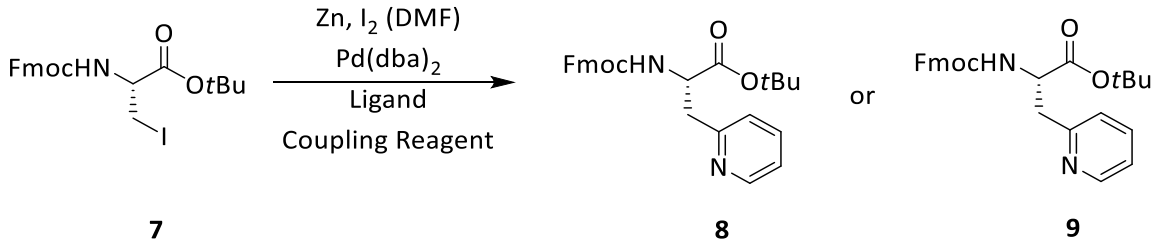

7 **8** **9**

Scheme 2.6: General scheme for the Negishi cross-coupling reactions to synthesize the new ***Fmoc***-protected pyridylalanine amino esters **8** and **9.** Compound **8** is afforded due to using 2-halopyridine derivatives as coupling reagents, and **9** uses 3-halopyridine derivatives (**Table 2.2**).

Table 2.2 shows the results for the set of reactions prepared to synthesize compounds **8** and **9**. The reaction did not work as desired when using P(*o*-tol)$_3$ as a ligand with either 2- or 3-bromopyridine as coupling reagents. However, it worked well with Sphos acting as ligand and 2- or 3-bromopyridine as coupling reagents, affording yields of 60% and 55% respectively. We believed that despite Sphos being larger ligand, its two cyclohexyl rings allowed flexibility, hence best addition to the intermediate and also elimination from the final product. As the normal order of reactivity of halogens is I > Br, we attempted to optimize the reaction yield by using 2- and 3-iodopyridine as coupling reagents. Nonetheless, lower yields of **8** and **9** were obtained, probably due to the formation of side products favoured by the higher reactivity of I.

Entry	Ligand	Coupling reagent	Yield (%)
			8 / **9**
2a / **2b**	P(*o*-tol)$_3$	2-bromopyridine / 3-bromopyridine	- -
2c / **2d**	Sphos	2-bromopyridine / 3-bromopyridine	60 55
2e / **2f**	Sphos	2-iodopyridine / 3-iodopyiridine	40 34

Table 2.2: Different reagents, such as ligand and coupling reagents, utilized to optimize the yield in the synthesis of **8** and **9**.

Figure 2.7 shows the ^{1}H NMR spectra of compounds **8** and **9** compared to the starting reagent **7** and shows evidence for the successful formation of the Fmoc-pyridylalanine *tert*-butyl ester compounds. The proton shifts of both the NH and *t*Bu signals in the ^{1}H NMR of **8** and **9** indicated the formation of new species starting from **7**, which were probably caused by internal hydrogen bonds. The shift of the CH_2 protons signal attached to the iodine in **7** moved when substituted by 2-pyridyl and 3-pyridyl motifs. Due to the distancing of the electronegative atom from the CH_2 group, the frequency decreased from I>2-pyridyl>3-pyridyl and the proton signals shifted upfield. The protons in the region of 4.75 to 4.00 ppm contained the α-proton together with the aliphatic protons of the Fmoc group.

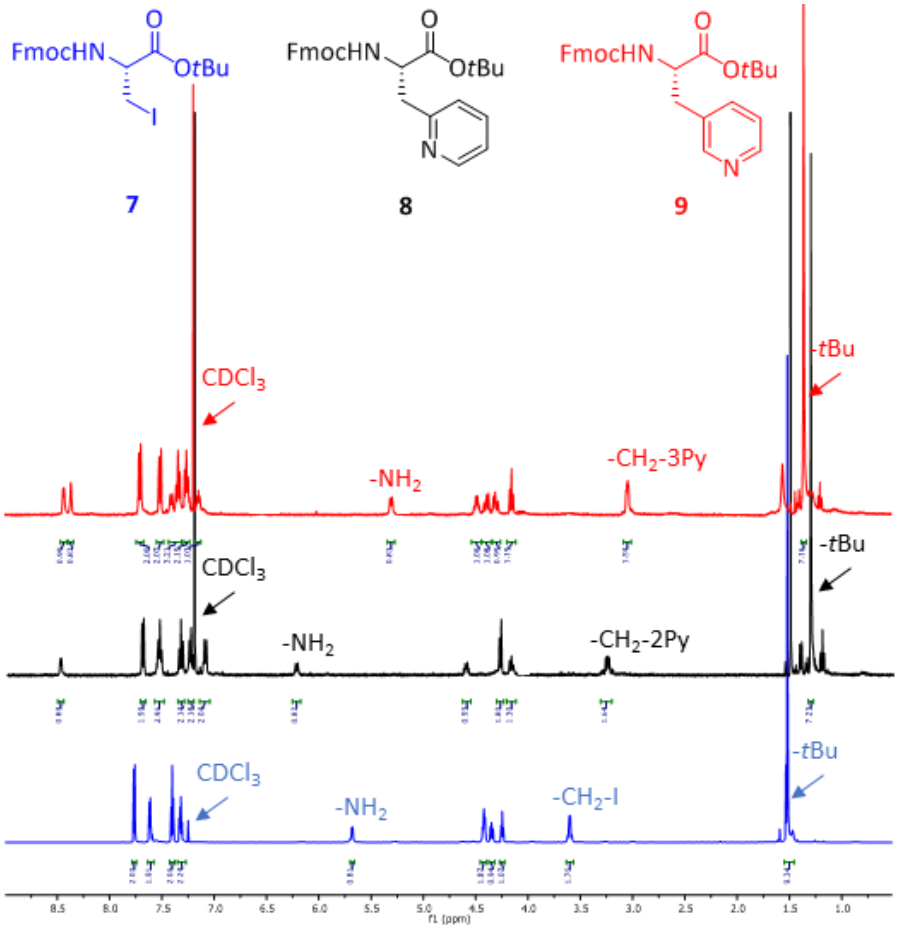

Figure 2.7: ^{1}H NMR spectra of **7** (in blue) compared to **8** (in black) and **9** (in red).

An expansion of the aromatic region (**Figure 2.8**) provided enough detail to confirm the formation of both **8** and **9** by ^{1}H NMR taking into account that we started from compound **7** with certainty. The aromatic protons of the Fmoc group are enclosed into blue squares and each of the pyridyl protons are assigned on the spectrum. Single mass analysis (TOF ESI-MS) supported the information provided by NMR that confirmed the formation of compounds **8** and **9**: for compound **8** (ES^{+}) *m/z* 445.3 $[M+H]^{+}$, 467.7 $[M+Na]^{+}$, 468.2 $[M+H+Na]^{+}$; for compound **9** (ES^{+}) *m/z* 445.4 $[M+H]^{+}$.

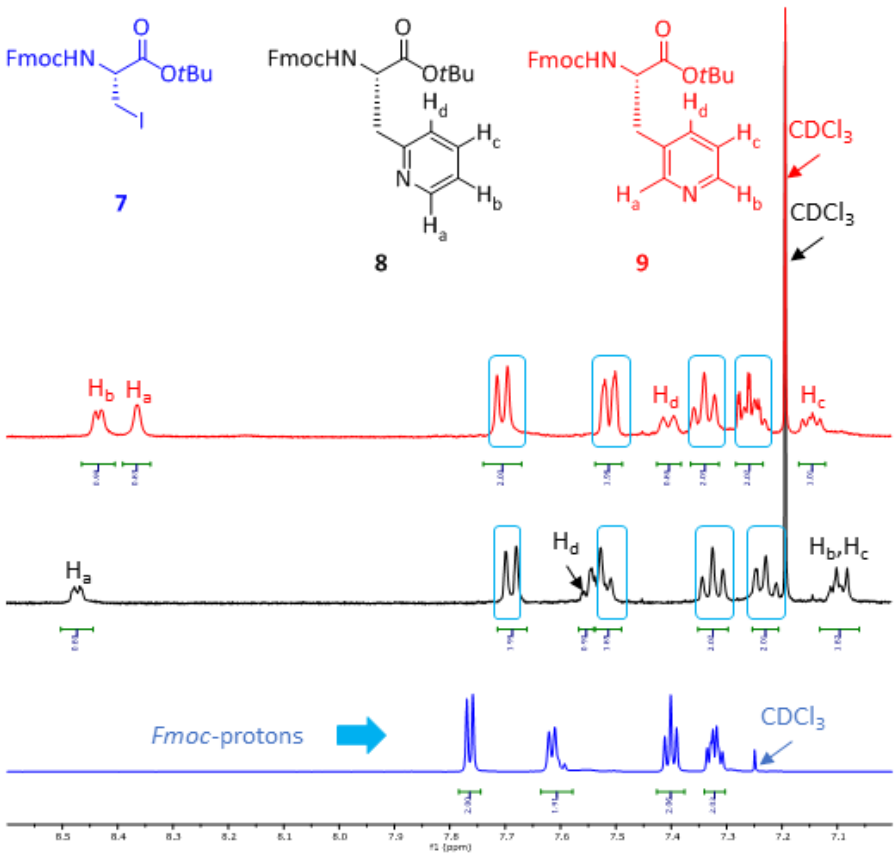

Figure 2.8: ^{1}H NMR spectra of the aromatic region of **7** (in blue) compared to **8** (in black) and **9** (in red).

Due to the fact that the achieved yields of **8** and **9** (these are the Fmoc-protected pyridylalanine amino esters) ranged from 34% to 60% and we aimed to obtain higher yields, we decided to follow a different strategy. Previously synthesized in our research group, the Boc-protected iodoalanine derivative **10** was available to be used. Thus, we decided to synthesize the Boc-protected pyridylalanine amino esters **11** and **12** to check if an increase in the yield was possible. **Scheme 2.7** shows the general scheme for the Negishi cross-coupling reactions to synthesize **11** and **12**.

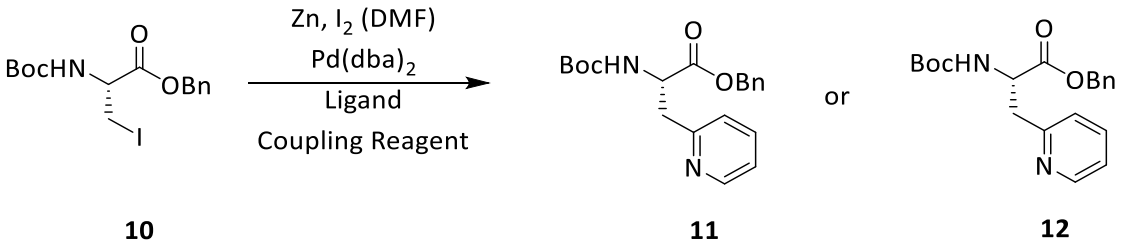

10 **11** **12**

Scheme 2.7: General scheme for the Negishi cross-coupling reactions to synthesize the new Boc-protected pyridylalanine amino esters **11** and **12.** Compound **11** is afforded due to using 2-halopyridine derivatives as coupling reagents, and **12** uses 3-halopyridine derivatives (**Table 2.3**).

Table 2.3 shows the results for the synthesis of **11** and **12**. As P(*o*-tol)$_3$ did not work as desired when synthesising the Fmoc-pyridylalanine derivatives **8** and **9**, we decided to use Sphos as ligand for this set of reactions. When using 2- and 3-bromopyridine as coupling reagents we produced **11** and **12** in 48% and 30% yields respectively which were lower yields than the obtained in the synthesis of the Fmoc-analogues. However, it provided higher yields than for the Fmoc-analogues when 2- and 3-iodopyridine were used as coupling reagents, producing compounds **11** and **12** in 51% and 45% yields respectively. As Xantphos is a more hindered ligand, we thought that using it could provide a higher selectivity in the synthesis of the final product. Hence, a final attempt to optimize the yields of **11** and **12** was made using the ligand Xantphos instead of Sphos. This was first used with 2-bromopyridine and a very low yield of **11** was achieved (9%). We then decided to try with 3-iodopyridine since the iodo-derivative should be more reactive than bromo-derivative for these type of compounds. However, a low yield of **12** was achieved (13%). Xantphos may turn into a highly hindered ligand which does not favour the formation of the pyridylalanine derivative but a different side product. We did not investigate this effect in detail or attempted to optimize the synthesis when using Xantphos since Sphos provided better yields in this set of experiments.

Entry	Ligand	Coupling reagent	Yield (%)
			11 / **12**
3a / **3b**	Sphos	2-bromopyridine / 3-bromopyridine	48 / 30
3c / **3d**	Sphos	2-iodopyridine / 3-iodopyiridine	51 / 45
3e / **3f**	Xantphos	2-bromopyridine / 3-iodopyiridine	9 / 13

Table 2.3: Different reagents (ligand and coupling reagents) used to optimize the yield of **11** and **12**.

Figure 2.9 shows the ^{1}H NMR spectra of compounds **11** and **12** compared to the starting reagent **10** and shows evidences for the successful formation of the Boc-pyridylalanine *O*-benzyl ester compounds. The proton signals of the *t*Bu groups in the ^{1}H NMR of **11** and **12** were at the same shift as **10**. The shift of the CH_2 protons signal next to the iodine in **10**, moved when substituted by 2-pyridyl and 3-pyridyl motifs as seen for the Fmoc-analogues. Due to the distancing of the electronegative atom from the CH_2 group, the frequency decreased from I>2-pyridyl>3-pyridyl and the proton signals shifted upfield. The protons in the region of 5.25 to 4.50 ppm contained the α-proton together with the protons of the CH_2 of the benzyl group of compound **12**.

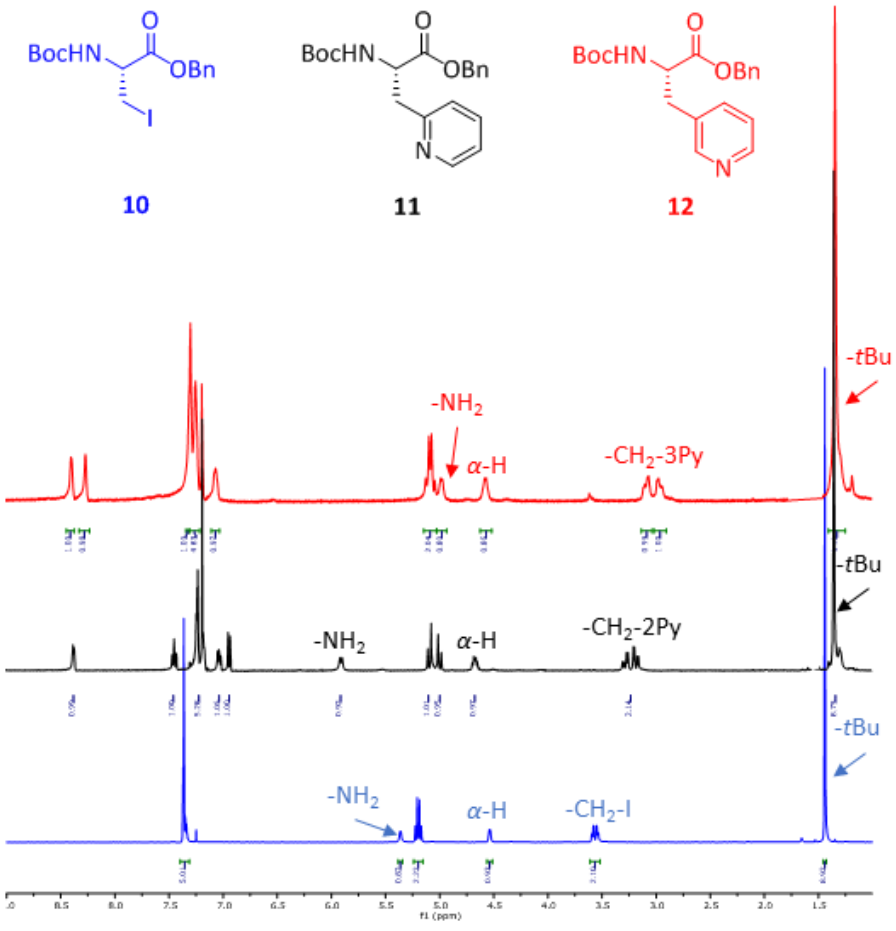

Figure 2.9: ^{1}H NMR spectra of **10** (in blue) compared to **11** (in black) and **12** (in red).

An expansion of the aromatic region (**Figure 2.10**) provided enough detail to confirm the formation of compounds **11** and **12** by ^{1}H NMR taking into account that we started from compound **10** with certainty. The aromatic protons of the benzyl group were

together under the same signal, and each of the pyridyl protons are assigned in the spectrum. Single mass analysis (TOF ESI-MS) of compounds **11** and **12** supported the information provided by NMR: for compound **11** (ES^+) *m/z* 380.3 $[M+H+Na]^+$; for compound **12** (ES^+) *m/z* 357.3 $[M+H]^+$.

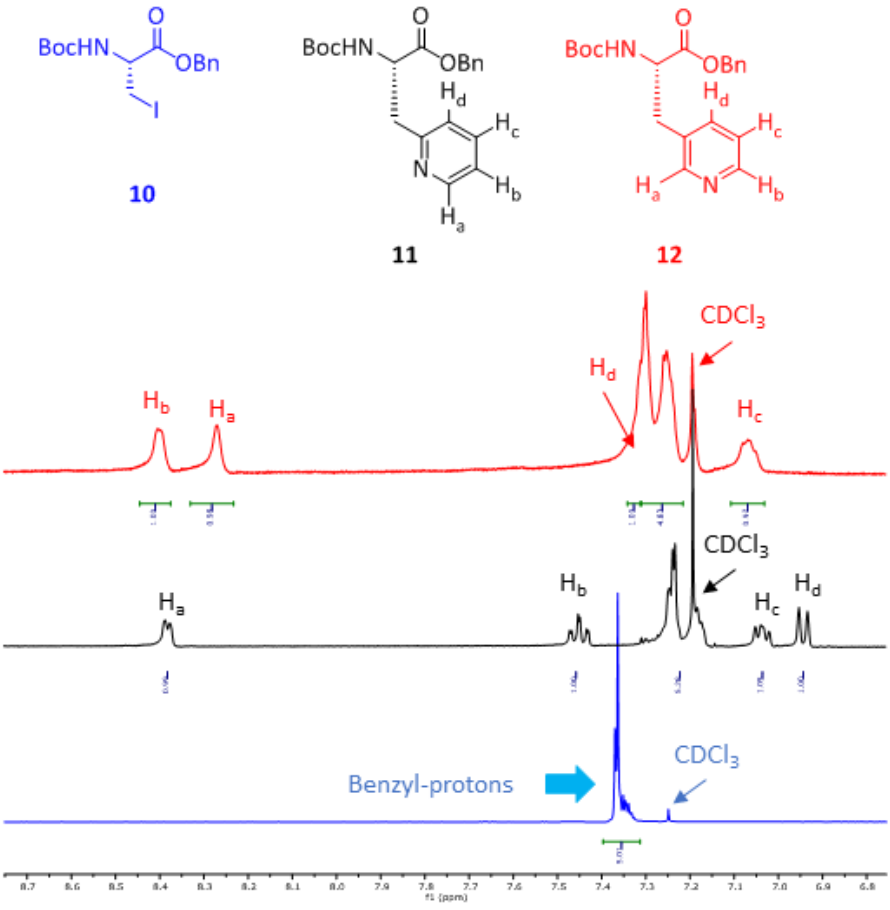

Figure 2.10: ^1H NMR spectra of the aromatic region of **10** (in blue) compared to **11** (in black) and **12** (in red).

2.3 Photoswitching as a method to generate conformational changes in peptide assemblies

As alternative to metal-binding as a method to generate conformational switching in our peptide designs, we decided to make use of light as energy source to induce conformational changes. In particular, we focused on azobenzenes since these molecules can be photoswitched between their *trans* and *cis* isomers, and this switching can be amplified up by attaching the azobenzenes onto the polypeptide

sequences on the verge of triggering. This may as well provide a potential power source for protein motors.

2.3.1 Synthesis of an azobenzene derivative to photo-control *α*-helical coiled-coil structures

The initial target compound was 3,3'-bis(sulfonato)-4,4'-bis(chloroacetamido)-azobenzene (**BSBCA, 19**), previously designed and synthesized in Woolley's lab.[31] **Scheme 2.8** shows the procedure for the synthesis of **19**.

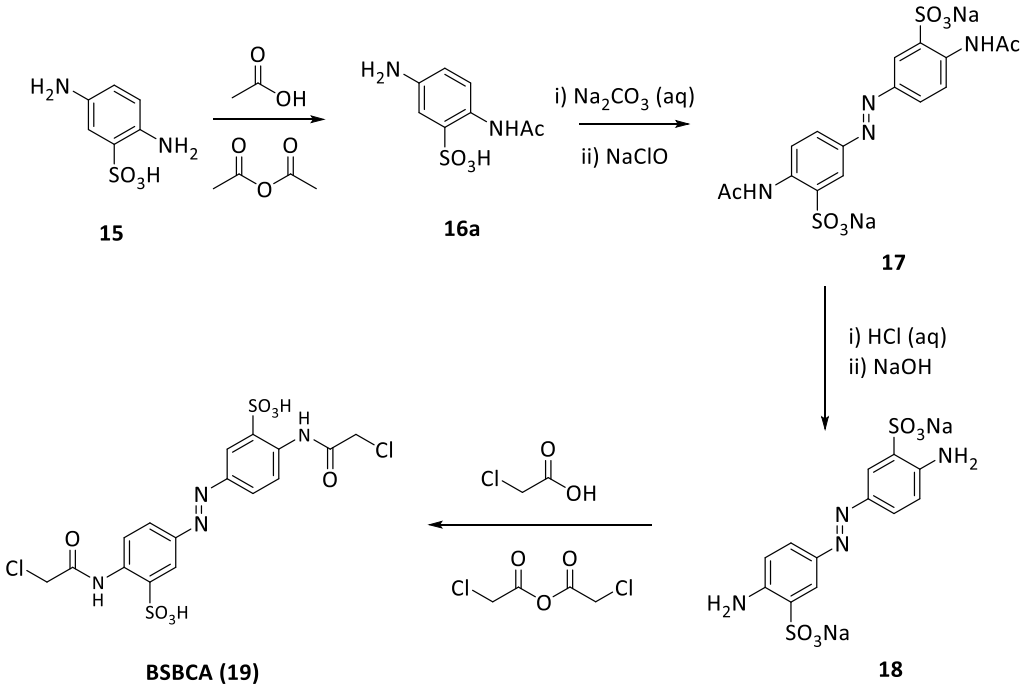

Scheme 2.8: Published synthesis of **BSBCA**.[31]

Following this procedure, the first step in the synthesis to afford **19** consisted of a selective protection step in which the amine group in position *ortho* to the sulfonic group from compound **15** reacted selectively with acetic anhydride in acetic glacial acid under reflux conditions. The resulting compound **16a** should be a mono-acetylated amino benzene sulfonic acid, however, we never achieved this step as a clean reaction. ^{1}H NMR and ESI-MS analysis of our crude of reaction showed a mixture

of products that indicated difficulties for selective protection of the amine group *ortho* to the sulfonic group. **Figure 2.11** shows the negative-ion mode electrospray ESI-MS spectrum of the crude of reaction. The detection of three different low-molecular-weight molecules is discussed and assigned as follows: compound **15** which is the starting material shows an $(ES)^-$ *m/z* 187.4 [M]; compound **16a** shows an $(ES)^-$ *m/z* 229.4 [M]; finally, compound **16b** shows an $(ES)^-$ *m/z* 271.5 [M].

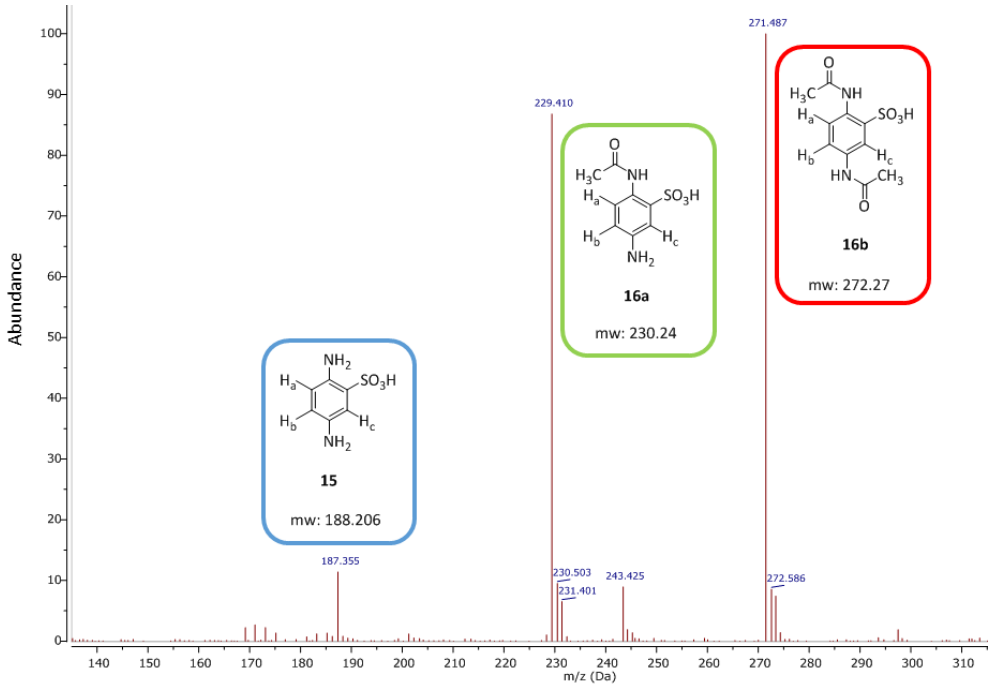

Figure 2.11: ESI-MS (negative-ion mode) of the crude in the first step for the synthesis of compound **19**.

NMR analysis of the crude product (**Figures 2.12** and **2.13**) was consistent with the ESI-MS analysis and confirmed a mixture of compounds: **15**, **16a** and **16b**. The ^{1}H NMR spectrum of the crude also showed a peak at 1.91 ppm from unreacted acetic acid, and a peak at 2.51 ppm from the solvent (DMSO-d_6). **Scheme 2.9** shows an overall view of the molecules involved in this first step of reaction: **15** is the starting reagent, **16b** is a by-product, and **16a** is the major component of this crude product (as confirmed by NMR, **Figure 2.13**) and the product of interest to carry on with the synthesis of **19**.

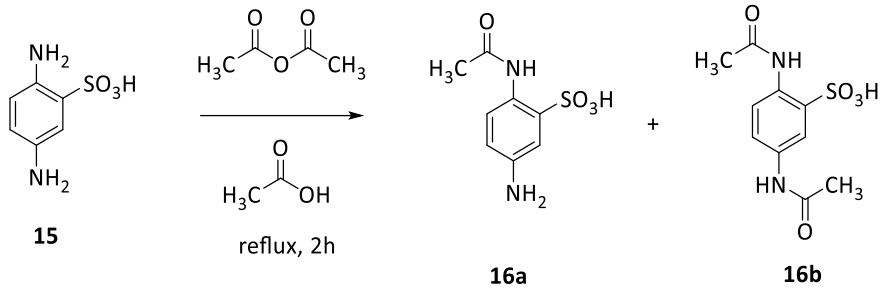

Scheme 2.9: Reaction scheme after the first step in the synthesis of **BSBCA** (**19**).

The ^{1}H NMR spectra shown in **Figure 2.12** shows the shifts for the NH and CH_3 protons of the products in the crude of reaction: **16a** showed a singlet at 10.34 ppm corresponding to the proton of the NH in the acetyl group, and a singlet at 2.09 ppm from the protons of the CH_3 group; **16b** showed two different singlets at 10.23 and 9.93 ppm from their two NH group protons, and two different singlets at 2.03 and 2.01 ppm from the CH_3 protons on the acetyl groups. The nearer these protons were to the sulfonic group (-SO_3H), the more shifted to low field (or high frequency) they appeared in the spectrum.

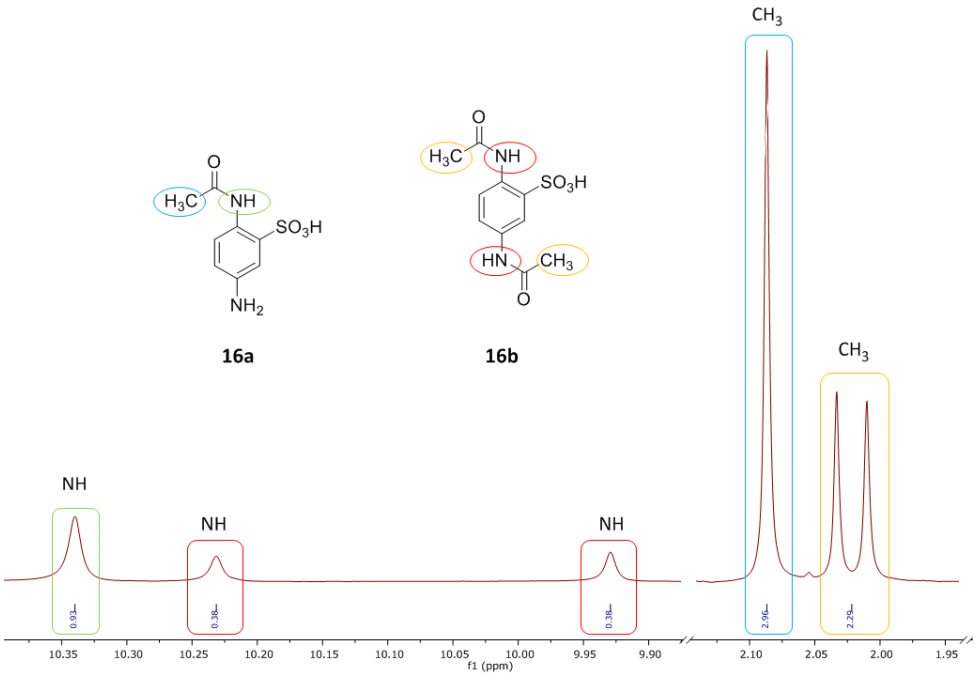

Figure 2.12: Assignment of the NH and CH_3 protons for compounds **16a** and **16b** by ^{1}H NMR.

Figure 2.13 shows an expansion of the ^{1}H NMR spectrum of the aromatic region and the assignment for each of the proton shifts: **16a** showed a doublet at 8.40 ppm (H_c), a doublet at 7.72 ppm (H_a) and a doublet of doublets at 7.33 ppm (H_b); **16b** was identified by a doublet at 8.17 ppm (H_c), a doublet at 7.86 ppm (H_a) and a doublet of doublets at 7.59 ppm (H_b). Finally, **15** (starting material) was identified by a doublet at 7.56 ppm (H_c), a doublet of doublets at 7.15 ppm (H_b) and a doublet at 7.06 ppm (H_a).

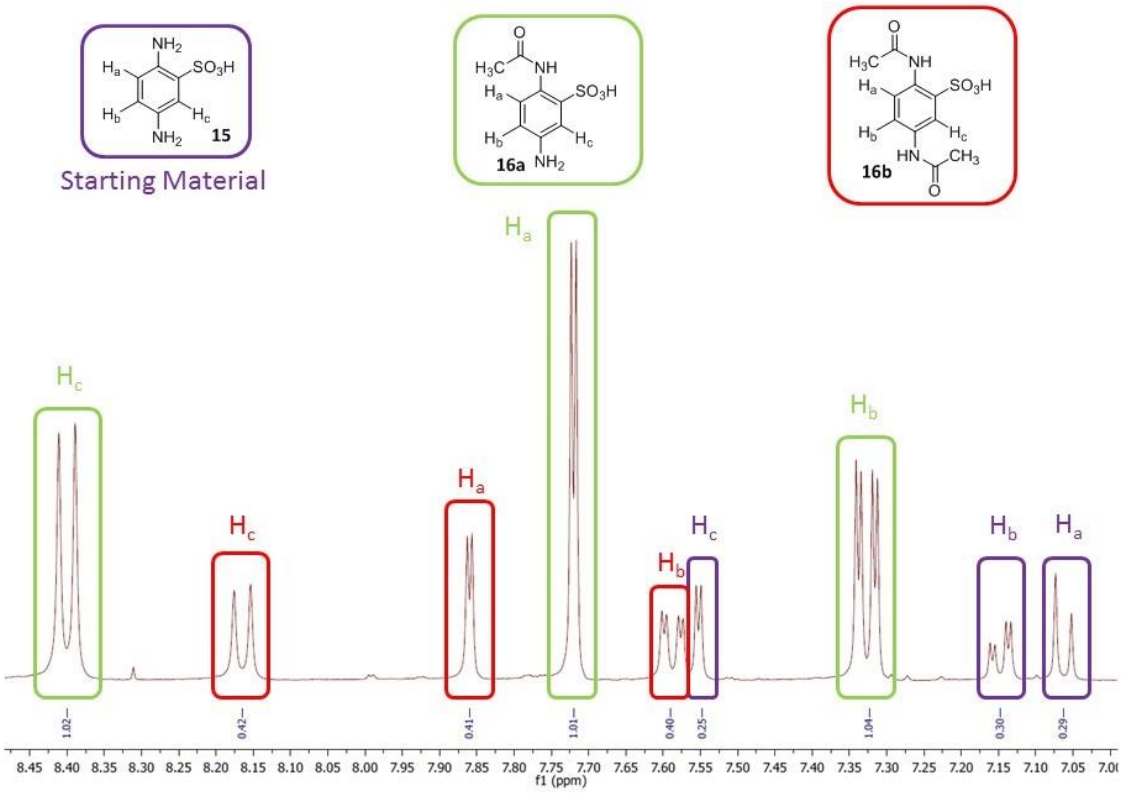

Figure 2.13: ^{1}H NMR spectrum of the crude of reaction from the aromatic region. All compounds from the crude of reaction were successfully assigned as showed. The ratio of compounds was assigned by NMR as follows: **15**/**16a**/**16b** (1:3:1), being **16a** the major product in a 59% as maximum yield.

Although we were able to identify all compounds from this first step, we never succeeded in synthesizing compound **17** by following the next step in the procedure. Initially, we started the second step of the synthesis from the crude mixture containing compounds **15**, **16a** and **16b** since we thought that an attempt to separate these products would mean a big loss of starting material. However, we also thought that having this mixture of compounds as starting material could affect the reaction conditions by not achieving the right pH conditions for compound **16a** to react as

expected, hence, not favoring the formation of **17**. Since this seemed to be the case, we decided to separate compounds **15**, **16a** and **16b** from the crude mixture of step 1 before starting step 2 by using RP-HPLC semi-preparative C18.

Figure 2.14 shows the chromatogram of this separation together with the ESI-MS analysis (positive-ion mode) of fractions 2 and 3, corresponding to compounds **16a** and **16b** respectively. Fraction 1 contained compound **15**: (ES) *m/z* 187.36 $[M]^+$; **16b** was found within fraction 3: (ES) *m/z* 270.9 $[M]^+$; finally, fraction 2 contained compound **16a** (ES) *m/z* 230.8 $[M]^+$; together with some residual **16b** (*m/z* 272.9 $[M+H]^+$).

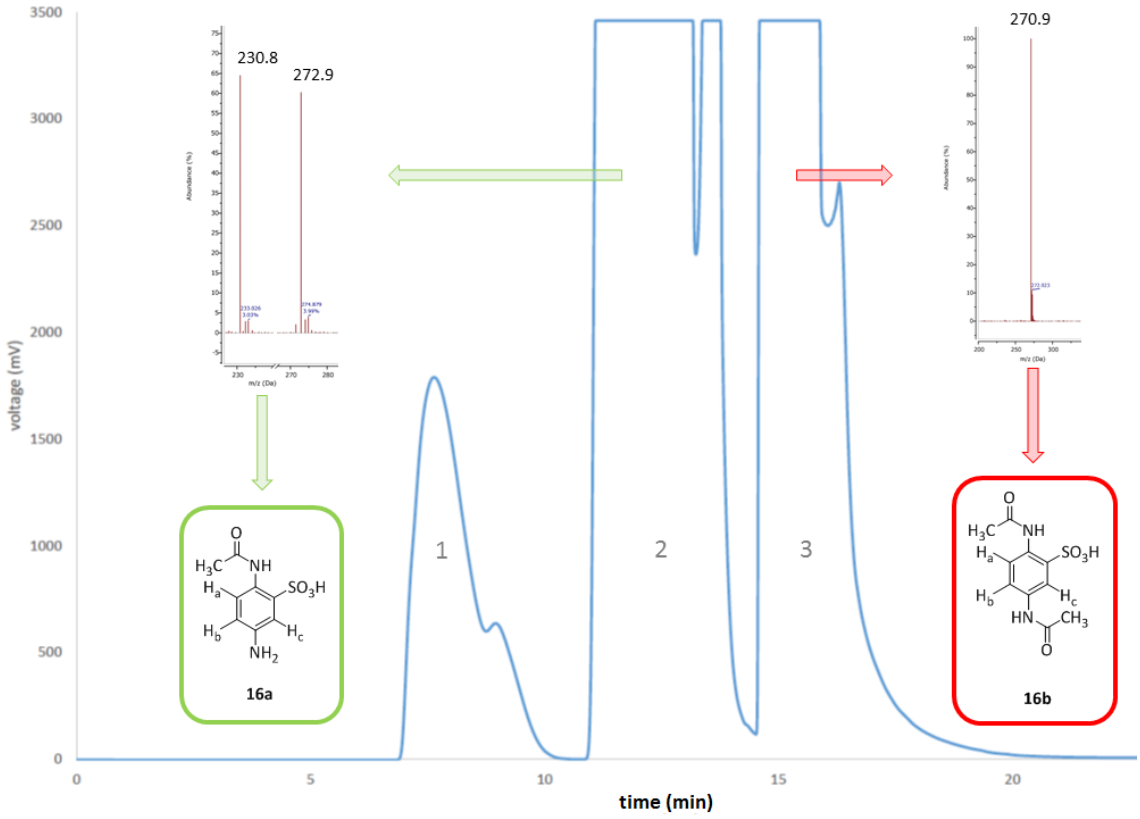

Figure 2.14: HPLC chromatogram of the mixture from step 1 of the procedure to make **19**. Fractions 2 and 3 show their ESI-MS spectra to identify compounds **16a** and **16b**.

Separate ^{1}H NMR analysis of fractions 2 and 3 collected from the RP-HPLC separation helped to confirm what observed by ESI-MS (**Figures 2.15** and **2.16**). However, the residual traces of **16b** observed in fraction 2 by ESI-MS were not detected by ^{1}H NMR as seen in the spectrum in **Figure 2.15**, with **16a** being the only compound detected. Compound **16b** was perfectly identified as shown in **Figure 2.16**.

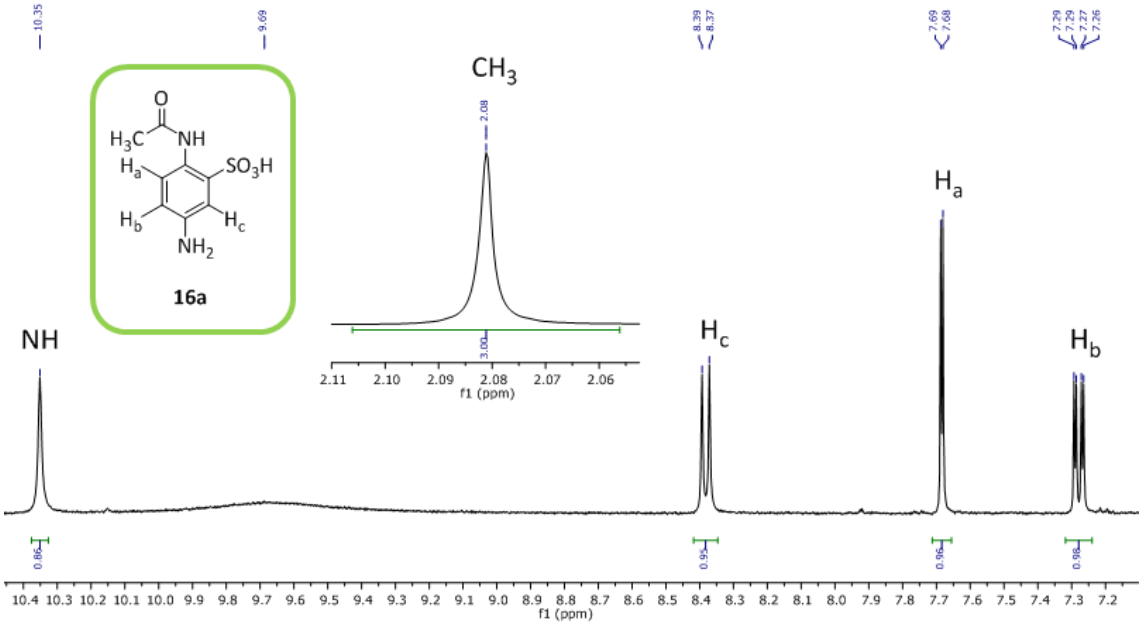

Figure 2.15: ^{1}H NMR spectrum in DMSO-d_6 of fraction 2 after HPLC separation of the crude of reaction from step 1 to synthesize **19**. Compound **16a** is identified and the proton signals assigned as shown: 2.06 ppm (CH_3), 7.27 ppm (CH^{b}_{Ar}), 7.69 ppm (CH^{a}_{Ar}), 8.38 ppm (CH^{c}_{Ar}), and 10.35 ppm (NH). **Chapter 7** provides ^{13}C NMR data and supports this information.

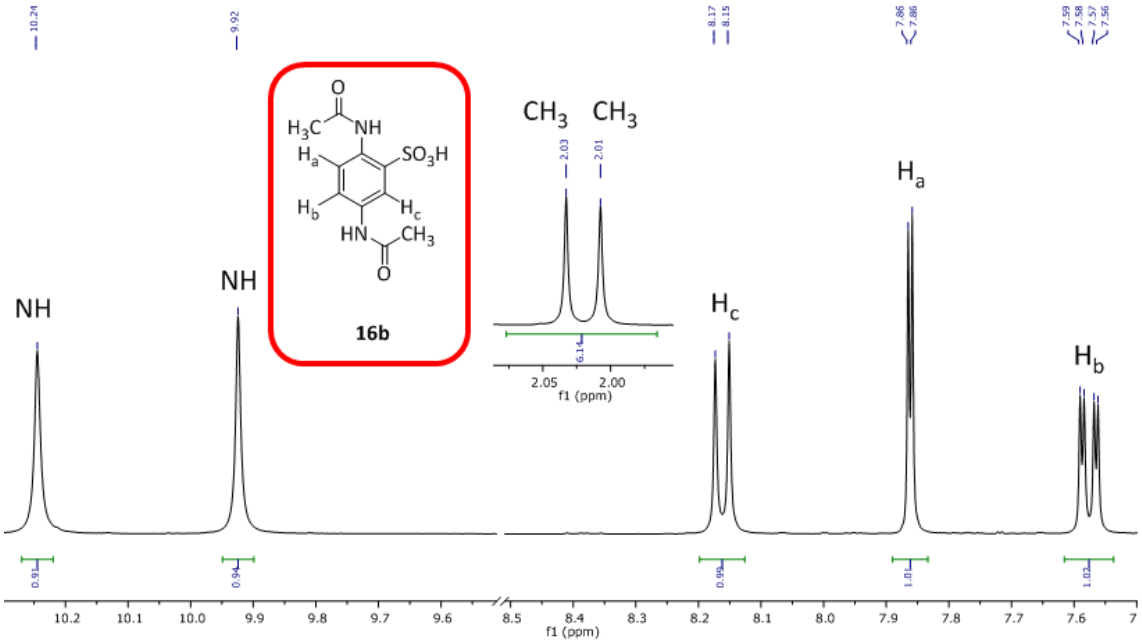

Figure 2.16: ^{1}H NMR spectrum in DMSO-d_6 of fraction 2 after HPLC separation of the crude of reaction from step 1 to synthesize **19**. Compound **16b** is identified and the proton signals assigned as shown: 2.01 ppm (CH_3), 2.03 ppm (CH_3), 7.57 ppm (CH^{b}_{Ar}), 7.86 ppm (CH^{a}_{Ar}), 8.16 ppm (CH^{c}_{Ar}), 9.92 ppm (NH), and 10.35 ppm (NH). **Chapter 7** provides ^{13}C NMR data and supports this information.

Using compound **16a** as showed in **Figure 2.15** to continue with the next step of the synthesis of **19** never produced **17**. Thus, we decided to find an alternative and synthesize an azobenzene derivative similar to compound **19**. Since we thought that we could be having issues in the synthesis of **17** due to the reactivity of the sulfonic groups which was not completely understood, we decided to synthesize an azobenzene analogue in which the sulfonic groups were not part of the molecule. The sulfonic groups provide higher solubility to the peptide sequences when they are in solution and that was the reason to try to make **19** in first instance. However, our final cross-linked peptides were found to be very soluble in aqueous conditions and we therefore did not find the loss of the water soluble groups to be an obstacle.

Our target compound then became 4,4'-dichloroacetamido-azobenzene (**24**). Fortunately, we saw in the literature that an analogue of this compound had already been made.[32] And, although this was taken into account, some modifications were applied to the original procedure to achieve higher yields. **Scheme 2.10** shows the synthetic route to produce **24**.

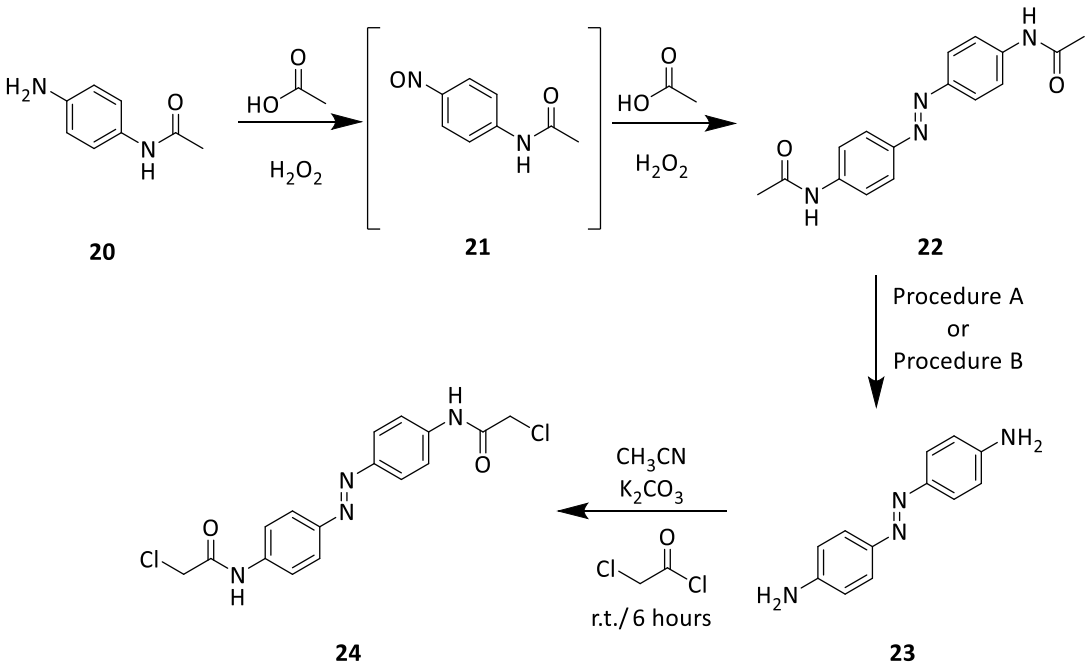

Scheme 2.10: Synthetic route to afford **24**. Procedures A and B are detailed in **Scheme 2.12**.

The synthesis of **24** was successful and achieved in three steps. The first step of the synthesis consisted of a partial oxidation of **20** in the presence of hydrogen peroxide and simultaneous coupling of the *in situ* formed 4-nitroso acetanilide (**21**) to unreacted 4-aminoacetanilide (**20**) in acetic acid (**Scheme 2.11**). This afforded **22** in a 13% yield.

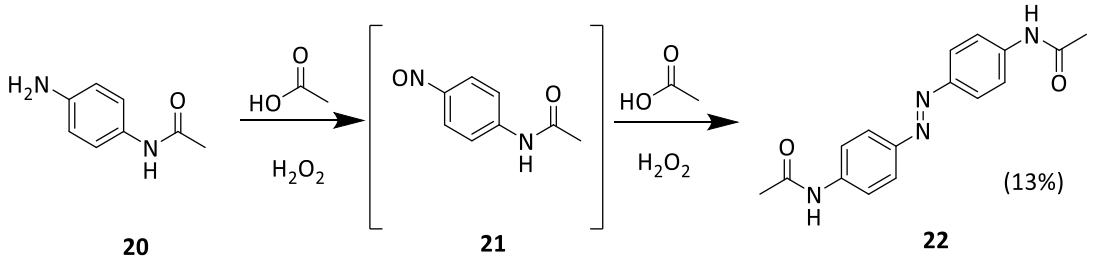

Scheme 2.11: Synthesis of 4,4'-diacetylamino azobenzene (**22**), followed as described in reference 32.

Figure 2.17 shows the ^{1}H NMR spectrum of **22** in DMSO-d_6. Since **22** is a symmetric molecule, the spectrum only shows half of the molecule. The NH protons were seen as a singlet at 10.28 ppm, the aromatic CH protons as two doublets between 7.85 and 7.78 ppm, the CH_3 protons from the acetyl groups as a singlet at 2.10 ppm, and H_2O from the DMSO-d_6 was seen at 3.35 ppm. ESI-MS (negative-mode ion) supported the ^{1}H NMR data: (ES^-) *m/z* 295.20 [M].

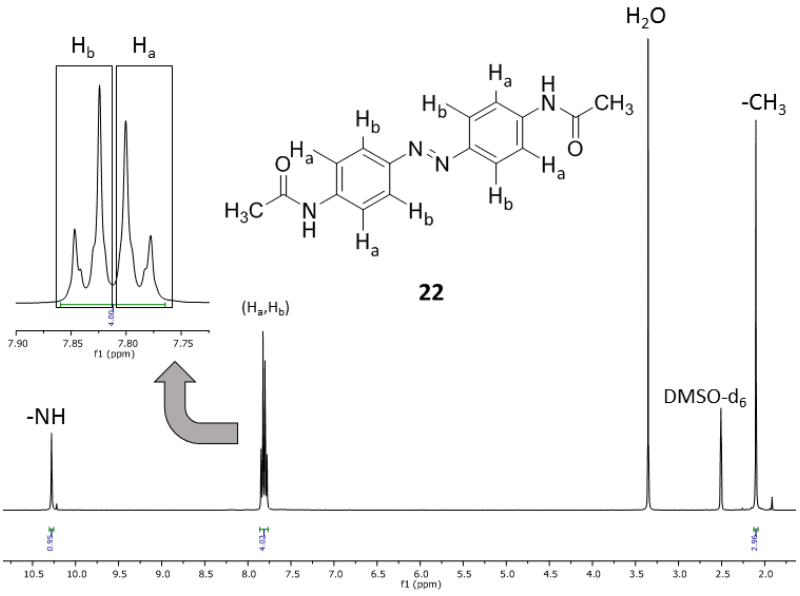

Figure 2.17: ^{1}H NMR spectrum of **22** and assignation of the proton signals.

Step two to synthesize compound **23** was achieved by following two different procedures found in the literature.[32, 33] We referred to them as procedure A and procedure B as detailed in the general synthetic route shown in **Scheme 2.10**. Procedure A afforded a 73% yield and consisted of removal of the N-acetyl groups by dissolving **22** in H_2O and refluxing it in concentrated hydrochloric acid (conc.HCl) for 3 hours. Procedure B increased the yield up to 84% when dissolving **22** in MeOH and refluxing it into conc.HCl for 1.5 hours until complete removal of the acetyl groups (**Scheme 2.12**).

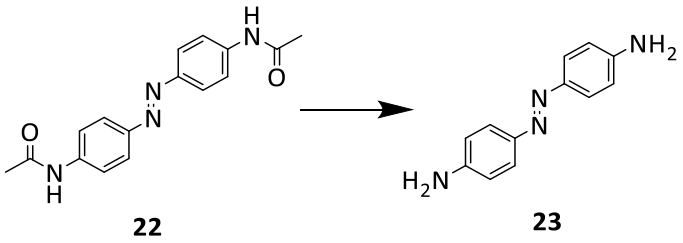

procedure	**A**	**B**
solvent	H_2O	MeOH
refluxing time	3 h	1.5 h
yield	73%	84%

Scheme 2.12: Synthesis of **23**: procedure A: (**22** in H_2O)/conc.HCl/reflux 3 hours; procedure B: (**22** in MeOH)/conc.HCl/reflux 3 hours

Figure 2.18 shows the ^{1}H NMR spectrum of **23**, which was also a symmetric compound as **22**, thus, the NMR only showed half of the molecule in the spectrum. The signal of the aromatic CH protons appeared as two doublets at 7.52 ppm and 6.63 ppm and the NH_2 protons as a singlet at 5.74 ppm. The spectrum was run in DMSO-d_6 which appeared at 2.51 ppm, and contained traces of H_2O that were seen at 3.35 ppm. ESI-MS (positive-mode ion) analysis was consistent with the ^{1}H NMR data and confirmed the formation of **23**: (ES^+) *m/z* 213.08 $[M+H]^+$.

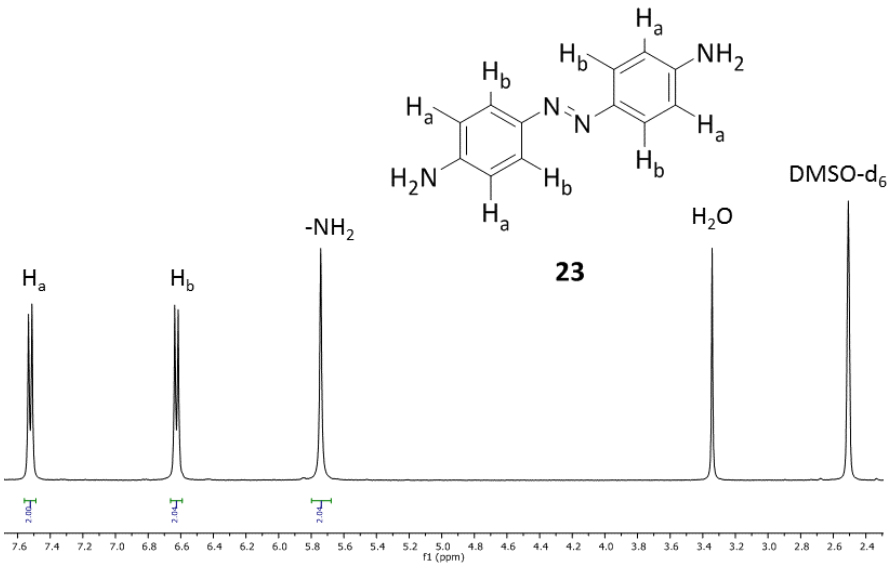

Figure 2.18: ^{1}H NMR spectrum of **23** and assignation of the proton signals.

The last step of the synthesis to finally produce 4,4'-dichloroacetamido azobenzene (**24**) consisted of suspending **23** in acetonitrile and the addition of chloroacetyl chloride at room temperature in the presence of a base (potassium carbonate) (**Scheme 2.13**).

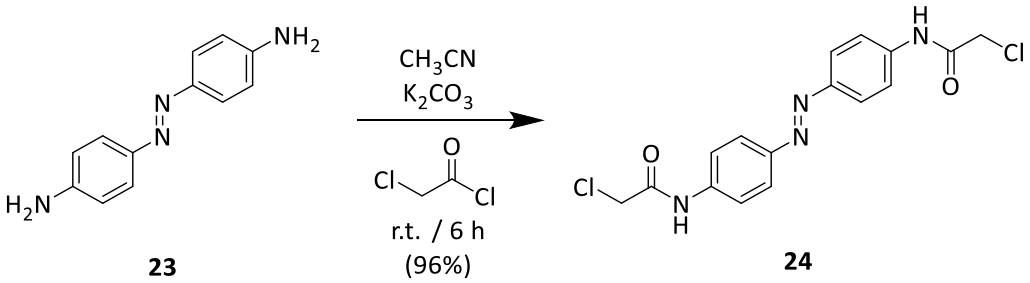

Scheme 2.13: Synthesis of 4,4'-dichloroacetamido azobenzene, **24**.

Compound **24** was obtained in a 96% yield and both ^{1}H NMR and ESI-MS data were consistent with the structure of the molecule. **Figure 2.19** shows the ^{1}H NMR spectrum of **24**, which was also a symmetric compound and only showed half of the molecule in the spectrum. The signal of the NH protons appeared as a singlet at 10.66 ppm which was consistent if compared with **22** as the chlorine atom is more electronegative and shifted the NH proton to lower field (higher frequency); the aromatic CH protons

appeared as two doublets at 7.89 ppm and 7.82 ppm which was also consistent if compared with **22** due to the similarity of their chemical environment; the CH_2 protons attached to the chlorine atoms appeared as a singlet at 4.33 ppm, which was expected due to the deshielding provoked by the high electronegativity of the chlorine. The spectrum was run in DMSO-d_6 which appeared at 2.51 ppm, and traces of H_2O were seen at 3.35 ppm as part of the solvent. ESI-MS (negative-mode ion) analysis of **24** showed *m/z* 362.9 [M]. The isotopic effects of the chlorine atom was indicative that the azobenzene **24** had the chlorine attached to the molecule and showed the highest intensity at the ^{35}Cl-^{35}Cl peak (**Figure 2.20**).

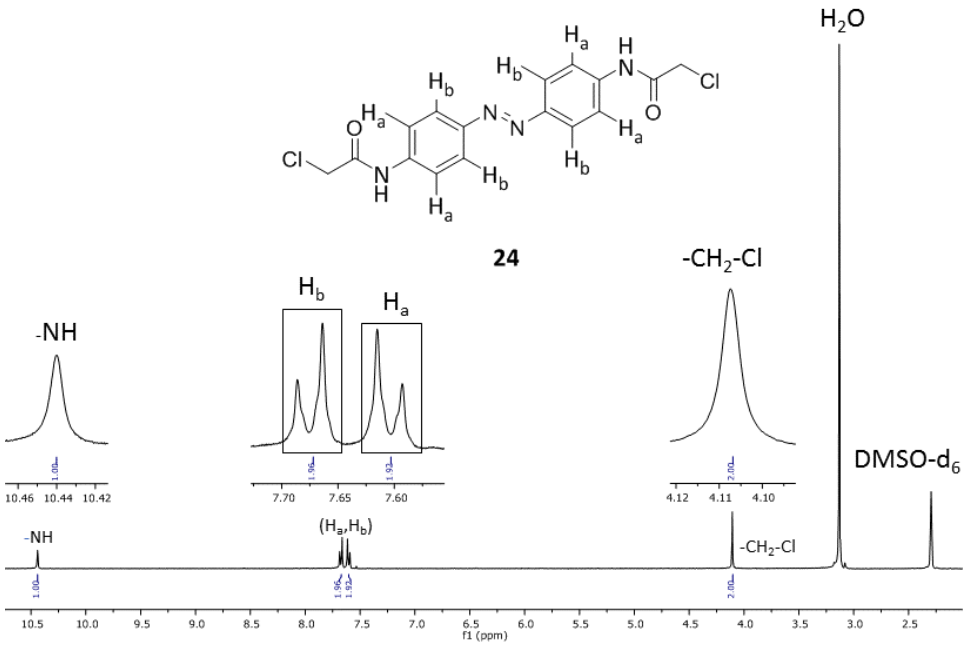

Figure 2.19: ^{1}H NMR spectrum of **24** and assignation of the proton signals.

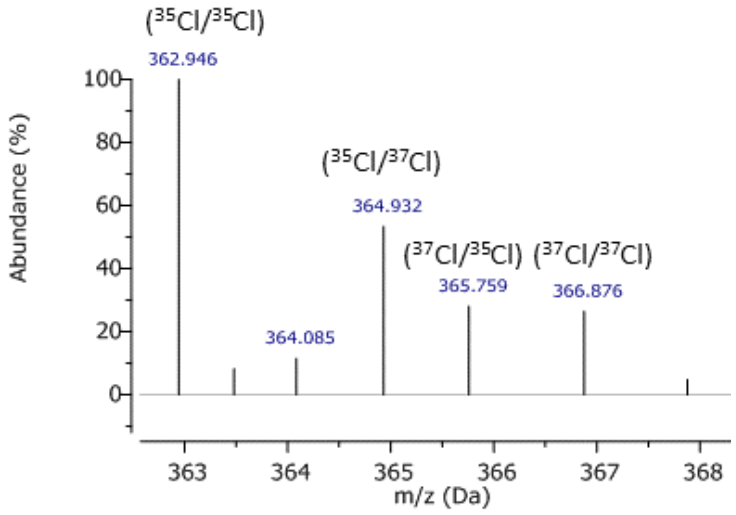

Figure 2.20: Expansion of the ESI-MS (negative-mode ion) spectrum of **24** where the isotopic effects caused by the chlorine atom show different ratio according to the abundance of the isotopes in nature ^{35}Cl (75.8%) and ^{37}Cl (24.2%).

Figure 2.21 shows the overlayed ^{1}H NMR spectra of **22** (black), **23** (red) and **24** (blue) for direct visual comparison of the proton signals of the different chemical groups in the molecules. There was clear evidence of some transformations from **22** to **24**. For instance, the CH_3 signal in **22** shifted to a higher frequency when converted into CH_2Cl in **24**. As previously explained, this was caused by the deshield effect of the CH_2 group due to the high electronegativity of the chlorine atom. This effect extended to the NH protons when going from **22** to **24**, however it was not as strong since the spacing between NH and Cl was bigger than the spacing between CH_2 and Cl. When comparing **22** and **24** with **23**, the aromatic protons shifted to a lower frequency. Again, the effects of the substituents directly attached to the phenyl rings were responsible for these changes. Whilst the acetyl or chloroacetyl groups are electron-releasing groups, hence the deshield effect shifted the aromatic protons to higher frequency, the amine groups are electron-donor and shifted the protons closer to them to a much lower frequency. The aromatic protons near the azo group were less affected by these changes.

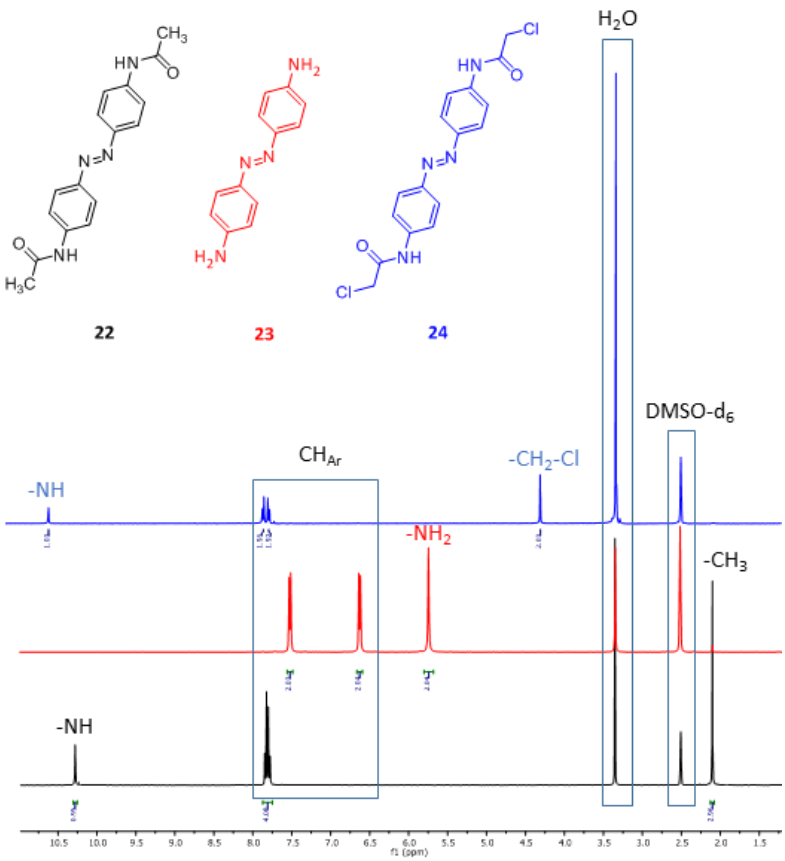

Figure 2.21: Overlayed ^{1}H NMR spectra of **22**, **23** and **24** and assignation of the proton signals.

2.3.2 UV/Vis spectroscopy for photoisomerization testing

As previously discussed in **Section 1.5.2**, the *trans* isomers of azobenzene derivatives are their most stable conformation and can photoisomerize to their *cis* isomers upon UV irradiation. Therefore, a UV/Vis analysis of **24** would be useful to confirm the presence of the azo bond in the molecule. **Figure 2.22** represents both *trans* and *cis* isomers of **24** upon UV-Vis radiation. Both conformational structures should switch from *trans*-to-*cis* upon irradiation with UV light (380 nm), and should return to the *trans* isomer upon irradiation with visible light (450 nm) or by thermal heating.

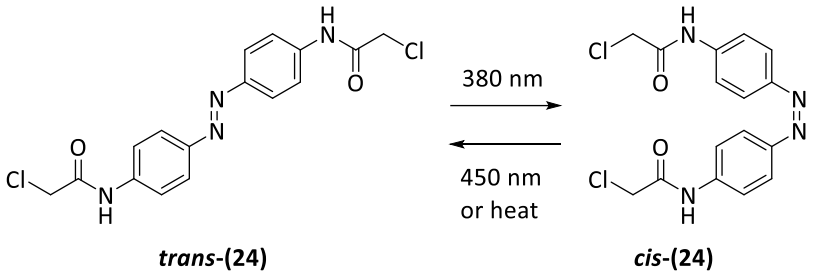

Figure 2.22: Photoisomerization of **24** by irradiation with UV/Vis light.

Figure 2.23 shows the UV/Vis spectra recorded after irradiating compound **24** (in DMSO) at both 380 nm and 450 nm. The initial UV/Vis spectrum, prior to any irradiation, showed the characteristic bands of absorption of an azobenzene derivative in its *trans* isomer (blue line). As discussed in **Section 1.5.2** these bands are low lying *n* → π* bands between 380 and 520 nm, while the π → π* bands appear at around 330 nm for the trans isomer and at around 275 nm for the cis isomer. Our azobenzene **24** showed a maximum of absorption, corresponding to a π → π* band, at 367 nm in the *trans* isomer. After irradiating **24** at 380 nm for 10 min, another UV/Vis measurement was recorded (red line). The band at 367 nm disappeared and seemed to be decreased and shifted to 330 nm, making 270 nm the maximum of absorbance for the *cis* isomer as previously described. This was a clear sign of the photoisomerization of our azobenzene derivative **24**. Irradiation of the *cis* isomer with 450 nm light for another 10 min returned *cis*-(**24**) to the *trans* conformational state (green line), however this was insufficient to return most of the molecules to the *trans* conformational state. Thus, irradiation at 450 nm for another 20 min was done and another spectrum recorded (purple line). As seen in **Figure 2.23**, this last irradiation was enough to return most of the molecules to the initial *trans*-conformational state.

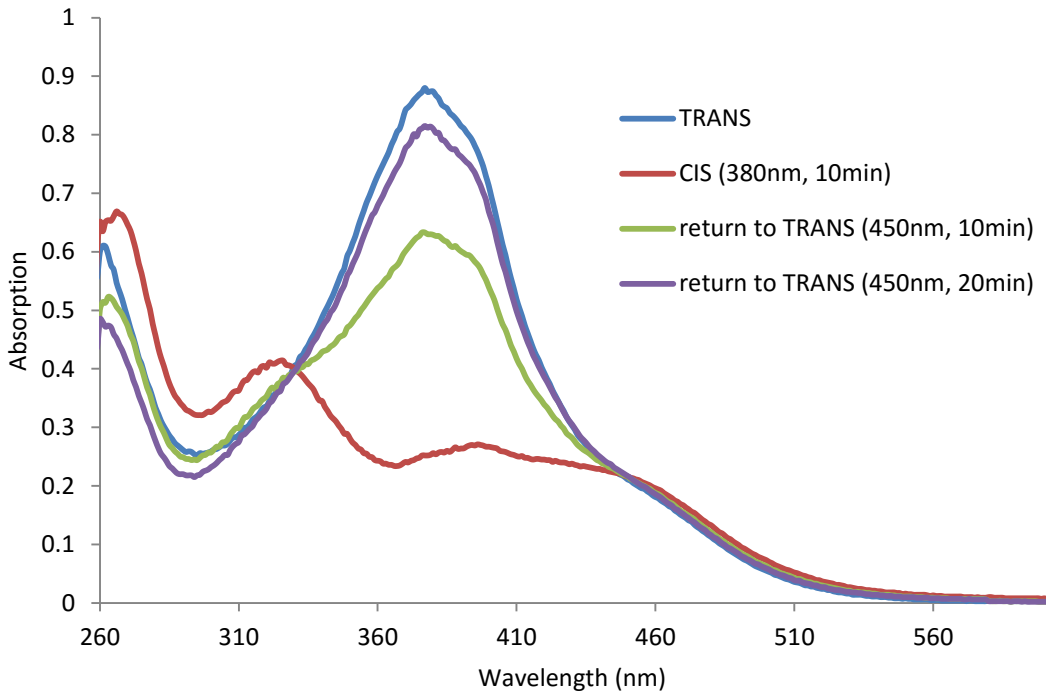

Figure 2.23: Overlayed UV/Vis spectra of the conformational switching (*trans*-to-*cis* and *cis*-to-*trans* isomerization) of 4,4'-dichloroacetamido azobenzene **(24)** 0.05 mM in DMSO.

2.4 Summary

We successfully synthesized unnatural amino acids for metal-binding investigations: Fmoc-2-Pal-O*t*Bu (**8**), Fmoc-3-Pal-O*t*Bu (**9**), Boc-2-Pal-OBn (**11**) and Boc-3-Pal-OBn (**12**). These will be incorporated into our designed self-assembling peptide sequences by SPPS methods. They will provide binding sites for metal-binding and will test the ability of a metal complex to modify the initial conformations of the peptide assemblies. On the other side, we were also able to synthesize an azobenzene derivative (4,4'-dichloroacetamido azobenzene, **24**) for photoswitching investigations, representing an alternative to metal-binding as a tool to generate conformational switch within peptide structures. The azobenzene derivative will be attached to our peptide designs through the thiol groups of Cys residues. This will help to investigate whether the photoisomerization of this switch, when attached to the peptide structure, can generate conformational changes to the structure of different peptide assemblies.

[1] Q. Lin, C.F. Barbas, and P.G. Schultz, *J. Am. Chem. Soc.* **2003**, 125, 612-613.

[2] M.M. Stevens, N.T. Flynn, C.Wang, D.A. Tirrel, and R. Langer, *Adv. Mater.* **2004**, 16, 915-918.

[3] B. Ciani, E.G. Hutchinson, R.B. Sessions, and D.N. Woolfson, *J. Biol. Chem.* **2002**, 277, 10150-1-155.

[4] M.J. Pandya, E. Cerasoli, A.Joseph, R.G. Stoneman, E. Waite, and D.N. Woolfson, *J. Am. Chem. Soc.* **2004**, 126, 17016-17024.

[5] X. Cao, X. Peng, L. Zhong, and R. Sun, *J. Agric. Food Chem.* **2014**, 62, 10000-10007.

[6] C.Y. Chiang, and C.C. Chu, *Carbohydr. Polym.* **2015**, 119, 18-25.

[7] N. Jotterand, D. A. Pierce, and B. Imperiali, *J. Org. Chem*. **2001**, 66, 3224-3228.

[8] M. L. Zastrow, A. F. A. Peacock, J. A. Stuckey, and V. L. Pecoraro, *Nat. Chem.*, **2012**, 4, 118-123.

[9] J. Fan, A. Fedorova, J. Hong, O. A. Kharenko, A. Y. Kornilova, R. C. Lasey, F. Xie, and M. Y. Ogawa, *J. Braz. Chem. Soc*. **2006**, 17, 1516-1521.

[10] G. Gilardi, and A. Fantuzzi, *Trends Biotechnol*. **2001**, 19, 468-476.

[11] A. I. Kornilova, J. F. Wishart, W. Z. Xiao, R. C. Lasey, A. Fedorova, Y. K. Shin, and M. Y. Owaga, *J. Am. Chem. Soc*. **2000**, 122, 7999-8006.

[12] J. Hong, O. A. Kharenko, and M. Y. Ogawa, *Inorg. Chem*. **2006**, 45, 9974-9984.

[13] M.V. Tsurkan, and M.Y. Ogawa, *Chem*. *Commun*. **2004**, 2092-2093.

[14] M.V. Tsurkan, and M.Y. Ogawa, *Inorg. Chem.* **2007**, 46, 6849-6851.

[15] M.V. Tsurkan, and M.Y. Ogawa, *Biomacromolecules* **2007**, 8, 3908-3913.

[16] D.V. Zaytsev, F. Xie, M. Mukherjee, A. Bludin, B. Demeler, R.M. Breece, D.L. Tierney, and M.Y. Ogawa, *Biomacromol.* **2010**, 11, 2602-2609.

[17] E. Negishi, N. Okukado, A.O. King, D.E. van Horn, B.I. Spiegel, *J. Am. Chem. Soc.* **1978**, 100, 2254-2256.

[18] N. Colgin, T. Flinn, and S.L. Cobb, *Org*. *Biomol*. *Chem*. **2011**, 9, 1864-1871.

[19] M. Ginisty, C. Gravier-Pelletier, and Y.L. Merrer, *Tetrahedron: Asymmetry* **2006**, 17, 142-150.

[20] L. Le-Corre, C. Gravier-Pelletier, and Y. Le-Merrer, *Eur. J. Org. Chem.* **2007**, 32, 5386-5394.

[21] S. Arndt, U. Emde, S. Bäurle, T. Friedrich, L. Grubert, and U. Koert, *Chem. – Eur. J.*, **2001**, 7, 993-1005.

[22] *Handbook of Organopalladium Chemistry for Organic Synthesis*; Negishi, E., Ed.; Wiley-Interscience: New York, **2002**; Volume 1, Part III

[23] S. Baba, and E. Negishi, *J. Am. Chem. Soc.* **1976**, 98, 6729-6731.

[24] E. Negishi, N. Okukado, A.O. King, D.E. van Horn, B.I. Spiegel, *J. Am. Chem. Soc.* **1978**, 100, 2254-2256.

[25] C.L. Oswald, T. Carrillo-Marquez, L. Caggiano, R.F.W. Jackson, *Tetrahedron* **2008**, 64, 681-687.

[26] C.S. Dexter and R.F.W. Jackson, *J. Or. Chem*., **1999**, 64, 7579-7585.

[27] M.S. Smyth and T.R. Burke Jr., *Tet. Lett.*, **1994**, 35, 551-554.

[28] A. Vaupel and P. Knochel, *J. Org. Chem.* **1996**, 61, 5743.

[29] E. Galardon, S. Ramdeehul, J.M. Brown, A. Cowley, K.K. Hii, A. Jutand, *Angew. Chem., Int. Ed.* **2002**, 41, 1760-1763.

[30] C.A. Tolman, *Chem. Rev.*, **1977**, 77, 313-348.

[31] D.C. Burns, F. Zhang, and G.A. Woolley, *Nature Protocols* **2007**, 2, 251-258.

[32] R. Pfister, J. Ihalainen, P. Hamm, and C. Kolano, *Org. Biomol. Chem*., **2008**, 6, 3508-3517.

[33] P.Santurri, F. Robbins, and R. Stubbings, *Org. Synth.*, Coll. Vol. 5, p.341 (**1973**); Vol. 40, p.18 (**1960**).

Chapter 3

Development of a chassis for *de novo* coiled-coil self-assembling peptide systems

3.1 Overview

As shown in **Section 1.3**, there is enough information for the design and construction of *α*-helical coiled-coil structures based on the *rules-of-thumb* which relate protein sequence and structure in coiled-coil domains. When considering the chemical synthesis of a peptide, we should aim for an approach which gives speed and simplicity for the synthesis. A linear stepwise synthesis – that is, one which the target is built one amino acid at a time as a single peptide strand – is conceptually simple and affords control over the incorporation of modifications within the sequence. Solid phase peptide synthesis (SPPS) is the methodology followed for the successful synthesis of our designed peptides and involves the appropriate choice of a solid support on to which the peptide sequence is going to be built (see **Section 3.2**).

3.2 Introduction to Solid Phase Peptide Synthesis (SPPS)

SPPS is the standard strategy used for the chemical synthesis of peptide sequences. A stepwise approach utilizing solid-phase Fmoc chemistry was adopted to proceed with the chemical transformations which were carried out on a solid support. SPPS presents advantages over solution-phase peptide synthesis, in particular in longer sequences where repetition of coupling and deprotections cycles are labour intensive, and often require purification of the intermediates. In addition, the use of a solid support in SPPS

allows the individual peptide coupling reactions to be pushed to completion through the use of excess reagents and multiple couplings.

SPPS proceeds via repeating cycle of coupling and deprotections steps which are assisted by microwave (MW) energy as this decreases reaction times and improves on the crude product yield and purity (**Scheme 3.1**). These reaction steps proceed inside a PTFE reaction vessel where the resin is left to swell in the appropriate solvent (dichloromethane, DCM, or dimethylformamide, DMF, in our synthesis) for a minimum time of 2 hours prior to any amino acid additions. A solution of the amino acid to be coupled together with an activating agent is then added and coupled with MW heating and agitation by bubbling nitrogen gas. Unreacted amino acids are removed by draining the solution-phase from the reaction vessel. The coupled amino acids are Fmoc-deprotected by addition of base – this is a 20% (*v*/*v*) solution of piperidine in DMF – and the subsequent amino acid is added to the growing peptide sequence. Upon completion of the sequence, the cleavage of the peptide from resin is achieved by treating the acid-labile peptide-resin with a trifluoro acetic (TFA) solution (in our case, with triisopropylsilane, TIPS, as scavenger to avoid undesirable acid-catalysed side reactions of the peptide) and this solution is shaken for a minimum of 3 hours at room temperature. The TFA solution also serves to remove side chain protecting groups present on amino acid side chains. For N-acetylation when capping peptides, the peptide-resin is suspended in a 20% (*v*/*v*) solution of acetic anhydride in DMF and shaken for 30 min before rinsing, DMF washing and rinsing again before TFA cleavage. All steps of the synthesis were run on a CEM Liberty1 automated peptide synthesizer equipped with a Discover microwave. Single couplings were carried out with activation using 5 equivalents of Fmoc amino acid under the default conditions (75 ˚C, 10 min). Removal of the Fmoc group was effected via treatment with 20% piperidine for 3 min with microwave assistance (75 ˚C) (see **Section 7.2.2** for experimental details of SPPS).

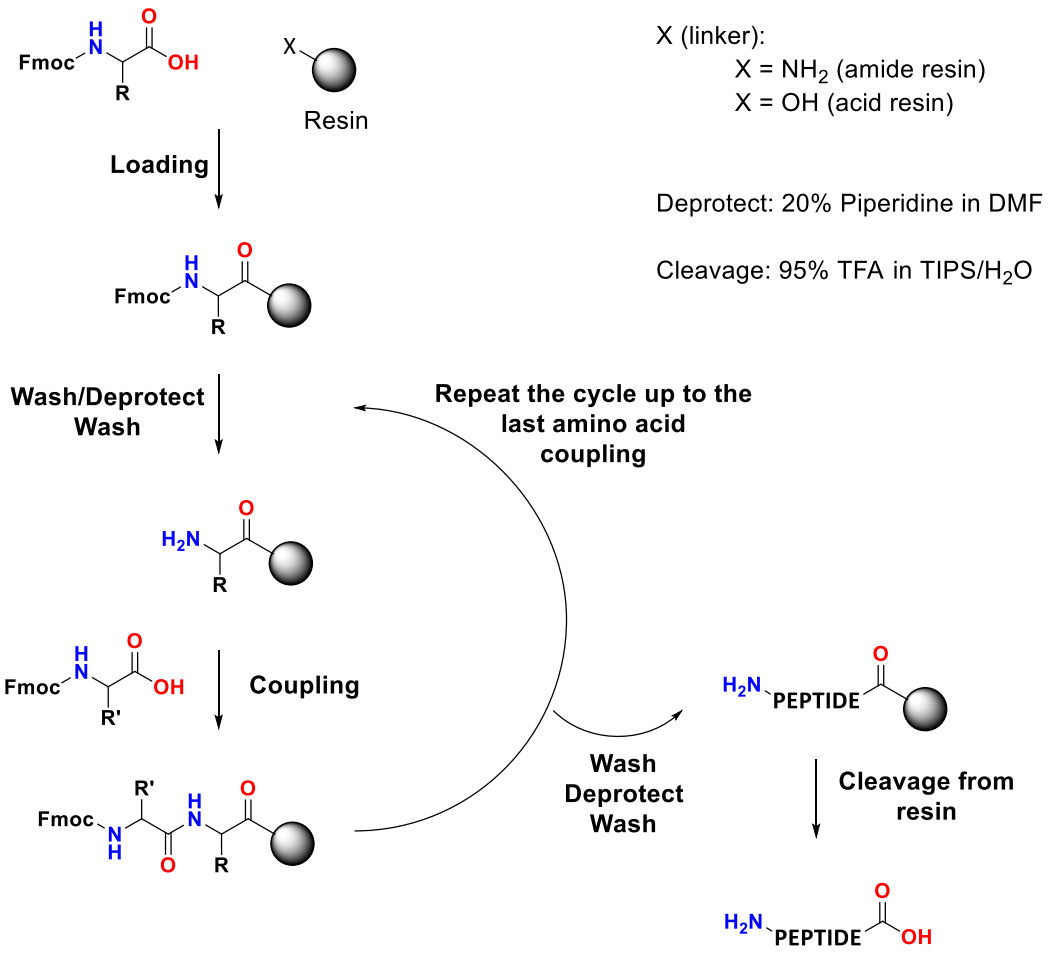

Scheme 3.1: Outline of the general procedure for Fmoc-SPPS.

The solid support

Careful selection of both the resin polymer and the linker type is crucial for an efficient peptide synthesis. The most common used polymers are polystyrene, poly(ethylene glycol) (PEG), PEG hybrid polystyrene, and polyamide (PA), each with different swelling properties in various solvents.[1] For the linkers (**Figure 3.1**) either a hydroxyl group (for an "acid resin") or amine group ("amide resin") on the linker is used to anchor the *C*-terminal amino acid onto the resin via an esterification or amide bond formation respectively during the initial resin loading. After elongation the peptide is cleaved from resin using 95% TFA (**Section 7.2.2**) to give either a peptide acid or peptide amide (depending on whether an acid or amide resin is used).

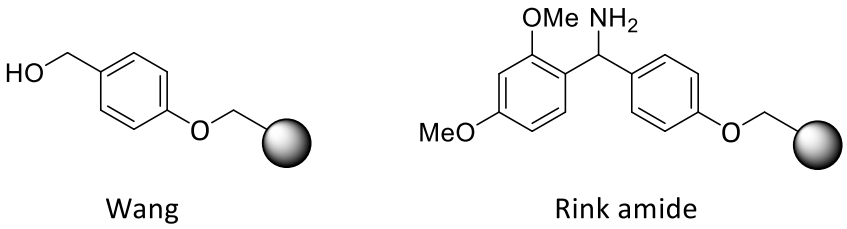

Wang Rink amide

Figure 3.1: Commonly used linkers for Fmoc SPPS. For Rink amide the C-terminal amino acid is attached via coupling to an amine, for Wang a hydroxyl group is used.

3.3 Synthesis of peptide sequences and discussion

3.3.1 Introduction to the design of coiled-coil systems

We aim to synthesize peptides with reasonable stability to produce a range of potential variants: (i) a blunt-ended coiled-coil; (ii) a sticky-ended fibre assembly similar to the SAF peptides to examine whether metal-binding can affect the morphology of the fibres; and (iii) a sticky ended assembly in the manner of the peptide nanostructures. The design principles are as follows:

a) We need a specifying polar residue to promote parallel dimer formation and to produce the sticky-ended coiled-coils (for enthalpic reasons the blunt-ended coiled-coil is always favourable unless the structure is heavily biased).
b) We need to use charge repulsion to prevent the formation of homo dimers (entropically favourable unless designed against).
c) We need four heptads of coiled-coil at least in order to provide reasonable stability particularly in the case of sticky-ended fibre assembly in the manner of SAF peptides.
d) At least two locations for metal binding amino acids must be found and be separate from the functional areas of the coiled-coil (including core residues, charged residues and chromophores).
e) Each peptide should have a net charge (to help solubility) and the complex should have an overall charge of +1 (to mimic the SAF system).

3.3.2 Synthesis of peptide sequences for coiled-coil formation

With all these requirements, the initial designed sequence Peptide1 (**PEP1**, **25**), its blunt-ended partner (**BEP**, **26**) and sticky-end partner (**SAF**, **27**) are as indicated in **Figure 3.2**, and their interaction mode is represented in **Figure 3.3** for (**PEP1**+**BEP**) – taken from **Section 1.4**, **Figure 1.10** – and **Figure 3.4** for (**PEP1**+**SAF**).

	gabcdefgabcdefgabcdefgabcdef
PEP1	KIAALKQKNAALKQEIAALEYEIEALEQ
BEP	EIAALEYENAALEQKIKALKQKIKALKQ
SAF	KIKALKQKIKALKQEIAALEYENAALEQ

Figure 3.2: Sequences of **PEP1**, **BEP** and **SAF**. In **PEP1**, amino acids for salt-bridging formation are highlighted in red, while in green for **BEP** and **SAF**. Positions *a* to *f* of the heptads are showed above the sequences and different tones of colour are used to highlight different heptads (4 heptads in total). Asn is placed in positions *a* of the third heptad to favor dimeric coiled-coil formation as explained in **Section 1.3**.

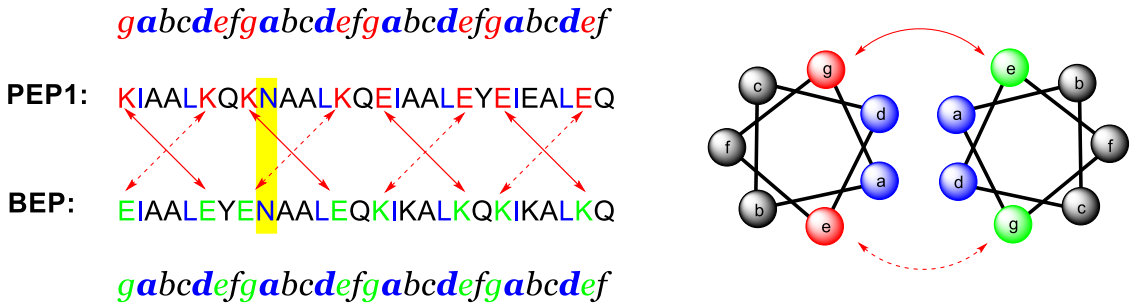

Figure 3.3: Interaction of sequences **PEP1** and **BEP** for dimeric coiled-coil formation. Amino acids for salt-bridging formation are highlighted in red in **PEP1** while in green in **BEP** and the red arrows indicate at where this happens – which is between positions *e* and *g* of complementary peptide sequences. Positions *a* to *f* of the heptads are showed above and below the sequences. Asn interactions is indicated in yellow. A wheel diagram of the heptads with both complementary sequences interacting is represented at the right-hand side of the figure with the hydrophobic residues (*a* and *d*) depicted in blue and the solvent-exposed residues (*b*, *c* and *f*) in grey.

Figure 3.4: Interaction of sequences **PEP1** and **SAF** for dimeric coiled-coil fibre formation. Amino acids for salt-bridging formation are highlighted in red in **PEP1** while in green in **SAF** and the red arrows indicate at where this happens between positions *e* and *g* of complementary peptide sequences. Positions *a* to *f* of the heptads are showed above and below the sequences. Asn interactions are indicated in yellow.

The synthesis of peptides **25**, **26** and **27** was successfully accomplished by automated Fmoc-MW-SPPS and purification by RP-HPLC afforded all the peptides with high purity as shown by MALDI-MS analysis. **PEP1** (**25**) was first synthesized on low loaded Fmoc-Gln(Trt)-wang resin (0.59 mmol/g substitution) at a 0.05 mmol scale following peptide synthesis – procedure 1 (**Section 7.2.3**) to afford 78 mg of crude peptide (50%). When **25** was synthesized at a 0.10 mmol scale, following peptide synthesis – procedure 2 (**Section 7.2.3**), the crude yield increased to 75% affording 235 mg of crude peptide. RP-HPLC of the crude peptide affords the pure peptide highly pure as determined by HRMS analysis (HRMS values are shown in **Section 7.5**). **Figure 3.5** shows the MALDI spectrum of the crude **PEP1** at the left and the MALDI spectrum of the pure **PEP1** after RP-HPLC purification at the right.

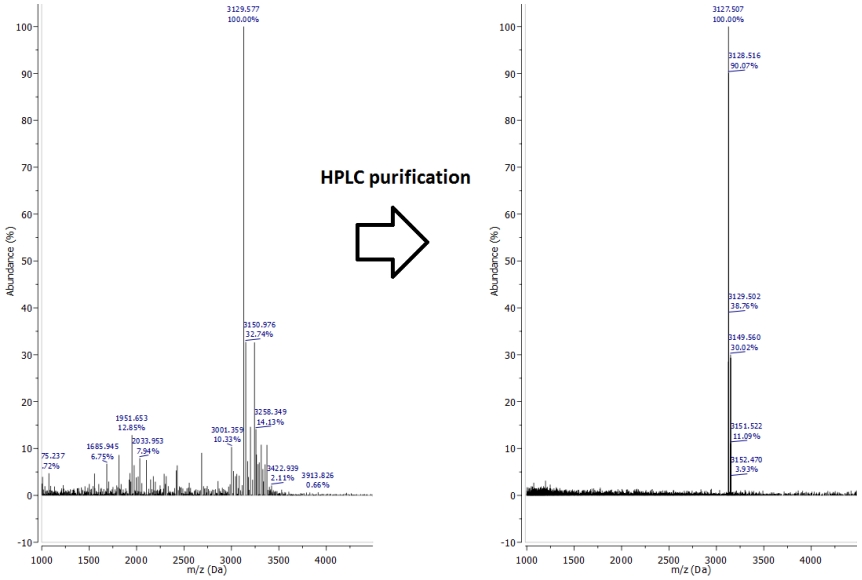

Figure 3.5: MALDI-TOF MS spectra of **PEP1** (**25**) before HPLC purification (at the left side) and after RP-HPLC purification (at the right).

Figure 3.6 shows the MALDI spectrum of **PEP1** after RP-HPLC purification, indicating the peaks found to confirm the presence of **25**: MALDI-TOF MS *m/z* 3127.5 $[M]^+$, 3128.5 $[M+H]^+$, 3149.6 $[M+Na]^+$, 3151.5 $[M+H+Na]^+$.

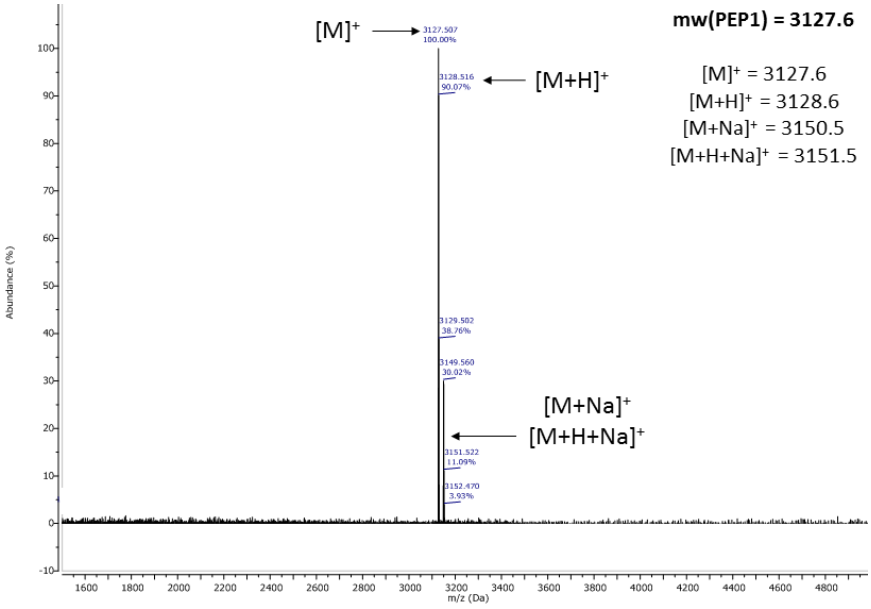

Figure 3.6: MALDI-TOF MS spectrum of **PEP1** (**25**). The molecular weight and different ions for the possible detectable species is at the top right corner. On the spectrum, detected ions are indicated.

Analytical RP-HPLC of the pure peptide **25** using a linear gradient of 0-100% of solvent B – this being (*v/v*) 5% H_2O/95% CH_3CN with 0.1% TFA as explained in **Section 7.1.4** – over 30 min was useful to confirm the presence of a single peptide sequence, and showed a retention time at 15.18 min (**Figure 3.7**).

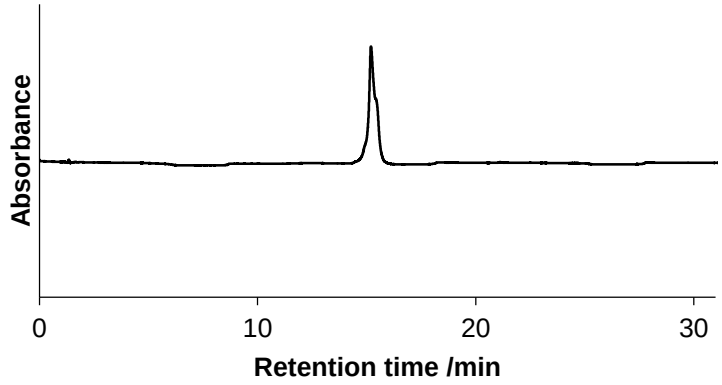

Figure 3.7: Analytical RP-HPLC chromatogram of **PEP1** (**25**) at 280 nm.

BEP (**26**) was synthesized on low loaded Fmoc-Gln(Trt)-wang resin (0.59 mmol/g substitution) at a 0.05 mmol scale following peptide synthesis – procedure 1 (**Section 7.2.3**) affording 90 mg of crude peptide (57%). **Figure 3.8** shows the MALDI spectrum of **BEP** after RP-HPLC purification: MALDI-TOF MS *m/z* 3183.5 $[M]^+$, 3184.5 $[M+H]^+$.

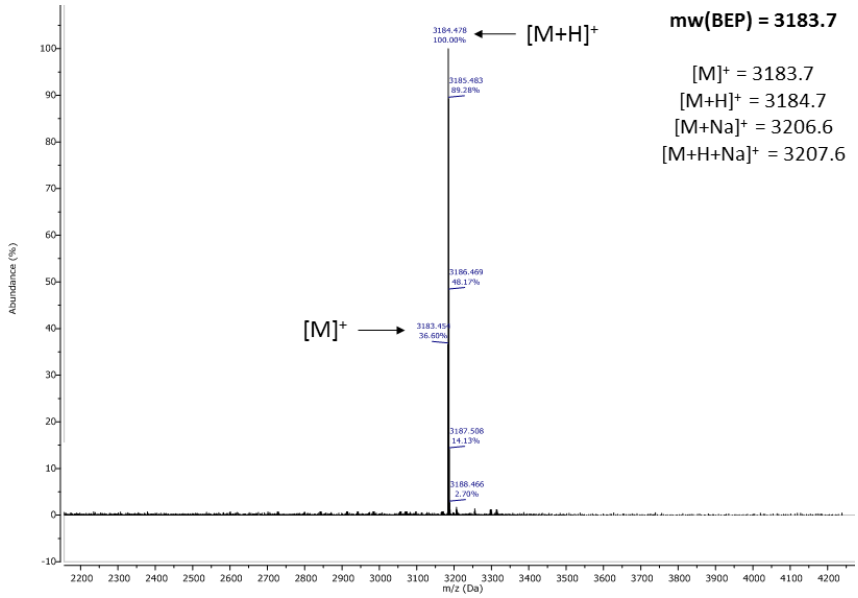

Figure 3.8: MALDI-TOF MS spectrum of **BEP** (**26**). The molecular weight and different ions for the possible detectable species is at the top right corner. On the spectrum, detected ions are indicated.

As for peptide **25**, analytical RP-HPLC of the pure peptide **26** using a linear gradient of 0-100% of solvent B – this being (*v/v*) 5% H_2O/95% CH_3CN with 0.1% TFA as explained in **Section 7.1.4** – over 30 min was also useful to confirm the presence of a single peptide sequence, showing a retention time at 13.86 min (**Figure 3.9**). Since **PEP1** (**25**) showed a retention time at 15.18 min using the same linear gradient, we conclude that peptide **25** is more hydrophobic than **26**.

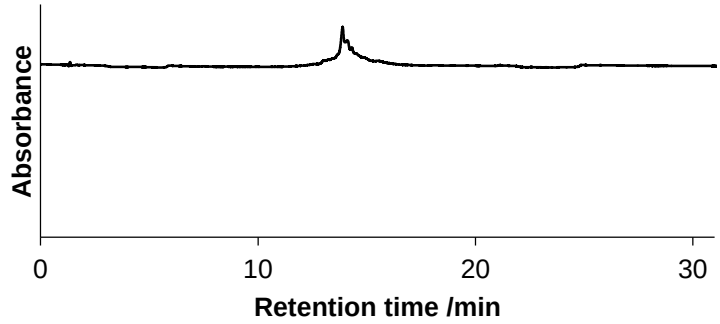

Figure 3.9: Analytical RP-HPLC chromatogram of **BEP** (**26**) at 280 nm.

SAF (**27**) was initially synthesized on low loaded Fmoc-Gln(Trt)-wang resin (0.59 mmol/g substitution) at a 0.05 mmol scale, using peptide synthesis – procedure 1 (**Section 7.2.3**) to afford 72 mg of crude peptide (45%). When synthesising **27** at a 0.10 mmol scale, following peptide synthesis – procedure 4 (**Section 7.2.3**) the crude yield increased to give 235 mg of crude peptide (74%). **Figure 3.10** shows the MALDI spectrum of **SAF** after RP-HPLC: MALDI-TOF MS *m/z* 3183.3 $[M]^+$, 3184.3 $[M+H]^+$, 3206.4 $[M+Na]^+$.

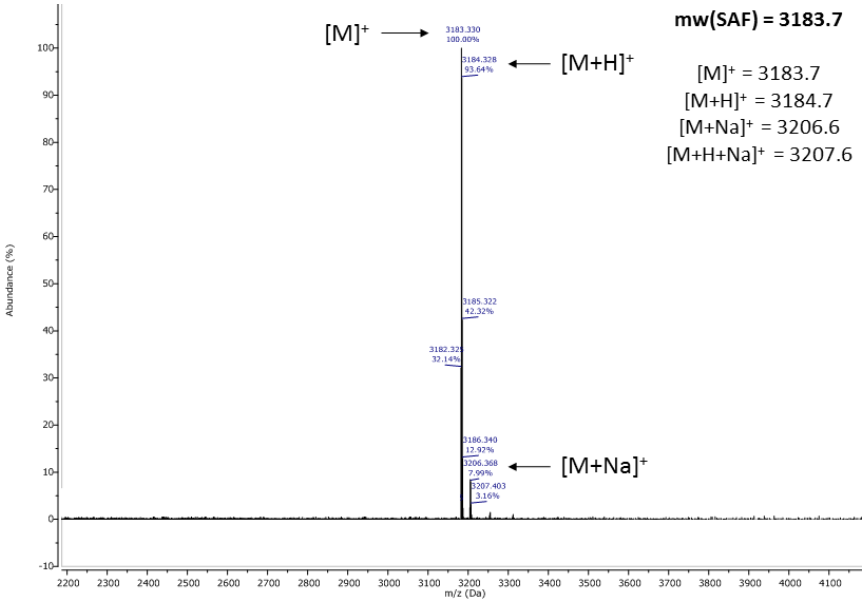

Figure 3.10: MALDI-TOF MS spectrum of **SAF** (**27**). The molecular weight and different ions for the possible detectable species is at the top right corner. On the spectrum, detected ions are indicated.

Analytical RP-HPLC of the pure peptide **27** using a linear gradient of 0-100% of solvent B – this being (*v/v*) 5% H_2O/95% CH_3CN with 0.1% TFA as explained in **Section 7.1.4** – over 30 min (as used for **25** and **26**), confirmed the presence of a single peptide sequence, showing a retention time at 13.50 min (**Figure 3.11**). Since **PEP1** (**25**) showed a retention time at 15.18 min, and **BEP** (**26**) at 13.86 min using the same linear gradient, we conclude that **SAF** (**27**) is the most hydrophobic of all these three peptides.

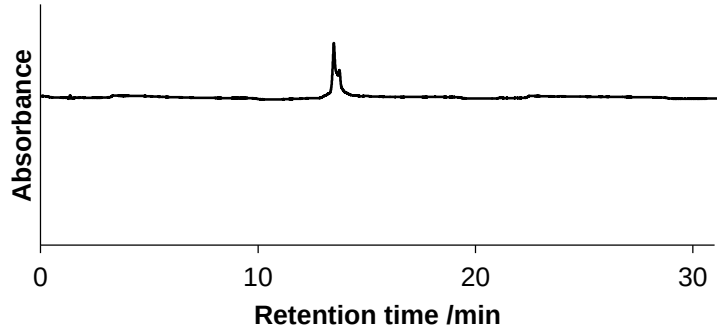

Figure 3.11: Analytical RP-HPLC chromatogram of **SAF** (**27**) at 280 nm.

CD analysis of the mixtures (**PEP1**+**BEP**) and (**PEP1**+**SAF**) at equal concentrations of each peptide provided information about the *α*-helical folding state of both systems. Measurements of both the single peptides **25**, **26** and **27**, and their mixtures (**25**+**26**) and (**25**+**27**) were carried out in PBS buffer at pH 7.4 at different concentrations of 20, 50, 100 and 200 μM to investigate if the self-assembly of the peptides and peptide systems depended on the concentration. However, all results at all concentrations for all these experiments indicated that both the single peptides and their corresponding mixtures were insensitive to concentration when promoting *α*-helical conformations. In this section, we only show the results of the CD spectra at 100 μM of peptides **25**, **26**, **27** and the CD spectra at 100 μM of their corresponding mixtures (**25**+**26**) and (**25**+**27**). We used room temperature (21 ˚C) as we had troubles with the temperature controller regulator and 21 ˚C was the temperature found in the room and read by the instrument. All the CD spectra at different concentrations can be found in the **Appendices**.

Figure 3.12 shows the CD spectra at room temperature (21 ˚C) of **PEP1** (**25**) in blue, **BEP** (**26**) in orange and their (1:1) mixture (**PEP1**+**BEP**) in green for coiled-coil formation, each of them at a concentration of 100 μM. The dotted green line shows an average of the single CD spectra of **PEP1** and **BEP** as a prediction for no interaction between these peptides. **PEP1** alone shows a minimum at 198 nm which is indicative that it does not predominantly have an *α*-helical but a random conformation. **BEP** alone shows two negative bands at 203 nm and 222 nm, intermediate between helical and disordered forms of the peptide. Upon mixture of both peptides, a clear interaction is denoted since two negative bands at 208 nm and 222 nm appear in the spectrum. These correspond with the same wavelength as for the typical CD spectrum of a coiled-coil structure. However, the θ_{222nm} (ellipticity at 222 nm) should have a similar or higher absolute value than the θ_{208nm} (ellipticity at 208 nm) in a fully folded *α*-helical coiled-coil structure. Thus, this indicates that the structure formed in the mixture (**25**+**26**) is not 100 % *α*-helical (only a 37.1 %) but contains other secondary structure elements.

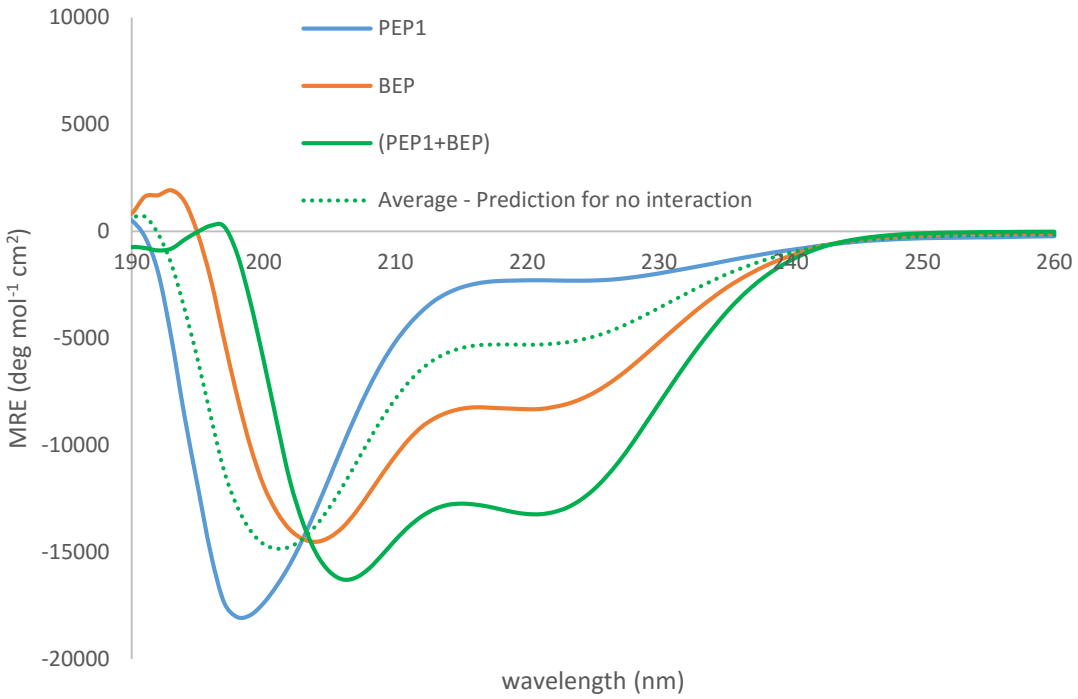

Figure 3.12: CD spectra of 100 µM solutions of **PEP1** (**25**), **BEP** (**26**) and (**PEP1**+**BEP**) (**25**+**26**) in PBS buffer at pH 7.4 at 21 ˚C.

Figure 3.13 shows the CD spectra at room temperature (21 ˚C) in PBS at pH 7.4 of **PEP1** (**25**) in blue, **SAF** (**27**) in orange and their (1:1) mixture (**PEP1**+**SAF**) in green for coiled-coil formation, each of them at a concentration of 100 µM. The dotted green line shows an average of the single CD spectra of **PEP1** and **BEP** as a prediction for no interaction between these peptides. As in the previous case, **PEP1** alone shows a minimum at 198 nm indicating that does not fold as an α-helix. **SAF** alone also shows a negative bands at 200 nm denoting the lack of an α-helical structure. When **PEP1** and **SAF** are mixed together, an interaction is observed as the negative band shifts to 202 nm. However, this is a clear evidence that a full α-helical conformation is not achieved. We conclude that the mixture of (**PEP1**+**SAF**) only forms a random coil and it is unable to form an α-helical coiled-coil as required.

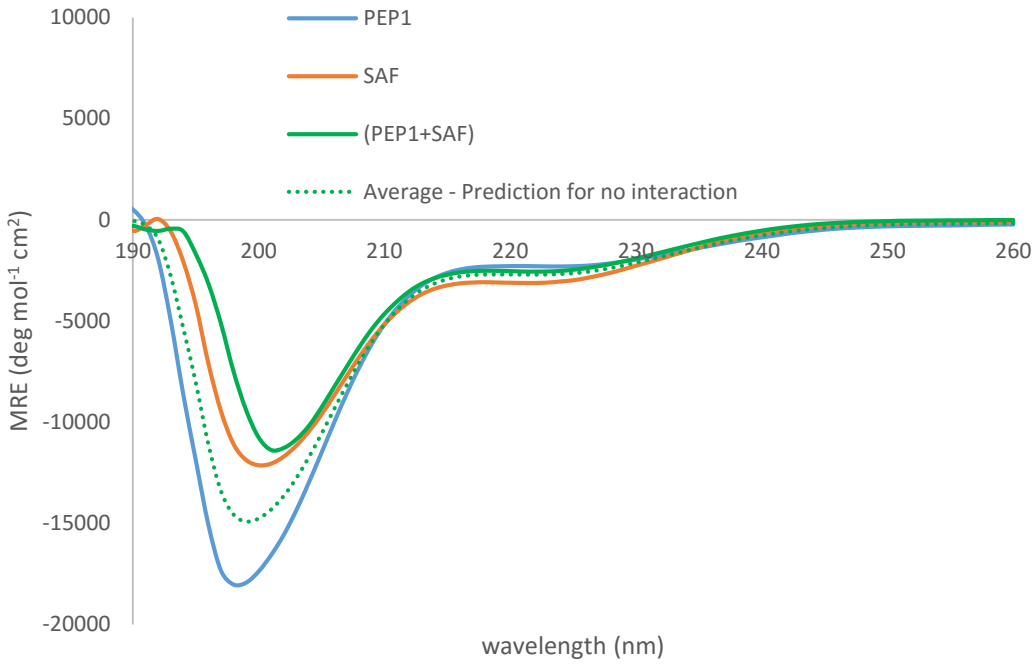

Figure 3.13: CD spectra of 100 µM solutions **PEP1** (**25**), **SAF** (**27**) and (**PEP1**+**SAF**) (**25**+**27**) in PBS buffer at pH 7.4 at 21 ˚C.

Table 3.1 summarises different data obtained at pH 7.4 from peptides **25**, **26** and **27** and their mixtures (**25**+**26**) and (**25**+**27**) at 100 µM in PBS at 21 °C. The helical contents of each peptide were calculated using the assumption that 100% helix gives a value of (-40000)*[(n-4)/n] where n is the number of residues in the peptide.[2] The percentage of helicity were calculated by using θ_{222} / [100% helix x (1-(2.57/n))].[3] The same type of data obtained at different concentrations for each one of the peptides and peptide mixtures can be found in the **Appendices**.

100 µM, pH 7.4	θ_{222nm}(deg mol^{-1} cm^2)	θ_{222nm}/ θ_{208nm}	% helicity
PEP1 (25)	-2292.99	0.31	7.4
BEP (26)	-8213.04	0.67	26.4
SAF (27)	-3122.39	0.46	10.0
PEP1 + BEP (25+26)	-13132.60	0.83	37.1
PEP1 + SAF (25+27)	-2556.91	0.41	7.2

Table 3.1: Summarised data obtained at pH 7.4 from peptides **25**, **26** and **27** and the mixtures (**25**+**26**) and (**25**+**27**) at 100 µM in PBS at 21 °C.

When looking at our peptide sequences and comparing them to the coiled-coil fibrous systems reviewed in the literature,[4,5,6] we found that these were double capped – this means N-terminal acetylated and C-terminal amidated. Since our peptide sequences have free both N- and C-terminus – this means in the form $–NH_3^+$ and $–OH^-$ at pH 7.4 – we attribute our results to the lack of both chemical groups (acetyl and amide) at the end of the sequences as they could provide a higher and more stable interaction between sequences for dimeric coiled-coil formation. As discussed in **Section 1.2**, the charged free ends may cause repulsive interactions between the sequences that avoid *α*-helical coiled-coil formation. Therefore, we decided to double capping both **PEP1** and **BEP** sequences – renaming them as **c-PEP1** (**28**) and **c-BEP** (**29**) – and leave **SAF** as firstly designed as we believed that **28** and **29** would provide enough stability for interaction and for coiled-coil formation when mixed with **SAF**. In addition, we thought that PBS might have a high percentage of salts that were interacting with our peptide sequences and could hinder the formation of coiled-coils. Thus, having a buffer solution with less salts than PBS could facilitate the formation of *α*-helical coiled-coil structures and also fibres for the (**PEP1**+**SAF**) mixture. As MOPS had been successfully utilized for the systems reviewed in the literature (references 4-6), a 10 mM solution of MOPS buffer at pH 8.5 was prepared and used in the CD measurements of these new peptides and peptide combinations.

Figure 3.14 shows the MALDI spectrum of **c-PEP1** (**28**) after RP-HPLC purification: MALDI-TOF MS *m/z* 3191.5 $[M+Na]^+$, 3207.4 $[M+K]^+$.

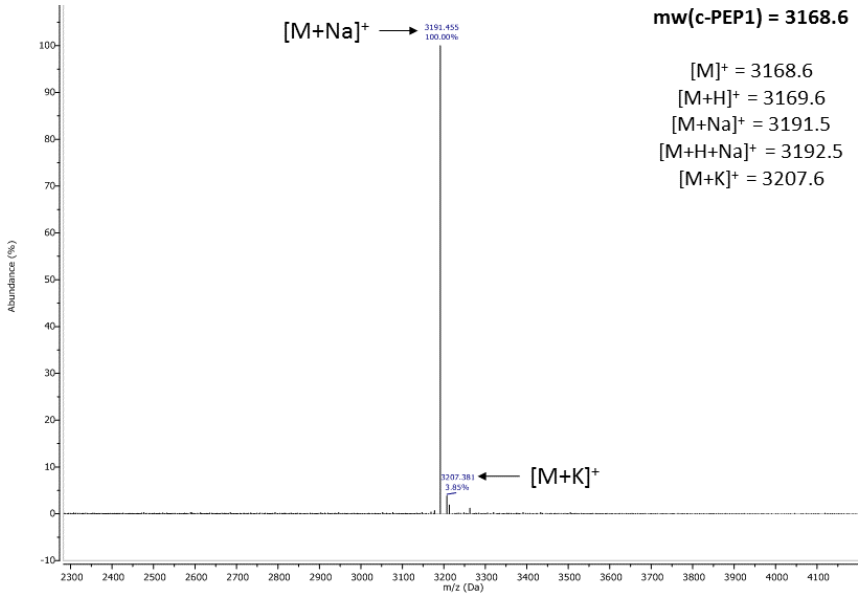

Figure 3.14: MALDI-TOF MS spectrum of **c-PEP1** (**28**): CH_3O-KIAALKQKNAALKQEIAALEYEIEALEQ-NH_2. The molecular weight and different ions for the possible detectable species is at the top right corner. On the spectrum, detected ions are indicated.

As previously, analytical RP-HPLC of the pure peptide **28** using a linear gradient of 0-100% of solvent B – this being (*v/v*) 5% H_2O/95% CH_3CN with 0.1% TFA as explained in **Section 7.1.4** – over 30 min was useful to confirm the presence of a single peptide sequence, and showed a retention time at 15.86 min (**Figure 3.15**). If we compare **28** to its analogue **25** (retention time at 15.18), we observe that double capping the peptide sequence provokes a small increase in the hydrophobicity of the peptide.

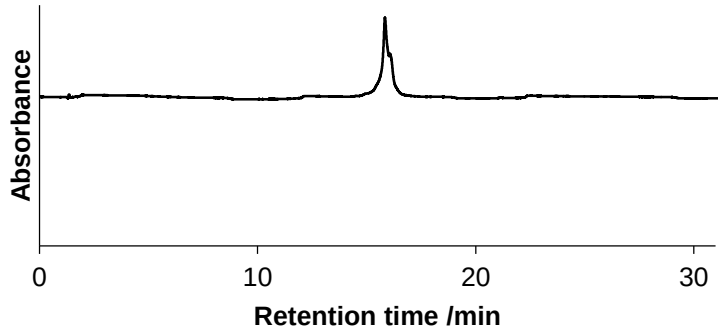

Figure 3.15: Analytical RP-HPLC chromatogram of **c-PEP1** (**28**) at 280 nm.

Figure 3.16 shows the MALDI spectrum of **c-BEP** after RP-HPLC purification: MALDI-TOF MS *m/z* 3224.7 $[M]^+$, 3225.7 $[M+H]^+$, 3246.7 $[M+Na]^+$.

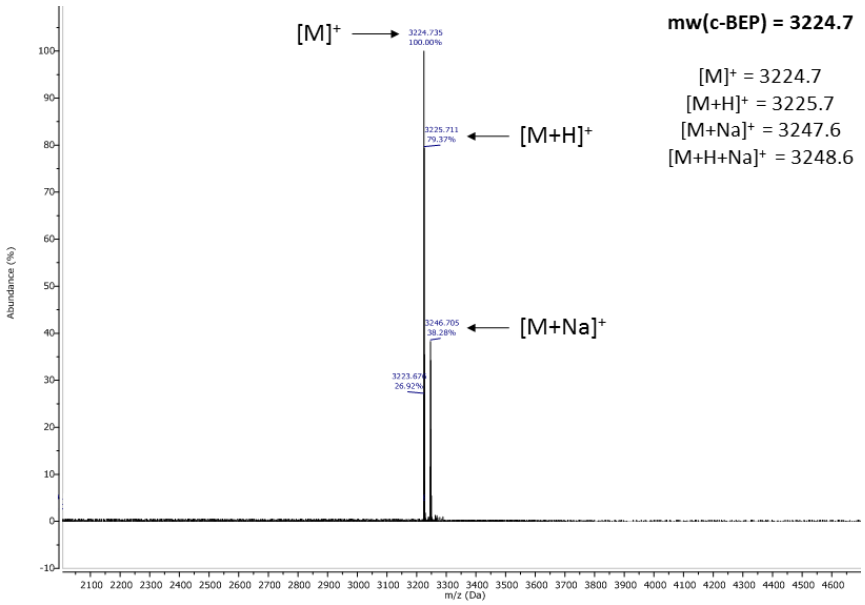

Figure 3.16: MALDI-TOF MS spectrum of **c-BEP** (**29**): CH_3O-EIAALEYENAALEQKIKALKQKIKALKQ-NH_2. The molecular weight and different ions for the possible detectable species is at the top right corner. On the spectrum, detected ions are indicated.

The analytical RP-HPLC of the pure peptide **29** using a linear gradient of 0-100% of solvent B – this being (*v/v*) 5% H_2O/95% CH_3CN with 0.1% TFA as explained in **Section 7.1.4** – over 30 min was also used to confirm the presence of a single peptide sequence, and showed a retention time at 14.68 min (**Figure 3.17**). As when comparing **25** and **28**, capping the initial **26** to convert it into **29** also makes the hydrophobicity slightly higher. However, as when comparing **25** and **26**, their analogues **28** and **29** also show the same tendency and **29** remains slightly more hydrophilic than **28**.

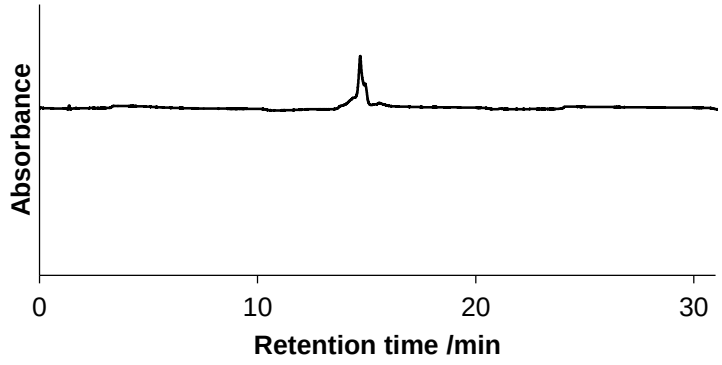

Figure 3.17: Analytical RP-HPLC chromatogram of **c-BEP** (**29**) at 280 nm.

CD analysis of the mixtures (**c-PEP1**+**c-BEP**) and (**c-PEP1**+**SAF**) showed more folding as anticipated. Measurements at 100 µM and 200 µM of the single peptides were carried out in MOPS buffer (10 mM) at pH 8.5 as to investigate the effect of the concentration on the self-assembly. However, no signs of dependence on the concentration were seen. The peptide mixtures were measured at 100 µM under the same conditions. As previously mentioned, in this section, we only show the CD spectra for 100 µM solutions of peptides **28**, **29**, **27** and their corresponding mixtures. As we chose 21 °C as the temperature conditions for our measurements, this is the temperature shown in our results. The CD spectra of the single peptides at 200 µM at pH 8.5 and 21 °C can be found in the **Appendices** together with the CD measurements of the single peptides and their mixtures at 100 µM in 10 mM MOPS at pH 8.5 and at 10 °C since coiled-coils are generally more folded at this temperature.

Figure 3.18 shows the CD spectra at room temperature (21 ˚C) of **28**, **29** and their mixture for coiled-coil formation, each of them at a concentration of 100 µM. In this case, **c-PEP1** (blue line) shows two negative bands at 208 nm and 222 nm typical of an α-helical peptide structure, with the absolute value at 208 nm slightly higher than the one at 222 nm. The same effect is observed in the CD spectrum of **c-BEP** (orange line). The dotted green line represents the average of the CD spectra of both peptides alone as a prediction for no interaction between them. When observing the CD signal of their mixture (green line), there exists a clear evidence of interaction between both of them.

The absolute value of θ_{222nm} becomes slightly higher than the one at θ_{208nm} this being a sign of α-helical coiled-coil formation.

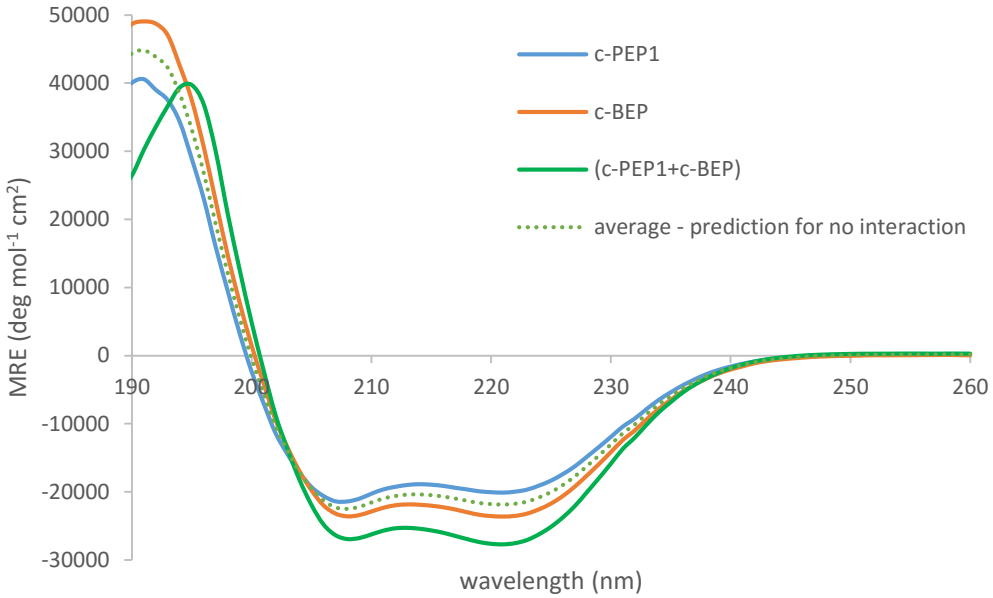

Figure 3.18: CD spectra of 100 µM solutions of **c-PEP1** (**28**), **c-BEP** (**29**) and (**c-PEP1**+**c-BEP**) (**28**+**29**) in 10 mM MOPS buffer at pH 8.5 and at 21 ˚C.

Thermal denaturation experiments were carried out to investigate the degree of thermal stability reached after coiled-coil formation. **Figure 3.19** shows an increase in the melting temperature (T_M) after mixing peptides **28** (blue line) and **29** (orange line). While T_M (**c-PEP1**) = 48.7 ˚C and T_M (**c-BEP**) = 49.4 ˚C, their mixture (green line) exhibited a T_M (**c-PEP1**+**c-BEP**) = 74.8 ˚C, which was a sign of higher thermal stability with coiled-coil formation. When looking at the curve, we found that the majority of this transition in which the initial helical structure was being disrupted happened in the range of 60 to 80 ˚C.

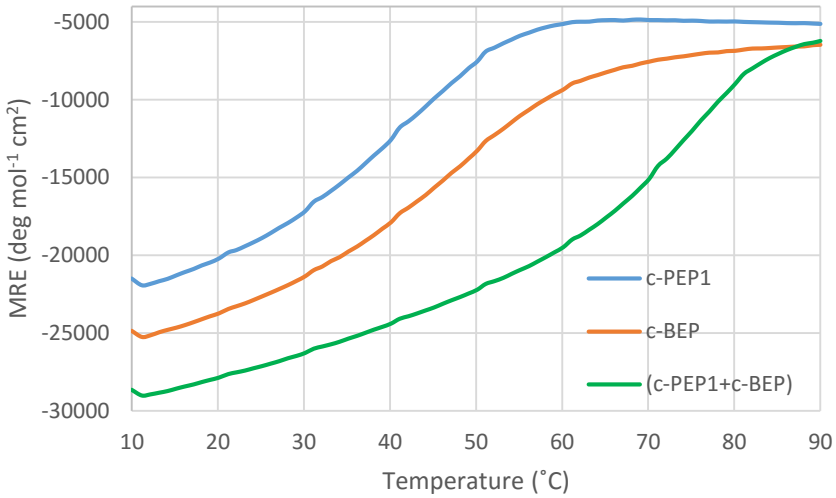

Figure 3.19: Thermal denaturation curves of 100 µM solutions of **c-PEP1** (**28**), **c-BEP** (**29**) and their mixture (**c-PEP1**+**c-BEP**) (**28**+**29**) in 10 mM MOPS buffer at pH 8.5.

Figure 3.20 shows the CD spectra at room temperature (21 ˚C) of **28**, **27** and their mixture for coiled-coil and fibre formation, each of them at individual concentrations of 100 µM. As previously seen, **c-PEP1** (blue line) showed two negative bands at 208 nm and 222 nm typical of a peptide structure with a high degree of *α*-helical content, with the absolute value at 208 nm slightly higher than the one at 222 nm. As we explained before, the CD spectrum of **SAF** (orange line) exhibited a negative band at 202 nm corresponding to the typical spectrum of a disordered structure. The dotted green line represents the average of the CD spectra of both peptides alone as a prediction for no interaction between them. Though, when observing the CD signal of the mixture (**28**+**27**) a clear evidence of interaction was seen. The association of both peptides (green line) exhibited an increase in the magnitude of the θ_{222nm} minimum in a larger magnitude that the one at θ_{208nm}. This provides a value of $\theta_{222nm}/\theta_{208nm} = 1.29$, which is indicative of the promotion of *α*-helical coiled-coil and fibre formation. In addition, the θ_{222nm} minimum showed a slight red-shift. This effect was noted in Bromley et *al*. and assigned to the chiral scattering provoked by the elongated *α*-helices into bundled fibres.[6] Moreover, this fibre formation was proved and supported by transmission electron microscopy (TEM) as showed in **Figure 3.22**.

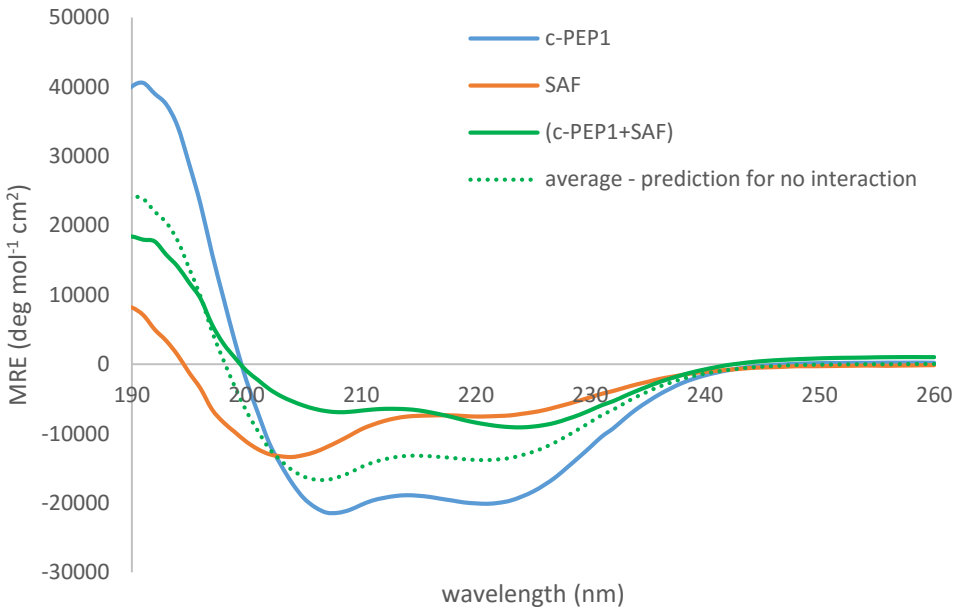

Figure 3.20: CD spectra of 100 µM solutions of **c-PEP1** (**28**), **SAF** (27) and (**c-PEP1**+**SAF**) (**28**+**27**) in 10 mM MOPS buffer at pH 8.5 and at 21 ˚C.

Figure 3.21 shows the thermal denaturation curves of 100 µM solutions of **29** (blue line), **27** (orange line) and their mixture (**27**+**29**) (green line) in 10 mM MOPS at pH 8.5. While T_M (**c-PEP1**) = 48.7 ˚C and T_M (**SAF**) = 19.7 ˚C, their mixture exhibited a slightly higher thermal stability than the individual peptides: T_M (**c-PEP1**+**SAF**) = 52.1 ˚C. The curve exhibited the largest change of this transition in the range of 35 to 55 ˚C.

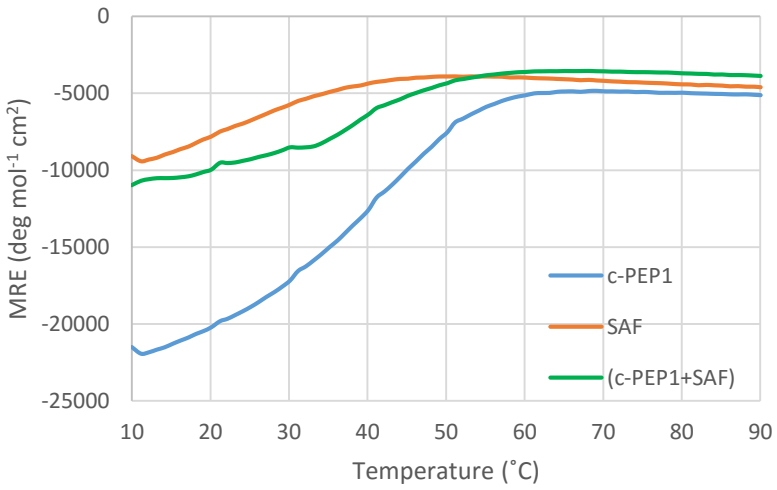

Figure 3.21: Thermal denaturation curves of 100 µM solutions of **c-PEP1** (**28**), **SAF** (**27**) and their mixture (**c-PEP1**+**SAF**) (**28**+**27**) in 10 mM MOPS buffer at pH 8.5.

Figure 3.22 shows different views and scales of the TEM spectra of (**c-PEP1**+**SAF**): Image A shows an overall view of the fibres longitudinally associated on the grid at a 10 µm scale. They look stiff thickened fibres between 6 to 36 µm length, and image B is a closer view from the fibres, at a 1 µm scale. Image C shows several of these fibres bending alongside their peptide chains at a 0.5 µm scale. Image D shows what it looks a longitudinally dimeric coiled-coil next to a higher order of fibre association which associate longitudinally (0.5 µm scale). Image E (at a 20 nm scale) shows the regular striation patterns seen for fibre formation previously reported by the Woolfson's lab,[5] which are indicative of internal organization and ultrastructure, in addition to providing information about the width of these fibres (~ 90nm). Finally, image F (at a 50 nm scale) shows the same pattern in multiple fibres that associate longitudinally.

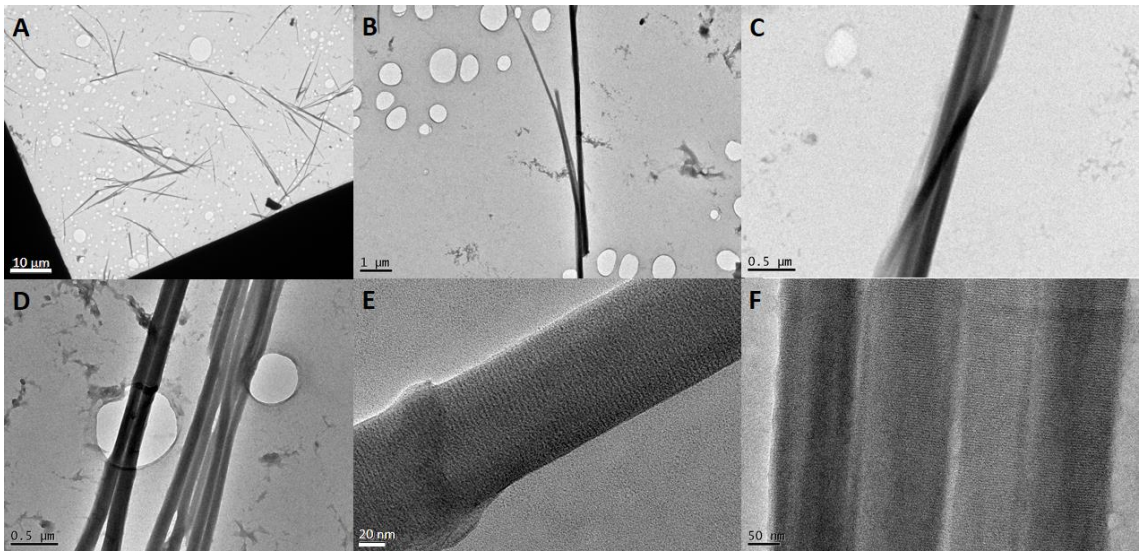

Figure 3.22: TEM spectra of (**c-PEP1**+**SAF**) (**28**+**27**) at different scales, in 10mM MOPS buffer at pH 8.5 at 21 ˚C. The image's scales range from 10 µm (in image A) to 50 nm (in image F).

Table 3.2 summarises different data obtained at pH 8.5 from peptides **28**, **29** and **27** and their mixtures (**28**+**29**) and (**28**+**27**) at 100 µM in MOPS at 21 °C. As explained, the helical contents of each peptide were calculated using the assumption that 100% helix gives a value of (-40000)*[(n-4)/n] where n is the number of residues in the peptide.[2] The percentage of helicity were calculated by using θ_{222} / [100% helix x (1-(2.57/n))].[3]

100 µM, pH 8.5	θ_{222nm}(deg mol^{-1} cm^2)	θ_{222nm}/ θ_{208nm}	% helicity	T_M (°C)
c-PEP1 (28)	-19975.2	0.93	64.1	48.7
c-BEP (29)	-23545.9	1.00	75.6	49.4
SAF (27)	-7460.8	0.67	24.0	19.7
(28+29)	-27534.7	1.02	77.7	74.8
(28+27)	-8919.9	1.29	25.2	52.1

Table 3.2: Summarised data obtained at pH 8.5 from peptides **28**, **29** and **27** and the mixtures (**28**+**29**) and (**28**+**27**) at 100 µM in MOPS at 21 °C.

Table 3.3 shows evidences of a higher folding of the peptides and peptide systems at 10 °C compared to the folding showed at 21 °C. As anticipated, the CD spectra at 10 °C can be found in the **Appendices**.

100 µM, pH 8.5	θ_{222nm} (deg mol^{-1} cm^2) 10 °C vs. 21°C	θ_{222nm}/ θ_{208nm} 10 °C vs. 21°C	% helicity 10 °C vs. 21°C
c-PEP1 (28)	-21815.0 vs. (-19975.2)	0.96 vs. 0.93	70.1 vs. 64.1
c-BEP (29)	-25155.4 vs. (-23545.9)	1.03 vs. 1.00	80.8 vs. 75.6
SAF (27)	-9348.7 vs. (-7460.8)	0.74 vs. 0.67	30.0 vs. 24.0
(28+29)	-28827.7 vs. (-27534.7)	1.04 vs. 1.02	81.3 vs. 77.7
(28+27)	-10853.7 vs. (-8919.9)	1.18 vs. 1.29	30.6 vs. 25.2

Table 3.3: Comparison of the data obtained at pH 8.5 from peptides **28**, **29** and **27** and the mixtures (**28**+**29**) and (**28**+**27**) at 100 µM in MOPS at both 10 °C and at 21 °C to show the higher folding of the structures at the lower temperature.

3.4 Summary

In this chapter we hence demonstrated the synthesis of the chassis for that our next experiments would be based on. We designed, synthesized and characterized the necessary peptide building blocks – **c-PEP1** (**28**), **c-BEP** (**29**) and **SAF** (**27**) – and successfully tested our initial aims described in **Section 3.3.1**: the formation of a blunt-ended *α*-helical coiled-coil from two individual peptides – (**c-PEP1**+**c-BEP**) or (**28**+**29**) – as well as the formation of a sticky-ended fibre assembly similar to the SAF peptides to examine whether metal-binding will affect the morphology of these fibres – this being (**c-PEP1**+**SAF**) or (**28**+**27**).

Table 3.4 summarises all the $\theta_{222nm}/\ \theta_{208nm}$ data and percentage of helicity obtained for the peptides and peptide systems at different conditions of buffer solution, pH and temperature made in this Chapter for a quicker comparison of results.

Peptide system	Buffer and pH	T (°C)	$\theta_{222nm}/\ \theta_{208nm}$	% helicity
PEP1	PBS pH 7.4	21	0.31	7.4
c-PEP1	MOPS pH 8.5	10	0.96	70.1
		21	0.93	64.1
BEP	PBS pH 7.4	21	0.67	26.4
c-BEP	MOPS pH 8.5	10	1.03	80.8
		21	1.00	75.6
SAF	PBS pH 7.4	21	0.46	10.0
	MOPS pH 8.5	10	0.74	30.0
		21	0.67	24.0
(PEP1+BEP)	PBS pH 7.4	21	0.83	37.1
(c-PEP1+c-BEP)	MOPS pH 8.5	10	1.04	81.3
		21	1.02	77.7
(PEP1+SAF)	PBS pH 7.4	21	0.41	7.2
(c-PEP1+SAF)	MOPS pH 8.5	10	1.18	30.6
		21	1.29	25.2

Table 3.4: Summary of all the peptide data obtained in this Chapter at different conditions of buffer solution, pH and temperature.

[1] M. Amblard, J.A. Fehrentz, J. Martinez, and G. Subra, *Mol. Biotechnol.* **2006**, 33, 239-254.
[2] N.R. Kallenbach and E.J. Spek, *Methods Enzymol*. **1998**, 295, 26-41.
[3] Y.H. Chen, J.T. Yang, and K.H. Chau, *Biochem*. **1974**, 13, 3350-3359.
[4] A.M. Smith, S.F.A. Acquah, N. Bone, H.W. Kroto, M.G. Ryadnov, M.S.P. Stevens, D.R.M. Walton, and D.N. Woolfson, *Angew. Chem. Int. Ed.* **2005**, 44, 325-328.
[5] D. Papapostolou, E.H.C. Bromley, C. Bano, and D.N. Woolfson, *J. Am. Chem. Soc.* **2008**, 130, 5124-5130.
[6] E.H.C. Bromley, K.J. Channon, P.J.S. King, Z.N. Mahmoud, E.F. Banwell, M.F. Butler, M.P. Crump, T.R. Dafforn, M.R. Hicks, J.D. Hirst, A. Roger, and D.N. Woolfson, *Biophys. J.* **2010**, 98, 1668-1676.

Chapter 4

Coiled-coil self-assembling peptide systems susceptible to conformational changes upon metal-binding

4.1 Design of coiled-coil assemblies susceptible to metal-binding

Our discussion in **Section 1.5.1** explained the possibility of controlling the self-assembly of peptide systems by introducing motifs within the polypeptide chains with the ability to coordinate metal ions that would bring a conformational change in the secondary structure of the system. The synthesis of pyridylalanine derivatives as unnatural amino acids (compounds **1** to **4** from **Section 2.3**) would provide a reacting site for metal-binding. We also mentioned that one of our aims is to investigate which of the effects are more important in determining the final structure: the peptide system itself (in our case, a designed α-helical coiled-coil structure) or the metal ion bound to the peptide system.

Although we successfully synthesized amino acids **1** to **4**, due to requiring a bigger mass of unnatural amino acid for automated SPPS and the laborious synthesis and work up of the products for high purity, we also obtained commercially: Fmoc-3-pyridylalanine (**2**) and Fmoc-4-pyridylalanine (**38**) amino acids (**Figure 4.1**).

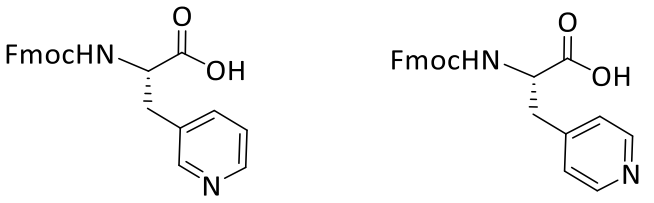

(2) **(38)**

Figure 4.1: Structures of the unnatural Fmoc-pyridylalanine amino acids purchased for automated SPPS use.

When designing the initial chassis peptide sequence **PEP1** (**25**), positions susceptible for conformational changes upon external stimulus were underlined (**Figure 3.2** and **Figure 4.2**). These correspond to positions *b*, *c* and *f* of the third and fourth heptad repeats, which are located at the hydrophilic face of the *α*-helical coiled-coil peptide structures. Since we aim to construct both blunt-ended heterodimers and sticky-end partners for fibre formation upon metal-binding and to compare these results with the initial peptide systems showed in **Section 3.3.2**, **PEP1** (**25**) is used as a template to swap either one or several of the underlined amino acids with one or several pyridylalanine amino acid derivatives. As **PEP1** did not provide stable self-assembly with **BEP** and/or **SAF** when lacking the N-acetyl and C-amide groups at the end of their peptide sequences, **c-PEP1** was used as the template instead.

Figure 4.2 shows the template or chassis sequence **c-PEP1** from which the subsequent peptide sequences susceptible for metal binding were synthesized. The names and compound numbers of these labelled peptides are shown next to the sequences, with the positions *a* to *f* of the heptads. Peptides **30** to **32** are labelled with unnatural amino acids at the indicated X positions. X = Pal = Pyridylalanine amino acid, being 3-Pal for peptides **30** to **32** and 4-Pal for peptide **33**. Their partners **29** (blunt-ended) and **27** (sticky-ended) for coiled-coil and fibre formation are also included for reference.

	gabcdefgabcdefgabcdefgabcdef
c-PEP1 (28)	CH_3O-KIAALKQKNAALKQEIAALEYEIEALEQ-NH_2
c-3PAL14 (30)	CH_3O-KIAALKQKNAALKXEIAALEYEIEALEQ-NH_2
c-3PAL10PAL14 (31)	CH_3O-KIAALKQKNXALKXEIAALEYEIEALEQ-NH_2
c-3PAL7PAL14 (32)	CH_3O-KIAALKXKNAALKXEIAALEYEIEALEQ-NH_2
c-4PAL14 (33)	CH_3O-KIAALKQKNAALKXEIAALEYEIEALEQ-NH_2
c-BEP (29)	CH_3O-EIAALEYENAALEQKIKALKQKIKALKQ-NH_2
SAF (27)	KIKALKQKIKALKQEIAALEYENAALEQ

Figure 4.2: Peptide sequences for the study of metal-binding when coiled-coil formation with X being a pyridylalanine residue.

4.2 Synthesis of peptides labelled with pyridylalanine amino acids

The synthesis of all the pyridylalanine labelled peptides **30** to **33** was fully accomplished by automated Fmoc-MW-SPPS using rink amide MBHA resin at a 0.10 mmol scale following the peptide synthesis procedure 5 from **Section 7.2.3**. **Table 4.1** shows all peaks found in the MALDI-TOF spectra of each of the pure peptides after RP-HPLC purification and the retention times found in the analytical RP-HPLC injections of the pure peptides using a linear gradient of 0-100% of solvent B (**Section 7.1.4**) over 30 min. These retention times are all slightly lower than the "template" peptide **c-PEP1** (**28**) which showed a retention time of 15.86 min. This indicates that all labelled peptides **30** to **33** are slightly more hydrophilic than **28**. The similar retention times of the labelled peptides is a sign of their similar hydrophobicity, **33** being the most hydrophobic peptide followed by **30**, then **32**, and finally **31**. From these observations we can conclude that insertion of a 4-pyridylalanine residue provokes a smaller effect with respect to decreasing the hydrophobicity of the chassis peptide (**28**) while insertion of 3-pyridylalanine residues induces a higher increase in the hydrophylicity of the peptides with respect to the original peptide sequence (**28**).

Peptide name and compound number	c-3PAL14 (30)	c-3PAL10PAL14 (31)	c-3PAL7PAL14 (32)	c-4PAL14 (33)
Molecular weight (mw)	3188.7	3265.9	3208.8	3188.7
MALDI-TOF MS (*m/z*) $[M]^+$			3208.3	
MALDI-TOF MS (*m/z*) $[M+Na]^+$	3211.8	3288.8	3231.2	3211.9
MALDI-TOF MS (*m/z*) $[M+H+Na]^+$			3232.2	
MALDI-TOF MS (*m/z*) $[M+2Na]^+$	3233.7		3254.3	
MALDI-TOF MS (*m/z*) $[M+K]^+$				3227.4
Retention time (min)	15.56	15.19	15.35	15.72

Table 4.1: Peaks found in the MALDI spectra of the pure peptides **30** to **33** after RP-HPLC purification together with their retention times after analytical RP-HPLC injections.

4.3 Formation of blunt-ended coiled-coil heterodimers

The mixture of peptides **c-PEP1** and **c-BEP** (**28**+**29**) produced blunt-ended coiled-coil heterodimers at a concentration of 100 µM in 10 mM MOPS at pH 8.5 at 21 °C. We expected to achieve the same results when mixing **c-BEP** with each one of the pyridyl-labelled peptides **30** to **33** under the same conditions. Thus, solutions of both the single peptides **29** and **30** to **33**, and their mixtures (**29**+**30**), (**29**+**31**), (**29**+**32**) and (**29**+**33**) were prepared and analysed by CD spectroscopy – and at room temperature (21 °C) as explained in **Section 3.3.2** (page 88). These results are shown and discussed next. We did not measure the CD spectra of these peptides and peptide systems at 10 °C as our measuring conditions were always room temperature because of the initial trouble we had with the temperature controller. However, as seen in **Table 3.4** from **Chapter 3**, we thought that the chassis peptides showed enough helicity at 21 °C compared to the one obtained at 10°C and this would provide reliable results.

Figure 4.3 shows the CD spectra of 100 µM solutions of **c-BEP** (**29**), **c-3PAL14** (**30**), and their mixture (**29**+**30**) in 10 mM MOPS at pH 8.5 at 21 °C. As expected, and previously seen (**Section 3.3.2**), **c-BEP** (**29**) (blue line) exhibited two negative bands at 208 nm and 222 nm. The magnitudes of their θ_{222nm} and θ_{208nm} values were very similar, producing a $\theta_{222nm}/\theta_{208nm}$ = 1.00, indicative of an α-helical conformation. The CD spectrum of **30**

(orange line) showed two negative bands at 208 nm and 222 nm with the absolute value of θ_{222nm} slightly smaller than θ_{208nm} and producing a $\theta_{222nm}/\theta_{208nm}$ = 0.91. This indicated that peptide **30** did not have a fully folded α-helical structure (39.2 %) but contained some degree of disordered forms of the peptide. The dotted green line represents the average of the CD spectra of both peptides alone as a prediction for no interaction. This line compared to the CD spectrum of the mixture (**29**+**30**) (green line) evidences signs of interaction between peptides **29** and **30**. An increase in the magnitude of the θ_{222nm} minimum produced a $\theta_{222nm}/\theta_{208nm}$ = 1.07, indicative of an increase in the α-helical content of the peptide structure (84.0 %) compared to the individual structures that **29** and **30** exhibited when alone. Therefore, we proved that the mixture (**29**+**30**) promoted the formation of α-helical coiled-coil heterodimers under these conditions.

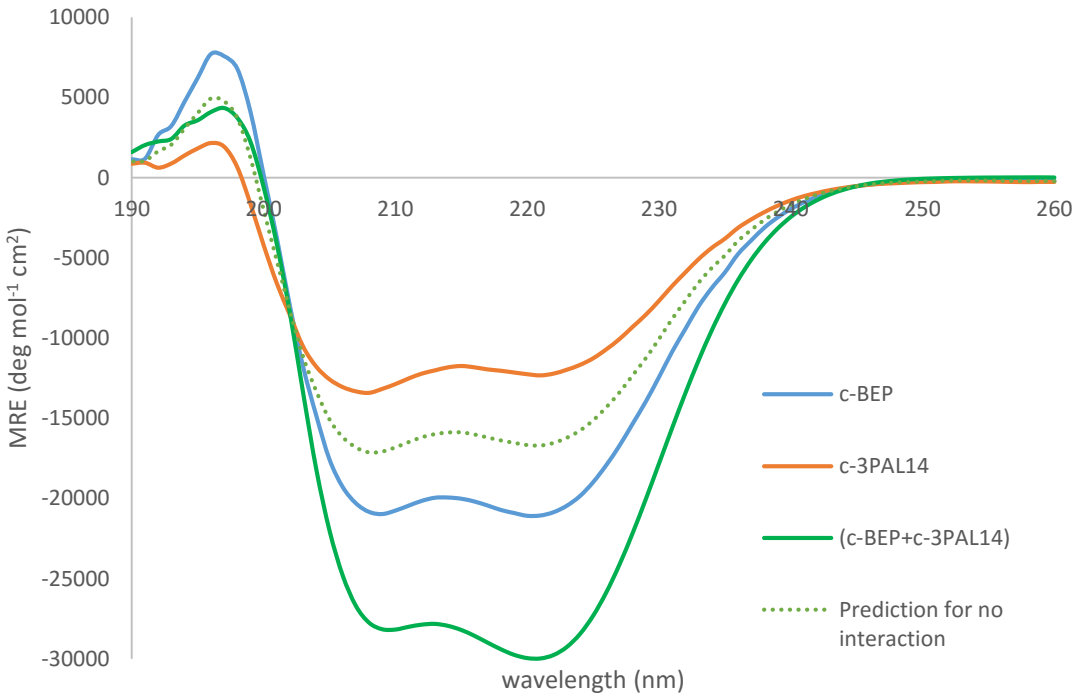

Figure 4.3: CD spectra of 100 µM solutions of **c-BEP** (**29**), **c-3PAL14** (**30**) and (**c-BEP**+**c-3PAL14**) (**29**+**30**) in 10 mM MOPS buffer at pH 8.5 at 21 ˚C. The peptide sequences are shown. **X** = 3-pyridylalanine (3-Pal)

c-BEP: Ac-EIAALEYENAALEQKIKALKQKIKALKQ-Am
c-3PAL14: Ac-KIAALKQKNAALK**X**EIAALEYEIEALEQ-Am

Figure 4.4 shows the thermal denaturation spectra recorded for the single peptides **29** and **30**, and their mixture (**29**+**30**) at a concentration of 100 µM in 10 mM MOPS at pH 8.5. Whilst peptide **29** (blue line) shows a melting temperature (T_M) of 50.6 ˚C and peptide **30** (orange line) shows a T_M (**30**) = 36.8 ˚C, the mixture of both peptides (green line) shows an important increase in this temperature (T_M = 69.1 ˚C). The melting point of the coiled-coil formed is about 20 ˚C higher than the most thermally stable of the single peptide components. We understand this effect as an increase of the thermal stability of the coiled-coil that has been formed compared to the ones for the single peptides.

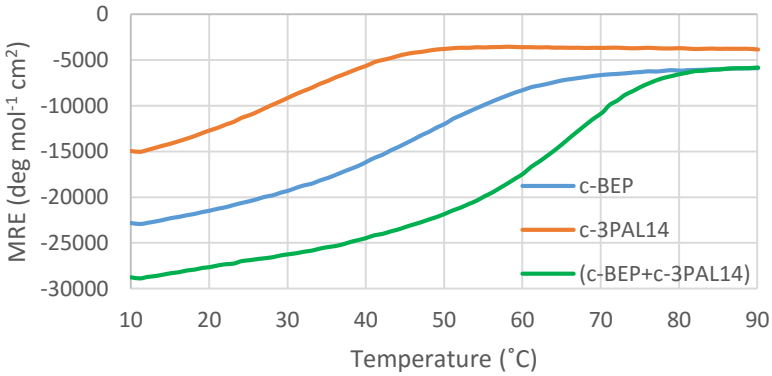

Figure 4.4: Thermal denaturation curves of 100 µM solutions of **c-BEP** (**29**), **c-3PAL14** (**30**) and (**c-BEP+c-3PAL14**) (**29**+**30**) in 10 mM MOPS buffer at pH 8.5. T_M (**c-BEP**) = 50.6 ˚C; T_M (**c-3PAL14**) = 36.8 ˚C; T_M (**c-BEP+c-3PAL14**) = 69.1 ˚C.

We then prepared 100 µM solutions of **c-BEP** (**29**), **c-3PAL10PAL14** (**31**), and their mixture (**29**+**31**) in 10 mM MOPS at pH 8.5. **Figure 4.5** shows the CD spectra of these solutions at room temperature. As previously, **29** (blue line) exhibited two negative bands at θ_{222nm} and θ_{208nm} typical of an α-helical conformation. The CD spectrum of **31** (orange line) showed two negative bands at 205 nm and 221 nm, being the absolute value of θ_{221nm} smaller than θ_{205nm}. The observed value of $\theta_{222nm}/\theta_{208nm}$ for **31** was 0.79, indicating that the structure of **31** had some degree of α-helical content (26.0 %) together with disordered forms of the peptide.

As previously, the dotted green line represents the average of the CD spectra of both peptides alone as a prediction for no interaction and the green line represents the CD spectrum of the mixture (**29**+**31**). The CD spectrum of the mixture evidenced signs of

interaction between peptides as an increase in the magnitude of the θ_{222nm} minimum was observed. This became slightly bigger than the magnitude of the θ_{208nm} minimum, producing a $\theta_{222nm}/\theta_{208nm}$ = 1.06, which was indicative of an increase in the α-helical content of the coiled-coil (67.2 %). As for the previous mixture (**29**+**30**), (**29**+**31**) was also able to promote the formation of α-helical coiled-coil under these conditions.

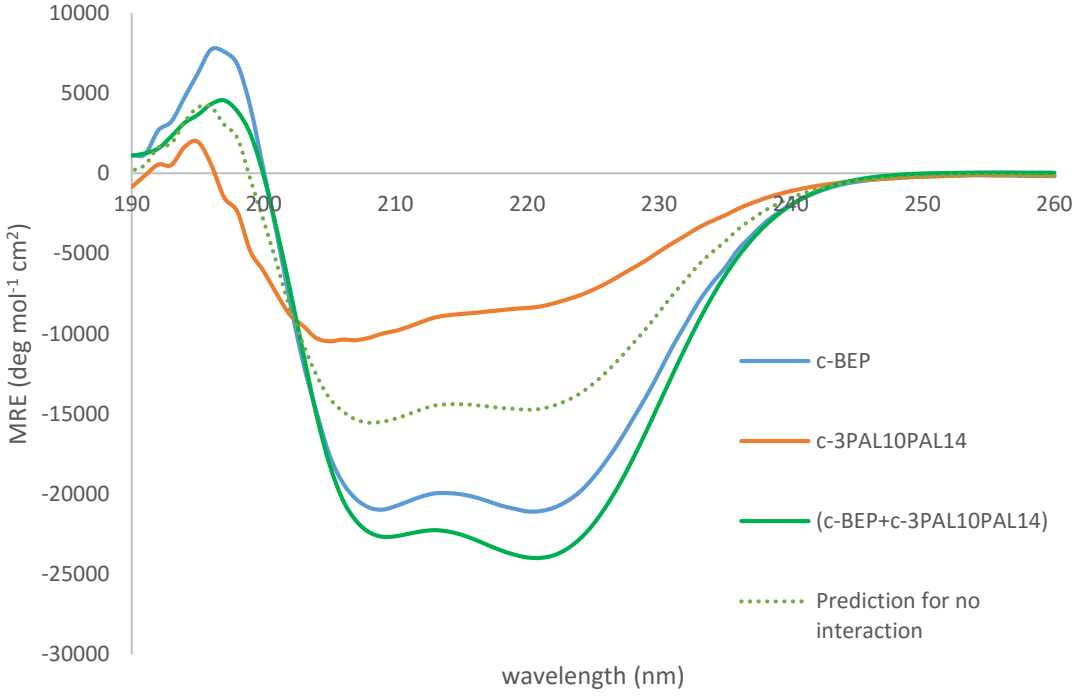

Figure 4.5: CD spectra of 100 µM solutions of **c-BEP** (**29**), **c-3PAL10PAL14** (**31**) and (**c-BEP+c-3PAL10PAL14**) (**29**+**31**) in 10 mM MOPS buffer at pH 8.5 at 21 ˚C. The peptide sequences are shown. **X** = 3-Pal:

c-BEP: Ac-EIAALEYENAALEQKIKALKQKIKALKQ-Am
c-3PAL10PAL14: Ac-KIAALKQKN**X**ALK**X**EIAALEYEIEALEQ-Am

The thermal denaturation curve of (**29**+**31**) (**Figure 4.6**) demonstrated an increase in the thermal stability of the peptide mixture compared to the ones exhibited by the individual peptides. The recorded melting temperatures were: T_M (**29**) = 50.6 ˚C (blue line); T_M (**31**) = 29.2 ˚C (orange line); and T_M (**29**+**31**) = 66.6 ˚C (green line). This indicated a large increase in the thermal stability of the peptide structure after coiled-coil formation compared to the thermal stability shown by the individual peptides.

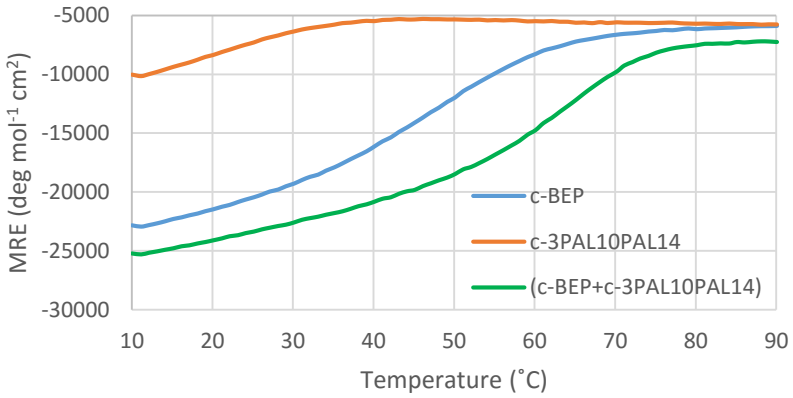

Figure 4.6: Thermal denaturation curves of 100 µM solutions of **c-BEP** (**29**), **c-3PAL10PAL4** (**31**) and (**c-BEP+c-3PAL10PAL14**) (**29**+**31**) in 10 mM MOPS buffer at pH 8.5. T_M (**c-BEP**) = 50.6 ˚C; T_M (**c-3PAL10PAL14**) = 29.2 ˚C; T_M (**c-BEP+c-3PAL10PAL14**) = 66.6 ˚C.

The CD analysis at room temperature of 100 µM solutions of **c-BEP** (**29**), **c-3PAL7PAL14** (**32**), and their mixture (**29**+**32**) in 10 mM MOPS at pH 8.5 is shown in **Figure 4.7**. From the previous experiments, we knew that **29** (blue line) was *α*-helical. The CD spectrum of **32** (orange line) showed two negative bands at 205 nm and 222 nm, very similar to the CD spectrum of peptide **31**. Though, these bands produced a smaller $\theta_{222nm}/\theta_{208nm}$ (0.72) than the observed for **31**. This indicated a decrease in the *α*-helical content of **32** compared to **30** and **31**. From this observations, we concluded that the insertion of two pyridylalanine residues within the sequence decreased the *α*-helical content (17.2 %) with respect to the original peptide **28** (64.1 %). Moreover, the longer the distance between the unnatural amino acids in the sequence (*i* → *i*+7 in this case), the higher the decrease of *α*-helicity in the peptide structure. However, this was found for the single peptides and we were investigating the interaction with the blunt-ended partner to form *α*-helical coiled-coils.

The dotted green line represents the average of the CD spectrum of **29** and **32** as a prediction for no interaction whilst the green line represents the CD spectrum of the interaction produced by the mixture (**29**+**32**). When observing the CD spectrum of the mixture, signs of interaction were identified by an increase in the magnitude of the θ_{222nm} minimum becoming this slightly bigger than the magnitude of θ_{208nm}. The formation of the coiled-coil produced a $\theta_{222nm}/\theta_{208nm}$ = 1.09 (77.7 % helicity), indicating that the interaction between **29** and **32** promoted *α*-helical coiled-coil formation.

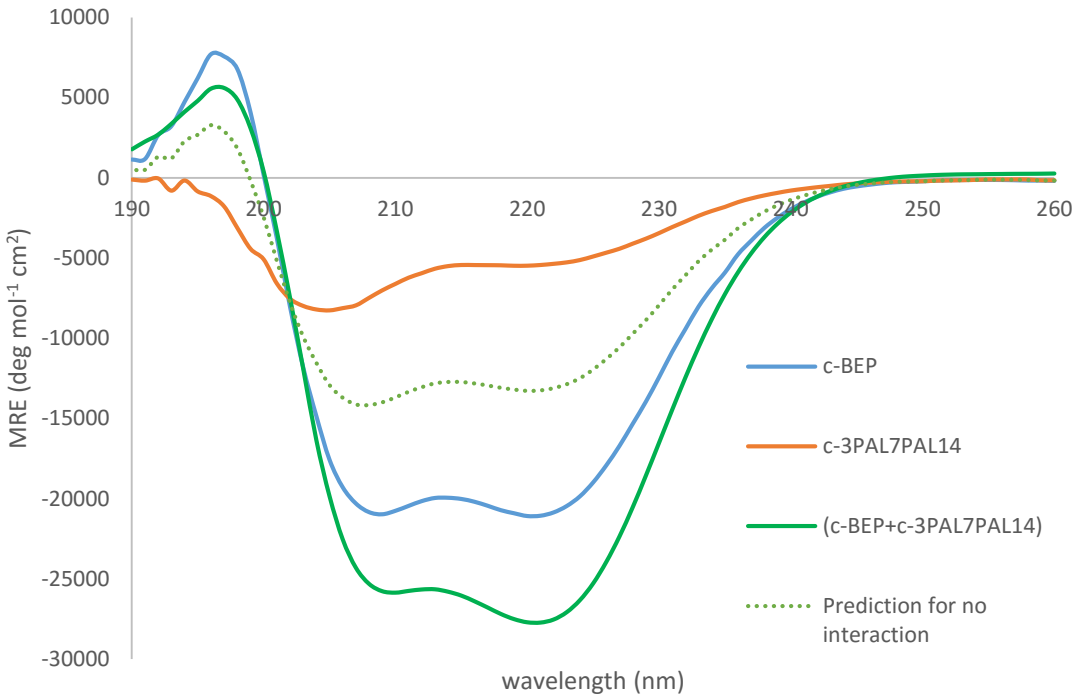

Figure 4.7: CD spectra of 100 µM solutions of **c-BEP** (**29**), **c-3PAL7PAL14** (**32**) and (**c-BEP**+**c-3PAL7PAL14**) (**29**+**32**) in 10 mM MOPS buffer at pH 8.5 at 21 ˚C. The peptide sequences are shown. **X** = 3-Pal

c-BEP: Ac-EIAALEYENAALEQKIKALKQKIKALKQ-Am
c-3PAL7PAL14: Ac-KIAALK**X**KNAALK**X**EIAALEYEIEALEQ-Am

Figure 4.8 shows the thermal denaturation of **29** (blue line), **32** (orange line), and their mixture (**29**+**32**) (green line) at a concentration of 100 µM in MOPS (10 mM) at pH 8.5. As previously, T_M (**29**) = 50.6 ˚C. The software used to obtain the T_M of each of our peptides or peptide mixtures was unable to provide us with a T_M value for **32** due to the shape of its melting curve. Thus, we estimated a value lower than 25 ˚C since we guessed a transitional change between 10 ˚C and 35 ˚C (orange line). This temperature was lower than the one found for peptide **31**: T_M (**31**) = 29.2 ˚C. When comparing peptides **31** and **32**, we found that the thermal stability of **31** was higher than the one of **32**: T_M (**31**) > T_M (**32**). We also saw that the secondary structure of **32** was slightly less α-helical than the found for **31** (17.2% vs. 26.0%). From these observations, we concluded that the higher degree of α-helicity in a single peptide the higher their thermal stability. For the mixture (**29**+**32**) we found a T_M = 66.8 ˚C, being this value very similar to the T_M obtained for the mixture (**29**+**31**) (66.6 ˚C). This evidenced an important increase in the melting point with respect to the structure shown by the

individual peptides, indicating a large increase of the thermal stability after coiled-coil formation.

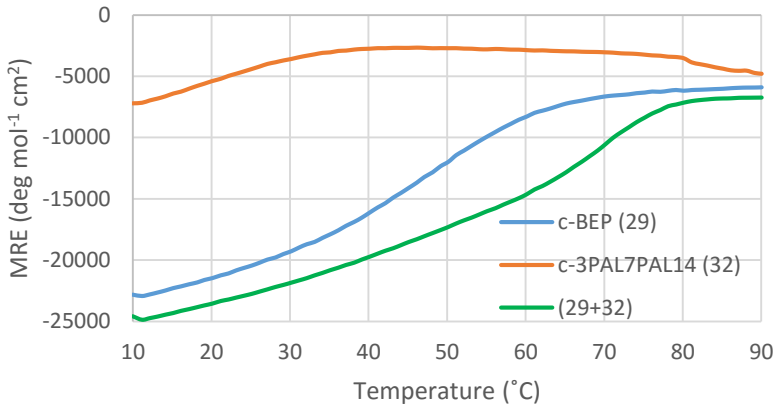

Figure 4.8: Thermal denaturation curves of 100 µM solutions of **c-BEP** (**29**), **c-3PAL7PAL4** (**32**) and (**c-BEP**+**c-3PAL7PAL14**) (**29**+**32**) in 10 mM MOPS buffer at pH 8.5. T_M (**c-BEP**) = 50.6 ˚C; T_M (**c-3PAL7PAL14**) < 25 ˚C; T_M (**c-BEP+c-3PAL7PAL14**) = 66.8 ˚C.

Figure 4.9 shows the CD analysis at room temperature of 100 µM solutions of **c-BEP** (**29**), **c-4PAL14** (**33**), and their mixture (**29**+**33**) in 10 mM MOPS at pH 8.5. Peptide **29** (blue line) was α-helical. The CD spectrum of **33** (orange line) showed two negative bands at 205 nm and 222 nm, with the absolute value of θ_{222nm} smaller than θ_{205nm}. This indicated that **33** could have some α-helical content (32.3 %) together with a random conformation structure. The dotted green line represents the average of the CD spectra of both peptides alone as a prediction for no interaction between them. When we measured the CD spectrum of the mixture (**29**+**33**) (green line), signs of interaction between both peptides were observed. The absolute value of θ_{222nm} became slightly bigger than the corresponding at θ_{208nm}. This produced a $\theta_{222nm}/\theta_{208nm}$ = 1.04, a sign of α-helical coiled-coil formation.

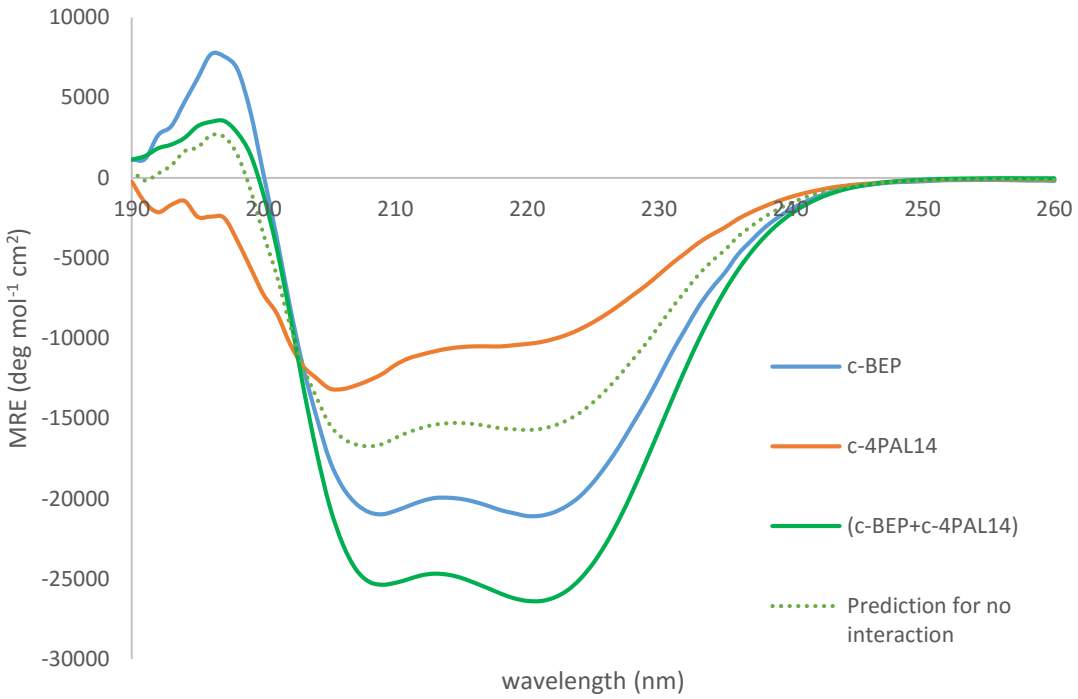

Figure 4.9: CD spectra of 100 µM solutions of **c-BEP** (**29**), **c-4PAL14** (**33**) and (**c-BEP+c-4PAL14**) (**29+33**) in 10 mM MOPS buffer at pH 8.5 at 21 ˚C. The peptide sequences are shown. **X** = 4-Pal

c-BEP: Ac-EIAALEYENAALEQKIKALKQKIKALKQ-Am
c-4PAL14: Ac-KIAALKQKNAALK**X**EIAALEYEIEALEQ-Am

Figure 4.10 shows the thermal denaturation spectra recorded for **29** (blue line), **33** (orange line), and their mixture (**29+33**) (green line) at a concentration of 100 µM in 10 mM MOPS 10 mM at pH 8.5. We knew that T_M (**c-BEP**) = 50.6 ˚C. Peptide **33** showed a T_M of 31.1 ˚C which was slightly lower than the analogous peptide **30**. In principle, and from this data, we could say that our labelled peptide including 3-pyridylalanine was more thermally stable than when including 4-pyridylalanine. The mixture of **29** and **33** recorded a T_M (**29+33**) = 68.0 ˚C. This indicated that there was an increase of the thermal stability after coiled-coil formation. Thought, T_M (**29+30**) = 69.1 showed a slightly higher melting point than the mixture formed by **29** and **33**. From this fact we believed that the insertion of the unnatural amino acid 3-pyridylalanine within the peptide sequence produced a slightly higher thermal stability than when inserting the 4-pyridylalanine analogue.

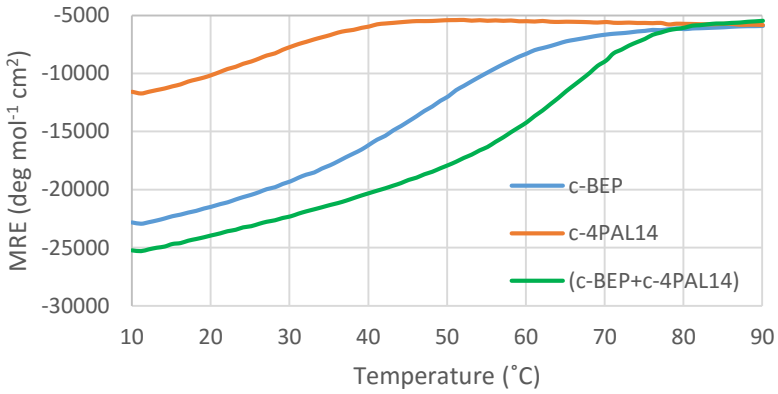

Figure 4.10: Thermal denaturation curves of 100 µM solutions of **c-BEP** (**29**), **c-4PAL4** (**33**) and (**c-BEP+c-4PAL14**) (**29**+**33**) in 10 mM MOPS buffer at pH 8.5. T_M (**c-BEP**) = 50.6 ˚C; T_M (**c-4PAL14**) = 31.1 ˚C; T_M (**c-BEP+c-4PAL14**) = 68.0 ˚C.

All combinations of **c-BEP** (**29**) with each of the pyridyl-labelled peptides (**30** to **33**) exhibited signs of coiled-coil formation (**Figures 4.3**, **4.5**, **4.7** and **4.9**). In all cases, the magnitude of their θ_{222nm} minimums in the mixtures increased, becoming slightly bigger than the magnitudes at θ_{208nm}. This produced values of $\theta_{222nm}/\theta_{208nm}$ higher than 1.00 in all cases, evidencing an increase in the α-helical content – with respect to the individual peptides – and promoting coiled-coil formation. When observing the thermal denaturation curves of each of the mixtures in **Figures 4.4**, **4.6**, **4.8** and **4.10**, signs of interaction between the individual peptides to form self-assembled systems were observed by an increase of their T_M. These temperatures increased in about 20 ˚C compared to the most thermally stable peptide component (**c-BEP** in all cases), and between 30 ˚C and 40 ˚C compared to the least thermally stable peptide component (the pyridyl-labelled peptides in all cases).

Despite achieving what we considered good results as to carry on with our research, we wondered whether these peptide mixtures would be able to form blunt-ended coiled-coils at a near-physiological pH. Therefore, we prepared the same peptide solutions at 100 µM in 10 mM MOPS at pH 7.2 and observed their CD spectra at room temperature (21 °C). We saw that coiled-coils were also able to form at this pH. The values produced for the $\theta_{222nm}/\theta_{282nm}$ coefficients were always equal or higher than 1.00 as a sign of α-helical content. When running thermal denaturation experiments of the mixtures at this pH, evidences of interaction between peptides were observed by

an increase in the thermal stability of each of the peptide mixtures. Their T_M values increased in about 30 ˚C with respect to the T_M that the individual peptides exhibited. These spectra and the data obtained with these peptide systems are shown in the **Appendices** in **Figures A4.1** to **A4.8** together with a table (**Table A4.1**) summarising some peptide data obtained at these conditions at pH (7.2) compared to the same type of peptide data obtained at pH 8.5.

Table 4.2 shows the obtained data of 100 µM solutions of all the individual peptides and peptide systems of this **Section 4.3** at pH 8.5 and at 21 °C. These data consists of: ellipticity at 222 nm (θ_{222}), the ellipticity ratio between 222 nm and 208 nm ($\theta_{222}/\theta_{208}$), the percentage of helicity, and the melting temperature (T_M).

Peptide or peptide systems	θ_{222} (deg mol^{-1} cm^2)	$\theta_{222nm}/\theta_{208nm}$	% helicity	T_M (°C)
c-BEP (29)	-20860.2	1.00	67.0	50.6
c-3PAL14 (30)	-12216.4	0.91	39.2	36.8
c-3PAL10PAL14 (31)	-8107.6	0.79	26.0	29.2
c-3PAL7PAL14 (32)	-5356.7	0.72	17.2	< 25
c-4PAL14 (33)	-10045.1	0.80	32.3	31.1
(29+30)	-29760.4	1.07	84.0	69.1
(29+31)	-23813.6	1.06	67.2	66.6
(29+32)	-27542.0	1.09	77.7	66.8
(29+33)	-26179.5	1.04	73.9	68.0

Table 4.2: Peptide data obtained for 100 µM solutions of **c-BEP** (**29**), the labelled peptides (**30** to **33**) and the peptide mixtures of **29** with each one of the labelled peptides in 10 mM MOPS at pH 8.5 at 21 °C.

4.3.1 Metal-binding experiments on the blunt-ended peptide systems

After examining the effects of the interaction between the pyridyl-labelled peptides **30** to **33** and the blunt-ended partner **29**, we wanted to investigate whether the addition of a metal complex to the blunt-ended coiled-coil peptide systems from **Section 4.3** could provide any conformational changes in their secondary structures. Since the pyridyl groups are soft ligands, we needed to find a soft metal to match, as described by the soft-hard theory of ligand-metal coordination: soft ligands (e.g. pyridyl or thiol

groups) bind relatively strongly to soft metals (e.g. Pt, Au, etc). We also saw how Mikhail Tsurkan had successfully used platinum complexes to bind pyridyl amino acids in previous investigations.[1,2,3] Thus, we decided to use a Pt(II) complex (K_2PtCl_4) in order to check the effects in the α-helical coiled-coil structures that we had formed. The platinum complex was completely soluble in the buffer solution used to record all the CD measurements, this is 10 mM MOPS at pH 8.5.

We then prepared 100 μM solutions of **29** to **33** and the corresponding mixtures of **29** with each one of them in 10 mM MOPS at pH 8.5. Several CD measurements of these peptide mixtures were recorded for a period of time where no spectral changes were observed after 48 hours. Thus, after incubation of the peptide systems for this period of time, volumes of 100 μL of a 100 μM solution of the metal complex were added into each one of the peptide mixtures, producing a total concentration of 66.7 μM. An initial CD measurement of the metal-peptide system was recorded and the evolution of these metal-peptide mixtures was monitored. Since we did not observe significant conformational changes in the CD spectra after 40 to 45 hours, 45 hours was the final recorded time. We thought that evaporation effects on the metal-peptide mixture provoked smooth differences in the CD signals. Thermal denaturation experiments of the metal-peptide systems were recorded and their thermal stability compared with the peptide systems without the metal additions.

Figure 4.11 shows the CD spectrum of the mixture (**29**+**30**) 48 hours later of being prepared (red line). The interaction between peptides exhibited a coiled-coil structure with certain degree of α-helical content as determined by their $\theta_{222nm}/\theta_{208nm}$ = 1.07 in this case. Upon the addition of the Pt(II) complex, no significant changes in the CD spectra were observed. An initial measurement showed a $\theta_{222nm}/\theta_{208nm}$ = 1.08, indicating that the degree of α-helical content in the type of structure generated remained similar (purple line). We did not observe significant conformational changes after 45 hours (green line). The addition of the metal complex to the peptide structure did not trigger any conformational change in the secondary structure, indicating that metal-binding is compatible with coiled-coil formation. We thought, therefore, that the peptide system was energetically more favourable in the initial conformation and

that the peptide assembly was the driving force to dictate the conformation of the system.

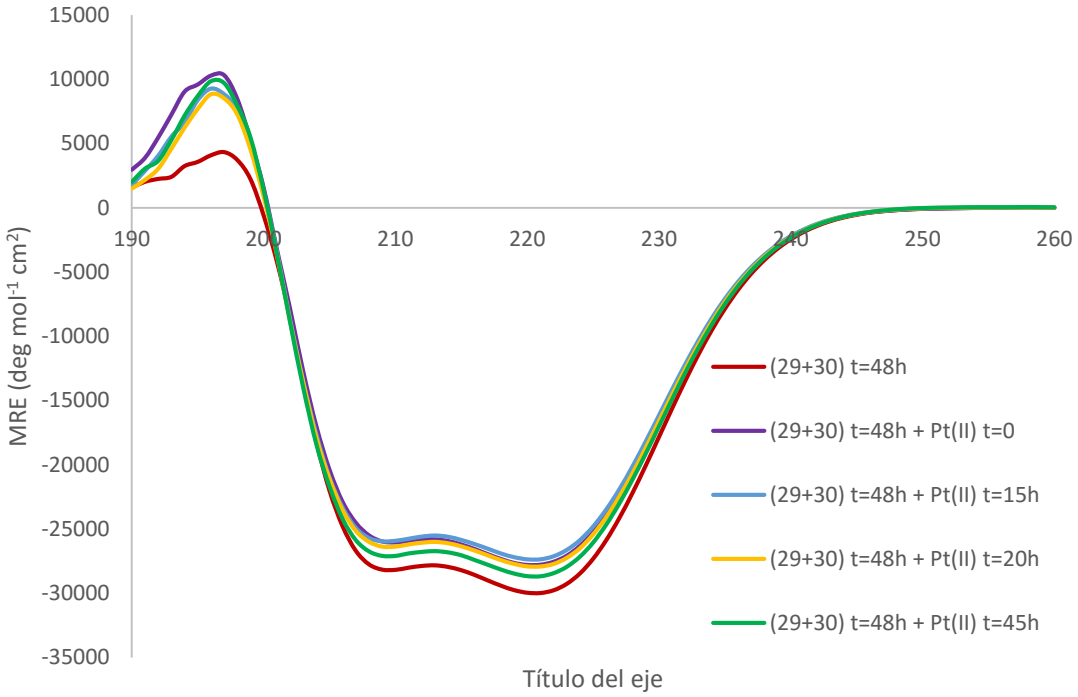

Figure 4.11: CD measurements of 100 µM (**c-BEP**+**c-3PAL14**) (**29**+**30**) in 10 mM MOPS at pH 8.5 at 21 ˚C and the metal-binding effects after addition of K_2PtCl_4.

Figure 4.12 shows the thermal denaturation curves 100 µM solutions of **29** (blue line), **30** (orange line), (**29**+**30**) (green line) and the metal-peptide mixture (**29**+**30**+**Pt(II)** (yellow line) in 10 mM MOPS at pH 8.5. The melting points seemed to be similar for the peptide mixtures before and after the addition of the metal complex, with T_M (**29**+**30**+**Pt(II)**) = 70.2 ˚C, this being indicative that metal-binding did not create conformational changes as previously mentioned.

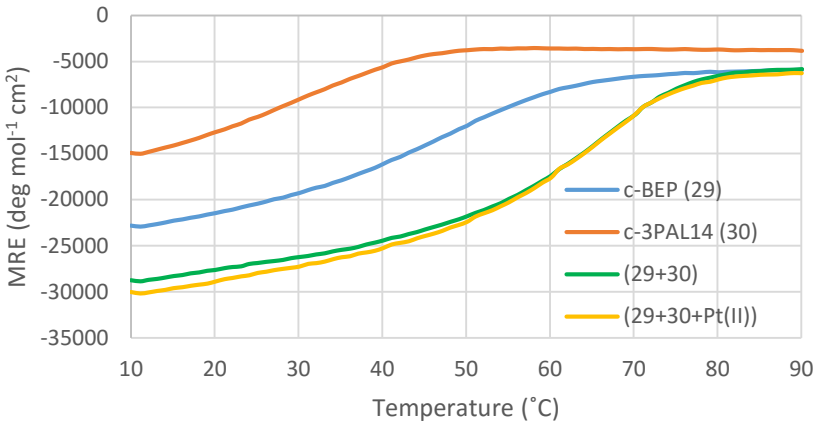

Figure 4.12: Thermal denaturation curves of 100 µM solutions of **c-BEP** (**29**), **c-3PAL14** (**30**), their mixture (**29**+**30**) and the mixture with K_2PtCl_4 (**29**+**30**+Pt(II)) in 10 mM MOPS buffer at pH 8.5. T_M (**29**) = 50.6 ˚C; T_M (**30**) = 36.8 ˚C; T_M (**29**+**30**) = 69.1 ˚C; T_M (**29**+**30+Pt(II)**) = 70.2 ˚C.

Figure 4.13 shows the CD spectra of the metal-binding experiments of the remaining 100 µM peptide mixtures of **29** with **31**, **32** and **33**. This exhibited the same tendency as the mixture (**29**+**30**) upon metal-binding with the Pt(II) complex: no significant conformational changes were observed. These spectra together with their thermal denaturation experiments can be found in the **Appendices** (**Figures A4.9** to **A4.14**).

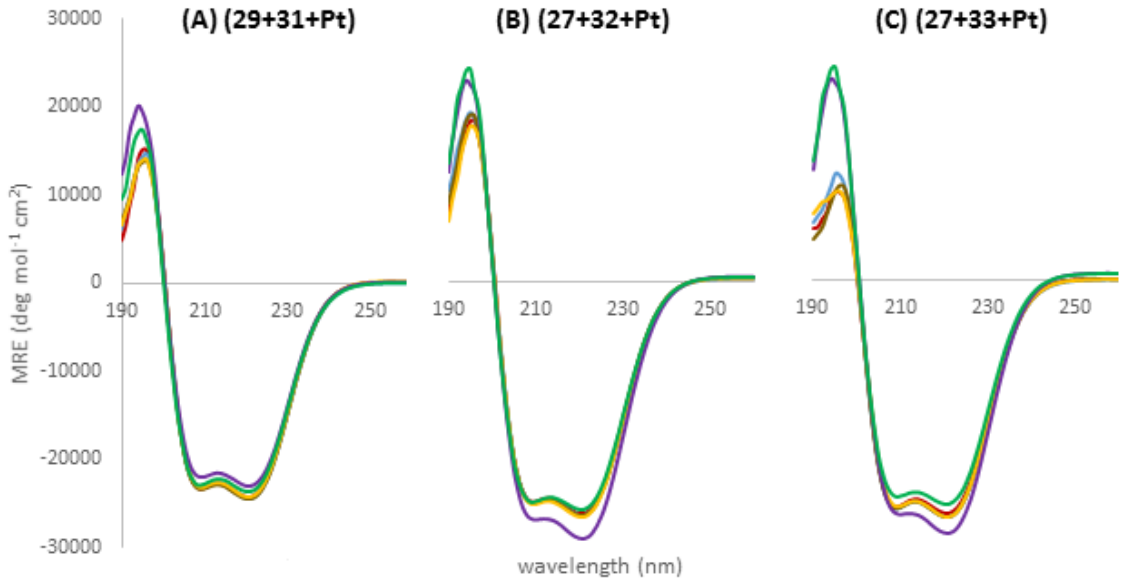

Figure 4.13: CD spectra of 100 µM solutions in 10 mM MOPS at pH 8.5 and at 21 ˚C of (A) (**29**+**31**); (B) (**29**+**32**); and (C) (**29**+**33**), and their metal-binding experiments with K_2PtCl_4. The red lines represent the first CD measurement of the peptide mixtures after being incubated for 48 hours. The purple lines represent the CD measurements in the initial time of the Pt(II) addition, the blue lines after 15 hours, the yellow lines after 20 hours, and the green lines after 45 hours.

Table 4.3 shows the T_M of the 100 μM solutions of the metal-peptide systems in 10 mM MOPS at pH 8.5 before and after the addition of the metal complex to demonstrate that metal-binding did not create conformational changes that affected their thermal stability.

Peptide system	T_M (˚C)	Peptide system (metal-binding)	T_M (˚C)
(29+30)	69.1	**(29+30+Pt)**	70.2
(29+31)	66.6	**(29+31+Pt)**	65.0
(29+32)	66.8	**(29+32+Pt)**	70.7
(29+33)	68.0	**(29+33+Pt)**	68.5

Table 4.3: T_M 100 μM solutions in MOPS at pH 8.5 of each one of the peptide systems of **c-BEP** (**29**) with the pyridyl labelled peptides (**30** to **33**) before and after metal-binding the Pt(II) complex.

The metal-peptide mixtures were also prepared at a concentration of 50 μM in 10 mM MOPS at pH 8.5 and their CD spectra recorded at 21 ˚C. This was measured only to test whether the concentration could affect the metal-binding in these type of peptide structures. However, the same behaviour as for the samples at 100 μM was found and no signs of concentration dependency was observed. Since the CD spectra recorded for the last hours did not show any significant conformational changes, the incubating times for these peptide mixtures was reduced. These CD spectra can be found in the **Appendices** (**Figures A4.15** to **A4.18**) and the incubating times indicated.

As a conclusion from all these set of metal-binding experiments with the blunt-ended coiled-coil heterodimers, we found that the peptide assemblies dictated the final structure of the peptide system and the addition of the Pt-complex did not appear to trigger any conformational change. The assembly provided by the association between peptides may be more energetically favourable than the possible structure produced by a conformational switch induced by the metal ion. All the peptide systems were more thermally stable after coiled-coil formation than the individual peptides as indicated by their T_M. In addition, the T_M of the metal-peptide structures exhibited a similar value to the one shown by the peptide structures without the metal additions.

4.4 Formation of sticky-ended coiled-coils

Similar to what we achieved in **Section 4.3**, we wanted to test whether the pyridyl-labelled peptides **30** to **33** – which were modifications of the **c-PEP1** (**28**) sequence – were able to interact with **SAF** (**27**) as sticky-ends heterodimers and form fibres in the same mode as the mixture (**28**+**27**) was able to achieve it. The peptide mixtures to test for fibre formation were as follows: (**27**+**30**), (**27**+**31**), (**27**+**32**) and (**27**+**33**). These were prepared at a concentration of 100 µM in 10 mM MOPS at pH 8.5 and at 21 °C (room temperature) and their CD spectra are discussed next. However, to avoid having many spectra lines within the same figures, here we only show the CD spectra of the peptide mixtures and their evolution with the time. The last recorded time was 24 hours in all cases as this was the time when the peptide mixtures stopped exhibiting significant conformational changes. The CD spectra of the individual peptides prior to the mixture and after being mixed at both the initial time and after incubation for 24 hours are shown in the **Appendices** in **Figures A4.19** to **A4.22**.

Figure 4.14 shows the CD measurements of a 100 µM solution of (**27**+**30**) in 10 mM MOPS at pH 8.5 at different intervals of time for 24 hours. The evolution of the CD signal obtained over time is prominent. From these results, we concluded that the fibrillogenesis process was time dependent. Thus, when observing the CD spectrum of the mixture at an initial time (red line), the magnitude of the θ_{222nm} and θ_{208nm} minimums indicated the formation of a partially folded α-helical structure together with some degree of random coiled-coil. Within the first two hours (yellow line) the CD spectrum became completely α-helical, showing a $\theta_{222nm}/\theta_{208nm} = 1.17$, typical of an α-helical coiled-coil structure with promotion to form fibres. After 8 hours (blue line), the tendency continued exhibiting a larger decrease in the magnitude of the θ_{208nm} minimum and a red shift of the band at θ_{222nm}. As previously discussed in **Section 3.3.2**, this effect had already been visualized by Bromley *et al*.[4] and was assigned to the chiral scattering provoked by the helices bundling in the fibres. After 20 hours, the change in spectrum became less noteworthy, with 24 hours being the last measurement time (green line) ($\theta_{222nm}/\theta_{208nm} = 1.40$).

After leaving the mixture (**27**+**30**) to mature the fibres for 24 hours, they had thicken and lengthen enough to be clearly detected by CD spectroscopy. We were also able to see by eye the formation of a blurred white precipitated within the cuvette. The appearance of these aggregates were not visible in the initial solution mixtures which appeared to be transparent. **Figure 4.15** shows a fresh prepared mixture of (**27**+**30**) at 100 µM in MOPS at pH 8.5 compared to a three days old mixture of a 100 µM mixture of (**27**+**30**) at the same conditions of pH.

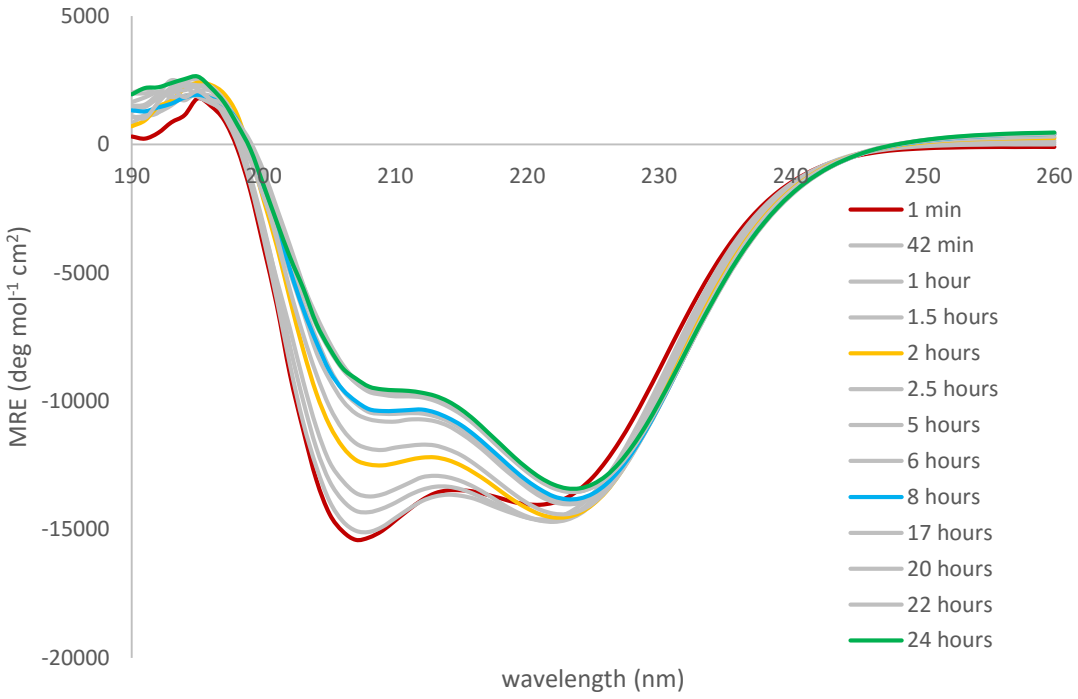

Figure 4.14: CD measurements at different times for a period of 24 hours of 100 µM (**SAF**+**c-3PAL14**) (**27**+**30**) in 10 mM MOPS buffer at pH 8.5 at 21 ˚C. The peptide sequences are shown. **X** = 3-Pal

SAF:	Ac-KIKALKQKIKALKQEIAALEYENAALEQ-Am
c-3PAL14:	Ac-KIAALKQKNAALK**X**EIAALEYEIEALEQ-Am

Figure 4.15: Visual comparison of 100 µM solutions of (**SAF**+**c-3PAL14**) (**27**+**30**) in 10 mM MOPS buffer at pH 8.5 at 21 ˚C at different times of their maturing process: just prepared sample at the left hand side vs a three-days old sample.

We found that incubating a 100 µM solution of the mixture (**27**+**30**) for 24 hours was enough to observe the formation of both *α*-helical coiled-coils and fibrous structures that could be detected by CD spectroscopy. Thus, we decided to use the same conditions in each of the remaining mixtures of the pyridyl-labelled peptides (**31**, **32** and **33**) with the **SAF** partner (**27**) and check whether they were also able to provide similar results.

Figure 4.16 shows the CD measurements of a 100 µM solution of (**27**+**31**) in MOPS at pH 8.5 recorded at different times for 24 hours. The mixture (**27**+**31**) did not show a fully folded *α*-helical coiled-coil pattern. The magnitude of the θ_{222nm} minimum was never able to reach the same or a higher value than the negative band at θ_{208nm}. Neither the freshly prepared sample (red line) nor the incubated sample after one day (green line) exhibited signs of *α*-helical coiled-coil formation or fibre formation by CD spectroscopy. However, as in the previous mixture of (**27**+**30**), a slightly blurred aggregation was observed within the cuvette after one day. Though, this was a tiny part of the total volume of the cuvette and stayed at the edge. We believed that this could be due to evaporation and the loss of this tiny volume from solution produced a reduction in the absolute signal of the CD spectrum.

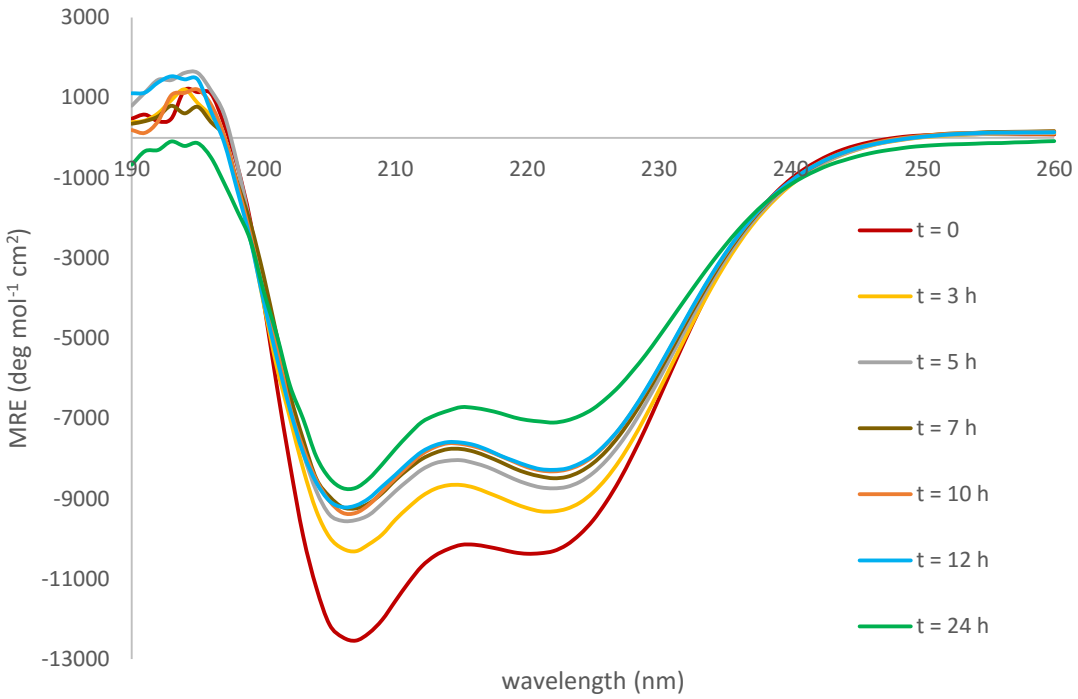

Figure 4.16: CD measurements at different times for a period of 24 hours of a 100 µM solution of (**SAF+c-3PAL10PAL14**) (**27+31**) in 10 mM MOPS buffer at pH 8.5 at 21 ˚C. The peptide sequences are shown. **X** = 3-Pal

SAF: Ac-KIKALKQKIKALKQEIAALEYENAALEQ-Am
c-3PAL10PAL14: Ac-KIAALKQKN**X**ALK**X**EIAALEYEIEALEQ-Am

We next prepared and investigated the mixture (**27**+**32**) at a concentration of 100 µM in 10 mM MOPS at pH 8.5. The results obtained by CD spectroscopy are shown in **Figure 4.17**. In this case, the initial sample recorded a spectrum that was not fully folded as an α-helical coiled-coil structure (red line). The magnitude of the negative band at θ_{222nm} was of a lower absolute value than the one at θ_{208nm}, showing an initial $\theta_{222nm}/\theta_{208nm}$ = 0.91. However, different measurements at different times in a total time of 24 hours exhibited a conformational change in the peptide structure by CD spectroscopy. As time increased, we believed that the peptide system was evolving to the formation of both α-helical coiled-coils and fibres. The green line shows the CD spectrum recorded 24 hours later than having prepared the peptide mixture. The negative band at 222 nm was then of a higher magnitude than the band at 208 nm, producing a $\theta_{222nm}/\theta_{208nm}$ = 1.11. We did not see any red-shift of the θ_{208nm}, however, we believed that the kinetics of this system might be slower than for the previous

peptide mixture (**27**+**30**). Since an increase in the α-helical content was observed, we supposed that the mixture (**27**+**32**) would be able to promote both α-helical coiled-coil formation and fibre formation at longer times than 24 hours.

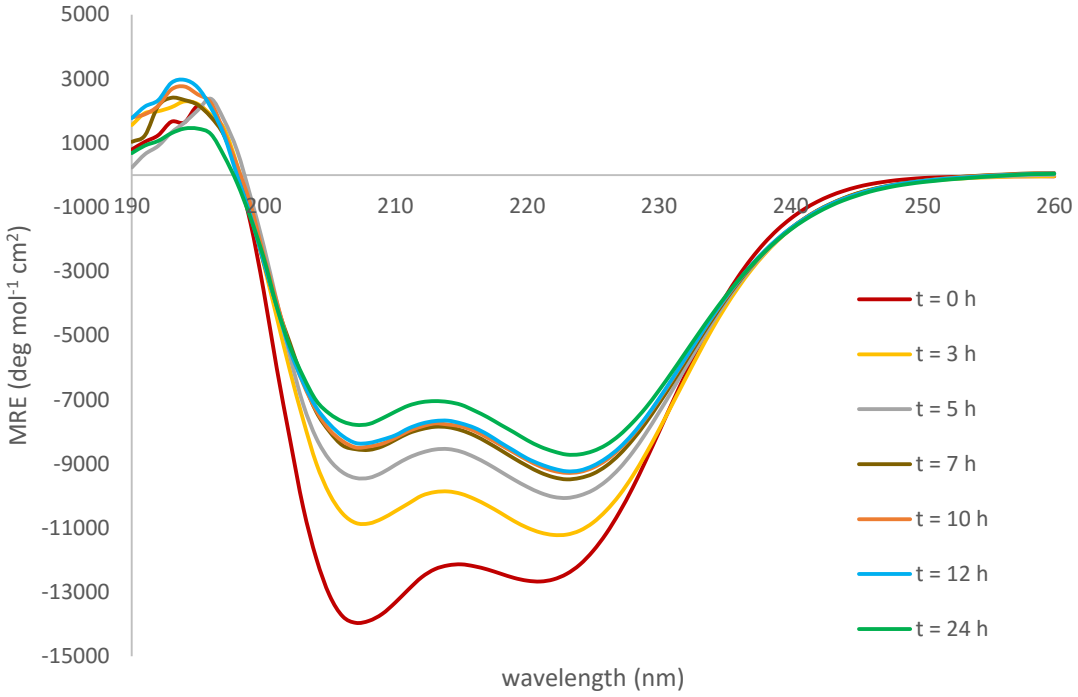

Figure 4.17: CD measurements at different times for a period of 24 hours of a 100 µM solution of (**SAF**+**c-3PAL7PAL14**) (**27**+**32**) in 10 mM MOPS buffer at pH 8.5 at 21 ˚C. The peptide sequences are shown. **X** = 3-Pal

SAF: Ac-KIKALKQKIKALKQEIAALEYENAALEQ-Am
c-3PAL7PAL14: Ac-KIAALK**X**KN**A**ALK**X**EIAALEYEIEALEQ-Am

The last of our peptide mixtures to test for α-helical coiled-coil and fibre formation was (**27**+**33**). **Figure 4.18** shows the CD measurements of a 100 µM solution in 10 mM MOPS at pH 8.5 recorded at different times for a period of one day. An initial measurement of the just prepared mixture exhibited a CD spectrum of a structure which was not fully folded as an α-helical coiled-coil (red line). The negative bands at 208 nm and 222 nm were of different magnitudes showing a $\theta_{222nm}/\theta_{208nm}$ = 0.79. Monitoring the evolution of the peptide mixture by CD spectroscopy did not show any conformational changes in the secondary structure after 24 hours. The magnitude of θ_{222nm} remained at a similar value as well as the magnitude at θ_{208nm}, producing a value of $\theta_{222nm}/\theta_{208nm}$ = 0.80 in the last measurement recorded (green line). This peptide

mixture did not show evidences for the formation of fully folded α-helical coiled-coil structures nor fibre formation. In addition, no visual signs of any blurred precipitate at the bottom or at the sides of the cuvette was detected.

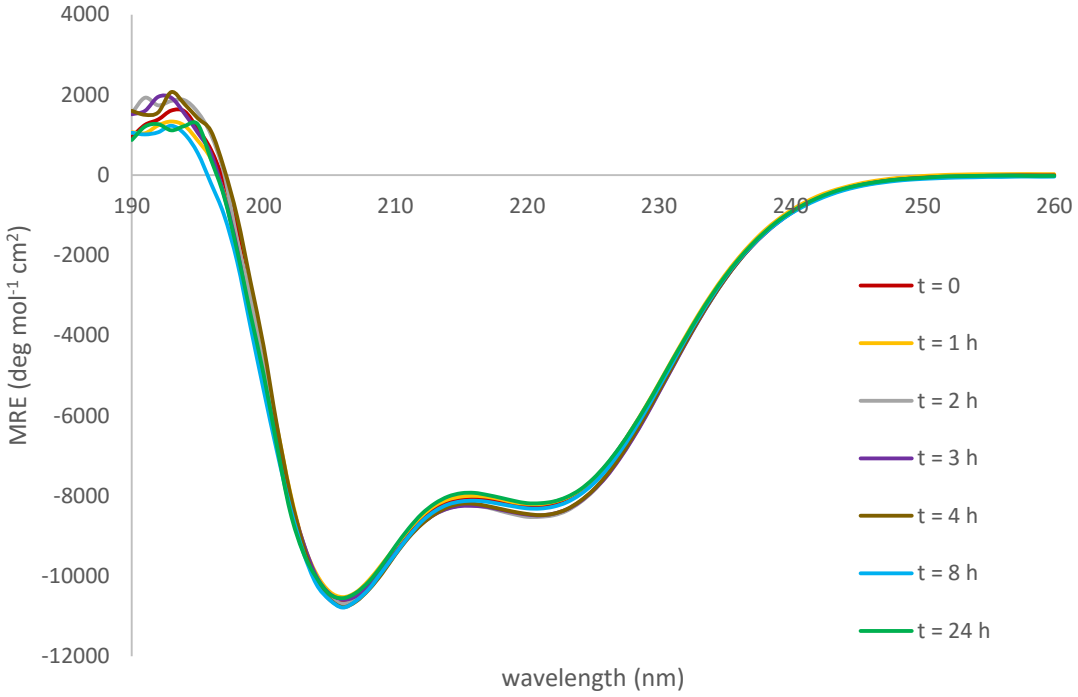

Figure 4.18: CD measurements at different times for a period of 24 hours of 100 µM (**SAF**+**c-4PAL14**) (**27**+**33**) in 10 mM MOPS buffer at pH 8.5 at 21 ˚C. The peptide sequences are shown. **X** = 4-Pal

SAF: Ac-KIKALKQKIKALKQEIAALEYENAALEQ-Am
c-4PAL14: Ac-KIAALKQKNAALK**X**EIAALEYEIEALEQ-Am

As observed, not all combinations of **SAF** (**27**) with the pyridyl-labelled peptides **30** to **33** exhibited signs of α-helical coiled-coil and fibre formation by CD spectroscopy. In addition, the magnitude of the minimums in the CD spectra appeared to be lower than what expected for these type of conformations (around -25,000 to -30,000 mdeg mol^{-1} cm^2). We believed that the insertion of the unnatural amino acids within the peptide sequences caused this effect since it was a common feature in the CD spectra of all these peptide mixtures. The combinations of (**27**+**30**) and (**27**+**32**) (**Figures 4.14** and **4.17**) showed the typical CD spectra pattern for α-helical coiled-coils and fibrous structures – although of a lower magnitude as just mentioned. In these two cases, the magnitudes of their θ_{222nm} minimums increased with respect to the magnitude of the negative bands at θ_{208nm}, which decreased and red-shifted as for the mixture (**27**+**30**).

From what we observed in the mixture (**27**+**32**) we also thought that higher concentrations of the peptide mixtures might show better and faster results of fibre formation, given that the kinetics of these processes are an important issue to take into account. On the other hand, when observing the CD spectra of the mixtures (**27**+**31**) and (**27**+**33**) a different behaviour was seen. These peptide mixtures did not exhibit a conformational change by CD spectroscopy that could indicate promotion of *α*-helical coiled-coil or fibre formation.

From these results and from a direct comparison of the mixtures (**27**+**30**) and (**27**+**33**), we could say that the insertion of a 3-pyridylalanine motif promoted *α*-helical coiled-coil and fibre formation whilst 4-pyridylalanine was unable to produce the same effect. We believed that the distancing from the nitrogen atom of the 3-pyridylalanine residue to the coiled-coil backbone could favor stabilizing interactions – such as hydrogen bonds – to promote the required structure. However, due to the distancing of the nitrogen atom in the 4-pyridylalanine residue together with the electronic effects of a para-substituted pyridyl ring did not produce the same effect. In the same way, when comparing (**27**+**31**) with (**27**+**32**), we observed that the assembly of **27** with **32** promoted *α*-helical coiled-coil and fibre formation in a way **31** was unable to achieve it. The different spacing of the two pyridylalanine motifs inserted within the sequences may be the cause of different effects: *i* → *i*+4 for peptide **31** and *i* → *i*+7 for peptide **32**. Perhaps, having both residues in **32** located on the same positions of the heptad (*f* and *f*) provided better stabilizing effects – hydrogen bonds – to favour the required structure whilst in peptide **31** (*f* and *b*) the stabilizing effects for this type of structure were lower than the hindrance caused by the pyridyl rings at different positions of the heptad repeat, producing a higher constrain, thus avoiding *α*-helical coiled-coil and fibre formation.

Table 4.4 shows the obtained data of ellipticity at 222 nm (θ_{222}) and the ratio $\theta_{222}/\theta_{208}$ for each one of the 100 µM solutions of all the individual peptides and peptide systems of this **Section 4.4** at pH 8.5 and at 21 °C.

Peptide or peptide systems	θ_{222} (deg mol^{-1} cm^2)	$\theta_{222nm}/\theta_{208nm}$
SAF (27)	-13764.8	0.84
c-3PAL14 (30)	-11990.5	0.86
(27+30) t_0	-13956.4	0.91
(27+30) t_{24h}	-13256.3	1.40
c-3PAL10PAL14 (31)	-5064.6	0.65
(27+31) t_0	-10306.3	0.83
(27+31) t_{24h}	-7102.2	0.84
c-3PAL7PAL14 (32)	-7431.8	0.78
(27+32) t_0	-12601.9	0.91
(27+32) t_{24h}	-8613.5	1.11
c-4PAL14 (33)	-5904.1	0.61
(27+33) t_0	-8192.4	0.80
(27+33) t_{24h}	-8139.8	0.80

Table 4.4: Peptide data obtained for 100 µM solutions of **SAF** (**27**), the labelled peptides (**30** to **33**) and the peptide mixtures of **27** with each one of the labelled peptides in 10 mM MOPS at pH 8.5 at 21 °C; $\mathbf{t_0}$ means the CD spectra recorded at the initial time of the mixture; $\mathbf{t_{24h}}$ means the CD spectra recorded after incubating the peptide mixture for 24 hours.

To complete this section, we were curious to find out whether the formation of fibres of these peptide-mixtures were concentration dependent. Since the peptide mixture (**27**+**30**) exhibited the biggest changes by CD spectroscopy after 8 hours, we prepared a 50 µM solution of (**27**+**30**) in 10 mM MOPS at pH 8.5 and monitored the evolution by CD spectra for 12 hours (**Figure 4.19**). As no changes in the secondary structure were observed, we thought that the process of fibre formation for these peptide mixtures was also concentration-dependent.

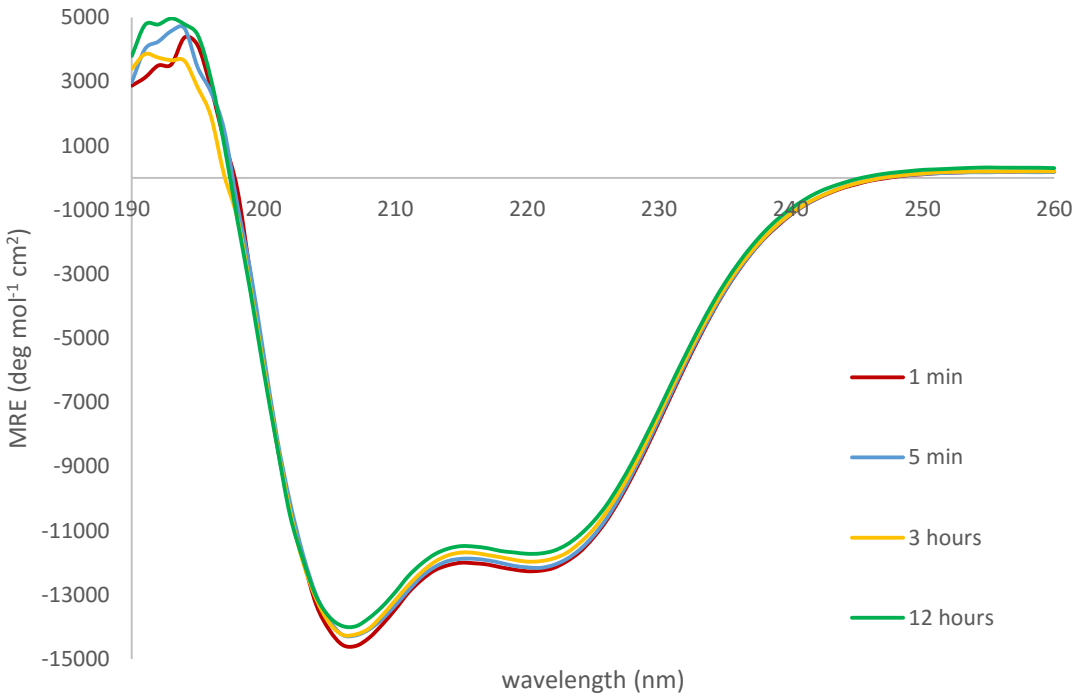

Figure 4.19: CD spectra at different intervals of time for 12 hours of 50 µM (**SAF+c-3PAL14**) (**27**+**30**) in 10 mM MOPS buffer at pH 8.5 at 21 ˚C.

4.4.1 Metal-binding experiments on the sticky-ended peptide systems

Once we were able to demonstrate that some of our pyridyl-labelled peptides (**30** and **32**) were able to promote *α*-helical coiled-coil and fibre formation upon their mixture with the **SAF** peptide (**27**), we wanted to test whether the addition of a metal complex would promote any conformational changes to the peptide structures. As mentioned in **Section 4.3.1**, pyridyl groups (soft ligands) bind relatively strong to soft metals, thus, we decided to use the Pt(II) complex K_2PtCl_4. We then proceeded to add aliquots of a 1 mM solution of K_2PtCl_4 to each of the peptide mixtures from **Section 4.4** – these were 100 µM solutions in MOPS at pH 8.5 of (**27**+**30**), (**27**+**31**), (**27**+**32**) and (**27**+**33**) – and observed the results by CD spectroscopy at different times for 24 hours.

Figure 4.20 shows the CD measurements of the metal-binding experiments of (**27**+**30**) with Pt(II). The red line shows the CD spectrum of the initial peptide mixture and the green line is the CD spectrum after 24 hours. These spectra match with **Figure 4.14**. As we discussed, for a 100 µM solution of (**27**+**30**), an increase in the magnitude in the θ_{222nm} minimum evidenced the promotion of fibre formation after 24 hours with a

$\theta_{222nm}/\theta_{208nm}$ of 1.40. The addition of 5 µL of a 1 mM solution of K_2PtCl_4 produced a total concentration of the metal-peptide system of 97.96 µM. An initial CD measurement exhibited a change in the response in the CD spectrum (purple line). The magnitude of the θ_{222nm} minimum increased producing a $\theta_{222nm}/\theta_{208nm}$ of 1.64. This effect remained after 24 hours (yellow line), producing a very similar $\theta_{222nm}/\theta_{208nm}$ of 1.61. In this particular case, we concluded that the addition of the platinum complex K_2PtCl_4 to the incubated peptide mixture accentuated the process of fibre formation and increased the degree of chiral scattering of the final coiled-coil structure.

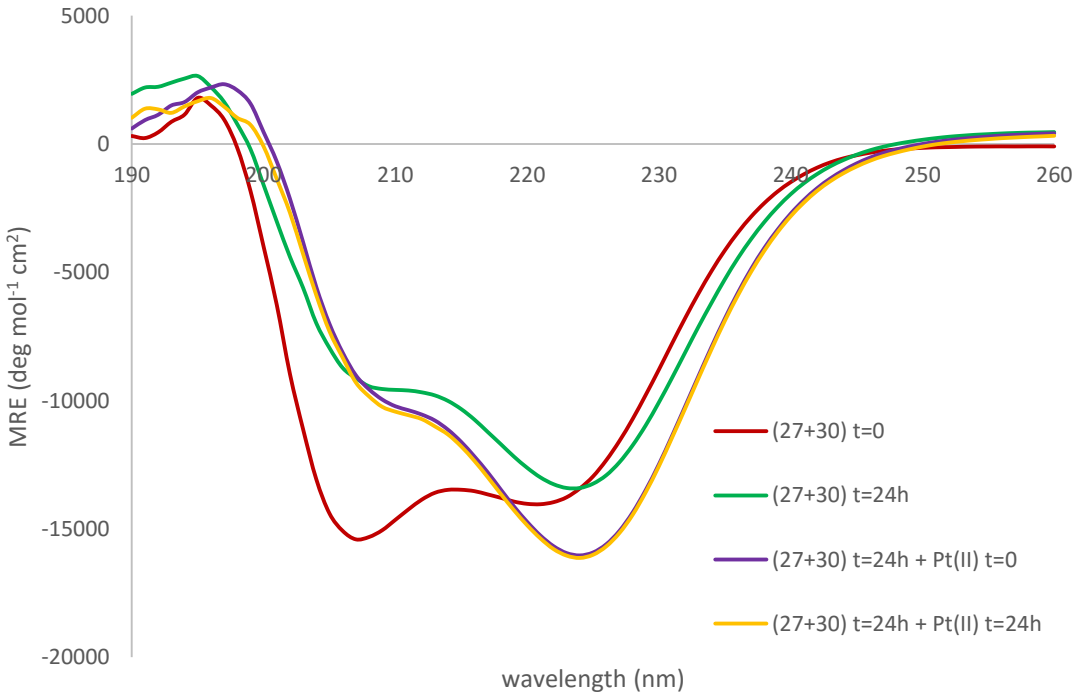

Figure 4.20: CD measurements of the metal-binding experiments of 100 µM (**SAF**+**c-3PAL14**) (**27**+**30**) with the Pt(II) complex in 10 mM MOPS buffer at pH 8.5 at 21 ˚C. The peptide sequences are shown. **X** = 3-pyridylalanine (3-Pal)

SAF:	Ac-KIKALKQKIKALKQEIAALEYENAALEQ-Am
c-3PAL14:	Ac-KIAALKQKNAALK**X**EIAALEYEIEALEQ-Am

Figure 4.21 shows the CD measurements of the metal-binding experiments of (**27**+**31**) with K_2PtCl_4. In this case, 25 µL of a 1 mM solution of K_2PtCl_4 were added to 240 µL of a 100 µM solution of (**27**+**31**) producing a final concentration of 90.57 µM, being this slightly lower than the starting concentration. The red line shows the CD spectrum of the initial peptide mixture and the green line after 24 hours. As we showed in **Figure**

4.16, the peptide mixture (**27**+**31**) prepared at a concentration of 100 µM in MOPS (pH 8.5) did not form fully folded α-helical coiled-coil structures nor promoted fibre formation. However, the addition of the Pt(II) complex showed to be crucial in causing conformational changes with respect to the initial structure. The purple line shows the CD spectrum of the mixture (**27**+**31**) right after the addition of Pt(II). The magnitude of θ_{222nm} increased compared to the negative band at θ_{208nm} indicating that coiled-coil formation was being promoted. Upon the addition of the Pt(II) complex, the $\theta_{222nm}/\theta_{208nm}$ value increased from 0.83 in the initial peptide mixture (**27**+**31**) to 0.97 in (**27**+**30**+**Pt-complex**). We recorded another CD spectrum after incubating the metal-peptide sample for 24 (yellow line). This showed a higher $\theta_{222nm}/\theta_{208nm}$ = 1.06, this being an evidence of promotion of α-helical coiled-coil. However, no evidences of fibre formation were observed.

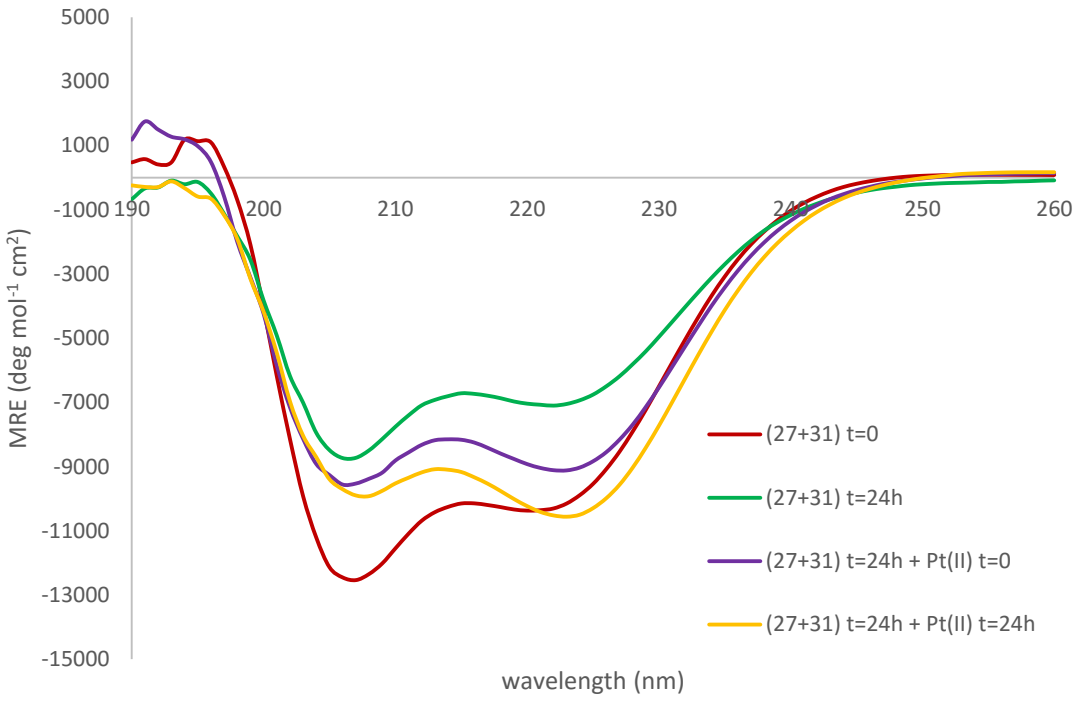

Figure 4.21: CD measurements of the metal-binding experiments of 100 µM (**SAF**+**c-3PAL10PAL14**) (**27**+**31**) with the Pt(II) complex in 10 mM MOPS buffer at pH 8.5 at 21 ˚C. The peptide sequences are shown. **X** = 3-pyridylalanine (3-Pal)

SAF: Ac-KIKALKQKIKALKQEIAALEYENAALEQ-Am
c-3PAL10PAL14: Ac-KIAALKQKN**X**ALK**X**EIAALEYEIEALEQ-Am

In this particular case (**27+31+Pt-complex**), we thought that the kinetics might be slow and longer times might be needed to produce higher values of $\theta_{222nm}/\theta_{208nm}$ that would evidence proof of fibre formation. Therefore, we concluded that the addition of the platinum complex K_2PtCl_4 to the peptide mixture produced a conformational change that increased the α-helicity in the final structure.

Figure 4.22 shows the CD measurements of the metal-binding experiments of (**27**+**32**) with Pt(II). Again, 25 µL of a 1 mM solution of K_2PtCl_4 were added to 240 µL of a 100 µM solution of (**27**+**32**) producing a final concentration of 90.57 µM, being this lower than the starting concentration. The red line shows the CD spectrum of the initial peptide mixture. As we showed in **Figure 4.17**, a 100 µM solution of (**27**+**32**) in 10 mM MOPS at pH 8.5 promoted α-helical coiled-coil and fibre formation after 24 hours (green line). The addition of the Pt(II) complex exhibited conformational changes increasing the propensity for fibre formation. The purple line shows the CD spectrum of the mixture (**27**+**32**) right after the addition of Pt(II). An increase in the magnitude of the θ_{222nm} minimum produced a higher value of $\theta_{222nm}/\theta_{208nm}$. This increased from 1.11 in the initial peptide mixture to 1.26 upon the addition of Pt(II). After incubating the sample for 24 hours, we recorded one last CD measurement (yellow line). The CD spectrum looked very similar to the one obtained right after the addition of the Pt(II) complex, producing a $\theta_{222nm}/\theta_{208nm}$ = 1.24. For this particular metal-peptide system, we concluded that the addition of the platinum complex K_2PtCl_4 to the peptide mixture provoked a morphological change in the final structure since an increase in the chiral scattering could be observed by the $\theta_{222nm}/\theta_{208nm}$ coefficient.

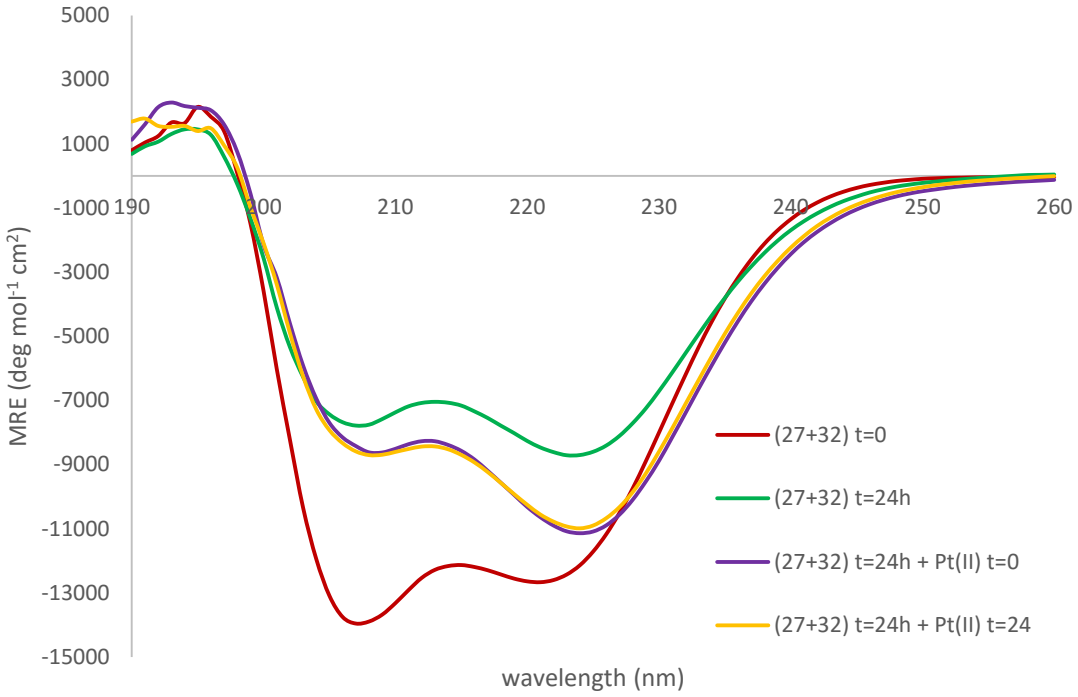

Figure 4.22: CD measurements of the metal-binding experiments of 100 µM (**SAF+c-3PAL7PAL14**) (**27+32**) with the Pt(II) complex in 10 mM MOPS buffer at pH 8.5 at 21 ˚C. The peptide sequences are shown. **X** = 3-pyridylalanine (3-Pal)

SAF: Ac-KIKALKQKIKALKQEIAALEYENAALEQ-Am
c-3PAL7PAL14: Ac-KIAALK**X**KN**A**ALK**X**EIAALEYEIEALEQ-Am

Figure 4.23 shows the CD measurements of the metal-binding experiments of (**27**+**33**) with Pt(II). Also in this case, 25 µL of a 1 mM solution of K_2PtCl_4 were added to 240 µL of a 100 µM solution of (**27**+**33**) producing a final concentration of 90.57 µM. The red line shows the CD spectrum of the initial peptide mixture. As we showed in **Figure 4.18**, a 100 µM solution of (**27**+**33**) in MOPS at pH 8.5 did not produce a fully folded α-helical coiled-coil structure after one day (green line). The CD spectrum recorded during the first minute after the addition of the Pt(II) complex did not show conformational changes to the initial structure of the peptide mixture (purple line). A remarkable conformational change was observed after 24 hours (yellow line). The magnitude of the θ_{222nm} minimum increased compared to the one at θ_{208nm} which slightly red-shifted. This change in magnitudes produced an increase in the $\theta_{222nm}/\theta_{208nm}$ coefficients from 0.83 to 0.99. Thus, for this particular peptide mixture, we concluded that the addition of K_2PtCl_4 provoked conformational changes helping to

increase the α-helical content of the coiled-coil. The metal complex may be folding up the N-terminal region of the peptide **33**, which may therefore have been unfolded in the assembly prior to metal addition. Though, we could not detect the formation of fibres by CD spectroscopy since the CD spectra did not match the patterns for this type of structure. This could be due to the slow kinetics of the system and leaving it for longer times might promote fibre formation.

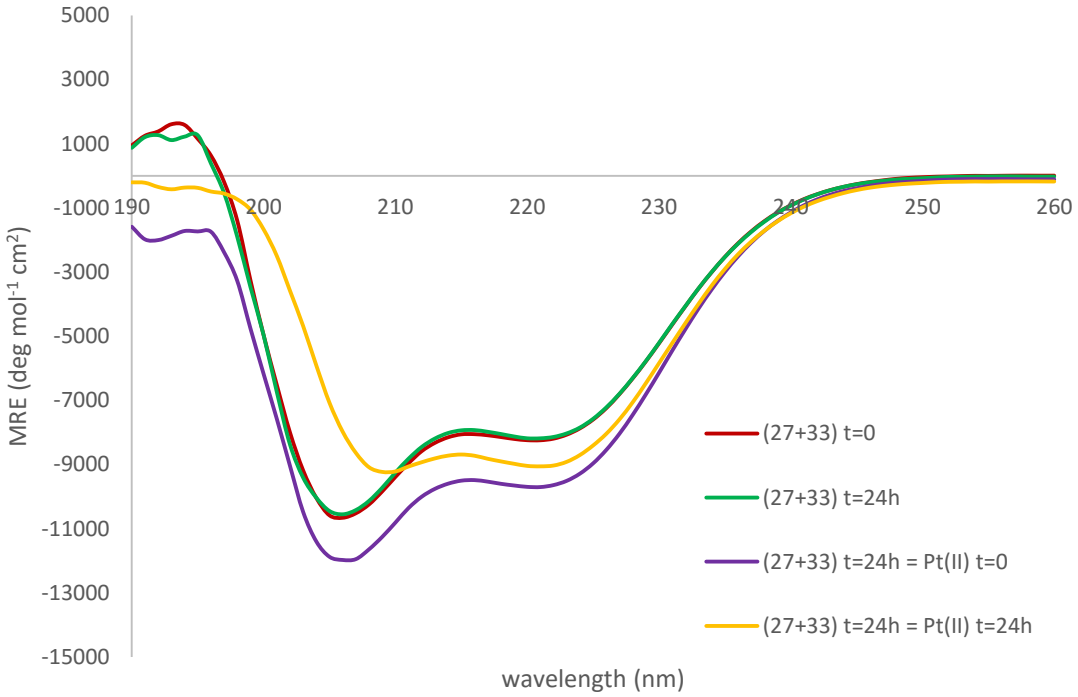

Figure 4.23: CD measurements of the metal-binding experiments of 100 µM (**SAF+c-4PAL14**) (**27+33**) with the Pt(II) complex in 10 mM MOPS buffer at pH 8.5 at 21 ˚C. The peptide sequences are shown. **X** = 4-pyridylalanine (4-Pal)

SAF:	Ac-KIKALKQKIKALKQEIAALEYENAALEQ-Am
c-4PAL14:	Ac-KIAALKQKNAALK**X**EIAALEYEIEALEQ-Am

Table 4.5 shows the obtained data of ellipticity at 222 nm (θ_{222}) and the ratio $\theta_{222}/\theta_{208}$ for each one of the 100 µM solutions of all the individual peptides and peptide systems of this first part of **Section 4.4.1** at pH 8.5 and at 21 °C and complements the obtained data from **Table 4.4** (which are written in grey).

Peptide or peptide systems	θ_{222} (deg mol^{-1} cm^2)	$\theta_{222nm}/\theta_{208nm}$
(27+30) t_0	-13956.4	0.91
(27+30) t_{24h}	-13256.3	1.40
[(27+30) t_{24h} + $Pt^{(II)}$] t_0	-15670.9	1.64
[(27+30) t_{24h} + $Pt^{(II)}$] t_{24h}	-15783.2	1.61
(27+31) t_0	-10306.3	0.83
(27+31) t_{24h}	-7102.2	0.84
[(27+30) t_{24h} + $Pt^{(II)}$] t_0	-9114.1	0.97
[(27+30) t_{24h} + $Pt^{(II)}$] t_{24h}	-10523.0	1.06
(27+32) t_0	-12601.9	0.91
(27+32) t_{24h}	-8613.5	1.11
[(27+30) t_{24h} + $Pt^{(II)}$] t_0	-10900.9	1.26
[(27+30) t_{24h} + $Pt^{(II)}$] t_{24h}	-10779.9	1.24
(27+33) t_0	-8192.4	0.80
(27+33) t_{24h}	-8139.8	0.80
[(27+30) t_{24h} + $Pt^{(II)}$] t_0	-9640.3	0.83
[(27+30) t_{24h} + $Pt^{(II)}$] t_{24h}	-9030.8	0.99

Table 4.5: Peptide data obtained for the peptide mixtures of **SAF** (**27**) with each one of the labelled peptides (**30** to **33**) after complexation with the platinum complex K_2PtCl_4 (**$Pt^{(II)}$**) in 10 mM MOPS at pH 8.5 at 21 °C; **t_0** is the CD spectra recorded at the initial time of the mixture; **t_{24h}** is the CD spectra recorded after incubating the mixture for 24 hours. Data from **Table 4.4** (in grey ink) shows the results prior to the addition of the platinum complex to compare the evolution after metal-binding.

We were also interested in investigating the effect that the single pyridyl-labelled peptides **30** to **33** would have upon interaction with the metal complex K_2PtCl_4 prior to be mixed with the **SAF** partner (**27**). Since none of the individual pyridyl-labelled peptides had a fully folded α-helical conformation, we thought that adding the Pt(II) complex could modify their structure rearranging them to be more or less α-helical. In addition, peptides **31** and **32** had two potential binding sites that could be used by the Pt(II) ion promoting changes in either the oxidation state or the coordination sphere of the metal centre. Thus, we prepared solutions in 10 mM MOPS at pH 8.5 of (**30**+K_2PtCl_4), (**31**+K_2PtCl_4), (**32**+K_2PtCl_4) and (**33**+K_2PtCl_4) and monitored the sample mixtures for one day. These samples were prepared as follows: aliquots of 100 µL of

K_2PtCl_4 200 µM were added to 200 µL of each of the pyridyl-labelled peptides at 200 µM, producing a peptide concentration of 133 µM. After this period of time 20 µL of the **SAF** peptide (**27**) at 2000 µM were added – producing a final concentration of 125 µM in the peptide mixture – to see if the metal ion was able to affect the interaction mode that the peptides had previously shown in **Section 4.4**.

The results obtained for all the metal-peptide mixtures exhibited the same tendency in this type of experiments. **Figure 4.24** shows the CD measurements of a freshly prepared solution of **30** (in orange), its mixture with the Pt(II) complex right after being mixed (purple line) and 24 hours later (yellow line), and the subsequent addition of **SAF** (**27**) right after being mixed (red line) and 28 hours later (green line). As explained, the final concentration of this sample was 125 µM in 10 mM MOPS at pH 8.5. The dotted green line represents the mixture of (**27**+**30**) incubated for 24 hours and then mixed with the Pt(II) complex and left for another 24 hours matching the yellow line from **Figure 4.20**. This allowed us to compare the difference in the CD spectra taking into account the order in which the components of the system were mixed. As previously seen, the CD spectrum of **30** (orange line) indicated that this did not have a fully folded α-helical conformation. An initial CD measurement right after addition of the Pt(II) complex did not exhibit any conformational change (purple line) and the same was observed after 24 hours (yellow line). We proceeded then to add **SAF** (**27**) and an initial CD measurement showed changes in the secondary structure (red line). The negative band at 208 nm had red-shifted and the magnitude of the θ_{222nm} minimum had increased producing a $\theta_{222nm}/\theta_{208nm} = 0.97$. This effect remained after 28 hours where the spectrum did not show large conformational changes (green line).

When comparing the green line and the dotted green line we observed how the order in which the components were mixed caused different structures. We also noticed the formation of a slightly blurred precipitated at the bottom of the cuvette which made us wonder whether some percentage of the fibrous structures were being formed. Perhaps, the kinetics of this type of structure were much slower due to the hindrance that the Pt(II) complex could cause on **30** prior to the addition of **27**.

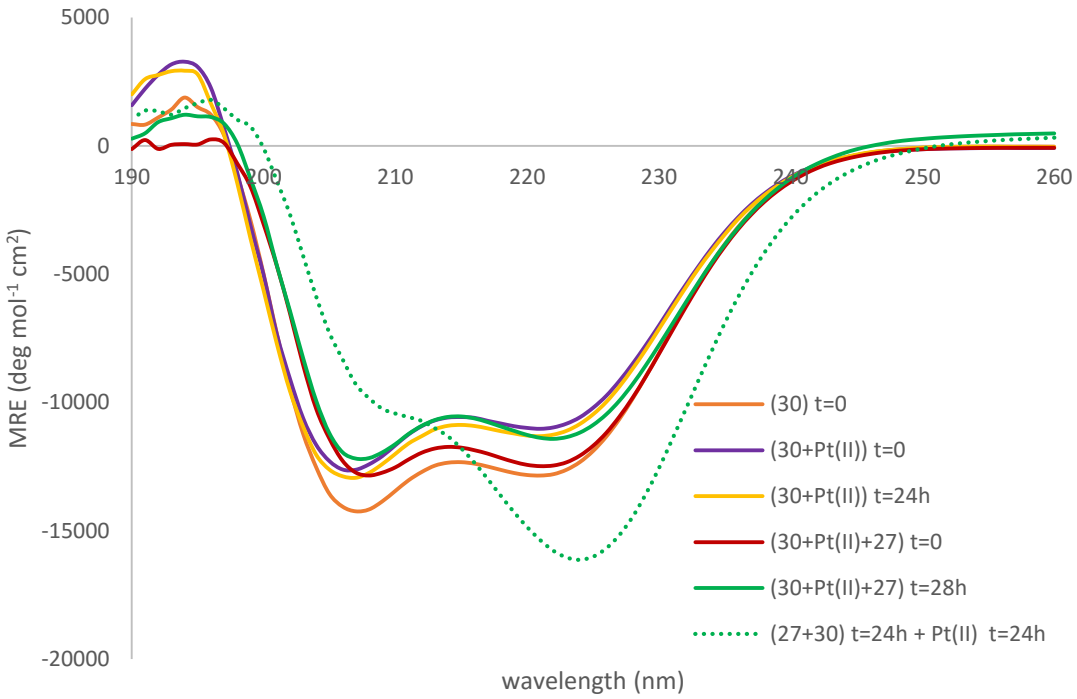

Figure 4.24: CD measurements at 21 ˚C of the metal-binding experiments in 10 mM MOPS buffer at pH 8.5 where the Pt(II) complex was first added to **30** and after a period of 24 hours, the **SAF** partner (**27**) was added to the mixture and monitored for another 28 hours. The peptide sequences are shown. **X** = 3-pyridylalanine (3-Pal)

SAF:	Ac-KIKALKQKIKALKQEIAALEYENAALEQ-Am
c-3PAL14:	Ac-KIAALKQKNAALK**X**EIAALEYEIEALEQ-Am

Figure 4.25 shows the CD measurements of a 200 µM solution of **31** freshly prepared (in orange), the mixture with the Pt(II) complex at different times (at a total concentration of 133.3 µM), and then the subsequent addition of **SAF** (**27**) (at a final concentration of 125 µM). The dotted green line represents the mixture of (**27**+**31**) incubated for 24 hours and then mixed with the Pt(II) complex and left for another 24 hours matching the yellow line from **Figure 4.21**. The CD spectrum of **31** (orange line) did not show the structure of a fully folded α-helical conformation but a structure that also contained some disordered forms of the peptide. After the addition of the Pt(II) complex, some structural changes could be seen by CD spectroscopy. A measurement at the initial time of the mixture (purple line) showed a red-shift in the negative band at 208 nm, and a similar structure was observed after 24 hours (yellow line). When **27** was added, conformational changes could be detected by CD spectroscopy. The negative band at 208 nm continued red-shifting and the magnitude of the θ_{222nm}

increased compared to the one at θ_{208nm} producing higher value of the $\theta_{222nm}/\theta_{208nm}$ coefficient (0.86) (red line). After 28 hours, the CD spectrum showed a $\theta_{222nm}/\theta_{208nm}$ = 0.92, indicating that the addition of the **SAF** partner was promoting an increase in the α-helicity of the structure (green line). However, this was not enough as to observe either a fully folded α-helical coiled-coil conformation or a fibrous structure.

We thought that the structure was evolving to a more α-helical structure but the kinetics were too slow to promote fibre formation in the period of time of our study. Again, when comparing the green line with the dotted green line we concluded that the addition of the Pt(II) complex K_2PtCl_4 to **31** and incubation for 24 hours prior to the addition of the **SAF** partner was hindering the interaction of both peptides, hence, not favoring the promotion of fully folded α-helical coiled-coils nor fibres.

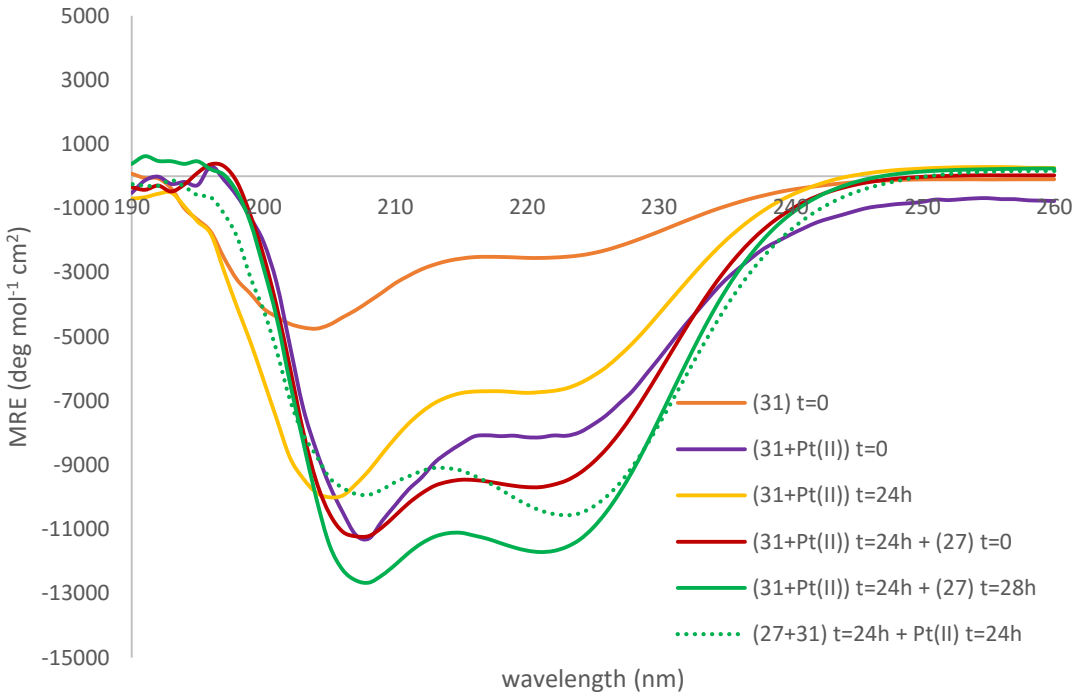

Figure 4.25: CD measurements at 21 ˚C of the metal-binding experiments in 10 mM MOPS buffer at pH 8.5 where the Pt(II) complex was first added to **31** and after a period of 24 hours, the **SAF** partner (**27**) was added to the mixture and monitored for another 28 hours. The peptide sequences are shown. **X** = 3-pyridylalanine (3-Pal)

SAF: Ac-KIKALKQKIKALKQEIAALEYENAALEQ-Am
c-3PAL10PAL14: Ac-KIAALKQKN**X**ALK**X**EIAALEYEIEALEQ-Am

Figure 4.26 shows the CD measurements of a 200 μM solution of **32** freshly prepared (in orange), the mixture with the Pt(II) complex at different times (at a total concentration of 133.3 μM), and then the subsequent addition of the **SAF** partner (**27**) (at a final concentration of 125 μM). The dotted green line represents the mixture of (**27**+**32**) incubated for 24 hours and then mixed with the Pt(II) complex and left for another 24 hours, matching the yellow line from **Figure 4.22**. The CD spectrum of **32** (orange line), as we already knew from previous discussions, did not show the structure of a fully folded α-helical conformation. After addition of Pt(II) and measuring the initial time of the mixture (purple line), the same type of structure was observed without any significant change for 24 hours (yellow line). After the addition of the **SAF** partner (**27**), the negative band at 208 nm red-shifted showing, in this case, a similar magnitude to the band at 222 nm. An increase in the magnitude of the θ_{222nm} minimum compared to θ_{208nm} produced a $\theta_{222nm}/\ \theta_{208nm} = 0.94$ (yellow line). This was indicative that the interaction with **SAF** was promoting an increase in the α-helical content of the system. The same effect remained after 28 hours (green line). The system seemed to evolve towards a more α-helical structure upon addition of **27**, however, this was insufficient to generate a fully folded α-helical coiled-coil conformation or to promote fibre formation. Again, the addition of the Pt(II) complex to the pyridyl-labelled peptide (**32**) and incubation for 24 hours prior to the addition of the **SAF** partner hindered the association of both peptides avoiding the promotion of a fully folded α-helical coiled-coil and fibrous structure.

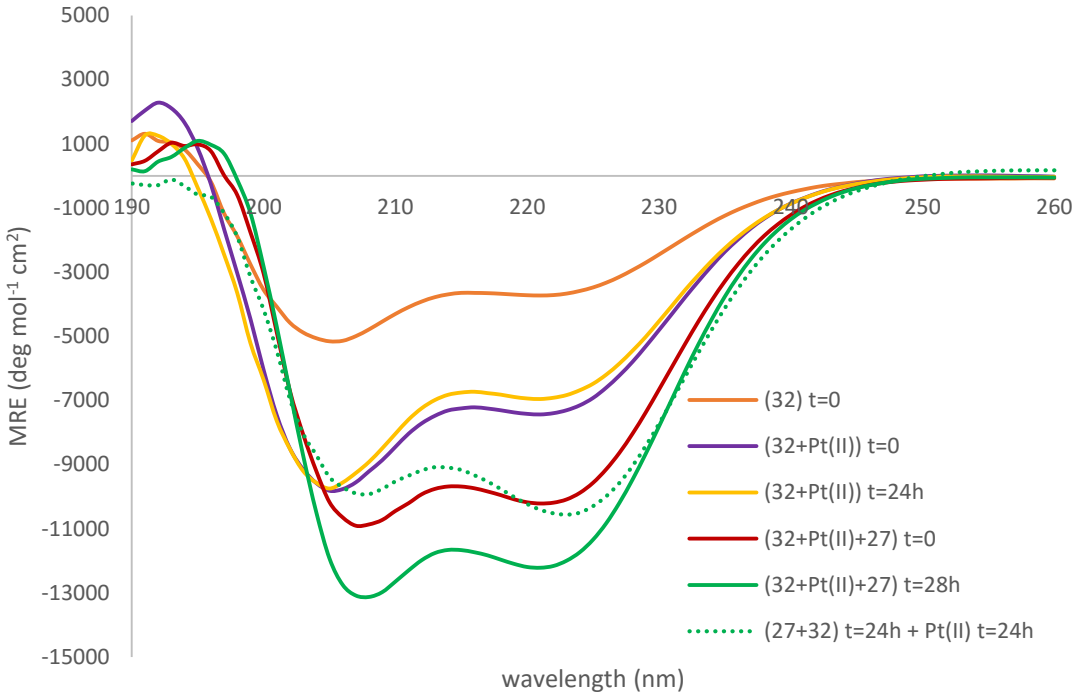

Figure 4.26: CD measurements at 21 ˚C of the metal-binding experiments in 10 mM MOPS buffer at pH 8.5 where the Pt(II) complex was first added to **32** and after a period of 24 hours, the **SAF** partner (**27**) was added to the mixture and monitored for another 28 hours. The peptide sequences are shown. **X** = 3-pyridylalanine (3-Pal)

SAF:	Ac-KIKALKQKIKALKQEIAALEYENAALEQ-Am
c-3PAL7PAL14:	Ac-KIAALK**X**KN**A**ALK**X**EIAALEYEIEALEQ-Am

Figure 4.27 shows the CD measurements of a 200 µM solution of **33** freshly prepared (in orange), the mixture with the Pt(II) complex at different times (at a total concentration of 133.3 µM), and then the subsequent addition of the **SAF** partner (**27**) (at a final concentration of 125 µM). The dotted green line represents the mixture of (**27**+**33**) incubated for 24 hours and then mixed with the Pt(II) complex and left for another 24 hours, matching the yellow line from **Figure 4.23**. Peptide **33** (orange line) did not have a fully folded α-helical conformation as previously seen. After the addition of Pt(II) and measuring the initial time of the mixture (purple line), a similar type of structure was observed without any changes after 24 hours (yellow line). Moreover, the $\theta_{222nm}/\ \theta_{208nm}$ value remained similar (0.61 vs. 0.65). When the **SAF** partner (**27**) was added, structural changes were observed. At the initial time of the mixture, the negative band at 208 nm had red-shifted although it did not show a similar magnitude as the band at 222 nm (red line). Though, these negative minimums

became closer in magnitude than in the absence of **27** after 28 hours, producing a $\theta_{222nm}/\ \theta_{208nm}$ = 0.91 (green line). The CD spectrum did not show a fully folded α-helical coiled-coil conformation nor fibre formation. The addition of **SAF** increased the α-helical content in the metal-peptide structure. However, when comparing the green line with the dotted green line, we could see that the addition of the Pt(II) complex to the pyridyl-labelled peptide **33** and incubation for 24 hours prior to the addition of **SAF** was hindering the association of both peptides avoiding the promotion of any type of fully folded α-helical coiled-coil or fibrous structures.

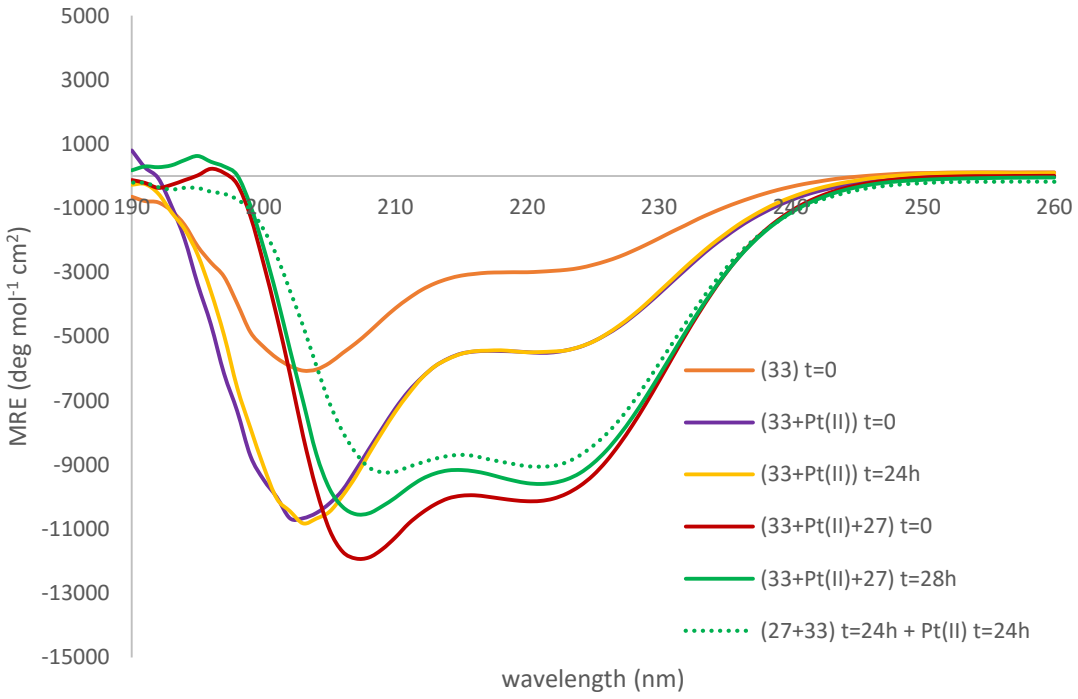

Figure 4.27: CD measurements at 21 ˚C of the metal-binding experiments in 10 mM MOPS buffer at pH 8.5 where the Pt(II) complex was first added to **33** and after a period of 24 hours, the **SAF** partner (**27**) was added to the mixture and monitored for another 28 hours. The peptide sequences are shown. **X** = 4-pyridylalanine (4-Pal)

SAF:	Ac-KIKALKQKIKALKQEIAALEYENAALEQ-Am
c-4PAL14:	Ac-KIAALKQKNAALK**X**EIAALEYEIEALEQ-Am

From these set of experiments we could see that the addition of the Pt(II) complex to the pyridyl-labelled peptides (**30** to **33**) showed a similar response by CD spectroscopy as for the individual peptides. The addition of the **SAF** partner (**27**) promoted structural changes as seen by CD spectroscopy increasing their degree of α-helicity in all the mixtures. However, this was never enough to produce fully folded α-helical coiled-coils

or fibres. Perhaps, the addition of the Pt(II) complex prior to the addition of **SAF** slowed the kinetics of the peptide system to avoid the formation of fibrous structures or the metal ion hindered an efficient folding between peptide partners. From these results, we concluded that the order in which the pyridyl-labelled peptides **30** to **33** were mixed either with **27** or the Pt(II) complex was important since both ways produced different results. **Table 4.6** summarises the peptide data of θ_{222} and $\theta_{222}/\theta_{208}$ obtained for the peptide mixtures of this last set of experiments.

Peptide or peptide systems	θ_{222} (deg mol^{-1} cm^2)	$\theta_{222nm}/\theta_{208nm}$
c-3PAL14 (30)	-12794.9	0.90
(30+Pt$^{(II)}$) t_0	-10973.2	0.88
(30+Pt$^{(II)}$) t_{24h}	-11253.6	0.88
[(30+Pt$^{(II)}$) t_{24h} + SAF] t_0	-12456.9	0.97
[(30+Pt$^{(II)}$) t_{24h} + SAF] t_{24h}	-11420.0	0.94
c-3PAL10PAL14 (31)	-2532.3	0.65
(31+Pt$^{(II)}$) t_0	-8076.8	0.72
(31+Pt$^{(II)}$) t_{24h}	-6688.0	0.73
[(31+Pt$^{(II)}$) t_{24h} + SAF] t_0	-9609.9	0.86
[(31+Pt$^{(II)}$) t_{24h} + SAF] t_{24h}	-11676.4	0.92
c-3PAL7PAL14 (32)	-3715.9	0.78
(32+Pt$^{(II)}$) t_0	-7397.2	0.80
(32+Pt$^{(II)}$) t_{24h}	-6915.9	0.78
[(32+Pt$^{(II)}$) t_{24h} + SAF] t_0	-10186.4	0.94
[(32+Pt$^{(II)}$) t_{24h} + SAF] t_{24h}	-12158.5	0.93
c-4PAL14 (33)	-2952.0	0.61
(33+Pt$^{(II)}$) t_0	-5492.7	0.65
(33+Pt$^{(II)}$) t_{24h}	-5464.9	0.63
[(33+Pt$^{(II)}$) t_{24h} + SAF] t_0	-12897.3	0.85
[(33+Pt$^{(II)}$) t_{24h} + SAF] t_{24h}	-12266.8	0.91

Table 4.6: Summarised peptide data of θ_{222} and $\theta_{222}/\theta_{208}$ obtained for the peptide mixtures of **SAF** (**27**) with each one of the previously incubated mixtures of the labelled peptides with the platinum complex **Pt(II)** in 10 mM MOPS at pH 8.5 and 21 °C. The obtained data for the individual labelled peptides **30** to **33** is also included to compare with their following mixtures. $\mathbf{t_0}$ is the CD measurement at the initial time of the mixture and $\mathbf{t_{24h}}$ is the CD measurement obtained after incubation of the mixture for 24 hours.

4.5 Summary

Some differences were observed when comparing the metal-binding experiments of **c-BEP** (**29**) and/or **SAF** (**27**) with the pyridyl-labelled peptides **30** to **33**. The first obvious thing was a decrease in the magnitude of the spectra when peptides **30** to **33** were mixed with **27**. We thought that the insertion of the unnatural amino acids within these peptide structures caused that effect by CD spectroscopy. Upon the addition of the Pt(II) complex to the peptide mixtures, the blunt-ended coiled-coil structures did not seem to exhibit any change in their secondary structure, indicating that metal-binding did not cause any conformational switch. We also thought that the peptide system was energetically stable and that was the reason to avoid conformational changes that the metal-binding could generate. However, after doing the same type of experiments with **27**, we found evidences of conformational switching by metal-binding. Either when we mixed both peptide partners and continued with the addition of the Pt(II) complex or when incubated the pyridyl-labelled peptides with the Pt(II) complex prior to the addition of their **SAF** partner, structural changes were observed. In this first case, the addition of Pt(II) to the peptide mixtures helped to increase their α-helical content and to promote fibre formation. In the second, we thought that the addition of the Pt(II) complex to the pyridyl-labelled peptides might slow the kinetics of the system towards the interaction with **SAF** and subsequent rearrangement.

[1] M.V. Tsurkan, and M.Y. Ogawa, *Chem*. *Commun*. **2004**, 2092-2093.
[2] M.V. Tsurkan, and M.Y. Ogawa, *Inorg. Chem.* **2007**, 46, 6849-6851.
[3] M.V. Tsurkan, and M.Y. Ogawa, *Biomacromol.* **2007**, 8, 3908-3913.
[4] E.H.C. Bromley, K.J. Channon, P.J.S. King, Z.N. Mahmoud, E.F. Banwell, M.F. Butler, M.P. Crump, T.R. Dafforn, M.R. Hicks, J.D. Hirst, A. Roger, and D.N. Woolfson, *Biophys. J.* **2010**, 98, 1668-1676.

Chapter 5

Photoswitching investigations in *de novo* coiled-coil peptide systems

5.1 Design of a peptide sequence to incorporate an azobenzene derivative for photoisomerization

As previously discussed in **Section 1.5.2** and **Section 2.3**, for proteins that present several folding states, it is possible to reversibly photo-control the isomerization states by irradiating light of a determined wavelength on a chromophore group within the protein structure. Here we design a peptide sequence with two binding sites for the attachment of an azobenzene derivative (4,4'-dichloroacetamide azobenzene, **24**) and to take advantage of the *trans*-to-*cis* isomerization switch (and viceversa) of these compounds for photoisomerization of its folding states when forming an α-helical coiled-coil. We still follow the same principles for peptide design explained in **Section 3.3**, hence, the design of a peptide partner of **PEP1** (**25**) for blunt-ended coiled-coil formation but with the ability of incorporating an azobenzene.

Since **BEP** (**26**) was designed to form an α-helical coiled-coil structure upon interaction with **PEP1** (**25**), we use peptide **26** as a template for the design and construction of a peptide partner for **25** with the addition of two binding sites for the attachment of the azobenzene unit are arranged. As we explained in **Section 1.5.2**, thiols can easily react with halo-compounds under the right conditions of pH. Cys residues contain thiol groups as side chains than can react with the halo-azobenzene (4,4'-dichloroacetamide azobenzene, **24**) synthesized for this purpose. As the design of these peptides is to form an α-helical coiled-coil in its native state, a spacing of $i \rightarrow i+11$ is selected for the incorporation of the Cys residues. This decision was made based on the information provided by Wooley where models placed at this spacing favoured the formation of an

α-helix in the dark adapted state when attached to an azobenzene derivative of similar structure to the one synthesized in this thesis.[1]

As *α*-helical coiled-coils are designed to assemble to bury their hydrophobic faces and these are positions *a* and *d* of the heptad, and positions *e* and *g* are used for salt-bridging interactions, the remaining heptad positions to allocate the Cys residues are *b*, *c* or *f*, which are in the hydrophilic face, hence designing a water-soluble azobenzene derivative (**Section 2.3**). Due to the greater effect that an azobenzene derivative has on a peptide when placed at the middle of the sequence, we decided to design a Cys-containing peptide that could achieve this, hence, suitably finding positions in the second and third heptad of the sequence to accommodate this. We decided to replace the Gln residue of position *f* of the second heptad and the corresponding amino acid at a spacing of *i* → *i*+11 which was an Ala residue in position *b* of the third heptad, which matched our planned requirements.

This new designed peptide, **CYS** (**34**), can then react with the azobenzene derivative (4,4'-dichloroacetamide azobenzene, **24**) to form a cross-linked peptide, **CL** (**35**), for heterodimer coiled-coil formation and for photoisomerization investigations. **Figure 5.1** illustrates a summary of what has been explained in the paragraphs before about the steps for the design of **34**, **35** and the coiled-coil dimer for photoisomerization.

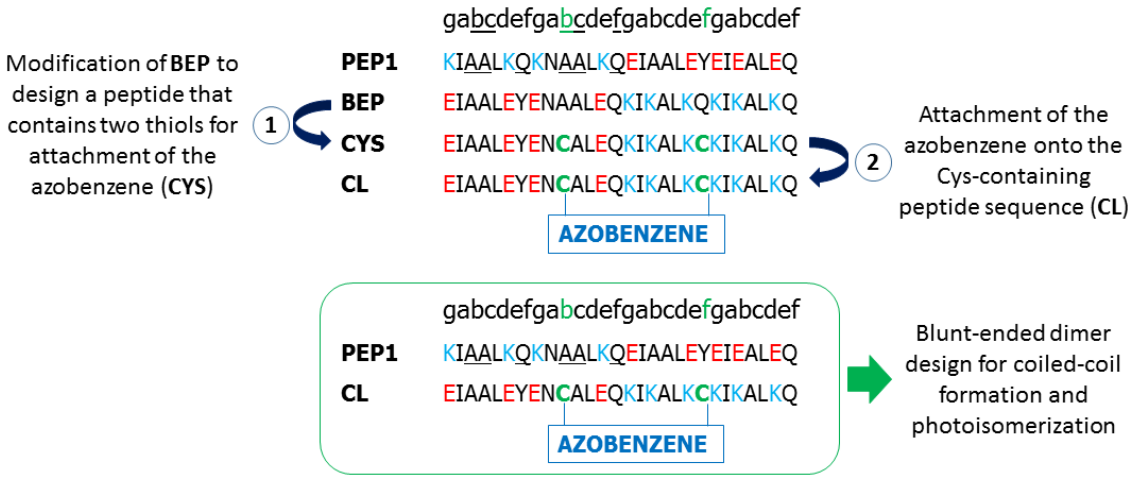

Figure 5.1: Steps for the design of **CYS** and **CL** from **BEP** and representation of the heterodimer design for coiled-coil formation and photoisomerization investigations.

Taking into consideration that our first designs in **Section 3.3** gave good results when the sequences were double capped – this is N-acetylated and C-amidated – we decided to synthesize the Cys-containing peptide also as a double capped peptide, **c-CYS** (**36**), and its cross-linking reaction with 4,4'-dichloroacetamide azobenzene (**24**) would provide **c-CL** (**37**) for heterodimer coiled-coil formation with **c-PEP1** (**28**) and subsequent photoisomerization investigations. Nevertheless, as we have **PEP1**, **c-PEP1**, **CL** and **c-CL**, it would be interesting to prepare all the possible combinations for coiled-coil formation to gain a better understanding of the photoisomerization effects on each type of structure. **Figure 5.2** shows the target heterodimer coiled-coil structures for photoisomerization investigations.

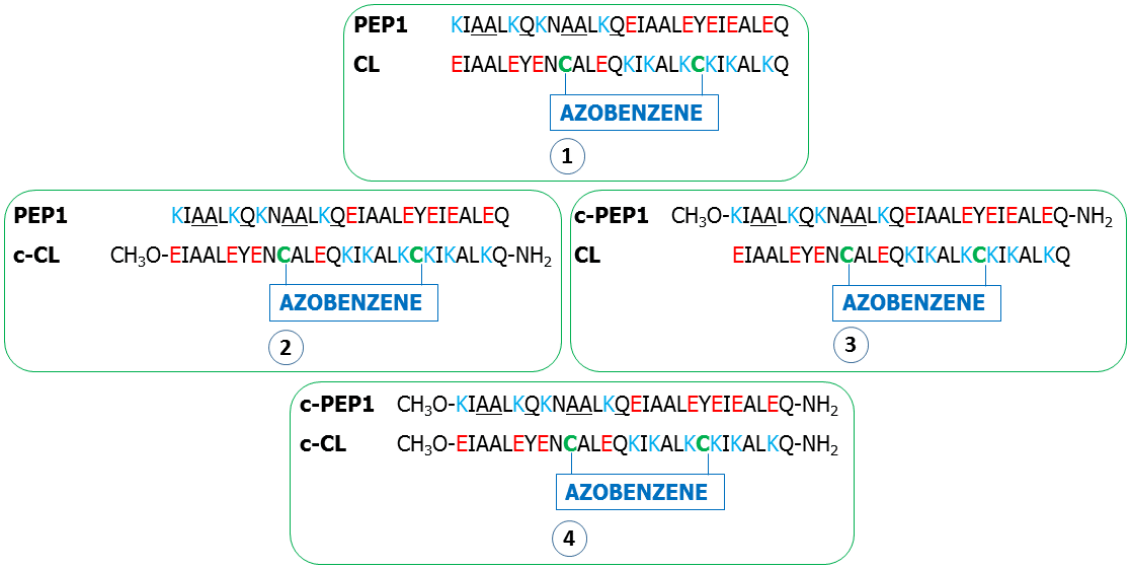

Figure 5.2: Potential combinations of coiled-coil heterodimers for photoisomerization investigations: (1) (**PEP1**+**CL**); (2) (**PEP1**+**c-CL**); (3) (**c-PEP1**+**CL**); and (4) (**c-PEP1**+**c-CL**).

5.2 Synthesis, characterization and discussion

5.2.1 Peptide synthesis

The synthesis of the Cys-containing peptides **34** and **36** was successfully accomplished by automated Fmoc-MW-SPPS. **CYS** (**34**) was synthesized on Fmoc-Gln(Trt)-wang resin at both 0.05 and 0.10 mmol scales following the peptide synthesis – procedures 1 and 2 respectively from **Section 7.2.3**. Procedure 1 afforded 77 mg of crude peptide (48%) whilst procedure 2 gave 175 mg of crude peptide (55%). **c-CYS** (**36**) was synthesized on rink amide MBHA resin at 0.10 mmol scale following the peptide synthesis – procedure 6 from **Section 7.2.3** and affording 170 mg of crude peptide (53%). Further purification of the crude material by RP-HPLC afforded both pure peptides with high purity of **c-CYS** (**37**) as seen by HRMS analysis (**Section 7.6**). **CYS**: MALDI-TOF MS *m/z* 3190.6 $[M]^+$, 3192.6 $[M+H]^+$; 3214.6 $[M+H+Na]^+$; while **c-CYS**: MALDI-TOF MS *m/z* 3231.5 $[M]^+$, 3253.5 *m/z* $[M+Na]^+$. **Figure 5.3** shows the MALDI spectrum of the crude **CYS** (**34**) peptide prior and after RP-HPLC purification; while **Figure 5.4** shows the corresponding MALDI spectra of the crude c-CYS (**36**) before and after RP-HPLC purification.

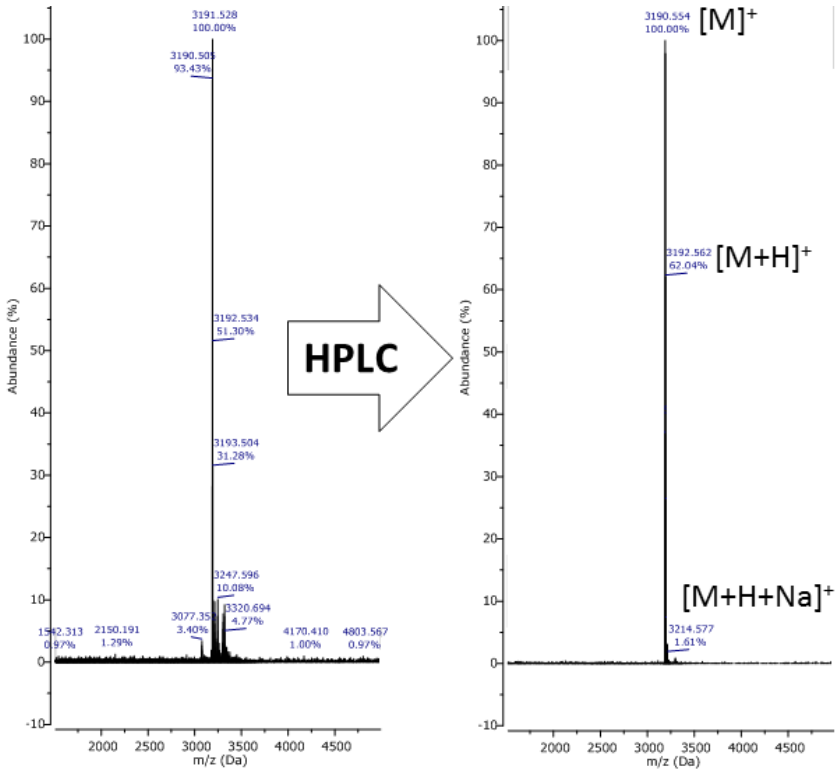

Figure 5.3: MALDI-TOF MS spectrum of **CYS** (**34**) before RP-HPLC (at the left) and after RP-HPLC (at the right).

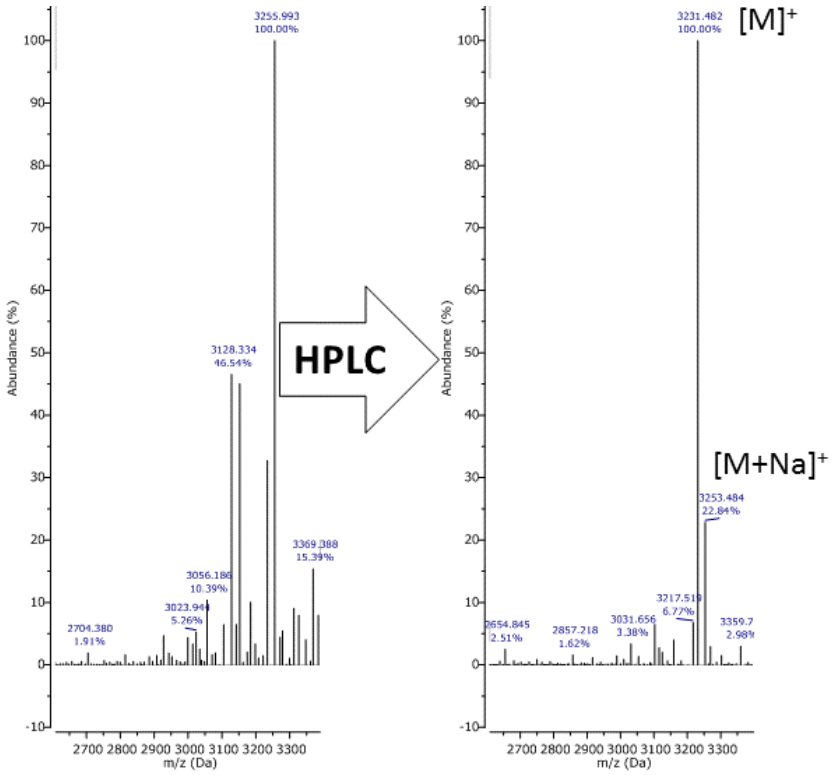

Figure 5.4: MALDI-TOF MS spectrum of **c-CYS** (**36**) before RP-HPLC (at the left) and after RP-HPLC (at the right).

5.2.2 Synthesis of azobenzene-peptide systems for photoisomerization

The cross-linking reactions are carried out into buffer solutions to favour the reaction processes. Here we use TCEP and tris-HCl. TCEP (tris(2-carboxyethylphosphine)) is a reducing agent commonly used in biochemistry to break disulfide bonds as preparatory step for further reactions; tris-HCl (tris(hydroxymethil)aminomethane) is a buffer solution widely used in biological reactions to preserve the pH of the media whilst the desired reaction is happening. As we need a slightly basic pH to preserve thiol groups in their reduced state and avoid disulfide bond formation, a tris-HCl solution (pH 8.5) together with TCEP at pH (8.5) is used to maintain these thiols in their reduced state (–SH) until the addition of 4,4'-dichloroacetamido azobenzene (**24**) in a nucleophilic substitution reaction.

The reaction is carried on in aqueous media with previous incubation of the peptide (either **34** or **36**) into the buffer solutions at room temperature for a minimum of 2 hours and under inert atmosphere (N_2 or Ar). The reaction proceeds with the addition

of the azobenzene derivative in excess (in DMSO to help solubility) in the dark and with heating at 40 ˚C. **Scheme 5.1** shows the conditions of reaction for cross-linking **24** with **CYS** (**34**) – the same conditions were applied to synthesize **c-CYS** (**36**) – and **Scheme 5.2** explains the mechanism of reaction by which this process happens. The crude of these reactions is lyophilized and purified by RP-HPLC.

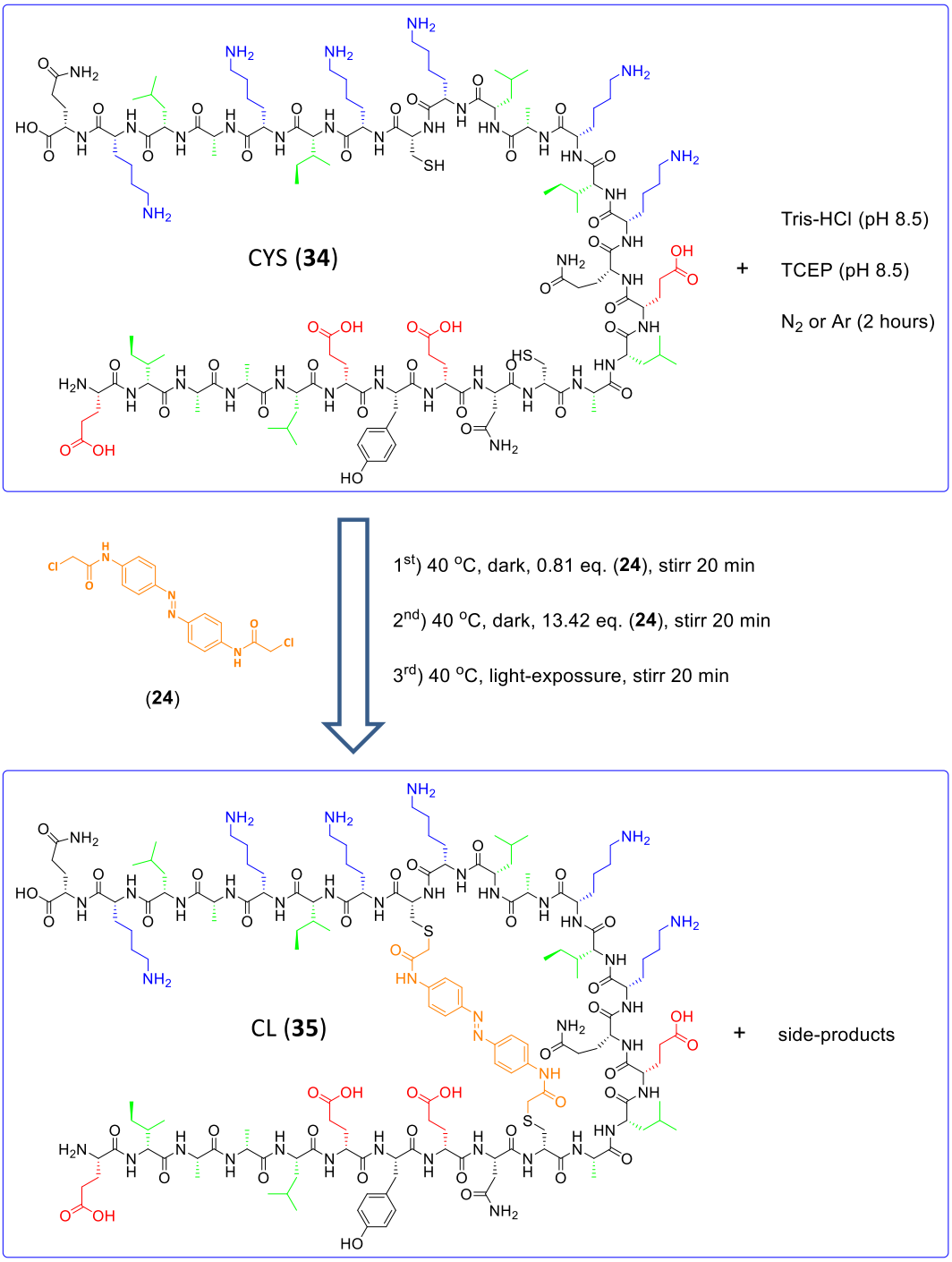

Scheme 5.1: Cross-linking reaction conditions to make **CL** (**35**) from **CYS** (**34**) and (**24**).

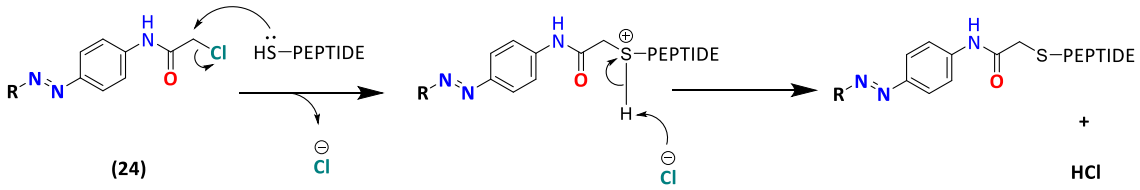

Scheme 5.2: Cross-linking reaction mechanism between azobenzene **24** and a thiol group from a peptide sequence. The nucleophilic substitution reaction generates HCl that stays in solution.

The MALDI-TOF spectra of the cross-linked peptides **35** and **37** after RP-HPLC purification showed the right *m/z* masses for the calculated ions (**Figure 5.5**). Thus, **CL** (**35**): MALDI-TOF MS *m/z* 3484.1 $[M+H]^+$, 3506.2 $[M+Na]^+$; while the corresponding masses peaks for the **c-CL** (**37**) were: MALDI-TOF MS *m/z* 3524.9 $[M]^+$, 3546.6 $[M+Na]^+$.

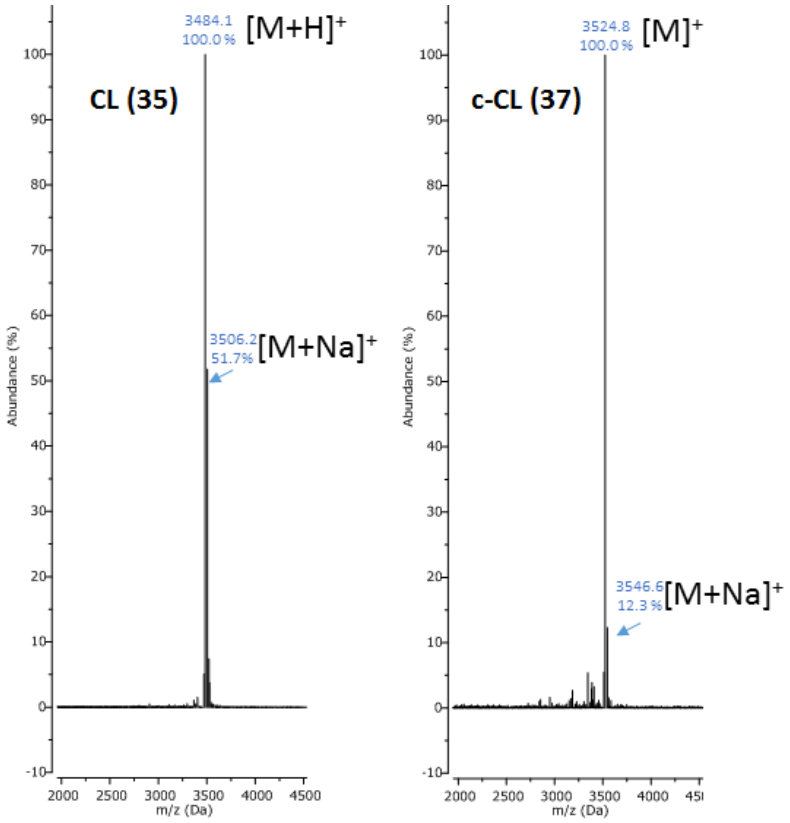

Figure 5.5: MALDI-TOF MS spectra of **CL** (**35**) at the left and of **c-CL** (**37**) at the right.

5.2.3 Photoisomerization of coiled-coil peptide systems

After successfully synthesized the azobenzene-peptide structures **35** and **37**, circular dichroism (CD) experiments were carried out to investigate: first, whether the combination of any of these with any of the peptide sequences **PEP1** (**25**) or **c-PEP1** (**28**) formed blunt-ended coiled-coils; and second, whether irradiation with UV light could photoswitch any of these systems. As we explained in **Figure 5.2**, our initial aim was to investigate the photoswitching effects in each of the possible combinations. However, because of the lack of peptide **35** and the difficulties we found when trying to resynthesize it, we decide to focus on systems 1, 2 and 4 from **Figure 5.2** and leave system 3 for future work. All CD measurements discussed next were recorded in PBS buffer at pH 7.4 at room temperature (21 °C).

CD analysis of the individual peptides **CL** (**35**) and **c-CL** (**37**) were carried out to test the photoisomerization effect. We first thought that irradiating the azobenzene-containing peptides with 380 nm light for 20 min would be enough to promote a conformational change in their secondary structure, and 450 nm light would return the peptides back to their initial conformation. This was deduced from observing the big conformational change of the azobenzene **24** alone by UV spectroscopy under these conditions (**Figure 2.19**). However, and due to the novelty of this type of experiment for us, we initially thought that irradiating **35** with 380 nm light for 20 min was not providing enough energy to induce the photoswitching of the peptide. Thus, we decided to increase the energy of irradiation to 340 nm to check whether that would be enough to confirm the photoisomerization of **35**.

Figure 5.6 shows the CD spectrum of **35** in the dark-adapted state (purple line) – this is, when the azobenzene is favored in the *trans*-isomer state – and the photoswitching effect after irradiating at 340 nm light for 20 min (red line). The concentration of this peptide solution was estimated to be around 50 μM (unfortunately, we did not have much of this peptide left when undertook this measurements, hence, the estimation). The negative bands at 222 nm and at 208 nm were indicative that this structure was not fully assembled as an α-helical conformation (purple line). The $\theta_{222nm}/\theta_{208nm}$ coefficient was 0.77, when for a fully folded α-helical conformation a coefficient of

1.00 or higher is expected. Moreover, the isodichroic point seen between 203 nm and 208 nm suggested the presence of a two-state equilibrium between helical and disordered forms of the peptide, being higher the α-helical content. Irradiation of this peptide at 340 nm for 20 min decreased the magnitude of the θ_{222nm} minimum in a higher magnitude than the θ_{208nm} minimum (dark red line). This produced a value of $\theta_{222nm}/\theta_{208nm}$ = 0.72 which was lower than that found in the initial state. This proved a conformational change of **35** upon light irradiation. To return the peptide to the initial conformation, 450 nm light was used for 20 min (dotted purple line). The $\theta_{222nm}/\theta_{208nm}$ coefficient was 0.76, which was almost the same as previously calculated when the peptide was in its initial state. Both bands at 222 nm and at 208 nm increased their magnitudes almost to the same point at where they were initially measured. This was another proof of the photoswitching ability of **35** and we concluded that peptide **35** could undergo both *trans*-to-*cis* and *cis*-to-*trans* photoisomerization, with 20 min being enough to return most of the molecules from the *cis* to the *trans*-initial state.

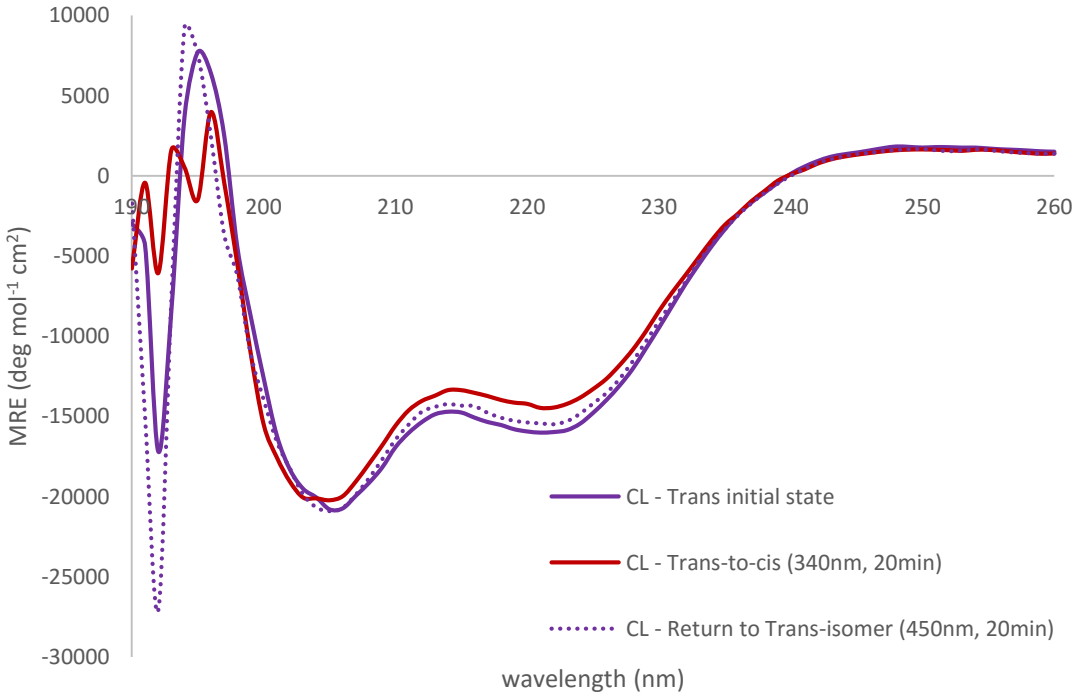

Figure 5.6: CD spectra of the photoisomerization of 50 µM **CL** (**35**) in PBS at pH 7.4 at 21 ˚C. The peptide sequence of **CL** (**35**) is shown. The residues Cys (in red on the sequence) are the binding sites through which the azobenzene **24** is attached:

CL: EIAALEYEN**C**ALEQKIKALK**C**KIKALKQ

We also tested the photoisomerization effects of **37**. As the level of experience in the synthesis of the cross-linked peptides at this point of the thesis was much higher, a larger amount of **37** was available for CD measurements. Samples at different concentrations of 20 µM, 50 µM, 100 µM and 200 µM in PBS at pH 7.4 and at room temperature (21 °C) were prepared to investigate the effects of concentration when photoswitching the peptide. Although the photoswitching effects were seen best when the concentration was higher, we found this a normal consequence as the more concentrated the more azobenzene-peptide structures can be found and detected, hence the better response when measuring CD. We only show the photoswitching effect at 100 µM (**Figure 5.7**) while the other spectra at different concentrations can be found in the **Appendices**.

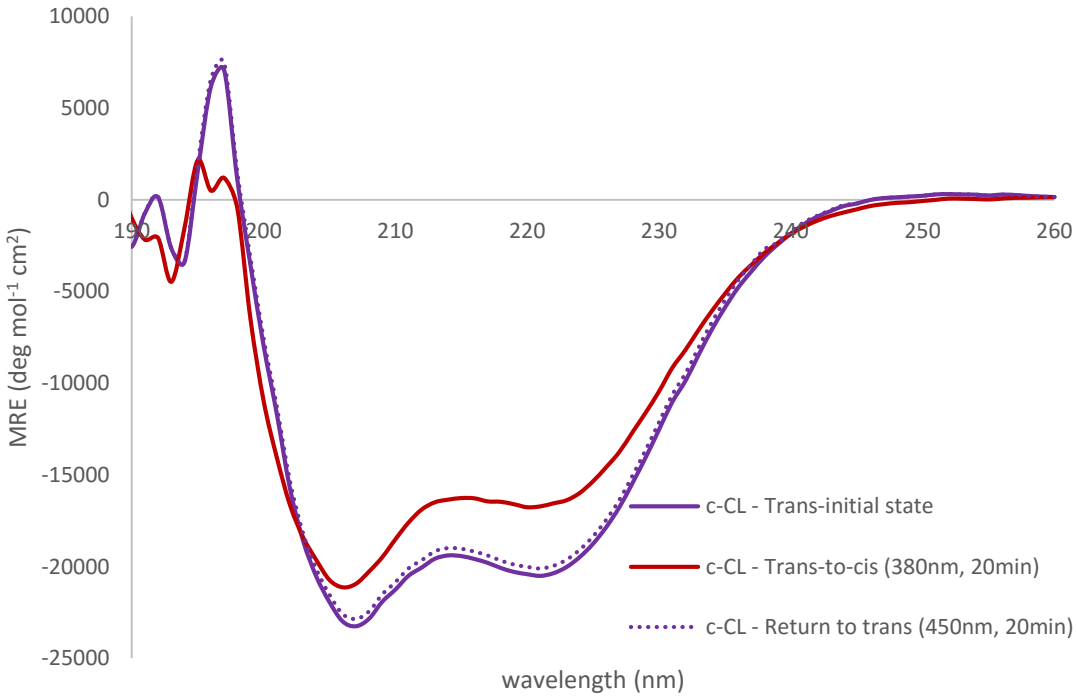

Figure 5.7: CD spectra of the photoisomerization of 100 µM **c-CL** (**37**) in PBS buffer at pH 7.4 at 21 ˚C. The peptide sequence (**37**) is shown. The residues Cys (in red on the sequence) are the binding sites through which the azobenzene **24** is attached:

c-**CL**: Ac-EIAALEYEN**C**ALEQKIKALK**C**KIKALKQ-Am

When observing the negative bands of the *trans*-initial state of **37** at the CD spectrum (purple line) in **Figure 5.7**, they showed a certain degree of *α*-helical content together with some disordered forms of the peptides as it happened with **35**. After irradiating the peptide with 380 nm light for 20 min, the magnitude of the θ_{222nm} minimum decreased producing a $\theta_{222nm}/\theta_{208nm}$ value of 0.82 when the initial $\theta_{222nm}/\theta_{208nm}$ = 0.89. This meant a significant loss in the *α*-helicity of the peptide structure. This turned out to be a clear proof of the *trans*-to-*cis* photoisomerization of the azobenzene-peptide structure. Irradiation of the *cis*-conformational state at 450 nm for 20 min seemed to be enough as to return most of the molecules of **37** to the *trans*-initial conformational state. Again, as for **35**, the reversible photoisomerization of **37** was proven by CD spectroscopy.

Since the azobenzene switch was strong enough to generate conformational changes in the structure of the individual peptides **35** and **37** upon 340 nm and 380 nm light respectively, we next mixed them with their partners **PEP1** (**25**) and **c-PEP1** (**28**) to investigate the photoswitching effects of such systems. As previously mentioned, we could only test these effects in the following coiled-coil systems (**Figure 5.2**):

1) (**PEP1**+**CL**) (**25**+**35**);
2) (**PEP1**+**c-CL**) (**25**+**37**);
3) (**c-PEP1**+**c-CL**) (**28**+**37**).

Figure 5.8 shows the CD spectrum of **PEP1** (**25**) (blue line), **CL** (**35**) (purple line), and their mixture (green line) in an equal molar ratio of (1:1) at a total concentration of 15 μM in PBS buffer at pH 7.4 at 21 °C. As we mentioned, we did not have much of **35**, thus, low concentrations were used in this case. **PEP1** showed a disordered structure with a $\theta_{222nm}/\theta_{208nm}$ = 0.25, and **CL** exhibited certain degree of *α*-helicity together with disordered forms of the peptide. The interaction between both peptides produced a $\theta_{222nm}/\theta_{208nm}$ = 0.84, indicating an increase in the *α*-helical content of the mixture, though, this structure contained some degree of random coil conformation. Irradiation of the peptide mixture with 340 nm light for 20 min exhibited a conformational change by CD spectroscopy (yellow line). The magnitude of the θ_{222nm} minimum decreased in a

higher magnitude compared to the θ_{208nm} minimum producing a $\theta_{222nm}/\theta_{208nm}$ = 0.81 and evidencing a loss in the α-helical content of the structure. This was indicative of a conformational switch from *trans*-to-*cis*. Though, the initial trans-conformation was recovered upon irradiation of the *cis*-isomer with 450 nm light for 20 min (dotted green line).

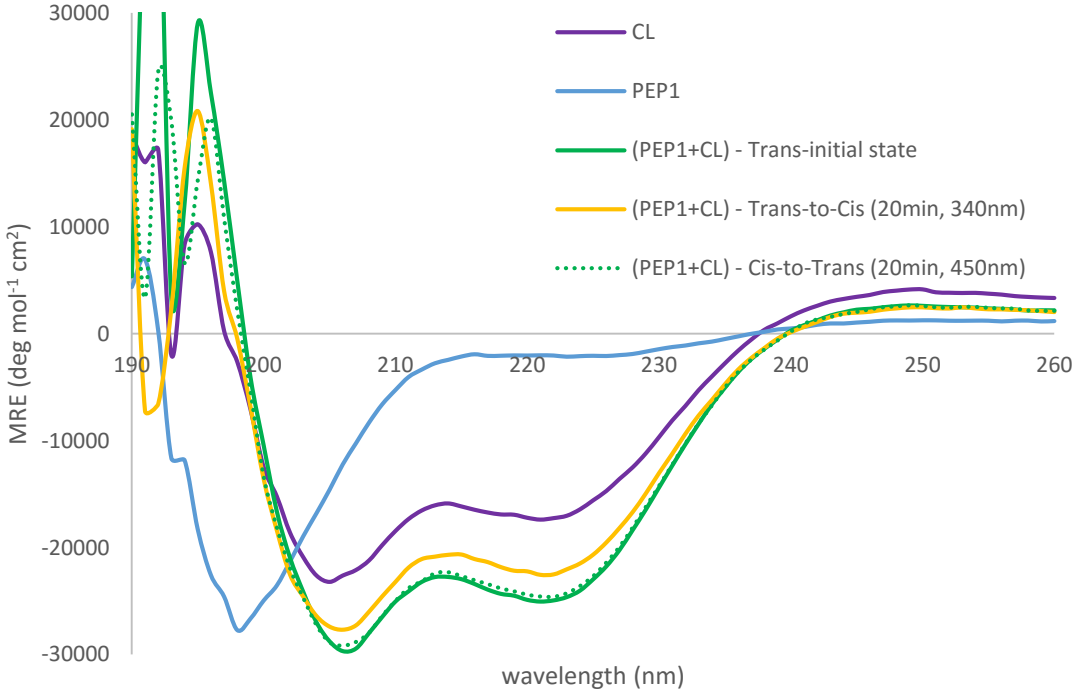

Figure 5.8: CD spectrum of 80 µM solutions of **PEP1** (**25**), **CL** (**35**), and their mixture (**25**+**35**) in PBS buffer at pH 7.4 at 21 ˚C, and the photoisomerization of the (**25**+**35**) system. The peptide sequences of **PEP1** (**25**) and **CL** (**35**) are shown. The residues Cys (in red on the sequence) are the binding sites through which the azobenzene **24** is attached:

PEP1:	KIAALKQKNAALKQEIAALEYEIALEQ
CL:	EIAALEYEN**C**ALEQKIKALK**C**KIKALKQ

This study confirmed the ability of the azobenzene chromophore (**24**) to photoswitch the conformational structure given by the peptide mixture of (**25**+**35**) despite the fact that the system did not fully assemble as an α-helical coiled-coil blunt-ended structure. In addition, we observed that irradiation at 450 nm for 20 min was almost enough to return all the azobenzene molecules to the *trans*-initial state making this a reversible process.

PEP1 was mixed in a molar ratio of (1:1) with **c-CL** at a total concentration of 100 µM in PBS buffer at pH 7.4 and at 21 °C forming what we considered a coiled-coil structure with a high degree of α-helical content as seen by CD spectroscopy in **Figure 5.9**. The CD spectrum of **PEP1** (dotted blue line) exhibited a negative band near 198 nm, typical of a disordered conformation. The CD spectrum of **c-CL** (dotted purple line) exhibited two negative bands at 208 nm and 222 nm, producing a $\theta_{222nm}/\theta_{208nm}$ = 0.89, which was a sign that its conformation had some degree of α-helicity together with disordered forms of the peptide. Irradiation of the **c-CL** peptide with 380 nm light for 20 min exhibited structural changes by CD spectroscopy. A larger decrease in the magnitude of the θ_{222nm} minimum than in θ_{208nm} exhibited a loss in the degree of α-helicity as determined by the coefficient $\theta_{222nm}/\theta_{208nm}$ = 0.82 (dotted red line).

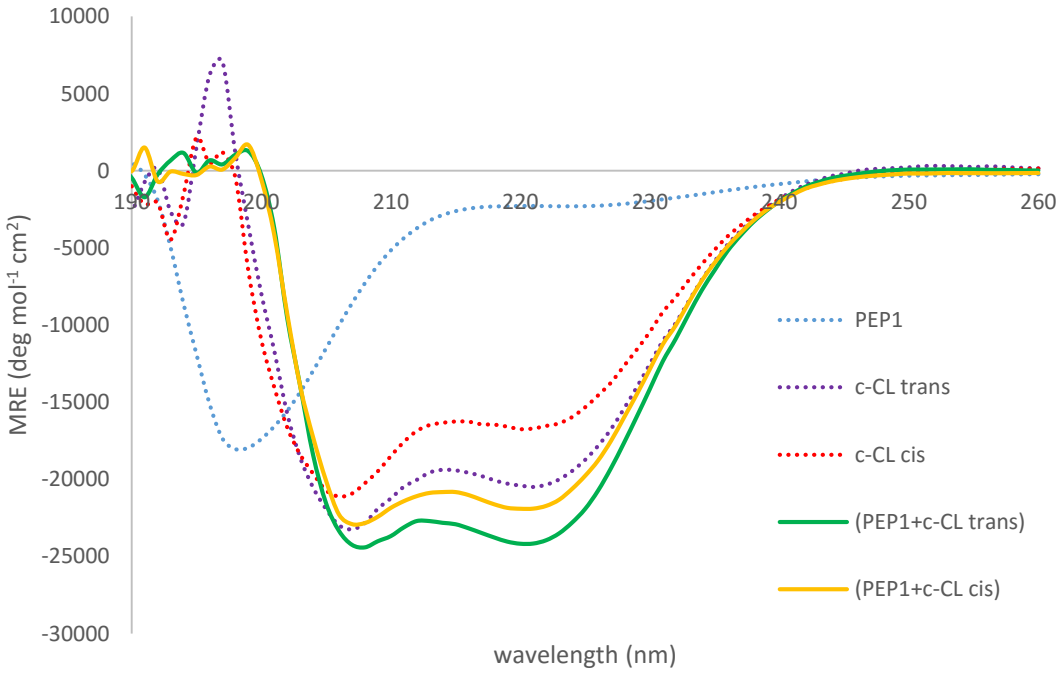

Figure 5.9: CD spectrum of 100 µM solutions of **PEP1** (**25**), **c-CL** (**37**), and their mixture (**25**+**37**) in PBS buffer at pH 7.4 at 21 ˚C, and the photoisomerization of the (**25**+**37**) system. The peptide sequences of **PEP1** (**25**) and **c-CL** (**37**) are shown. The residues Cys (in red on the sequence) are the binding sites through which the azobenzene **24** is attached:

PEP1: KIAALKQKNAALKQEIAALEYEIALEQ
c-**CL**: Ac-EIAALEYEN**C**ALEQKIKALK**C**KIKALKQ-Am

When **25** and **37** were mixed together (green line), an increase in the magnitude of the θ_{222nm} minimum was indicative of a higher degree of α-helical content in the coiled-coil structure compared to the helical content shown by the individual peptides, producing a $\theta_{222nm}/\theta_{208nm}$ = 0.98 for the *trans*-conformation. Irradiation of the mixture (**25**+**37**) with 380 nm light for 20 min induced a conformational change that meant a loss in the α-helical content of the peptide assembly (yellow line). Both the negative bands at 208 nm and 222 nm decreased their magnitudes, exhibiting the θ_{222nm} minimum a larger decrease compared to θ_{208nm} and producing a $\theta_{222nm}/\theta_{208nm}$ = 0.95 for the *cis*-irradiated structure.

When we compared the conformational changes exhibited by **c-CL** (**37**) itself and by the mixture (**25**+**37**), we observed different responses that suggested a difference in sensitivity to UV light irradiation. Peptide **37** showed a higher change in the magnitude of the θ_{222nm} minimum but also in the $\theta_{222nm}/\theta_{208nm}$ value than when irradiating the peptide mixture. Irradiation of **37** with 380 nm light decreased this coefficient in 7 units while (**25**+**37**) only decreased it in 3 units. As mentioned, we understood this response to irradiation with UV light as a sign of different sensitivity to photoisomerization depending on the stability of the peptide structure. In other words, the same level of energy put into *trans*-to-*cis* isomerization of the azobenzene when attached in the single peptide was not enough to cause the same effect when (**25**+**37**) were mixed together.

Figure 5.10 shows the thermal denaturation curve of a 100 µM solution of (**25**+**37**) compared to a 100 µM solution of **37**, each of them in PBS at pH 7.4. The melting point of the peptide mixture was slightly higher than the found for peptide **37** alone: T_M (**PEP1**+**c-CL**) = 58.6 ˚C > T_M(**c-CL**) = 54.6 ˚C. If we observe the curve of **37** (purple line), we see that the transition is not as noticeable as for (**25**+**37**) (green line). In the mixture, there is a large transition in the region of 40 to 60 ˚C that indicates evidences of disruption of the coiled-coil. From this data, we concluded that association of both peptides (**PEP1**+**c-CL**) increased the magnitude of the thermal stability of the coiled-coil structure.

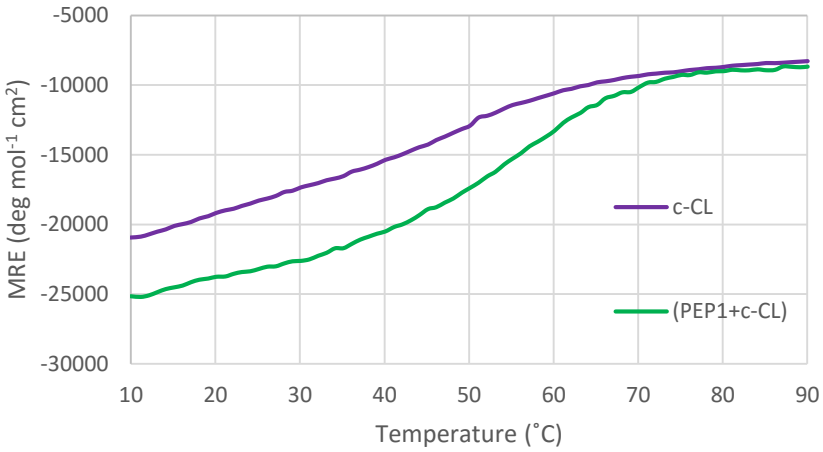

Figure 5.10: Thermal denaturation curves of 100 µM **PEP1** (**25**), **c-CL** (**37**), and (**PEP1+c-CL)** (**25**+**37**) in PBS buffer at pH 7.4: T_M (**25**) estimated lower than 32.3 ˚C; T_M (37) = 54.6 ˚C; T_M (28+37) = 58.6 ˚C. The peptide sequences of **PEP1** (**25**) and **c-CL** (**37**) are shown. The residues Cys (in red on the sequence) are the binding sites through which the azobenzene **24** is attached:

PEP1: KIAALKQKNAALKQEIAALEYEIALEQ
c-**CL**: Ac-EIAALEYEN**C**ALEQKIKALK**C**KIKALKQ-Am

To summarise, we verified that the peptide mixture (**PEP1**+**c-CL**) produced a blunt-ended coiled-coil structure with the ability to generate reversible photoisomerization upon irradiation with the appropriate wavelength. This mixture of peptides was found to be more α-helical, slightly more resistant to the photoswitching effect, and also showed a higher thermal stability than their single peptides **PEP1** (**25**) and **c-CL** (**37**) when these were alone.

When comparing systems 1 and 2, this is (**PEP1**+**CL**) and (**PEP1**+**c-CL**), we observed that the only difference was the double capping of **CL** in system 2. It seemed that the α-helical content of the peptide mixture was higher when half of the peptide sequences from the mixture were bearing a N-terminal acetyl group and a C-terminal amide group. This effect produced interactions between peptides that provided higher resistance to the photoswitching effect. Thus, the photoswitching effect of the mixture (**PEP1**+**CL**) was larger than that of the mixture (**PEP1**+**c-CL**). For this reason, since **28** and **37** were both double capped, we predicted a lower photoswitching effect for their mixture (**c-PEP1**+**c-CL**) than for the previous investigations.

Figure 5.11 shows the CD spectra of 100 µM solutions in PBS buffer at pH 7.4 and at 21 °C of **c-PEP1** (**28**) (dotted dark blue line), **c-CL** (**37**) (dotted purple line), and their mixture (**28**+**37**) (green line), as well as the photoisomerization effects showed after UV irradiation. The negative bands at 208 nm and 222 nm of **28** and **37** indicate some degree of α-helicity in their structures in equilibrium with disordered forms of the peptides. After mixing both peptides together, signs of association were observed by an increase in the magnitude of the θ_{222nm} minimum. This produced a $\theta_{222nm}/\theta_{208nm}$ = 0.99 indicating an increase in the degree of α-helicity of the peptide structure. We believed that the mixture (**28**+**37**) favoured dimeric blunt-ended coiled-coils with a high α-helical content. Since irradiation of the peptide mixture with 380 nm light for 20 min in a first attempt, 45 min in a second attempt, and 35 min in a last attempt did not generate any conformational change (yellow line), we also thought that the effect of the double capping of both individual peptides provided interactions that helped to stabilize the formation of blunt-ended heterodimers in a higher percentage. Thus, the energy used to photoswitch the azobenzene was insufficient in this case.

Figure 5.12 shows the thermal denaturation curve of the coiled-coil structure (**28**+**37**) at 100 µM in PBS at pH 7.4 compared to the ones for **28** and **37** under the same conditions. The melting point of **28** was about 20 ˚C lower than the melting point of **37**, indicating that **37** was thermally more stable than **28**: T_M (**c-PEP1**) = 32.3 ˚C < T_M (**c-CL**) = 54.6 ˚C. However, the melting point observed for the peptide mixture after coiled-coil formation was of a higher magnitude than any of the T_M observed for the individual peptides: T_M(**c-PEP1**+**c-CL**) = 67.7 ˚C. That indicated a higher thermal stability of the peptide mixture when assembled. This temperature was even higher than the T_M observed for the previous coiled-coil structure (**PEP1**+**c-CL**). We concluded that the interactions provided for both the N-acetyl group and the C-amide group at the end of the peptide sequences seemed to be crucial to gain thermal stability when forming α-helical blunt-ended coiled-coil structures.

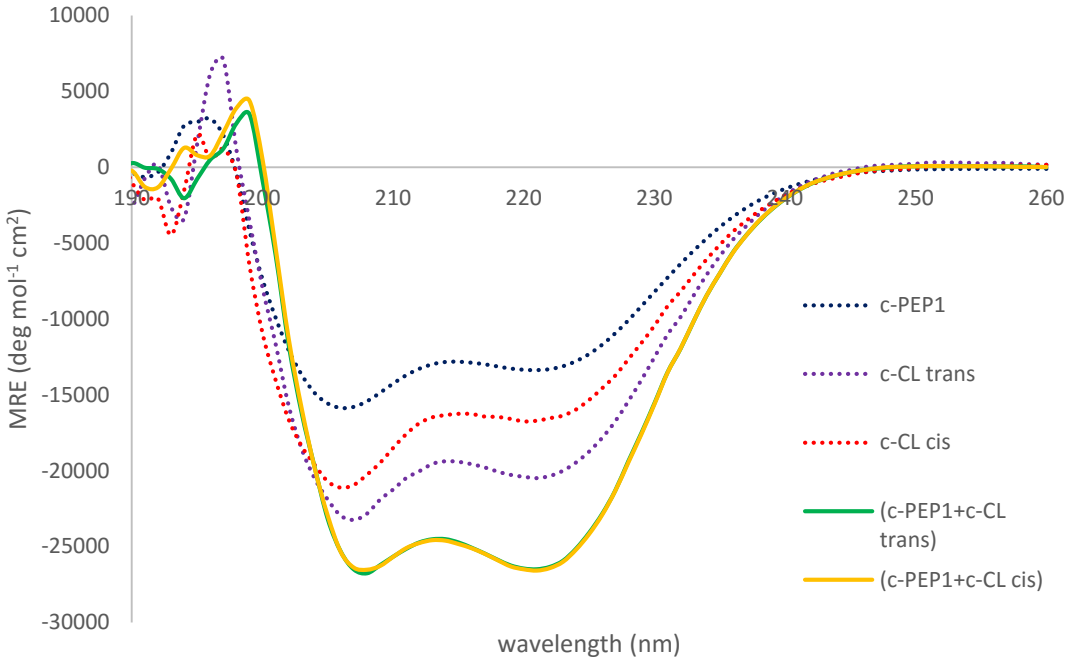

Figure 5.11: CD spectrum of 100 µM solutions of **c-PEP1** (**28**), **c-CL** (**37**), and their mixture (**28**+**37**) in PBS buffer at pH 7.4 at 21 ˚C, and the photoisomerization of the (**28**+**37**) system. The peptide sequences of **PEP1** (**25**) and **c-CL** (**37**) are shown. The residues Cys (in red on the sequence) are the binding sites through which the azobenzene **24** is attached:

c-PEP1: Ac-KIAALKQKNAALKQEIAALEYEIALEQ-Am
c-**CL:** Ac-EIAALEYEN**C**ALEQKIKALK**C**KIKALKQ-Am

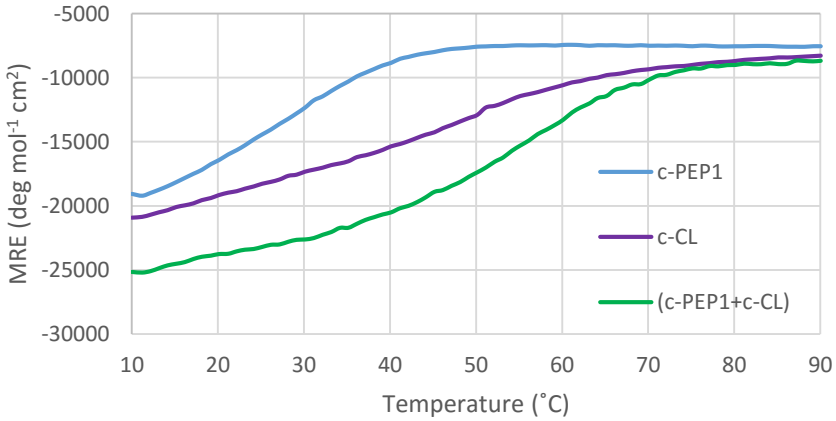

Figure 5.12: Thermal denaturation curves of 100 µM **c-PEP1** (**28**), **c-CL** (**37**), and (**c-PEP1+c-CL)** (**28**+**37**) in PBS buffer at pH 7.4: T_M (**28**) = 32.3 ˚C; T_M (**37**) = 54.6 ˚C; T_M (**28**+**37**) = 67.7 ˚C.

With all these results in hand, we could predict the results for the remaining peptide mixture (**c-PEP1**+**CL**) – this is system 3 from **Figure 5.2**, which we were not able to investigate as previously mentioned. Thus, as seen for the individual peptides, they would not form fully folded *α*-helical structures when alone. Instead, they would show some degree of *α*-helical content together with disordered forms of the peptides. However, upon their mixture, a peptide assembly with a higher *α*-helical content would be obtained. Since one of the individual peptides is double capped, this mixture would exhibit a higher *α*-helical content than that of (**25**+**35**) but similar to that of (**25**+**37**). In addition, this peptide system would be able to produce reversible photoisomerization by CD spectroscopy as observed in systems 1 and 2 – these are (**25**+**35**) and (**25**+**37**). Finally, the melting temperature would be higher than that of system 1 (**PEP1**+**CL**) but similar to system 2 (**PEP1**+**c-CL**), and lower than that of system 4 (**c-PEP1**+**c-CL**).

Figure 5.13 represents the θ_{222nm} values of peptide **37** and each one of the peptide assemblies discussed in this section as a sign of the stability of their structures at room temperature (in the *trans*-conformation state), *versus* the magnitudes of the photoswitching effects in each of them (this being given as an absolute value). The lower the θ_{222nm} value, the higher the *α*-helical content of each structure, and the higher the stability. Thus, the peptide assembly of (**28**+**37**) exhibited the largest degree of *α*-helical content and highest stability, this being due to the double capping of both individual peptides. In addition, (**28**+**37**) exhibited the largest resistance to the photoswitching effect. On the other hand, **37** showed the lowest degree of *α*-helical content, the least stability, and the largest photoswitching effect.

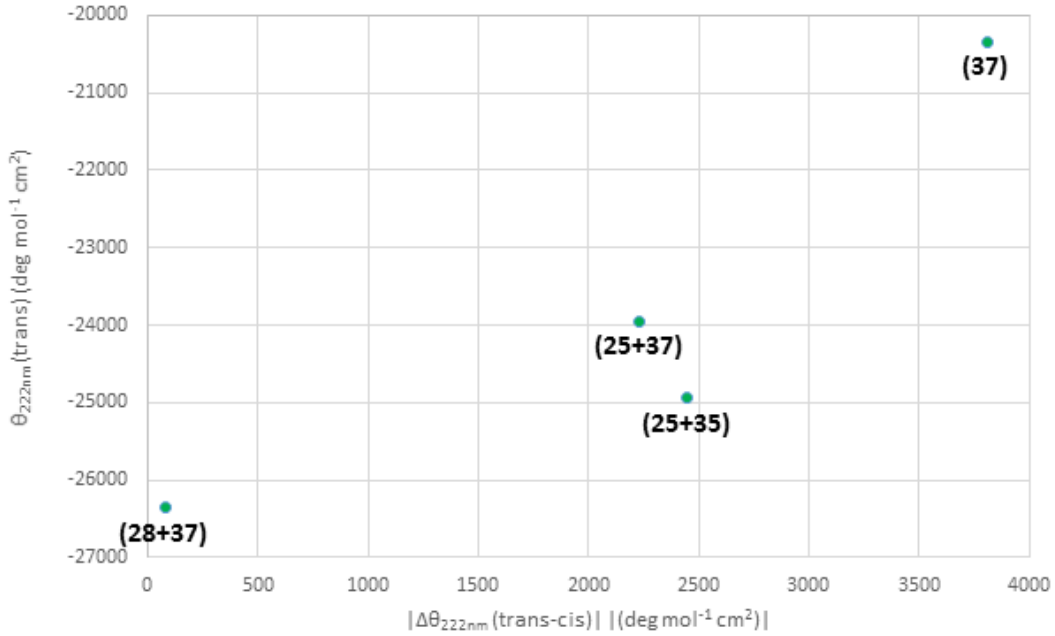

Figure 5.13: Representation of the stability (θ_{222nm} *trans*) (*y axys*) *vs*. the photoswitching effects (*x axys*) of **37**, (**25**+**35**), (**25**+**37**) and (**28**+**37**).

Table 5.1 summarises peptide data of θ_{222nm}, the ratio $\theta_{222nm}/\theta_{208nm}$ and some values of T_M obtained for the peptides and peptide mixtures from this **Chapter**.

Peptide or peptide system	conformation	θ_{222} (deg mol^{-1} cm^2)	$\theta_{222}/\theta_{208}$	T_M (°C)
CL (35)	*trans*	-15963.2	0.77	Not calc.
	cis	-14445.7	0.72	
c-CL (37)	*trans*	-20352.3	0.89	54.6
	cis	-16543.0	0.82	
(PEP1+CL)	*trans*	-24946.0	0.84	Not calc.
	cis	-22499.6	0.81	
(PEP1+c-CL)	*trans*	-23946.4	0.98	58.6
	cis	-21716.1	0.95	
(c-PEP1+c-CL)	*trans*	-26343.8	0.99	67.7
	cis	-26535.9	0.99	

Table 5.1: Peptide data obtained for **CL** (**35**), **c-CL** (**37**), (**PEP1**+**CL**) or (**25**+**35**), (**PEP1**+**c-CL**) or (**25**+**37**) and (**c-PEP1**+**c-CL**) or (**28**+**37**) in PBS at pH 7.4 and at 21 °C. The T_M values were not calculated for all peptide mixtures due to a lack of peptide **35**.

5.3 Summary

We were able to synthesize peptide partners – both capped and uncapped – for blunt-ended associations and for *α*-helical coiled-coil formation. These peptides were developed from the designed chassis **BEP** (**26**) and **c-BEP** (**29**) peptides described in **Chapter 3**. From them, we built Cys-containing peptides (**34** and **36**). These had the ability to attach the azobenzene derivative **24** through the thiols from the Cys residues. The resulting peptides were referred to as cross-linked peptides (**35** and **37**) and exhibited reversible photoswitching properties. The photoswitching degree was different depending on the peptide system they were forming. Peptides **35** and **37** exhibited a larger switch when alone but also exhibited a certain degree of photoswitching when they were forming *α*-helical coiled-coil peptide assemblies: (**25**+**35**), (**25**+**37**) and (**28**+**37**). The lower the θ_{222nm} value of each of the peptide assemblies, the higher the *α*-helical content of each structure, and the higher the stability. The structure produced by the mixture (**28**+**37**) exhibited the largest degree of *α*-helical content and highest stability, this being due to the double capping of both individual peptides. In addition, (**28**+**37**) exhibited the largest resistance to the photoswitching effect.

[1] G.A. Woolley, *Acc. Chem. Res.* **2005**, 38, 486-493.

Chapter 6

Conclusions

As we mentioned in the abstract and in the introductory chapter, this is considered to be an interdisciplinary research project in nature. It involves biomolecular design, for peptide design, and also both organic and inorganic chemistry, for the synthesis of biomolecular components that are incorporated into the peptide sequences to generate conformational switching.

By making use of Pd-catalysed cross-coupling methodologies (Negishi reaction), we have been able to synthesize both Fmoc- and Boc-protected unnatural amino acids (pyridylalanine derivative analogues) for metal-minding investigations. These were: Fmoc-2-Pal-O*t*Bu (**8**), Fmoc-3-Pal-O*t*Bu (**9**), Boc-2-Pal-OBn (**11**) and Boc-3-Pal-OBn (**12**). The conditions of the syntheses and yields of the target compounds were optimized, being Sphos the ligand used in all cases: compound **8** achieved 60% as maximum yield being 2-bromopyridine the coupling reagent; compound **9** achieved 55% as maximum yield with 3-bromopyiridine as the coupling reagent; compound **11** achieved 51% as maximum yield with 2-iodopyridine as coupling reagent; and, compound **12** achieved 45% as maximum yield being 3-iodopyridine the coupling reagent. This opens a wider scope to be used for the synthesis of other pyridyl-type amino acid analogues by using the Negishi methodology.

We were not able to synthesize the initial target **BSBCA** for the photoisomerization experiments on our peptide systems. This azobenzene derivative was desired since we believed that the sulfonic groups forming part of the molecule would provide a higher solubility when attached to our peptide designs. Though, an alternative azobenzene derivative to **BSBCA** was successfully synthesized: 4,4'-dichloroacetamido-azobenzene (**24**), being this achieved in a maximum yield of 96% (0.495 g). Compound **24** was found to be completely soluble under our working conditions (either ddH2O or PBS

buffer at pH 7.4), and its photoisomerization properties were proved to be efficiently incorporated in our peptide designs. As achieved in the synthesis of the unnatural amino acids, we also enhanced the conditions and increased the reaction yields of **24**.

We first designed and then built a chassis for *de novo* coiled-coil self-assembling peptide systems in both modes of blunt-ended and sticky-ended heterodimers. We found out that for the formation of *α*-helical coiled-coil and fibrous structures, we needed to double cap the peptide sequences (**28** and **29**) in order to provide the required stabilization to produce these conformations. The design of these peptide sequences included tuneable positions to incorporate either the synthetic pyridylalanine amino acids, with metal-binding properties, or to be swapped with Cys residues, for the attachment of the azobenzene derivative (**24**) through thiol-bridge formation.

When the chassis peptide-systems incorporated the unnatural pyridylalanine amino acid derivatives, some changes in their conformational structures were observed. In the case of the formation of blunt-ended heterodimers, all combinations of **c-BEP** (**29**) with each of the pyridyl-labelled peptides (**30** to **33**) produced thermally stable *α*-helical coiled-coil structures as verified by thermal denaturation experiments. Their thermal denaturation curves proved that these peptide assemblies increased their T_M about 20 ˚C compared to the most thermally stable peptide component (**c-BEP** in all cases) and between 30 ˚C and 40 ˚C compared to the least stable peptide component (the pyridyl-labelled peptides in all cases). Upon addition of the metal complex K_2PtCl_4, we found that the peptide assemblies dictated the final structure of the peptide systems and the addition of the Pt-complex did not appear to trigger any conformational changes. We thought that the assembly provided by the association between these peptides may be more energetically favourable than the possible structure produced by a conformational switch induced by the metal ion. All the peptide systems were more thermally stable after coiled-coil formation than the individual peptides as indicated by their T_M. In addition, the T_M of the metal-peptide structures exhibited a similar value to the one shown by the peptide structures without the metal additions.

In the case of the formation of sticky-ends heterodimers, not all combinations of **SAF** (**27**) with the pyridyl-labelled peptides **30** to **33** exhibited signs of *α*-helical coiled-coil and fibre formation by CD spectroscopy: the peptide assemblies of (**27**+**30**) and (**27**+**32**) showed the typical CD spectra pattern for *α*-helical coiled-coils and fibrous structures whilst the mixtures (**27**+**31**) and (**27**+**33**) did not exhibit evidences of *α*-helical coiled-coil or fibre formation. From the assemblies that promoted fibre formation, and after checking the mixture (**27**+**30**) at a lower concentration (50 μM), we believed that higher concentrations of the peptide mixtures (higher than 100 μM) might show better and faster results of fibre formation (concentration-dependent), with the kinetics of these processes an important issue to take into account. In addition, the magnitude of the θ_{208nm} and θ_{222nm} minimums in the CD spectra of all these peptide assemblies appeared to be lower than what expected for these type of conformations. We thought that the insertion of the unnatural amino acids within the peptide sequences caused this effect since it was a common feature to all of the peptide mixtures.

Moreover, when comparing (**27**+**30**) and (**27**+**33**), we observed that the insertion of the 3-pyridylalanine motif promoted *α*-helical coiled-coil and fibre formation, whilst 4-pyridylalanine was unable to produce the same effect. We thought that the distancing from the nitrogen atom of the 3-pyridylalanine residue to the coiled-coil backbone could favor stabilizing interactions – such as hydrogen bonds – to promote the required structure. However, due to the distancing of the nitrogen atom in the 4-pyridylalanine residue together with the electronic effects of a para-substituted pyridyl ring did not produce the same effect. When comparing (**27**+**31**) with (**27**+**32**), we thought that the different spacing of the two pyridylalanine motifs inserted within the sequences may be the cause of the different effects: the spacing *i* → *i*+4 in peptide **31** (positions *f* and *b* of the heptad repeat) was insufficient, increasing steric hindrance between them and preventing fibre formation, whilst for an *i* → *i*+7 the greater spacing in peptide **32** (positions *f* and *f* of the heptad repeat) allowed for fibre formation.

The metal-binding investigations that we undertook of the mixtures of **SAF** with the pyridyl-labelled peptides provided us with important information. In the first set of

experiments, where the metal complex was added to the 24 hours matured peptide assemblies, an increase in the chiral scattering of all the coiled-coils was observed. However, in the second set of experiments, different results were obtained. In this case, the Pt(II) complex was first mixed with the individual pyridyl-labelled peptides (not showing important conformational changes), and 24 hours later the **SAF** peptide was added. In this cases, the addition of SAF promoted conformational changes increasing the degree of α-helicity in all the mixtures. However, this was never enough to produce fully folded α-helical coiled-coils or fibres. We thought that the addition of the Pt(II) complex prior to the addition of **SAF** slowed the kinetics of the peptide assembly preventing the formation of fibrous structures. From these results, we concluded that the order in which the pyridyl-labelled peptides **30** to **33** were mixed either with **27** or the Pt(II) complex was important since the two ways produced different rearrangements. Therefore, in the mixtures of **SAF** with the pyridyl-labelled peptides, we observed that metal-binding produced conformational changes and was responsible for the final structure of the assemblies.

As a future work for these metal-binding experiments, obtaining crystal structures of the metal-peptide assemblies would provide information about the precise arrangements. This would be a useful tool to understand the interaction modes between peptides and to what extent the conformation is driven by the metal complex. TEM of the matured fibres from all the peptide mixtures between **SAF** (**27**) and the pyridyl-labelled peptides could be used to compare whether the length or thickness of these fibres changes from that formed by the chassis peptides. In the same direction, different stoichiometries of metal-to-peptide could be investigated with the same peptide systems and compare their results. Since we tested 3- and 4-pyridylalanine derivatives, it would be interesting to investigate the effects of 2-pyridylalanine, as well as the effects of the insertion of different mixtures of these, e.g: 2- and 3-pyridylalanines, 2- and 4-pyridylalanines, etc. It would also be interesting to use different type of ligands such as bipyridyl-derivatives and investigate it these could promote α-helical coiled-coil and fibre formation. In the same way, different metal ions and metal complexes could be examined for metal-binding. Different sizes of

metal ions or metal ions with different coordination geometries could produce different peptide assemblies at different metal-peptide stoichiometries.

With respect to the photoswitching investigations of the peptide systems that we were able to build with the azobenzene derivative (**24**), we found different photoswitching efficiencies. We were able to synthesize peptide partners – both capped and uncapped – for blunt-ended like associations and for α-helical coiled-coil formation. These peptides were developed from the designed chassis **BEP** (**26**) and **c-BEP** (**29**) peptides, from which we built peptides **34** and **36**. These peptides successfully attached the azobenzene derivative **24** through the thiol groups of the Cys residues forming the cross-linked peptides (**35** and **37**), which exhibited reversible photoswitching properties. The photoswitching degree was different in each peptide system: **35** and **37** exhibited larger switches when alone but also exhibited a certain degree of photoswitching when they were forming α-helical coiled-coil peptide assemblies with their corresponding partners, always in a blunt-ended mode. In addition, the thermal stability of the peptide systems increased as the C-terminus and N-terminus of the peptide sequences were capped. Thus, the more capped ends, the higher the thermal stability, but also, the lower the switch efficiency of the peptide systems.

The success of this photoswitching effect in simple systems encourages us to try it in larger systems which would add a whole extra layer of complexity to the assemblies. The use of azobenzene derivatives for photo-regulation of peptide sequences may provide a potential power source for protein motors, e.g. in a motor hub to influence the direction and efficiency of stepping.

Overall, in this thesis, we were able to achieve our goals of designing and synthesizing self-assembling peptide sequences for both blunt-ended and sticky-ended coiled-coil formation. The use of molecular components generated conformational switching in the designed structures. The tools utilized for these structural rearrangements were both metal-binding – by incorporating unnatural amino acid analogues – and light irradiation – by amplifying up the photoswitching effect of the azobenzene chromophore after attachment on to different coiled-coil forming peptides.

Chapter 7

Experimental

7.1 General experimental

7.1.1 Reagents

For the synthesis of unnatural amino acids, the reagents iodine, triphenyl phosphine, bis(dibenzylideneacetone)palladium(0), and imidazole were purchased from Alfa Aesar (Heysham, Lancashire, UK). The amino acid Fmoc-L-Ser-OH was purchased from both Novabiochem (Darmstadt, Germany) and Mimotopes Ltd. (Wirral, UK). All the other reagents were purchased from Sigma-Aldrich Company Ltd. (Gillingham, Dorset, UK). All reagents, except Zn(dust) which was acid washed, were used as received without further purification.

For the synthesis of the azobenzene derivatives, all the reagents: 2,5-diaminobenzenesulfonic acid (**15**), 4,4'-aminoacetanilide (**20**), glacial acetic acid, acetic anhydride, hydrogen peroxide (33%), sodium hydroxide, hydrochloric acid (37%), chloroacetyl chloride and potassium carbonate were purchased from Sigma-Aldrich Company Ltd. (Gillingham, Dorset, UK) and used as received withouth further purification.

For the synthesis of the peptide sequences, the Fmoc-protected L-amino acid derivatives, dimethyl sulfoxide (DMSO), Tris(2-carboxyethyl)phosphine hydrochloride solution (TCEP-HCl), trifluoroacetic acid (TFA), Tris(hydroxymethyl)aminomethane hydrochloride (Tris-HCl), piperidine, 1-Methyl-2-pyrrolidinone (NMP), and triisopropylsilane (TIPS) were purchased from Sigma-Aldrich Company Ltd. (Gillingham, Dorset, UK). Amino acid side chain functionality was protected as follows: Fmoc-Asn(Trt)-OH, Fmoc-Cys(Trt)-OH, Fmoc-Gln(Trt)-OH, Fmoc-Glu(*t*Bu)-OH, Fmoc-Lys(Boc)-OH, Fmoc-Tyr(*t*Bu)-OH. Alanine, Isoleucine and Leucine were not side chain protected.

N,*N'*-Diisopropylethylamine (DIPEA), *N,N'*-Dimethylformamide (DMF), and the Fmoc-protected unnatural amino acids Fmoc-L-3-pyridylalanine-OH and Fmoc-L-4-pyridylalanine-OH were purchased from AGTC Bioproducts Ltd. (Hessle, UK). Both the preloaded Fmoc-Gln(Trt)-wang resin (100-200 mesh) and rink amide MBHA resin were purchased from Novabiochem (Darmstadt, Germany). *N*,*N*'-Diisopropylcarbodiimide (DIC) was purchased from Fluorochem (Derbyshire, UK). Anhydrous 1-hydroxybenzotriazole (HOBt) was purchased from CEM peptides (Buckingham, UK). (Benzotriazol-1-yloxy)tripyrrolidinophosphonium hexafluorophosphate (PyBOP) was purchased from Apollo Scientific Limited (Stockport, Cheshire, UK). All reagents were used as received without further purification.

For the metal-binding investigations, the platinum complex K_2PtCl_4 was purchased from Sigma-Aldrich Company Ltd. (Gillingham, Dorset, UK). This was used as received without further purification.

For the synthesis of the azobenzene-peptide systems, the reagents dimethyl sulfoxide (DMSO), Tris(2-carboxyethyl)phosphine hydrochloride solution (TCEP-HCl), Tris(hydroxymethyl)aminomethane hydrochloride (Tris-HCl), and sodium hydroxide (NaOH) were purchased from Sigma-Aldrich Company Ltd. (Gillingham, Dorset, UK). A solution of NaOH (0.1M) was used to adjust the pH to 8.5 for both TCEP and Tris buffer solutions. The peptides were used as obtained after HPLC purification.

7.1.2 General experimental: NMR, IR and ESI-MS spectroscopy

NMR spectra were collected using a Bruker Avance 400 MHz at 400 MHz for ^{1}H NMR measurements and at 100 MHz for ^{13}C NMR measurements. Chemical shifts are reported in ppm and are referenced to residual solvent peaks: $CHCl_3$ (^{1}H 7.26 ppm, ^{13}C 77.0 ppm) and DMSO (^{1}H 2.50 ppm, ^{13}C 39.5 ppm); multiplicities; s = singlet, d = doublet, dd = doublet of doublets, ddd = doublet of doublet of doublets, dt, doublet of triplets, m = multiplet, t = triplet, q = quartet, bd = broad doublet, bs = broad singlet, app s = apparent singlet, app d = apparent doublet, app t = apparent triplet, app td = apparent triplet doublet. J couplings are measured in Hertz (Hz). All reactions were monitored by TLC using Merck precoated silica gel plates. Column chromatography

was performed using silica gel (40-60 mM) using the solvent system indicated. All reported yields refer to the isolated yield and the product purity was estimated to be >95% by ^{1}H NMR.

IR spectra were recorded on a Perkin Elmer Spectrum RX1 fitted with an ATR attachment, intensities as; s = strong, m = medium, w = weak, v = very, bd = broad. All absorptions measured in cm^{-1}.

Electro-Spray Ionization Mass Spectra (ESI-MS) were collected on a Waters TQD mass spectrometer and accurate mass spectra were collected on a Waters LCT Premier XE mass spectrometer.

7.1.3 Matrix-Assisted Laser Desorption/Ionization Time-Of-Flight mass spectrometry (MALDI-TOF MS)

Characterization of peptides was achieved by MALDI-TOF mass spectrometry. MALDI spectra were collected using an Autoflex II ToF/ToF mass spectrometer (Bruker Daltonik GmBH) equipped with a 337 nm nitrogen laser. All peptides were dissolved in deionized water (1 mg/mL) for MS analysis. MS data was processed using FlexAnalysis 2.0 (Bruker Daltonik GmBH).

7.1.4 Purification of crude peptides by RP-HPLC

Crude peptides were purified by reversed-phase high-performance liquid chromatography (RP-HPLC) using a Speck and Burke Analytical C-18 column (5.0 µm, 10.0 x 250 mm) attached to a PerkinElmer Series 200 LC Pump and 785A UV/Vis Detector. For preparative runs, concentrations up to 30 mg/mL (1.0 mL) were injected and peak fractions of interest pooled and lyophilized. Since all the peptide sequences synthesized in this thesis were water soluble, all samples were prepared by dissolving the peptide powder in H_2O and the solution centrifuged before injection to remove undissolved material. A flow rate of 2 mL/min was used for all separations. The aqueous phase (solvent A) consisted of a mixture (*v/v*) 95% H_2O/5% CH_3CN with 0.1% TFA while the organic phase (solvent B) consisted of a mixture (*v/v*) 5% H_2O/95%

CH_3CN with 0.1% TFA. Initial HPLC injections of each peptide sample were set to 90 min for linear gradients of 0-100% of solvent B to detect different compound peaks, and either shorter times (60 min) or shorter gradients (from solvent A to B) applied for subsequent injections depending on each peptide sequence. Analytical runs of the crude peptides after MALDI analysis were used to confirm the presence of a single peptide within the pure fraction. These were small-scale runs (1 mg/mL loading) in a 30 minutes linear gradient of 0-100% of solvent B. A UV-Vis lamp was used as detector and 280 nm was the wavelength selected in all cases to monitor and detect the chromophore of the Tyr amino acid – which was part of all the peptide sequences.

7.1.5 Ultraviolet-visible spectroscopy (UV-Vis)

UV/Vis absorbance spectra were measured with a Unicam UV2-300 spectrometer using quartz cuvettes of 10 mm pathlength. All peptides were dissolved and measured in double distilled water (ddH_2O) for peptide-concentration determination when using PBS (10x) as the buffer solution of the sample, and were dissolved within the buffer solution when either PBS (1x) or MOPS were used as solvent/buffer of the samples. Peptide samples were prepared from 1-5 mg of peptide powder dissolved in 1-2 mL of solvent (ddH_2O, PBS or MOPS) and the absorbance recorded maximums at 280 nm corresponding to the absorption of Tyr, which is the chromophore for all the peptide sequences and shows a molar extinction coefficient of $\varepsilon = 1280\ cm^{-1}mol^{-1}$ at 280 nm at neutral pH.[1] For the labelled peptides with pyridylalanine amino acids, a maximum at 262 nm was observed and a molar extinction coefficient of $\varepsilon = 3400\ cm^{-1}mol^{-1}$ at 262 nm was used as this is the value for picoline, which shows similarity with the chemical structure of the pyridylalanine motifs.

Photoisomerization of the azobenzene derivative (**24**) in DMSO was monitored by UV/Vis and the concentration of the dark-adapted (*trans* isomer) azobenzene derivative was determined by the molar exctinction coefficient at 367 nm ($\varepsilon = 28000\ cm^{-1}mol^{-1}$).[2]

The Beer-Lambert law (**Equation 7.1**) was used to calculate the concentration of each peptide sample:

$$A = \varepsilon \, x \, c \, x \, l \qquad \textit{(Eq. 7.1)}$$

A being the absorbance, *c* being the concentration of the peptide sample (mol/L), *l* being the path length of the beam of light throughout the cuvette that contains the sample (1 cm in our case), and *ε* the molar extinction coefficient ($cm^{-1}mol^{-1}$).

Since the absorbance was determined by the spectrometer and we knew the values of *l* = 1 and the molar extinction coefficient (ε) at 280 nm (for the Tyr), at 262 nm (for the picoline), or at 367 nm (for the azobenzene), the concentration was calculated by:

$$c = \frac{A}{\varepsilon} \qquad (\textit{Eq. 7.2})$$

7.1.6 Circular dichroism spectroscopy (CD)

Circular dichroism (CD) is the biophysical technique used to determine the secondary structure of our peptides and peptide mixtures. It gives us a value of the differential absorbance of left- and right- handed circularly polarised light (**Equation 7.3**):

$$\Delta A = A\,(LHCP) - (RHCP) \qquad (\textbf{Eq. 7.3})$$

Where *A* is absorbance, *LHCP* is left-handed circularly polarised light, and *RHCP* is right-handed circularly polarised light.

In general, when compound concentration and cell path length are taken into account, we obtain the molar circular dichroism (Δε) (**Equation 7.4**):

$$\Delta\varepsilon = \varepsilon\,(LHCP) - \varepsilon\,(RHCP) = \frac{\Delta A}{(c \, x \, l)} \qquad (\textbf{Eq. 7.4})$$

Where *c* is the molar concentration, *l* is the path length (cm), and *ε (LHCP)* and *ε (RHCP)* are the molar extinction coefficients for the left- and right-handed circularly polarised light respectively.

However, CD measurements are usually reported in degrees of ellipticity (θ) or molar ellipticity (or mean residue ellipticity, MRE), which is circular dichroism corrected for concentration and it is calculated as shown in **Equation 7.5** next:

$$MRE = \frac{\theta\ (222nm)}{(c\ x\ N)} \qquad \textbf{(Eq. 7.5)}$$

Where θ_{222nm} is the ellipticity at 222 nm, *c* is the molar concentration, and *N* is the number of amino acids involved in the peptide or peptide mixture being measured.

CD measurements were performed using a Jasco Model J-1500 spectropolarimeter fitted with a Jasco J815 MCB-100 mini circulation bath. All measurements were carried out in thermostated quartz cuvettes of 1 mm path length. Temperatures were measured using a microprobe placed directly into the sample cell. All peptide samples for CD analysis were measured in buffer solutions of either PBS or MOPS. These solutions were prepared from stock solutions of higher concentrations than the required ones mixed with a 1/10 (v/v) of buffer solution when the buffer was PBS (10x). When using PBS (1x) or MOPS, the stock solutions were prepared in the buffer solutions and diluted to the required concentration. CD measurements were recorded at concentrations of: 20, 50, 100 and 200 µM to investigate concentration-dependence effects. Both PBS and MOPS buffer solutions were adjusted with NaOH to the corresponding pH: PBS at pH 7.4 and MOPS at pH 8.5.

Thermal denaturation curves were measured by monitoring the θ_{222nm} (mean residue ellipticity at 222 nm) at various temperatures ranging from 10 ˚C to 90 ˚C with a temperature gradient of 0.5 ˚C/min and equilibrating each reached temperature for 10 seconds prior to next measurement. The thermal denaturation multianalysis program calculator method was based on what is explained next.

Assuming that the peptide (or peptide mixture) in solution is in equilibrium at certain temperature such (**Equation 7.6**):

$$N \rightleftharpoons D \qquad K_D = \frac{[D]}{[N]} \qquad \textbf{(Eq. 7.6)}$$

Where N and D are the peptide (or peptide mixture) before and after denaturation respectively, K_D is the equilibrium constant for peptide denaturation and [N] and [D] represent the concentration of non-denaturated and denaturated peptides.

If denaturation occurs or not can be evaluated thermodynamically using the ΔG_D free energy, which can be expressed in terms of K_D as:

$$\Delta G_D = -RT\ ln\ KD \quad \textbf{(Eq. 7.7)}$$

In addition, since:

$$\Delta G_D = -\Delta H - T\Delta S \quad \textbf{(Eq. 7.8)}$$

The enthalpy and entropy can be determined using the following equation:

$$\ln K_D = -\frac{\Delta H}{R}\ x\ \frac{1}{T} + \frac{\Delta S}{R} \quad \textbf{(Eq. 7.9)}$$

Since K_D and T are known, the ΔH value can be found from the slope of a graph of *ln* K_D against –(1/T), and the ΔS value from the intercept of a van't Hoff graph. In addition, if K_D = 1, in **Eq. 7.9**, that would mean that [N] = [D], so this would give the denaturation temperature value (**T_M**) (**Equation 7.10**):

$$T_M = \frac{\Delta H}{\Delta G} \quad \textbf{(Eq. 7.10)}$$

Photo-isomerization of the cross-linked peptides was accomplished by irradiating peptide solutions with either 380 nm or 450 nm light for a minimum of 20 min.

7.1.7 Transmission electronic microscopy (TEM)

For TEM measurements, images were obtained using a JEOL 2100F FEG TEM with a schottky field emitter operating at 200 kV, a Gatan Orius camera for acquiring high quality images over a wide field of view as well as diffraction patterns, a video capturing software using Digital Micrograph platform for dynamic experiments, a GATAN GIF tridiem with 4 megapixel Ultrascan™ 1000 CCD camera used for energy filtered imaging and CBED, and a JEOL HAADF/bright field PMT and Gatan ADF/bight field PMT for STEM imaging.

Samples at 100 μM of the corresponding peptides in 10 mM MOPS at pH 8.5 were prepared. Fixation and embedding of the samples is carried out on the dark side of a carbon film grid. A droplet of the sample is added onto the grid and left for 30 seconds before sucking off the excess of liquid with filter paper. A droplet of double distilled water (ddH_2O) is added onto the grid to avoid it getting dry and after 20 seconds is sucked off with filter paper. This washing step with ddH_2O is repeated once more before continuing with the negative staining. A droplet of an uranyl acetate solution (used as negative staining) is added onto the grid and dried with filter paper after 30 seconds. The sample is then ready to be inserted into the microscope and be analysed.

7.2 General experimental procedures

7.2.1 General procedure for the palladium-catalysed cross-coupling of protected iodoalanines: Negishi chemistry.

Acid washed zinc dust (4 eq.) was placed in a pyrex test tube flask fitted with a screw top that could be opened when chemicals were added at the time that vacuum or argon were applied. The reaction flask was evacuated under heating at 100 ˚C for at least 30 minutes with vigorous stirring. After cooling to 70 ˚C under argon, and having stopped the vacuum line, anhydrous DMF (0.5 mL) and I_2 (20 mg) were added and the light grey suspension stirred for 15 minutes. The reaction mixture was then cooled to 50 ˚C followed by the addition of the corresponding iodoalanine, **7** or **10** (1 eq) in DMF (1 mL). After stirring for 5 minutes under argon, addition of the catalyst $Pd(dba)_2$ (0.03 eq), the ligand (0.09 eq) and the relevant aryl halide (1 eq) were added and the resulting black mixture stirred at 50 ˚C under argon for a minimum of 5 hours. The reaction mixture was sealed to keep in the Argon and cooled to room temperature whilst stirring overnight. Next step was purification *via* column chromatography without work-up (SiO_2; 80/20 Hexane/EtOAc → 100% EtOAc). After purification, work-up was needed to remove the DMF remaining in the pyridylalanine derivatives.

7.2.2 Automated Fmoc Solid-Phase Peptide Synthesis

All peptides were synthesized using solid-phase methods on an automated CEM Liberty1 single-channel microwave peptide synthesizer equipped with a Discover microwave unit. All resins were left to swell in the appropriate solvent (DMF or DCM, see individual syntheses in **Section 7.2.3**) for a minimum of 2 hours at room temperature before starting the couplings. All reactions were carried out using the 30 mL polytetrafluoroethylene (PTFE) reaction vessel, with microwave heating and agitation by bubbling nitrogen gas. Couplings were carried out using a 5-fold excess of Fmoc-protected amino acid, activator (10 equiv) and activator base (20 equiv) unless otherwise stated. For double and triple couplings the reaction vessel was drained after each cycle and fresh reagents were added. Amino acid side chain functionality was protected as described in **Section 7.1.1**. Fmoc deprotections were carried out using a 20% (*v*/*v*) solution of piperidine in DMF in all cases.

Microwave-assisted couplings

Microwave couplings at 0.05 mmol scale were carried out for 10 min at 75 ˚C and 20 W power unless otherwise stated. Cys residues were coupled at low temperature: 30 min at room temperature followed by 10 min at 50 ˚C (20 W). The Fmoc group was removed by a single treatment with piperidine solution at 75 ˚C (35 W) for 3 min. For 0.1 mmol scale syntheses the power was increased to 25 W for couplings and 45 W for deprotections.

Room temperature couplings

Couplings at room temperature were carried out for 60 min. The Fmoc group was removed by two successive treatments with piperidine solution (5 min, then 10 min).

Peptide sequences capping

Acetylation of the N-terminus was accomplished by suspending the peptide-resin in a 20% (v/v) solution of acetic anhydride in DMF for 30-45 min.

Cleavage of peptides from resin

TFA cleavage of all peptides from resin was achieved by treating the acid-labile peptide-resin with 2.85 mL TFA and 0.15 mL deionized water, with 0.15 mL TIPS as scavenger for a minimum of 3 hours at room temperature. The resin was then removed by filtration and the filtrate was added dropwise to 35 mL of ice-cold diethyl ether. After centrifugation the supernatant was removed and the pellets suspended in fresh ether and centrifuged again. Following further centrifugation, the supernatant was discarded. The resulting solid peptide was dissolved in deionized water and lyophilized.

7.2.3 General experimental procedures for peptide synthesis

Peptide synthesis – Procedure 1

Fmoc-Gln(Trt)-wang resin was used (0.59 mmol/g substitution, 0.05 mmol) and swollen in DMF for three hours. Both couplings and deprotections were carried out under microwave-assistance (see **Section 7.2.2**). PyBOP was the activator and DIPEA/NMP used as the activator base. Peptide cleavage from resin was carried out as described in **Section 7.2.2**.

Peptide synthesis – Procedure 2

Fmoc-Gln(Trt)-wang resin was used (0.59 mmol/g substitution, 0.10 mmol) and swollen in DMF for three hours. Couplings were microwaved-assisted whilst deprotections were carried out under conditions of room temperature (see **Section 7.2.2**). PyBOP was the activator and DIPEA/NMP the activator base. Peptide cleavage from resin was carried out as described in **Section 7.2.2**.

Peptide synthesis – Procedure 3

Fmoc-rink amide MBHA resin was used (0.59 mmol/g substitution, 0.01) and swollen in DCM for three hours. Both couplings and deprotections were carried out under microwave-assistance (see **Section 7.2.2**). HOBt was the activator and DIC the coupling reagent. After completion of the synthesis, the peptide was capped on the N-terminus. Peptide cleavage from resin was carried out as described in **Section 7.2.2**.

Peptide synthesis - Procedure 4

Fmoc-Gln(Trt)-wang resin was used (0.59 mmol/g substitution, 0.10 mmol) and swollen in DCM for three hours. Both couplings and deprotections were carried out under microwave-assistance (see **Section 7.2.2**). HOBt was the activator and DIC the coupling reagent. Peptide cleavage from resin was carried out as described in **Section 7.2.2**.

Peptide synthesis – Procedure 5

Fmoc-rink amide MBHA resin was used (0.59 mmol/g substitution, 0.10 mmol) and swollen in DCM for three hours. Microwave conditions of couplings and deprotections were used from residues 1 to 14. Room temperature conditions of couplings and deprotections were used from position 15 until completion of the peptide sequence (see **Section 7.2.2**). HOBt was the activator and DIC the coupling reagent. After completion of the synthesis, the peptide was capped on the N-terminus. Peptide cleavage from resin was carried out as described in **Section 7.2.2**.

Peptide synthesis – Procedure 6

Fmoc-rink amide MBHA resin was used (0.59 mmol/g substitution, 0.10 mmol) and swollen in DCM for three hours. Microwave coupling and deprotection conditions were used except for couplings 1 and 25 to 28 which used room temperature coupling and deprotections conditions (see **Section 7.2.2**). Cys residues were coupled at low temperature: 30 min at room temperature followed by 10 min at 50 ˚C (20 W). HOBt was the activator and DIC the coupling reagent. After completion of the synthesis, the peptide was capped on the N-terminus. Peptide cleavage from resin was carried out as described in **Section 7.2.2**.

7.2.4 General procedure for metal-binding investigations

A stock solution of the metal-complex K_2PtCl_4 was prepared by dissolving the red crystals in a 10 mM MOPS buffer solution at pH 8.5 and at room temperature (21 ˚C). By diluting this stock solution with the same buffer solution, different concentrations were prepared as needed for each one of the combinations of the metal-peptide assemblies. The solutions at a known concentration were mixed with the peptide mixtures and CD measurements were recorded at different times at 21 ˚C.

7.2.5 General procedure for intramolecular cross-linking of the azobenzene derivative (24) to a Cys-containing peptide

Intramolecular cross-linking of the Cys-containing peptides by compound **24** could be achieved as follows. A solution of the Cys-containing peptide in ddH_2O (1 eq, 0.079 mM to 3.1 mM) was combined with a 5 mM Tris-buffer solution (pH 8.5) and TCEP (5 mM, pH 8.5) and incubated at room temperature under inert conditions (N_2 or Ar) for a minimum of 1 hour. The reaction flask was protected from light with aluminium foil and immersed into an oil bath at 40 ˚C. When the temperature of the solution reached 40 ˚C, a solution of azobenzene (**24**) in DMSO (0.78 eq) was added dropwise and stirred for 20 min in the dark. Another addition of a more concentrated solution of **24** in DMSO (13.6 eq) was added dropwise and stirred for another 20 min in the dark. The reaction flask was then exposed to light while stirring for another 20 min. The crude product was lyophilized before purification by RP-HPLC.

7.3 Synthesis of pyridylalanine containing amino acids and precursors

Fmoc-Ser(OH)-OtBu (6)

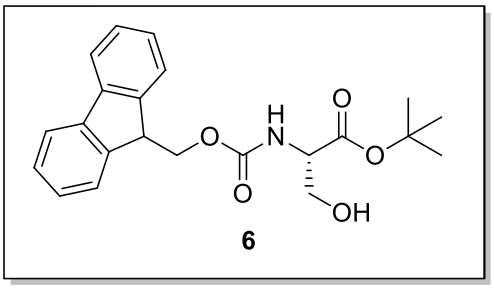

6

Fmoc-L-Serine (5.00 g, 15.27 mmol) and *tert*-butyl 2,2,2-trichloroacetimidate (8.85 g, 22.91 mmol) were dissolved in ethyl acetate (75 mL) and the reaction was left to stir at r.t. for 24 h. The reaction mixture was concentrated under vacuum and the crude product was then purified via column chromatography (SiO_2; 80/20 hexane/EtOAc → 100% EtOAc) to afford **6** as a white solid (5.54 g, 94%). ν_{max}(solid)/cm^{-1} 3479.4 (w bd, O-H), 3373.3 (w, N-H), 2963.5 (w, C-H_{Ar}), 1736.8 (s, C=O), 1678.6 (vs, C=O), 1537.4 (s, N-H), 1259.4 (C-O); ^{1}H NMR δ 1.42 (s, 9H, *t*Bu), 3.87 (m, 2H, β-CH_2), 4.16 (t, 1H, J = 7.2 Hz, Fmoc-CH), 4.26 (m, 1H, α-H), 4.35 (d, 2H, J = 9.6 Hz, Fmoc-CH_2), 5.60 (d, 1H, J = 7.2 Hz, NH), 7.25 (app td, 2H, J_{ortho} = 7.2 Hz, J_{meta} = 1.2 Hz, Ph), 7.34 (app td, 2H, J_{ortho} = 7.2 Hz, J_{meta} = 1.2 Hz, Ph), 7.54 (app d, 2H, J = 7.2 Hz, Ph), 7.70 (app d, 2H, J = 7.2 Hz, Ph); ^{13}C NMR δ 26.9 (*t*Bu), 46.2 (α-CH), 55.6 (Fmoc-CH), 62.7 (β-CH_2), 66.2 (Fmoc-CH_2), 81.9 (*t*Bu), 118.9 (CH_{Ar}), 124.1 (CH_{Ar}), 126.1 (CH_{Ar}), 126.7 (CH_{Ar}), 140.3 (C_{Ar}), 142.7 (C_{Ar}), 155.3 (NH-CO), 168.4 (COO*t*Bu); (ESI$^+$) *m/z* 407.2 [M+Na]$^+$; HRMS calculated for $C_{22}H_{25}NO_5Na$ 406.1630 [M+Na]$^+$, found 406.1612.

The data obtained is consistent with that given in the literature.[3]

Fmoc-Ala(I)-OtBu (7)

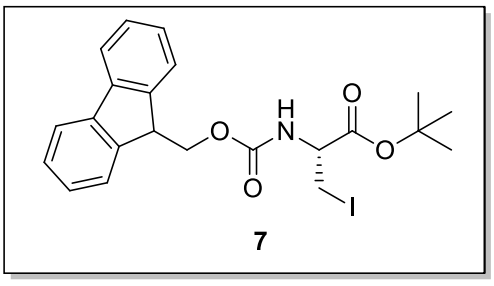

7

Fmoc-Ser(OH)-O*t*Bu **6** (5.19 g, 13.50 mmol), triphenylphosphine (3.56 g, 13.58 mmol), imidazole (0.92 g, 13.58 mmol) and iodine (solid) (1.75 g, 13.83 mmol) are dissolved in DCM (100 mL) . The reaction was left to stir at r.t. for 24 h. and then concentrated under vacuum. The crude product was purified via column chromatography (SiO_2; 90/10

hexane/EtOAc → 100% EtOAc) to give **7** as a sticky yellow solid (3.58 g, 54%). ν_{max}(solid)/cm^{-1} 3383.6 (w, N-H), 2968.0 (w, C-H$_{Ar}$), 1734.9 (s, C=O), 1698.4 (vs, C=O), 1510.3 (s, N-H), 1387.5 (s, C-O); ^{1}H NMR δ 1.52 (s, 9H, *t*Bu), 3.60 (m, 2H, β-CH$_2$-I), 4.25 (app t, 1H, *J* = 4.4 Hz, α-H), 4.35 (dd, 1H, *J* = 4.4 and 4.0 Hz, Fmoc-CH), 4.42 (m, 2H, Fmoc-CH$_2$), 5.68 (d, 1H, *J* = 4.0 Hz, NH), 7.32 (m, 2H, Ph), 7.4 (t, 2H, *J* = 4.4 Hz, Ph), 7.61 (d, 2H, *J* = 4.4 Hz, Ph), 7.76 (d, 2H, *J* = 4.4 Hz, Ph); ^{13}C NMR δ 27.9 (*t*Bu), 47.1 (α-CH), 54.0 (Fmoc-CH), 67.1 (I-CH$_2$), 67.3 (Fmoc-CH$_2$), 83.6 (*t*Bu), 120.0 (CH$_{Ar}$), 125.2 (CH$_{Ar}$), 127.1 (CH$_{Ar}$), 127.7 (CH$_{Ar}$), 141.3 (C$_{Ar}$), 143.7 (C$_{Ar}$), 155.3 (NHCO), 168.1 (COO*t*Bu); (ESI$^+$) *m/z* 516.2 [M+Na]$^+$; HRMS calculated for $C_{22}H_{24}NO_4INa$ 516.0625 [M+Na]$^+$, found 516.0648.

The data obtained is consistent with that given in the literature.[4]

Fmoc-2-Pyridylalanine-OtBu (8)

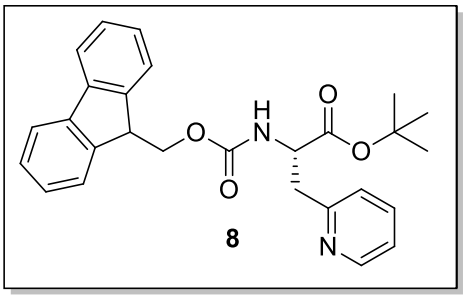

8

According to general procedure, coupling of zinc reagent **14**, prepared from iodide **7** (0.71 mmol, 0.35 g) with 2-bromopyridine (0.71 mmol, 67 µL) gave **8** as a light yellow-orange sticky solid (0.25 g, 60%). ν_{max}(solid)/cm^{-1} 3380.5 (w bd, N-H), 2965.3 (w, C-H$_{Ar}$), 1719.1 (s bd, C=O), 1449.6 (m, N-H), 1151.9 (s, C-O); ^{1}H NMR δ 1.30 (s, 9H, *t*Bu), 3.25 (m, 2H, β-CH$_2$), 4.16 (app t, 2H, *J* = 7.6 Hz, Fmoc-CH), 4.27 (d, 2H, *J* = 7.6 Hz, Fmoc-CH$_2$), 4.60 (m, 1H, α-H), 6.22 (d, 1H, *J* = 8 Hz, NH), 7.09 (d, 2H, *J* = 7.6 Hz, Py), 7.23 (app t, 2H, *J* = 7.2 Hz, Ph), 7.32 (t, 2H, *J* = 7.6 Hz, Ph), 7.52 (m, 3H; 1H from Py and 2H from Ph), 7.69 (d, 2H, *J* = 7.2 Hz, Ph), 8.47 (bd, 1H, *J* = 3.2 Hz, Py); ^{13}C NMR δ 27.9 (*t*Bu), 39.4 (Fmoc-CH$_2$), 47.2 (Fmoc-CH), 53.9 (α-CH), 67.0 (β-CH$_2$), 81.8 (*t*Bu), 119.9 (CH$_{Ar}$), 121.8 (CH$_{Py}$), 123.8 (CH$_{Py}$), 125.2 (CH$_{Ar}$), 127.0 (CH$_{Ar}$), 127.6 (CH$_{Ar}$), 136.4 (CH$_{Py}$), 141.2 (C$_{Ar}$), 144.0 (C$_{Ar}$), 149.1 (CH$_{Py}$), 156.0 (C$_{Py}$), 157.4 (NHCO), 170.5 (COO*t*Bu); (ESI$^+$) *m/z* 467.7 [M+Na]$^+$; HRMS calculated for $C_{29}H_{27}N_2O_4Na$ 467.1971 [M+Na]$^+$, found 467.1934.

Fmoc-3-Pyridylalanine-OtBu (9)

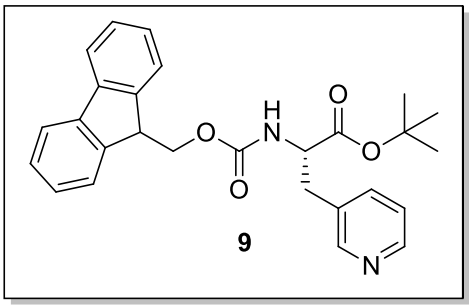

9

According to general procedure, coupling of zinc reagent **14**, prepared from iodide **7** (0.72 mmol, 0.35 g) with 3-bromopyridine (0.72 mmol, 0.11 g) gave **9** as a light yellow-orange sticky solid (0.17 g, 55%). ν_{max}(solid)/cm^{-1} 3379.9 (w bd, N-H), 2960.8 (w, C-H$_{Ar}$), 1714.1 (s bd, C=O), 1449.5 (m, N-H), 1150.6 (s, C-O); ^{1}H NMR δ 1.35 (s, 9H, *t*Bu), 3.03 (m, 2H, β-CH$_2$), 4.14 (t, 2H, *J* = 6.4 Hz, α-H), 4.34 (m, 2H, Fmoc-CH$_2$), 4.48 (m, 1H, Fmoc-CH), 5.30 (d, 1H, *J* = 9.6 Hz, NH), 7.14 (app dd, 2H, *J* = 4.0 and 8.0 Hz, Py), 7.26 (m, 2H, Ph), 7.34 (app t, 2H, *J* = 7.2 Hz, Ph), 7.40 (d, 1H, *J* = 7.6 Hz, Py), 7.51 (m, 2H, Ph), 7.70 (d, 2H, *J* = 7.6 Hz, Ph), 8.36 (s, 1H, Py), 8.43 (bd, 1H, *J* = 4.0 Hz, Py); ^{13}C NMR δ 28.0 (*t*Bu), 35.7 (Fmoc-CH$_2$), 47.2 (Fmoc-CH), 54.8 (α-CH), 66.9 (β-CH$_2$), 83.0 (*t*Bu), 120.0 (CH$_{Ar}$), 123.2 (CH$_{Py}$), 125.0 (CH$_{Ar}$), 127.0 (CH$_{Ar}$), 127.7 (CH$_{Ar}$), 136.9 (CH$_{Py}$), 141.3 (C$_{Ar}$), 143.7 (C$_{Ar}$), 148.4 (CH$_{Py}$), 150.6 (CH$_{Py}$), 155.5 (C$_{Py}$), 157.8 (NHCO), 170.0 (COO*t*Bu); (ESI$^+$) *m/z* 445.4 [M+H]$^+$; HRMS calculated for $C_{29}H_{27}N_2O_4$ 445.2127 [M+H]$^+$, found 445.2130.

Boc-2-Pyridylalanine-OBn (11)

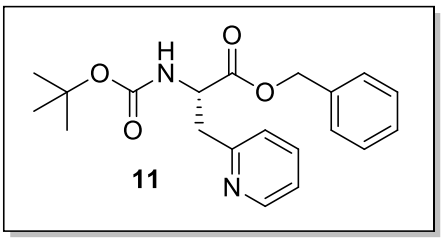

11

According to general procedure, coupling of zinc reagent **14**, prepared from **Boc-Ala(I)-OBn, 10** (1.23 mmol, 0.50 g) with 2-iodopyridine (1.23 mmol, 0.25 g) gave the Boc-protected pyridyl amino ester **11** as a sticky and bright yellow oil (0.22 g, 51%). ν_{max}(solid)/cm^{-1} 3199.6 (w, N-H), 2979.3 (w, C-H$_{Ar}$), 1706.3 (s bd, C=O), 1497.5 (m, N-H), 1159.1 (vs, C-O); ^{1}H NMR δ 1.35 (s, 9H, *t*Bu), 3.18 (dd, 1H, *J* = 4.4 and 14.4 Hz, β-CH$_2$), 3.28 (dd, 1H, *J* = 5.2 and 14.4 Hz, β-CH$_2$), 4.67 (m, 1H, α-H), 4.99 (d, 1H, *J* = 12.4 Hz, OCH$_2$Ph), 5.09 (d, 1H, *J* = 12.4 Hz, OCH$_2$Ph), 5.91 (d, 1H, *J* = 8.0 Hz, NH), 6.94 (d, 1H, *J* = 7.6 Hz, Py), 7.03 (m, 1H, Py), 7.22 (m, 5H, Ph), 7.45 (td, 2H, *J* = 1.6 and 7.6 Hz, Py), 8.38 (bd, 1H, *J* = 4 Hz, Py); ^{13}C NMR δ 28.3 (*t*Bu), 39.1 (CH$_2$Py), 53.0 (α-CH), 66.9 (CH$_2$OBn), 79.7 (C$_{t\text{Bu}}$), 121.7 (CH$_{Py}$), 123.7 (CH$_{Py}$), 128.0 (CH$_{Ph}$), 128.2 (CH$_{Ph}$), 128.4

(CH_{Ph}), 130.9 (C_{Ph}), 135.3 (C_{Py}), 136.4 (CH_{Py}), 149.1 (CH_{Py}), 155.5 (COOBn), 171.8 (OCONH); (ESI$^+$) *m/z* 380.3 $[M+H+Na]^+$; HRMS calculated for $C_{20}H_{24}N_2O_4$ 357.1824 $[M+H]^+$, found 357.1814.

Boc-3-Pyridylalanine-OBn (12)

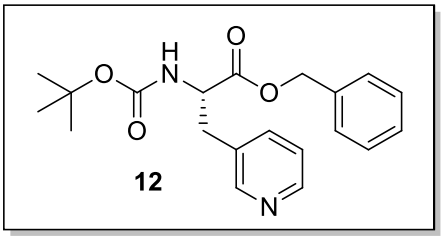

12

According to general procedure, coupling of zinc reagent **14**, prepared from **Boc-Ala(I)-OBn, 10** (1.32 mmol, 0.54 g) with 3-iodopyridine (1.32 mmol, 0.27 g) gave the Boc-protected pyridyl amino acid **12** as a yellow powdery solid (0.21 g, 45%). ν_{max} (solid)/cm^{-1} 3197.9 (w, N-H), 2976.2 (w, C-H_{Ar}), 1738.3 (s, C=O), 1704.0 (vs, C=O), 1537.4 (m, N-H), 1165.2 (vs, C-O); ^{1}H NMR δ 1.34 (s, 9H, *t*Bu), 2.97 (dd, 1H, *J* = 5.2 Hz and 14.4, β-CH_2), 3.07 (dd, 1H, *J* = 4.4 and 14.4 Hz, β-CH_2), 4.57 (m, 1H, α-H), 4.98 (m, 1H, NH), 5.05 (d, 1H, *J* = 12.0 Hz, OCH_2Ph), 5.11 (d, 1H, *J* = 12.0 Hz, OCH_2Ph), 7.07 (m, 1H, Py), 7.26 (m, 5H, Ph), 7.31 (m, 1H, Py), 8.27 (s, 1H, Py), 8.40 (bd, 1H, *J* = 2.4 Hz, Py); ^{13}C NMR δ 28.2 (*t*Bu), 35.5 (CH_2Py), 54.1 (α-CH), 67.4 (CH_2OBn), 80.1 (C_{tBu}), 123.3 (CH_{Py}), 128.61 (CH_{Ph}), 128.63 (CH_{Ph}), 128.64 (CH_{Ph}), 131.6 (C_{Ph}), 134.9 (C_{Py}), 136.7 (CH_{Py}), 148.4 (CH_{Py}), 150.5 (CH_{Py}), 154.9 (COOBn), 171.1 (OCONH); (ESI$^+$) *m/z* 357.3 $[M+H]^+$; HRMS calculated for $C_{20}H_{24}N_2O_4$ 357.1804 $[M+H]^+$, found 357.1814.

7.4 Synthesis of azobenzene derivative and precursors

2-Acetylamino-5-aminoazobenzenesulfonic acid (16a)

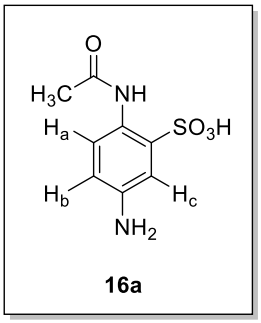

16a

2,5-Diaminobenzenesulfonic acid (**15**) (8.20 g, 43.56 mmol) was suspended in glacial acetic acid (200 mL). The reaction flask is sealed and immersed in an oil bath at 94 ˚C. Acetic anhydride (5.1 mL, 53.58 mL) is then added dropwise while stirring under reflux. The reaction is left to stir for 2 hours and 30 min at 94 ˚C. The flask is removed from the oil bath and its reaction content is left to cool down to room temperature. The mixture was filtered through P8 coarse

filter paper using a Hirsch funnel under aspirator vacuum. The reaction flask was rinsed with hot acetic anhydride (3 x 5 mL). The crude product was collected from the filter and left to dry using a vacuum pump. A pink solid was yielded (9.52 g, 97%) which after RP-HPLC purification in a gradient 0-100% of solvent B – this being (*v/v*) 5% H_2O/95% CH_3CN with 0.1% TFA as explained in **Section 7.1.4** – over 20 min afforded compound **16a** at a retention time of 9.90 min (5.93 g, 59%). ν_{max}(solid)/cm^{-1} 3389.5 (w, N-H), 1670.6 (m, C=O), 1525.0 (s, C_{Ar}-C_{Ar}), 1289.6 (m, C-O) 1016.9 (s, C-N); ^{1}H NMR (DMSO-d_6) δ 2.06 (s, 3H, CH_3), 7.27 (dd, 1H, *J* = 6.4 and 8.8 Hz, CH^b_{Ar}), 7.69 (d, 1H, *J* = 2.4 Hz, CH^a_{Ar}), 8.38 (d, 1H, *J* = 8.8 Hz, CH^c_{Ar}), 10.35 (s, 1H, NH); ^{13}C NMR (DMSO-d_6) δ 25.3 (CH_3), 121.1 (C_c), 121.8 (C_a), 121.9 (C_b), 124.4 (C_{NH2}) 134.9 (C_{SO3H}) 136.6 ($C_{acetamido}$), 168.3 (CO); (ESI^-) *m/z* 230.8 $[M]^-$; HRMS calculated for $C_{16}H_{14}Cl_2N_4O_2$ 230.2406 $[M+H]^+$, found 229.9103.

The data obtained is consistent with that given in the literature.[5]

2,5-Diacetylaminobenzenesulfonic acid (16b)

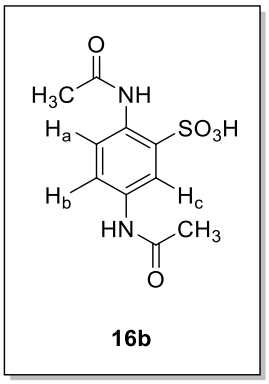

16b

2,5-Diaminobenzenesulfonic acid (**15**) (8.20 g, 43.56 mmol) was suspended in glacial acetic acid (200 mL). The reaction flask was sealed and immersed in an oil bath at 94 ˚C. Acetic anhydride (5.1 mL, 53.58 mL) was then added dropwise while stirring under reflux. The reaction was left to stir for 2 hours and 30 min at 94 ˚C. The flask was removed from the oil bath and its content was left to cool down to room temperature. The mixture was filtered through P8 coarse filter paper using a Hirsch funnel under aspirator vacuum. The reaction flask was rinsed with hot acetic anhydride (3 x 5 mL). The crude product was collected from the filter and left to dry using a vacuum pump. A pink solid was yielded (9.52 g, 97%) which after RP-HPLC purification in a gradient 0-100% of solvent B – this being (*v/v*) 5% H_2O/95% CH_3CN with 0.1% TFA as explained in **Section 7.1.4** – over 20 min afforded compound **16b** at a retention time of 12.88 min (2.22 g, 24%). ν_{max} (solid)/cm^{-1} 3390.7 (w, N-H), 1675.0 (m, C=O), 1530.7 (s, C_{Ar}-C_{Ar}), 1291.5 (m, C-O) 1019.0 (s, C-N); ^{1}H NMR (DMSO-d_6) δ 2.01 (s, 3H, CH_3), 2.03 (s, 3H,

CH_3), 7.57 (dd, 1H, *J* = 2.4 and 8.8 Hz, CH^b_{Ar}), 7.86 (d, 1H, *J* = 2.4 Hz, CH^a_{Ar}), 8.16 (d, 1H, *J* = 8.8 Hz, CH^c_{Ar}), 9.92 (s, 1H, NH), 10.35 (s, 1H, NH); ^{13}C NMR (DMSO-d_6) δ 24.3 (CH_3), 25.3 (CH_3), 118.2 (CH_{Ar}), 120.3 (CH_{Ar}), 120.4 (CH_{Ar}), 130.9 (C_{SO3H}), 134.2 ($C_{Acetamido}$), 135.9 ($C_{Acetamido}$), 167.6 (CO), 168.4 (CO); (ESI$^-$) *m/z* 270.9 [M]$^-$; HRMS calculated for $C_{16}H_{14}Cl_2N_4O_2$ 272.2703 [M+H]$^+$, found 270.9762.

4,4'-Di(acetylamino)-azobenzene (22)

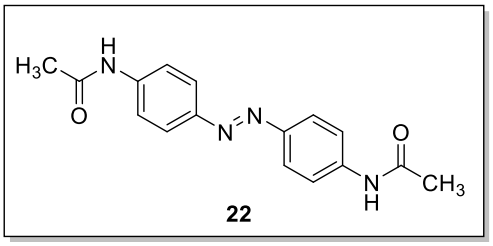

22

4,4' aminoacetanilide (**20**) (15.00 g, 0.099 mol) was dissolved in acetic acid (297 mL). The flask was wrapped with aluminium foil to protect the reaction from light. Hydrogen peroxide (33%) (30 mL) was then added slowly whilst stirring at room temperature. After 6 hours stirring the mixture, deionized water (350 mL) was added and left to stir for 20 minutes. The precipitated brown product was filtered off and washed with water (250 mL). After drying under reduced pressure, compound **22** was afforded as a brown solid (4.21 g, 14%). ν_{max}(solid)/cm^{-1} 3318-3192 (s bd, N-H amide), 2983 (s, C-H_{Ar}), 1646 (m, C=O), 1599 and 1533 (s, N=N), 1270 (C-O), 1155 (m, Ph-N); ^{1}H NMR (DMSO-d_6) δ 2.10 (s, 6H, CH_3), 7.79 (d, 4H, *J* = 8.8 Hz, CH_{Ar}), 7.83 (d, 4H, *J* = 8.8 Hz, CH_{Ar}), 10.28 (s, 2H, NH); ^{13}C NMR (DMSO-d_6) δ 23.1 (CH_3), 118.1 (CH_{Ar}), 122.3 (CH_{Ar}), 140.9 (C_{Ar}), 146.5 (C_{Ar}), 167.7 (CO); (ESI$^-$) *m/z* 295.20 [M]$^-$; HRMS calculated for $C_{16}H_{16}N_4O_2$ 296.3317 [M+H]$^+$, found 297.1347.

The data obtained is consistent with that given in the literature.[6]

4,4'-Diamino-azobenzene (23)

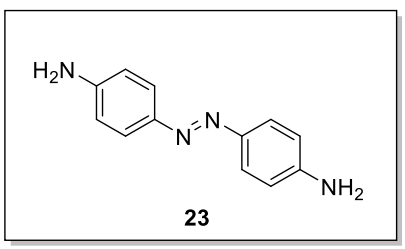

23

4,4'-di(acetylamino)-azobenzene (**22**) (1.45 g, 4.89 mmol) was suspended in methanol (80 mL). Whilst stirring, concentrated HCl (40 mL) was added and the mixture was heated under reflux for 3 hours. The solvent was removed *in vacuo*, and the residue was

taken up in water (80 mL). The solution was basified to pH 8.5 by adding dropwise NaOH (1M). The precipitated product was filtered off, and was washed twice with water (40 mL). The filter cake was taken up in acetone. Removal of the solvent yielded **23** as a dark brown solid (0.67 g, 84%). ν_{max}(solid)/cm^{-1} 3352 (m, N-H_2 stretching vibrations), 2982 (m, C-H_{Ar}), 1623 and 1581 (s, N=N), 1148 (m, Ph-N); ^{1}H NMR (DMSO-d_6) δ 5.74 (s, 4H, NH_2), 6.63 (d, 4H, J = 2.0 Hz, CH_{Ar}), 7.52 (d, 4H, J = 2.0 Hz, CH_{Ar}); ^{13}C NMR (DMSO-d_6) δ 113.9 (CH_{Ar}), 124.2 (CH_{Ar}), 143.6 (C_{NH2}), 151.4 ($C_{N=N}$); (ESI$^+$) *m/z* 213.08 [M]$^+$**,** 236.06 [M+Na]$^+$; HRMS calculated for $C_{12}H_{12}N_4$ 212.2678 [M+H]$^+$, found 213.1117.

The data obtained is consistent with that given in the literature.[7]

4,4'-Dichloroacetamide-azobenzene (24)

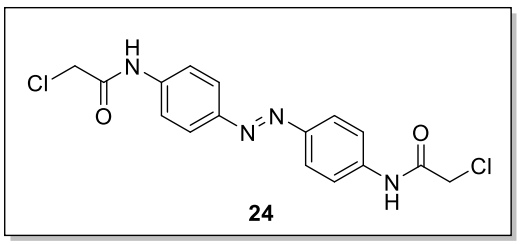

24

4,4'-diamino-azobenzene (**23**) (0.30 g, 1.88 mmol) was suspended in acetonitrile (150 mL). Whilst stirring at room temperature, potassium carbonate (0.78 g, 5.65 mmol) and chloroacetyl chloride (0.45 mL, 5.65 mmol) are added and left to stir for 6 hours at room temperature. The reaction flask is immersed in an ice bath for 30 min before filtering it off under reduced pressure. Water (20 mL) is used to wash the reaction flask. Drying the product under reduced pressure yielded **24** as a dark purple solid (0.495 g, 96%). ν_{max}(solid)/cm^{-1} 3272-3143 (m bd, N-H amide), 2982 (s, C-H_{Ar}), 1676 (m, C=O), 1619 and 1553 (s, N=N), 1295 (C-O), 1246 (vs, CH_2-Cl), 1150 (m, Ph-N); ^{1}H NMR (DMSO-d_6) δ 4.33 (s, 4H, CH_2), 7.82 (d, 4H, J = 8.8 Hz, CH_{Ar}), 7.89 (d, 4H, J = 8.8 Hz, CH_{Ar}), 10.66 (s, 2H, NH); ^{13}C NMR (DMSO-d_6) δ 43.6 (CH_2), 119.6 (CH_{Ar}), 123.5 (CH_{Ar}), 141.1 (C_{Ar}), 148.0 (C_{Ar}), 165.0 (CO); (ESI$^-$) *m/z* 363.09 [M]$^-$; HRMS calculated for $C_{16}H_{14}Cl_2N_4O_2$ 365.2106 [M+H]$^+$, found 365.0578.

The data obtained is consistent with the iodo-derivative given in the literature.[8]

7.5 Synthesis of peptide sequences

PEP1, KIAALKQKNAALKQEIAALEYEIEALEQ (25)

Synthesized via automated SPPS on low loaded Fmoc-Gln(Trt)-wang resin (0.59 mmol/g substitution). Peptide synthesis – procedure 1 (**Section 7.2.3**) at a 0.05 mmol scale produced 78 mg crude peptide (50%) whilst procedure 2 (**Section 7.2.3**) at a 0.10 mmol scale gave 235 mg crude peptide (75%). Analytical RP-HPLC using a linear gradient of 0-100% of solvent B – this being (*v/v*) 5% H_2O/95% CH_3CN with 0.1% TFA as explained in **Section 7.1.4** – over 30 min showed a retention time of the pure peptide at 15.18 min. Final purification was achieved by RP-HPLC as described in **Section 7.1.4**. MALDI-TOF MS *m/z* 3127.5 $[M]^+$, 3128.5 $[M+H]^+$, 3149.6 $[M+Na]^+$, 3151.5 $[M+H+Na]^+$; HRMS calculated for $C_{140}H_{236}N_{36}O_{44}$ 1564.3761 $[M+2H]^{2+}$, found 1564.3783 $[M+2H]^{2+}$.

BEP, EIAALEYENAALEQKIKALKQKIKALKQ (26)

Synthesized via automated SPPS on low loaded Fmoc-Gln(Trt)-wang resin (0.59 mmol/g substitution) following peptide synthesis – procedure 1 (**Section 7.2.3**) at a 0.05 mmol scale produced 90 mg crude peptide (57%). Analytical RP-HPLC using a linear gradient of 0-100% of solvent B – this being (*v/v*) 5% H_2O/95% CH_3CN with 0.1% TFA as explained in **Section 7.1.4** – over 30 min showed a retention time of the pure peptide at 13.86 min. Final purification was achieved by RP-HPLC as described in **Section 7.1.4**. MALDI-TOF MS *m/z* 3183.5 $[M]^+$, 3184.5 $[M+H]^+$; HRMS calculated for $C_{144}H_{248}N_{38}O_{42}$ 1592.4312 $[M+2H]^{2+}$, found 1592.4298 $[M+2H]^{2+}$.

SAF, KIKALKQKIKALKQEIAALEYENAALEQ (27)

Synthesized via automated SPPS on low loaded Fmoc-Gln(Trt)-wang resin (0.59 mmol/g substitution) using peptide synthesis – procedure 1 (**Section 7.2.3**) on a 0.05 mmol scale produced 72 mg crude peptide (45%) whilst using procedure 4 (**Section 7.2.3**) at a 0.10 mmol scale produced 235 mg (74%). Analytical RP-HPLC using a linear gradient of 0-100% of solvent B – this being (*v/v*) 5% H_2O/95% CH_3CN with 0.1% TFA as explained in **Section 7.1.4** – over 30 min showed a retention time of the pure peptide

at 13.50 min. Final purification was achieved by RP-HPLC as described in **Section 7.1.4**. MALDI-TOF MS *m/z* 3183.3 $[M]^+$, 3184.3 $[M+H]^+$, 3206.4 $[M+Na]^+$; HRMS calculated for $C_{144}H_{248}N_{38}O_{42}$ 1592.4312 $[M+2H]^{2+}$, found 1592.9265 $[M+2H]^{2+}$.

c-PEP1, CH_3O-KIAALKQKNAALKQEIAALEYEIEALEQ-NH_2 (28)

Synthesized via automated SPPS on low loaded Fmoc-rink amide MBHA resin (0.59 mmol/g substitution) following peptide synthesis – procedure 3 (**Section 7.2.3**) at a 0.10 mmol scale gave 258 mg crude peptide (82%). Analytical RP-HPLC using a linear gradient of 0-100% of solvent B – this being (*v/v*) 5% H_2O/95% CH_3CN with 0.1% TFA as explained in **Section 7.1.4** – over 30 min showed a retention time of the pure peptide at 15.86 min. Final purification was achieved by RP-HPLC as described in **Section 7.1.4**. MALDI-TOF MS *m/z* 3191.5 $[M+Na]^+$, 3207.4 $[M+K]^+$; HRMS calculated for $C_{142}H_{239}N_{37}O_{44}$ 1584.8894 $[M+2H]^{2+}$, found 1584.8926 $[M+2H]^{2+}$.

c-BEP, CH_3O-EIAALEYENAALEQKIKALKQKIKALKQ-NH_2 (29)

Synthesized via automated SPPS on low loaded Fmoc-rink amide MBHA resin (0.59 mmol/g substitution) using peptide synthesis – procedure 3 (**Section 7.2.3**) at a 0.10 mmol scale gave 222 mg crude peptide (69%). Analytical RP-HPLC using a linear gradient of 0-100% of solvent B – this being (*v/v*) 5% H_2O/95% CH_3CN with 0.1% TFA as explained in **Section 7.1.4** – over 30 min showed a retention time of the pure peptide at 14.68 min. Final purification was achieved by RP-HPLC as described in **Section 7.1.4**. MALDI-TOF MS *m/z* 3224.7 $[M]^+$, 3225.7 $[M+H]^+$, 3246.7 $[M+Na]^+$; HRMS calculated for $C_{146}H_{251}N_{39}O_{42}$ 1612.9445 $[M+2H]^{2+}$, found 1613.4443 $[M+2H]^{2+}$.

c-3PAL14, CH_3O-KIAALKQKNAALK(Pal)EIAALEYEIEALEQ-NH_2 (30)

Synthesized via automated SPPS on low loaded Fmoc-rink amide MBHA resin (0.59 mmol/g substitution) using peptide synthesis – procedure 5 (**Section 7.2.3**) on a 0.10 mmol scale gave 208 mg crude peptide (65%). Analytical RP-HPLC using a linear gradient of 0-100% of solvent B – this being (*v/v*) 5% H_2O/95% CH_3CN with 0.1% TFA as

explained in **Section 7.1.4** – over 30 min showed a retention time of the pure peptide at 15.56 min. Final purification was achieved by RP-HPLC as described in **Section 7.1.4**. MALDI-TOF MS *m/z* 3211.8 $[M+Na]^+$, 3233.7 $[M+2Na]^+$; HRMS calculated for $C_{145}H_{239}N_{37}O_{43}$ 1063.5972 $[M+3H]^{3+}$, found 1063.9231 $[M+3H]^{3+}$.

c-3PAL10PAL14, CH_3O-KIAALKQKN(Pal)ALK(Pal)EIAALEYEIEALEQ-NH_2 (31)

Synthesized via automated SPPS on low loaded Fmoc-rink amide MBHA resin (0.59 mmol/g substitution) using peptide synthesis – procedure 5 (**Section 7.2.3**) at a 0.10 mmol scale gave 274 mg crude peptide (84%). Analytical RP-HPLC using a linear gradient of 0-100% of solvent B – this being (*v/v*) 5% H_2O/95% CH_3CN with 0.1% TFA as explained in **Section 7.1.4** – over 30 min showed a retention time of the pure peptide at 15.19 min. Final purification was achieved by RP-HPLC as described in **Section 7.1.4**. MALDI-TOF MS *m/z* 3288.8 $[M+Na]^+$; HRMS calculated for $C_{150}H_{242}N_{38}O_{43}$ 1633.4052 $[M+2H]^{2+}$, found 1633.4093 $[M+2H]^{2+}$.

c-3PAL7PAL14, CH_3O-KIAALK(Pal)KNAALK(Pal)EIAALEYEIEALEQ-NH_2 (32)

Synthesized via automated SPPS on low loaded Fmoc-rink amide MBHA resin (0.59 mmol/g substitution) using peptide synthesis – procedure 5 (**Section 7.2.3**) at a 0.10 mmol scale produced 137 mg crude peptide (43%). (Some peptide was lost during preparation). Analytical RP-HPLC using a linear gradient of 0-100% of solvent B – this being (*v/v*) 5% H_2O/95% CH_3CN with 0.1% TFA as explained in **Section 7.1.4** – over 30 min showed a retention time of the pure peptide at 15.35 min. Final purification was achieved by RP-HPLC as described in **Section 7.1.4**. MALDI-TOF MS *m/z* 3208.3 $[M]^+$, 3231.2 $[M+Na]^+$; 3232.2 $[M+H+Na]^+$; 3254.3 $[M+2Na]^+$; HRMS calculated for $C_{147}H_{235}N_{37}O_{43}$ 1070.2561 $[M+3H]^{3+}$, found 1070.2534 $[M+3H]^{3+}$.

c-4PAL14, CH_3O-KIAALKQKNAALK(Pal)EIAALEYEIEALEQ-NH_2 (33)

Synthesized via automated SPPS on low loaded Fmoc-rink amide MBHA resin (0.59 mmol/g substitution) following peptide synthesis – procedure 5 (**Section 7.2.3**) at a

0.10 mmol scale gave 190 mg crude peptide (60%). Analytical RP-HPLC using a linear gradient of 0-100% of solvent B – this being (*v/v*) 5% H_2O/95% CH_3CN with 0.1% TFA as explained in **Section 7.1.4** – over 30 min showed a retention time of the pure peptide at 15.72 min. Final purification was achieved by RP-HPLC as described in **Section 7.1.4**. MALDI-TOF MS *m/z* 3211.9 $[M+Na]^+$, 3227.4 $[M+K]^+$; HRMS calculated for $C_{145}H_{239}N_{37}O_{43}$ 1594.8920 $[M+2H]^{2+}$, found 1594.9025 $[M+2H]^{2+}$.

CYS, EIAALEYENCALEQKIKALKCKIKALKQ (34)

Synthesized via automated SPPS on low loaded Fmoc-Gln(Trt)-wang resin (0.59 mmol/g substitution) following peptide synthesis – procedures 1 and 2 (**Section 7.2.3**). Procedure 1 (0.05 mmol scale) gave 77 mg crude peptide (48%) whilst procedure 2 (0.10 mmol scale) afforded 175 mg crude peptide (55%). Analytical RP-HPLC using a linear gradient of 0-100% of solvent B – this being (*v/v*) 5% H_2O/95% CH_3CN with 0.1% TFA as explained in **Section 7.1.4** – over 30 min showed a retention time of the pure peptide at 13.33 min. Final purification was achieved by RP-HPLC as described in **Section 7.1.4**. MALDI-TOF MS *m/z* 3190.6 $[M]^+$, 3192.6 $[M+H]^+$; 3214.6 $[M+H+Na]^+$.

c-CYS, CH_3O-EIAALEYENCALEQKIKALKCKIKALKQ-NH_2 (36)

Synthesized via automated SPPS on low loaded Fmoc-rink amide MBHA resin (0.59 mmol/g substitution) using peptide synthesis – procedure 6 (**Section 7.2.3**) at a 0.10 mmol scale gave 170 mg crude peptide (53%). Analytical RP-HPLC using a linear gradient of 0-100% of solvent B – this being (*v/v*) 5% H_2O/95% CH_3CN with 0.1% TFA as explained in **Section 7.1.4** – over 30 min showed a retention time of the pure peptide at 12.29 min. Final purification was achieved by RP-HPLC as described in **Section 7.1.4**. MALDI-TOF MS *m/z* 3231.5 $[M]^+$, 3253.5 *m/z* $[M+Na]^+$; HRMS calculated for $C_{144}H_{248}N_{38}O_{41}S_2$ 646.5535 $[M+5H]^{5+}$, found 646.9664 $[M+5H]^{5+}$.

7.6 Synthesis of cross-linked azobenzene-peptide systems

CL, (EIAALEYENCALEQKIKALKCKIKALKQ + 24) (35)

A solution of **CYS** (**34**) in water (2 mL, 0.079 mM) was incubated in Tris-HCl pH 8.5 (4 mL, 5 mM) and TCEP-HCl pH 8.5 (2 mL, 0.088 mM) and stirred at room temperature, for a minimum of 2 hours under N_2. The reaction flask was protected from light with aluminium foil and the solution heated up to 40 ˚C. When the temperature of the solution reached 40 ˚C, a solution of azobenzene (**24**) in DMSO (4 mL, 0.064 mM) was added dropwise and left to stir for 20 min in the dark. Another addition of a more concentrated solution of **24** in DMSO (3 mL, 1.06 mM) was added dropwise and left to stir for another 20 min in the dark. The reaction flask was then exposed to light while stirring for 20 min. The crude product was then lyophilized and final purification was achieved by RP-HPLC as described in **Section 7.1.4**. MALDI-TOF MS *m/z* 3484.1 $[M+H]^+$, 3506.2 $[M+Na]^+$.

c-CL, (CH_2O-EIAALEYENCALEQKIKALKCKIKALKQ-NH_2 + 24) (37)

A solution of **c-CYS** (**36**) in water (15 mL, 3.47 mM) was incubated in Tris-HCl pH 8.5 (5 mL, 5 mM) and TCEP-HCl pH 8.5 (5 mL, 5 mM) and stirred at room temperature, for a minimum of 2 hours under N_2. The reaction flask was protected from light with aluminium foil and the solution heated up to 40 ˚C. When the temperature of the solution reached 40 ˚C, a solution of azobenzene (**24**) in DMSO (4 mL, 3.5 mM) was added dropwise and left to stir for 20 min in the dark. Another addition of a more concentrated solution of **24** in DMSO (2 mL, 65 mM) was added dropwise and left to stir for another 20 min in the dark. The reaction flask was then exposed to light while stirring for 20 min. The crude product was then lyophilized and final purification was achieved by RP-HPLC as described in **Section 7.1.4**. Analytical RP-HPLC using a linear gradient of 0-100% of solvent B – this being (*v/v*) 5% H_2O/95% CH_3CN with 0.1% TFA as explained in **Section 7.1.4** – over 30 min showed a retention time of the pure peptide at 15.19 min. MALDI-TOF MS *m/z* 3524.9 $[M]^+$, 3546.6 $[M+Na]^+$; HRMS calculated for $C_{160}H_{260}N_{42}O_{43}S_2$ 705.5765 $[M+5H]^{5+}$, found 705.5862 $[M+5H]^{5+}$.

[1] C. Gribbon, K.J. Channon, W. Zhang, E.F. Banwell, E.H.C. Bromley, J.B. Chaudhuri, R.O.C. Oreffo, and D.N. Woolfson, *Biochem.* **2008**, 47, 10365-10371.

[2] J.R. Kumita, D.G. Flint, G.A. Woolley, and O.S. Smart, *Faraday Discuss*. **2002**, 122, 89-103.

[3] L. Le Corre, C. Gravier-Pelletier, Y. Le Merrer, *Eur. J. Org. Chem.* **2007** (32), 5386-5394.

[4] L. Jobron, G. Hummel, *Org. Letters.* **2000**, 2 (15), 2265-2267.

[5] D.C. Burns, F. Zhang, and G.A. Woolley, *Nat. Protocols* **2007**, 2, 251-258.

[6] A.C. Sousa, L.O. Martins, and M.P. Robalo, *Adv. Synth. Catal*. **2013**, 355, 2908-2917.

[7] J.B. Kyziol, and H. Frej, *Chem. Papers* **1988**, 42, 781-793.

[8] R. Pfister, J. Ihalainen, P. Hamm, and C. Kolano, *Org. Biomol. Chem*. **2008**, 6, 3508-3517.

APPENDICES

Chapter 3 – Development of the chassis of de novo coiled-coil self-assembling peptide systems

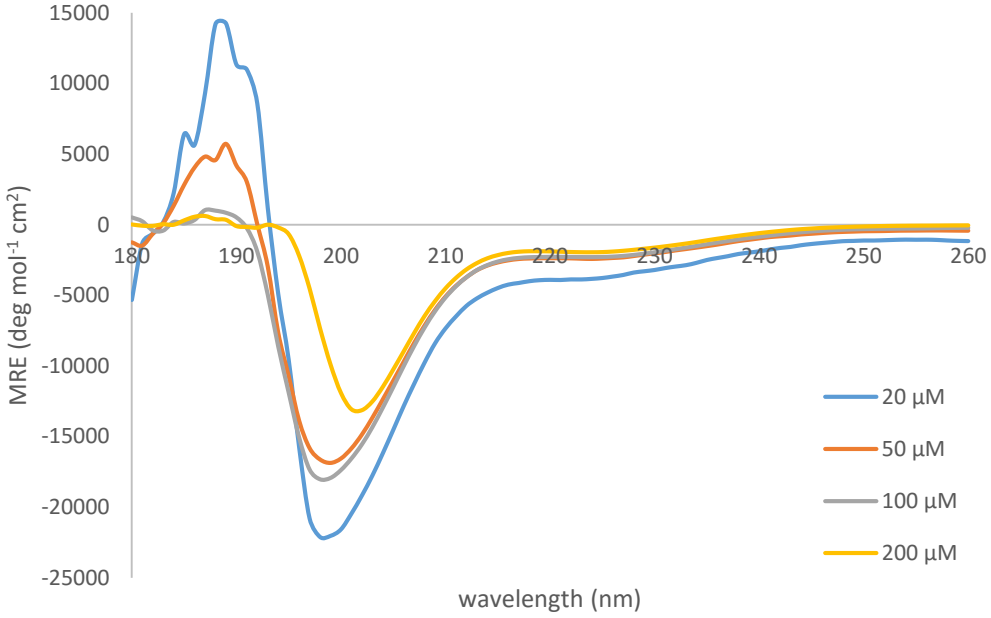

Figure A3.1: CD spectra of **PEP1** (**25**) in PBS buffer at pH 7.4 at different concentrations at 21 ˚C.

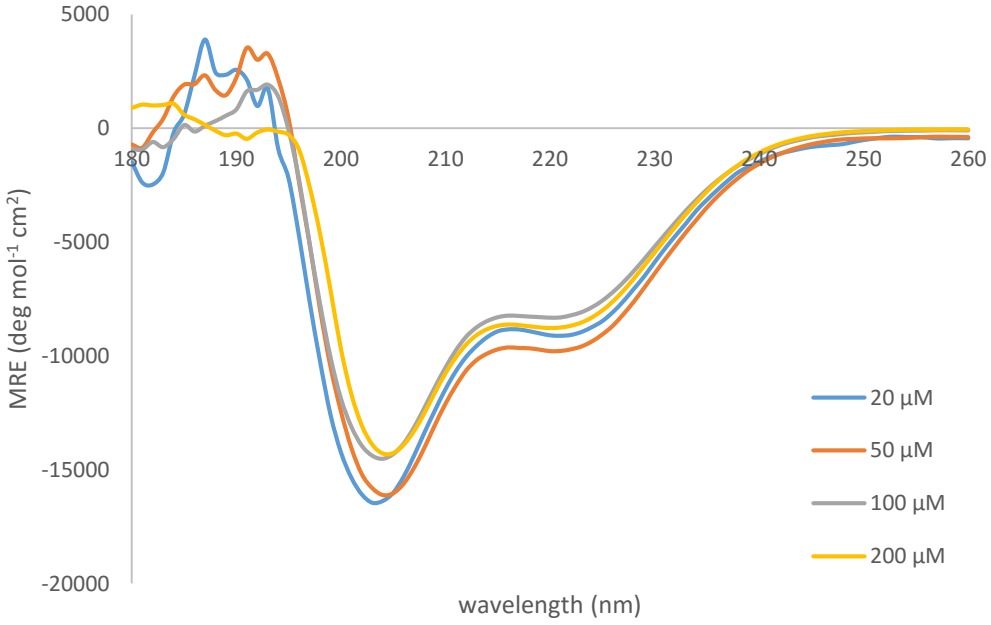

Figure A3.2: CD spectra of **BEP** (**26**) in PBS buffer at pH 7.4 at different concentrations at 21 ˚C.

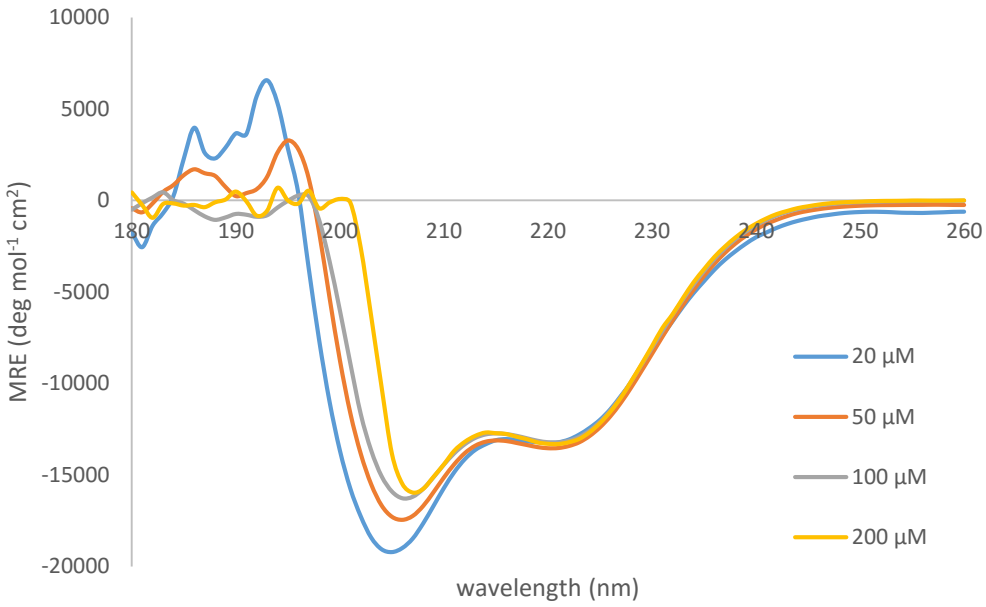

Figure A3.3: CD spectra of (**PEP1**+**BEP**) (**25**+**26**) in PBS buffer at pH 7.4 at different concentrations and at 21 ˚C.

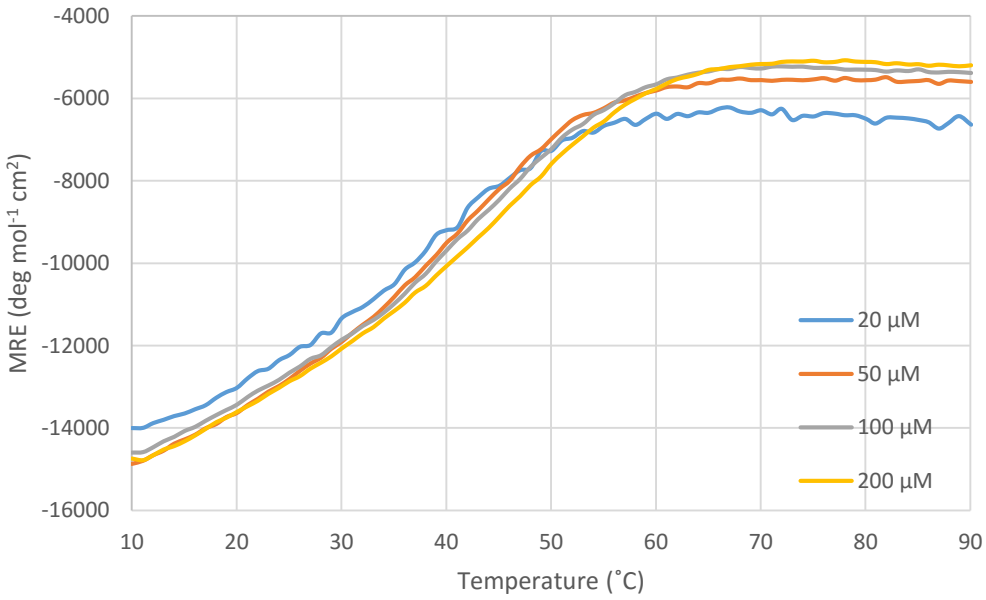

Figure A3.4: Thermal denaturation curves of (**PEP1**+**BEP**) (**25**+**26**) in PBS buffer at pH 7.4 at different concentrations.

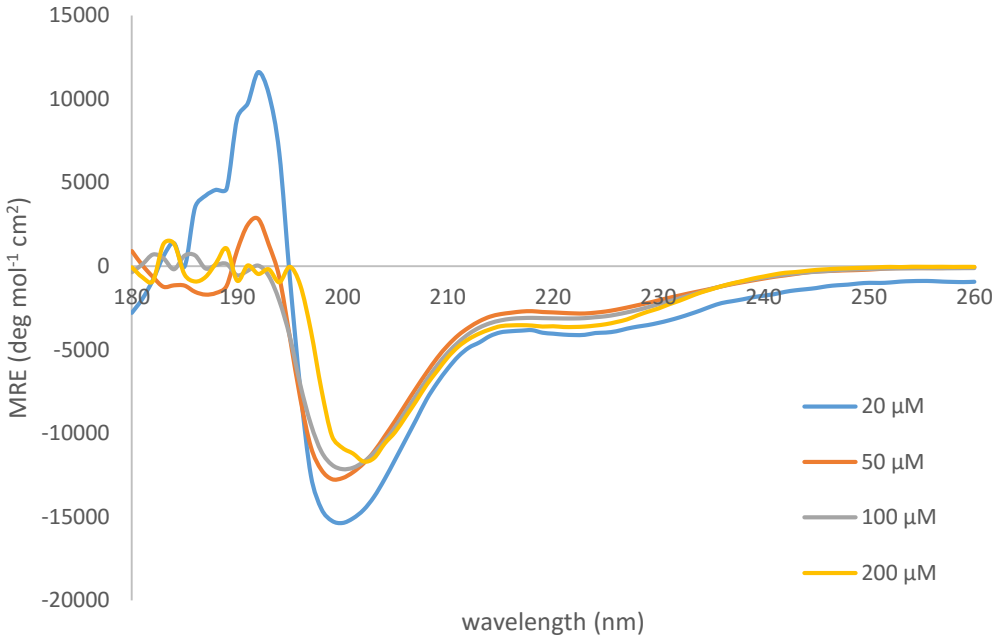

Figure A3.5: CD spectra of **SAF** (**27**) in PBS buffer at pH 7.4 at different concentrations at 21 ˚C.

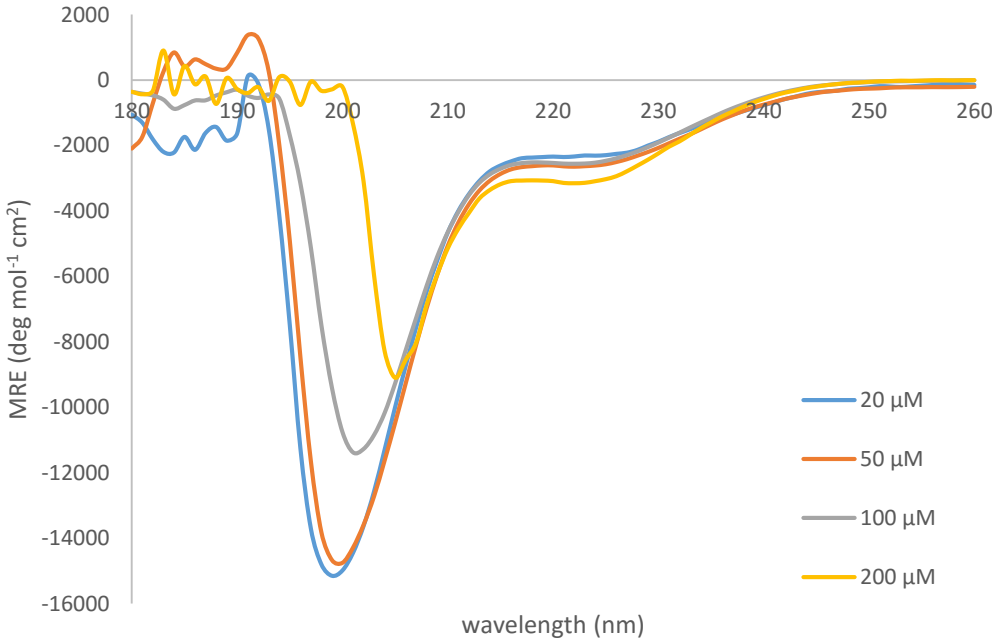

Figure A3.6: CD spectra of (**PEP1**+**SAF**) (**25**+**27**) in PBS buffer at pH 7.4 at different concentrations and at 21 ˚C.

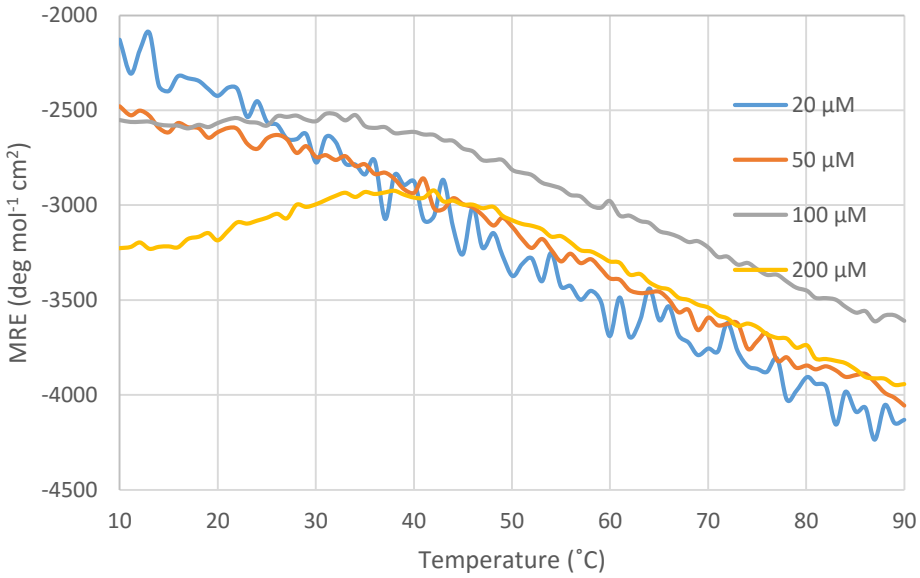

Figure A3.7: Thermal denaturation curves of (**PEP1**+**SAF**) (**25**+**27**) in PBS buffer at pH 7.4 at different concentrations.

20 µM, pH 7.4	θ_{222nm}(deg mol^{-1} cm^2)	θ_{222nm}/ θ_{208nm}	% helicity
PEP1 (25)	-3870.34	0.40	12.4
BEP (26)	-9080.66	0.68	29.2
SAF (27)	-4123.95	0.52	13.2
PEP1 + BEP (25+26)	-13072.90	0.74	36.9
PEP1 + SAF (25+27)	-2334.43	0.36	6.6

Table A3.1: Summarised data obtained at pH 7.4 from peptides **25**, **26** and **27** and the mixtures (**25**+**26**) and (**25**+**27**) at 20 µM in PBS at 21 °C.

50 µM, pH 7.4	θ_{222nm}(deg mol^{-1} cm^2)	θ_{222nm}/ θ_{208nm}	% helicity
PEP1 (25)	-2382.16	0.33	7.7
BEP (26)	-9712.21	0.69	31.2
SAF (27)	-2833.79	0.45	9.1
PEP1 + BEP (25+26)	-13417.70	0.80	37.9
PEP1 + SAF (25+27)	-2648.90	0.38	7.5

Table A3.2: Summarised data obtained at pH 7.4 from peptides **25**, **26** and **27** and the mixtures (**25**+**26**) and (**25**+**27**) at 50 µM in PBS at 21 °C.

200 µM, pH 7.4	θ_{222nm}(deg mol^{-1} cm^2)	θ_{222nm}/ θ_{208nm}	% helicity
PEP1 (25)	-1931.11	0.30	6.2
BEP (26)	-8674.98	0.69	27.9
SAF (27)	-3633.71	0.51	11.7
PEP1 + BEP (25+26)	-13218.30	0.84	37.3
PEP1 + SAF (25+27)	-3154.03	0.46	8.9

Table A3.3: Summarised data obtained at pH 7.4 from peptides **25**, **26** and **27** and the mixtures (**25**+**26**) and (**25**+**27**) at 200 µM in PBS at 21 °C.

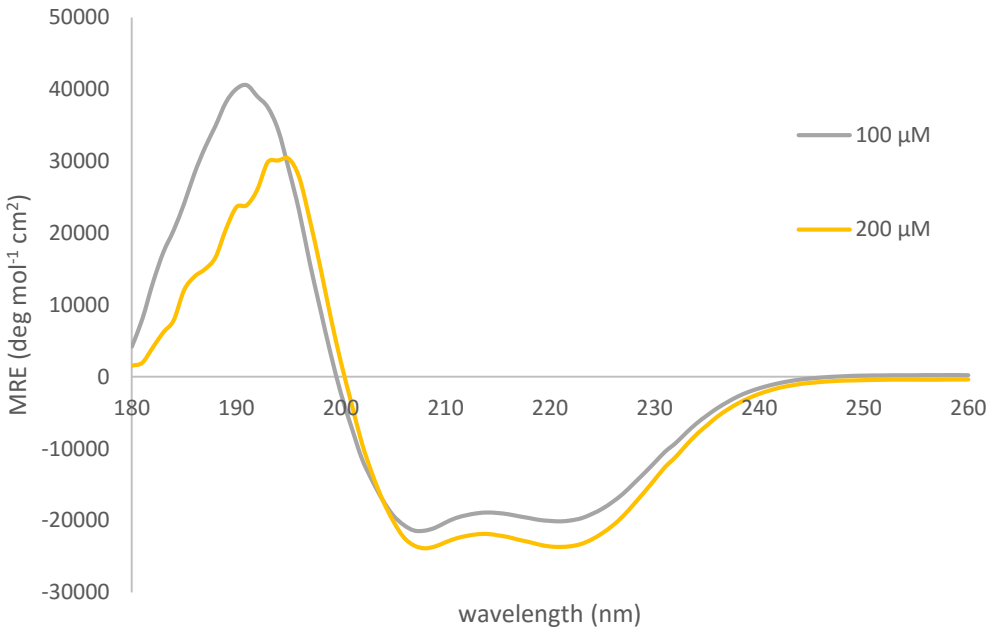

Figure A3.8: CD spectra of **c-PEP1** (**28**) in MOPS at pH 8.5 at different concentrations at 21 ˚C.

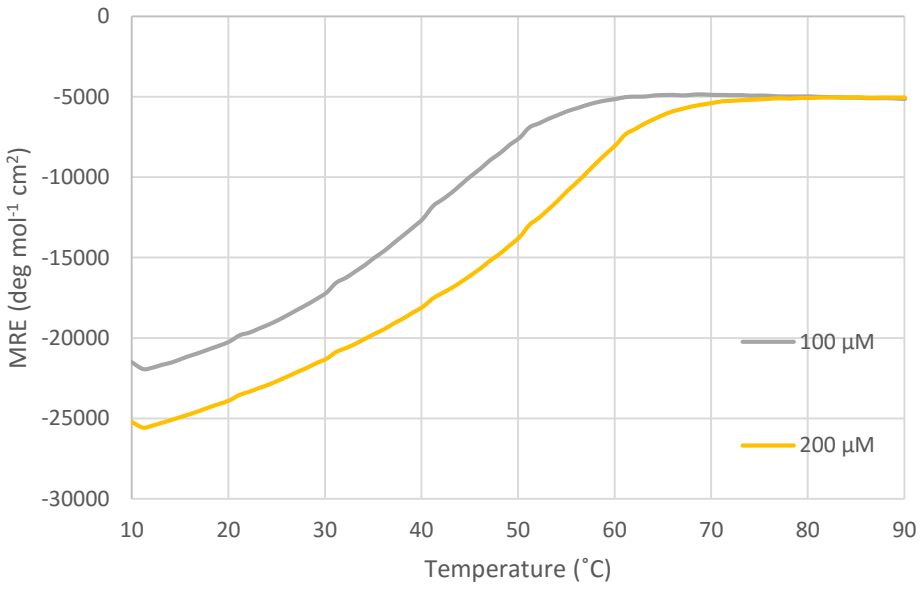

Figure A3.9: Thermal denaturation curves of **c-PEP1** (**28**) in MOPS at pH 8.5 at different concentrations.

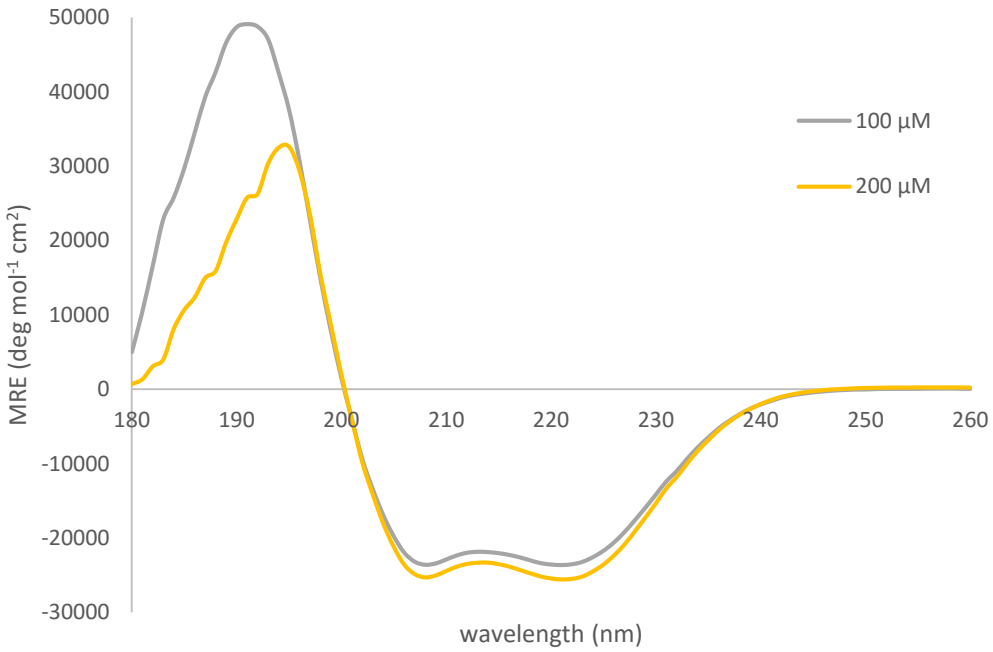

Figure A3.10: CD spectra of **c-BEP** (**29**) in MOPS at pH 8.5 at different concentrations at 21 ˚C.

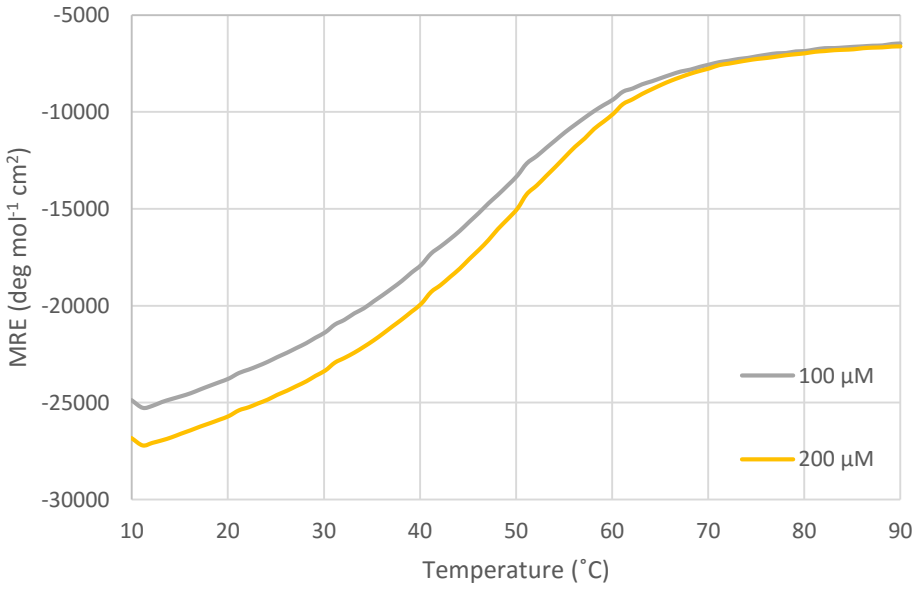

Figure A3.11: Thermal denaturation curves of **c-BEP** (**29**) in MOPS at pH 8.5 at different concentrations.

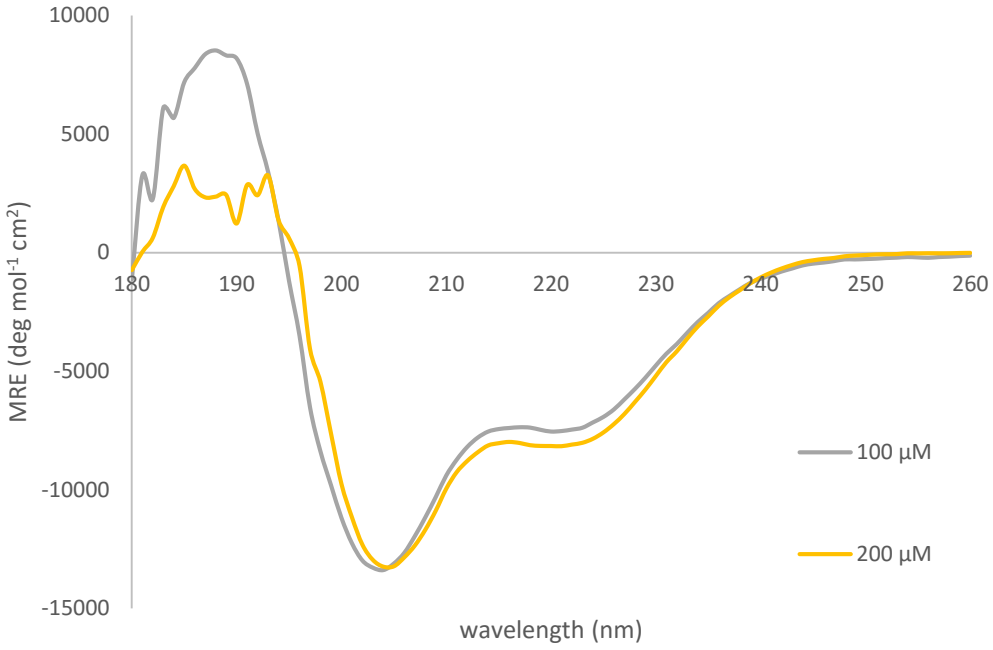

Figure A3.12: CD spectra of **SAF** (**27**) in MOPS at pH 8.5 at different concentrations at 21 ˚C.

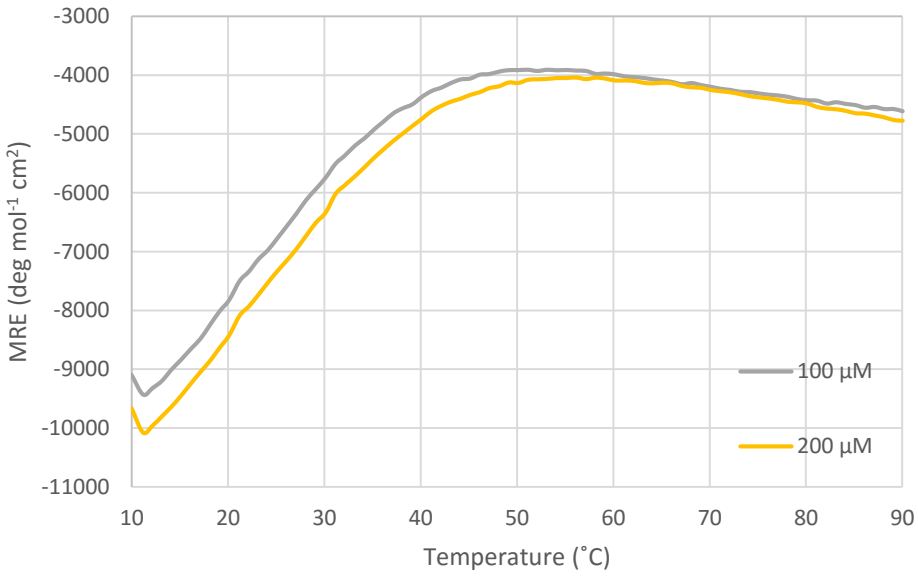

Figure A3.13: Thermal denaturation curves of **SAF** (**27**) in MOPS at pH 8.5 at different concentrations.

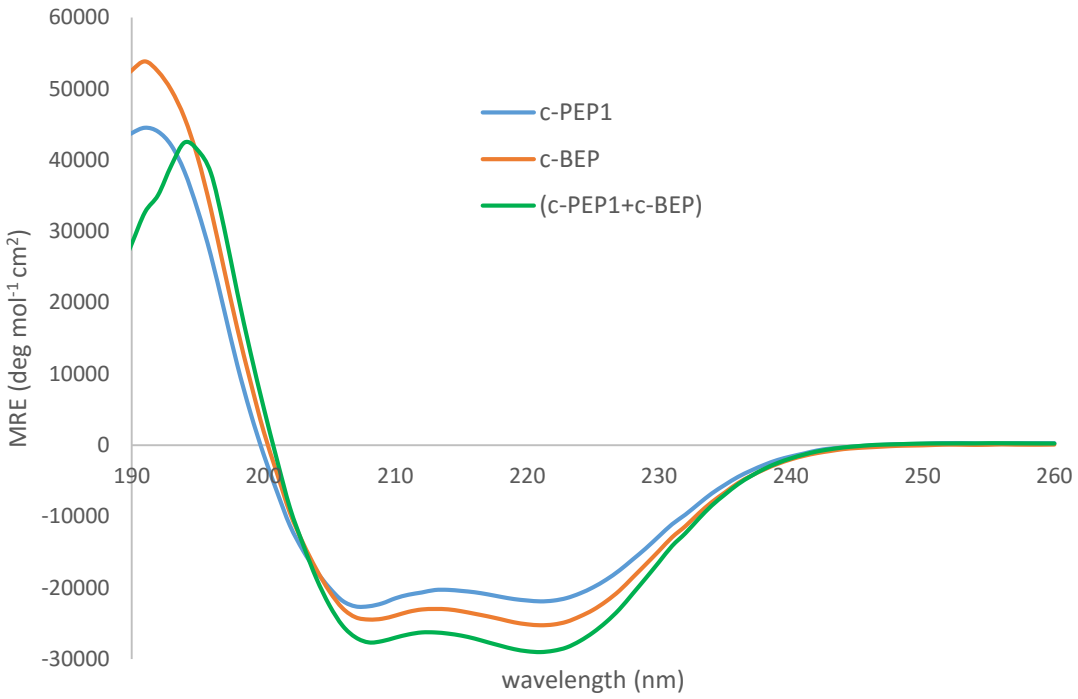

Figure A3.14: CD spectra of 100 µM solutions of **c-PEP1** (**28**), **c-BEP** (**29**) and (**c-PEP1**+**c-BEP**) (**28**+**29**) in 10 mM MOPS buffer at pH 8.5 and at 10 ˚C.

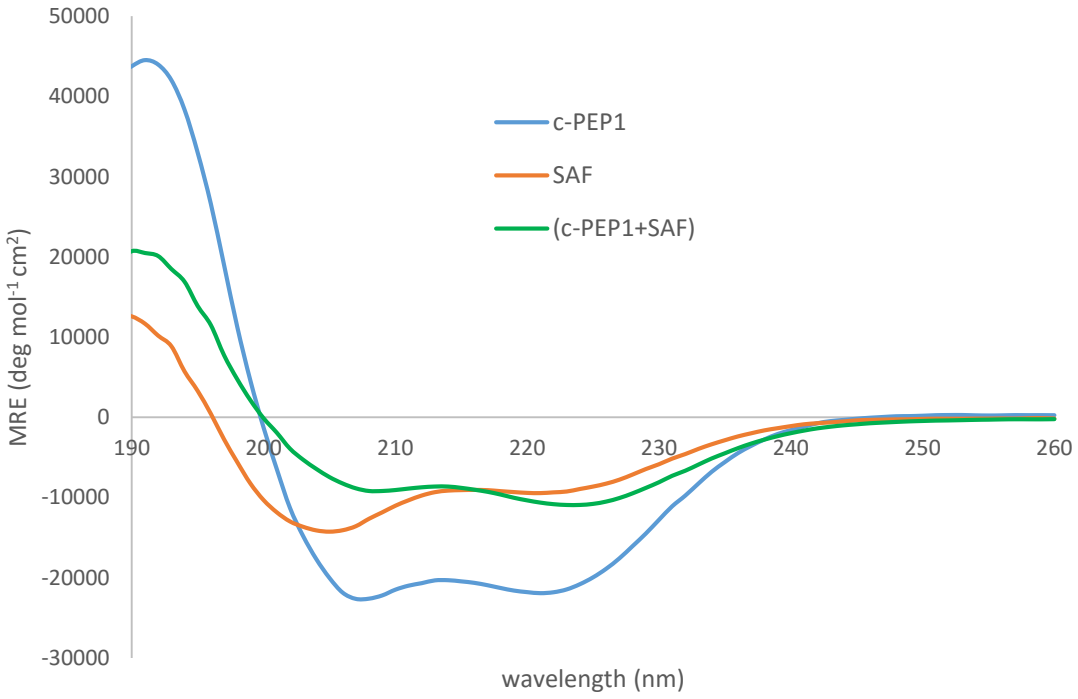

Figure A3.15: CD spectra of 100 µM solutions of **c-PEP1** (**28**), **SAF** (27) and (**c-PEP1**+**SAF**) (**28**+**27**) in 10 mM MOPS buffer at pH 8.5 and at 10 ˚C.

Chapter 4 – Coiled-coil self-assembling peptide systems susceptible to conformational changes upon metal-binding

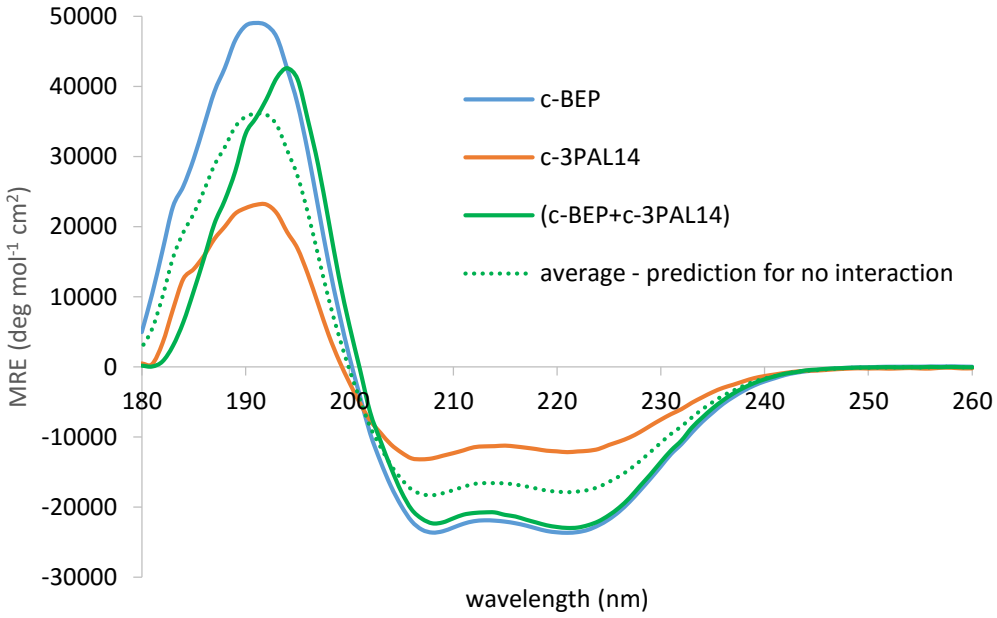

Figure A4.1: CD spectra of 100 µM solutions of **c-BEP** (**29**), **c-3PAL14** (**30**) and (**c-BEP+c-3PAL14**) (**29+30**) in 10 mM MOPS buffer at pH 7.2 at 21 ˚C. The peptide sequences are shown. **X** = 3-pyridylalanine (3-Pal)

c-BEP: Ac-EIAALEYENAALEQKIKALKQKIKALKQ-Am
c-3PAL14: Ac-KIAALKQKNAALK**X**EIAALEYEIEALEQ-Am

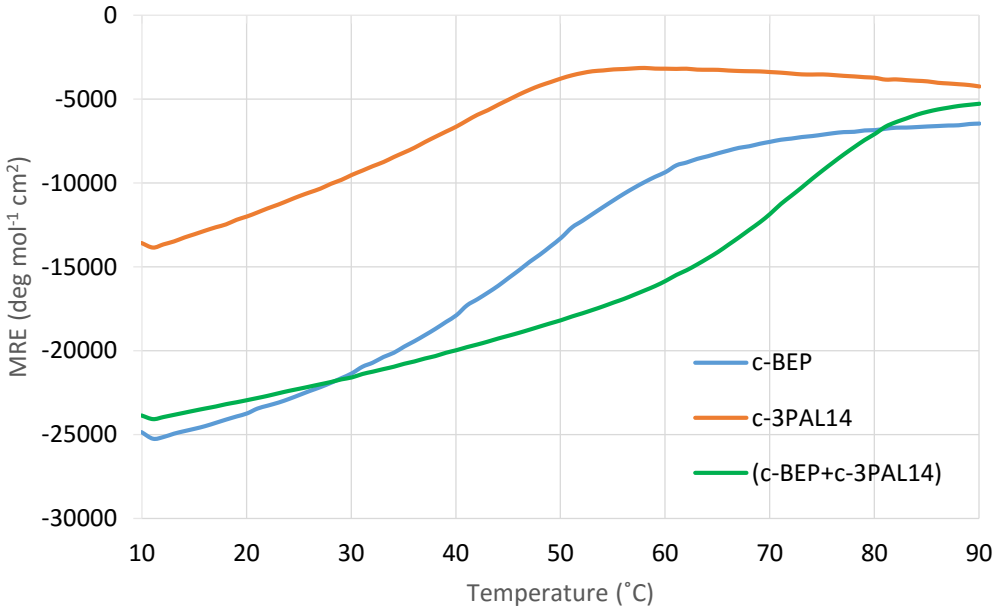

Figure A4.2: Thermal denaturation curves of 100 µM solutions of **c-BEP** (**29**), **c-3PAL14** (**30**) and (**c-BEP+c-3PAL14**) (**29+30**) in 10 mM MOPS buffer at pH 7.2. T_M (**c-BEP**) = 49.4 ˚C; T_M (**c-3PAL14**) = 34.2 ˚C; T_M (**c-BEP+c-3PAL14**) = 70.0 ˚C.

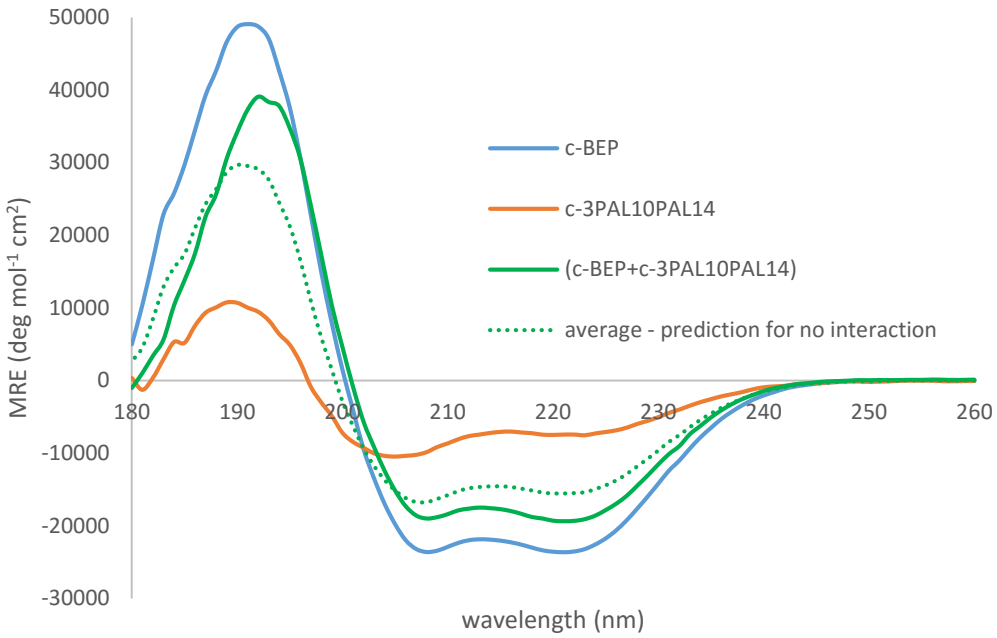

Figure A4.3: CD spectra of 100 µM solutions of **c-BEP** (**29**), **c-3PAL10PAL14** (**31**) and (**c-BEP+c-3PAL10PAL14**) (**29**+**31**) in 10 mM MOPS buffer at pH 7.2 at 21 ˚C. The peptide sequences are shown. **X** = 3-Pal:

c-BEP: Ac-EIAALEYENAALEQKIKALKQKIKALKQ-Am
c-3PAL10PAL14: Ac-KIAALKQKN**X**ALK**X**EIAALEYEIEALEQ-Am

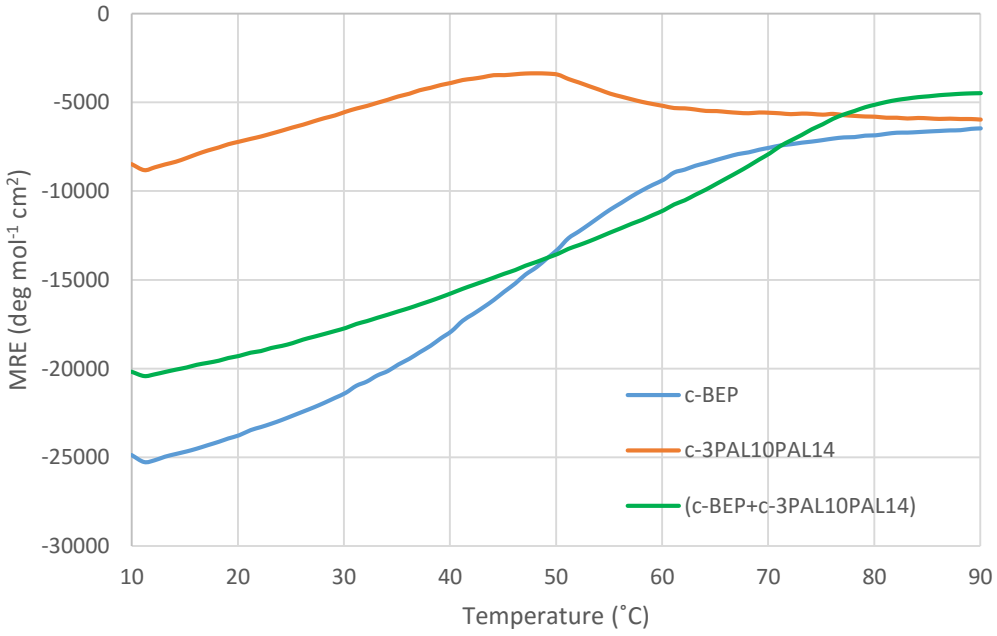

Figure A4.4: Thermal denaturation curves of 100 µM solutions of **c-BEP** (**29**), **c-3PAL10PAL14** (**31**) and (**c-BEP+c-3PAL10PAL14**) (**29**+**31**) in 10 mM MOPS buffer at pH 7.2. T_M (**c-BEP**) = 49.4 ˚C; T_M (**c-3PAL10PAL14**) = 31.4 ˚C; T_M (**c-BEP+c-3PAL10PAL14**) = 68.2 ˚C.

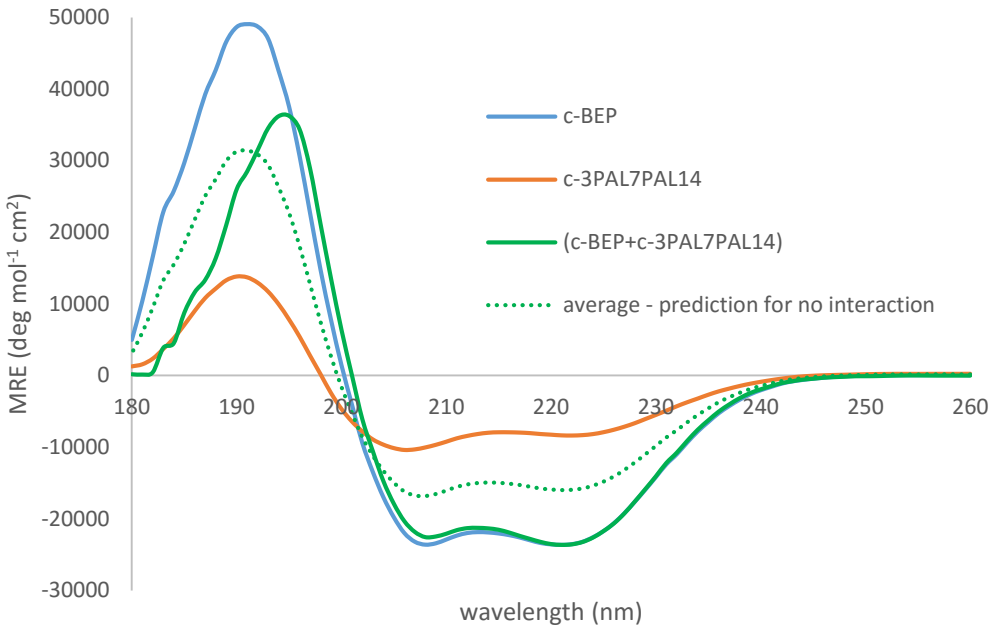

Figure A4.5: CD spectra of 100 µM solutions of **c-BEP** (**29**), **c-3PAL7PAL14** (**32**) and (**c-BEP+c-3PAL7PAL14**) (**29**+**32**) in 10 mM MOPS buffer at pH 7.2 at 21 ˚C. The peptide sequences are shown. **X** = 3-Pal

c-BEP: Ac-EIAALEYENAALEQKIKALKQKIKALKQ-Am
c-3PAL7PAL14: Ac-KIAALK**X**KNAALK**X**EIAALEYEIEALEQ-Am

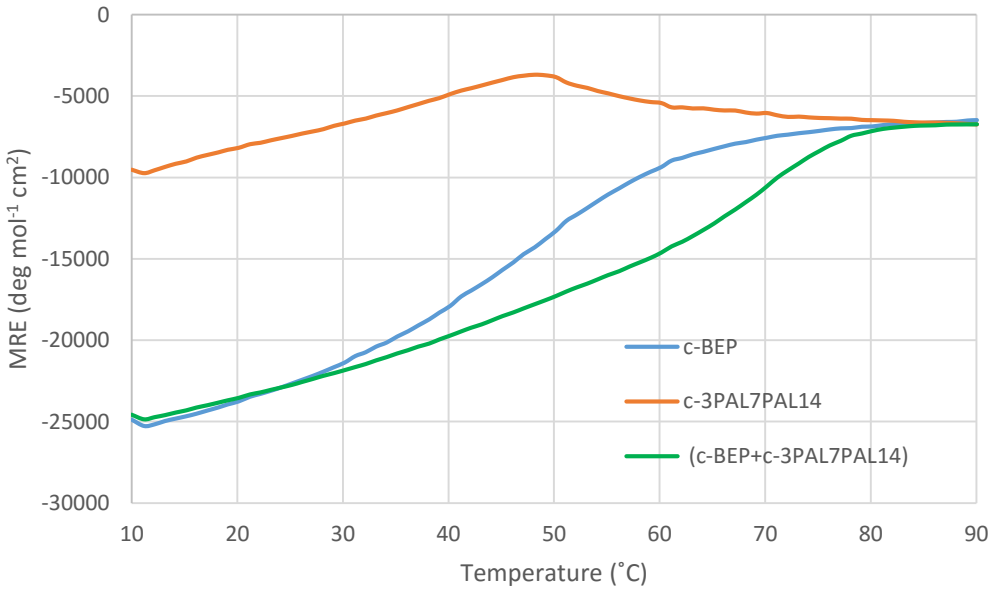

Figure A4.6: Thermal denaturation curves of 100 µM solutions of **c-BEP** (**29**), **c-3PAL7PAL14** (**32**) and (**c-BEP+c-3PAL7PAL14**) (**29**+**32**) in 10 mM MOPS buffer at pH 7.2. T_M (**c-BEP**) = 49.4 ˚C; T_M (**c-3PAL7PAL14**) = 30.0 ˚C; T_M (**c-BEP+c-3PAL7PAL14**) = 66.2 ˚C.

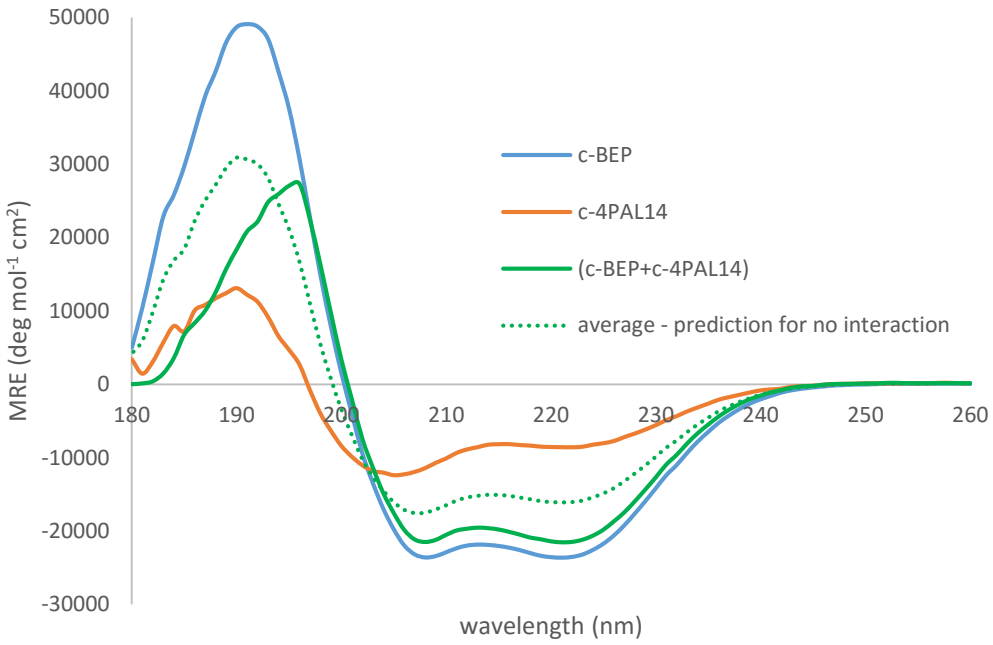

Figure A4.7: CD spectra of 100 µM solutions of **c-BEP** (**29**), **c-4PAL14** (**33**) and (**c-BEP+c-4PAL14**) (**29**+**33**) in 10 mM MOPS buffer at pH 7.2 at 21 ˚C. The peptide sequences are shown. **X** = 4-Pal

c-BEP: Ac-EIAALEYENAALEQKIKALKQKIKALKQ-Am
c-4PAL14: Ac-KIAALKQKNAALK**X**EIAALEYEIEALEQ-Am

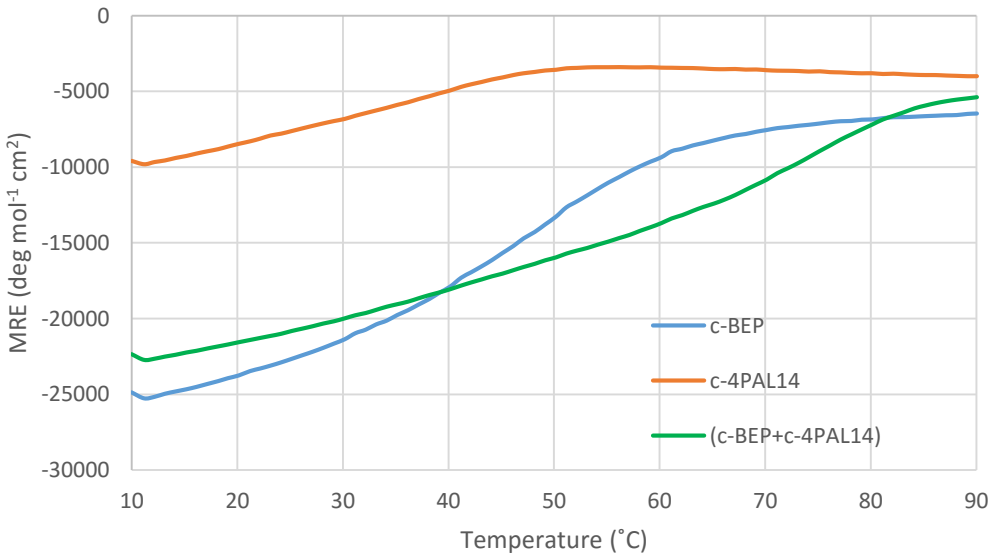

Figure A4.8: Thermal denaturation curves of 100 µM solutions of **c-BEP** (**29**), **c-4PAL14** (**33**) and (**c-BEP+c-4PAL14**) (**29**+**33**) in 10 mM MOPS buffer at pH 7.2. T_M (**c-BEP**) = 49.4 ˚C; T_M (**c-4PAL14**) = 30.2 ˚C; T_M (**c-BEP+c-4PAL14**) = 65.2 ˚C.

Peptide or peptide systems	pH	θ_{222} (deg mol^{-1} cm^2)	$\theta_{222}/\theta_{208}$	% helicity	T_M (°C)
c-BEP (29)	7.2	-22912.9	0.97	73.6	49.4
	8.5	-20860.2	1.00	67.0	50.6
c-3PAL14 (30)	7.2	-12033.5	0.92	38.6	34.2
	8.5	-12216.4	0.91	39.2	36.8
c-3PAL10PAL14 (31)	7.2	-7445.4	0.75	23.9	31.4
	8.5	-8107.6	0.79	26.0	29.2
c-3PAL7PAL14 (32)	7.2	-8358.0	0.83	26.8	30.0
	8.5	-5356.7	0.72	17.2	< 25.0
c-4PAL14 (33)	7.2	-8564.4	0.75	27.5	30.2
	8.5	-10045.1	0.80	32.3	31.1
(29+30)	7.2	-22575.5	1.01	63.7	70.0
	8.5	-29760.4	1.07	84.0	69.1
(29+31)	7.2	-19306.8	1.02	54.5	68.2
	8.5	-23813.6	1.06	67.2	66.6
(29+32)	7.2	-23560.0	1.04	66.5	66.2
	8.5	-27542.0	1.09	77.7	66.8
(29+33)	7.2	-21462.7	1.00	60.6	65.2
	8.5	-26179.5	1.04	73.9	68.0

Table A4.1: Summary of the obtained data of 100 µM solutions of all the individual peptides and peptide systems of **Section 4.3** in 10 mM MOPS at pH 8.5 and at 21 °C compared to the obtained data at pH 7.2 under the same conditions of peptides concentration and temperature. These peptide data consists of: ellipticity at 222 nm (θ_{222}), the ellipticity ratio between 222 nm and 208 nm ($\theta_{222}/\theta_{208}$), the percentage of helicity, and the melting temperature (T_M).

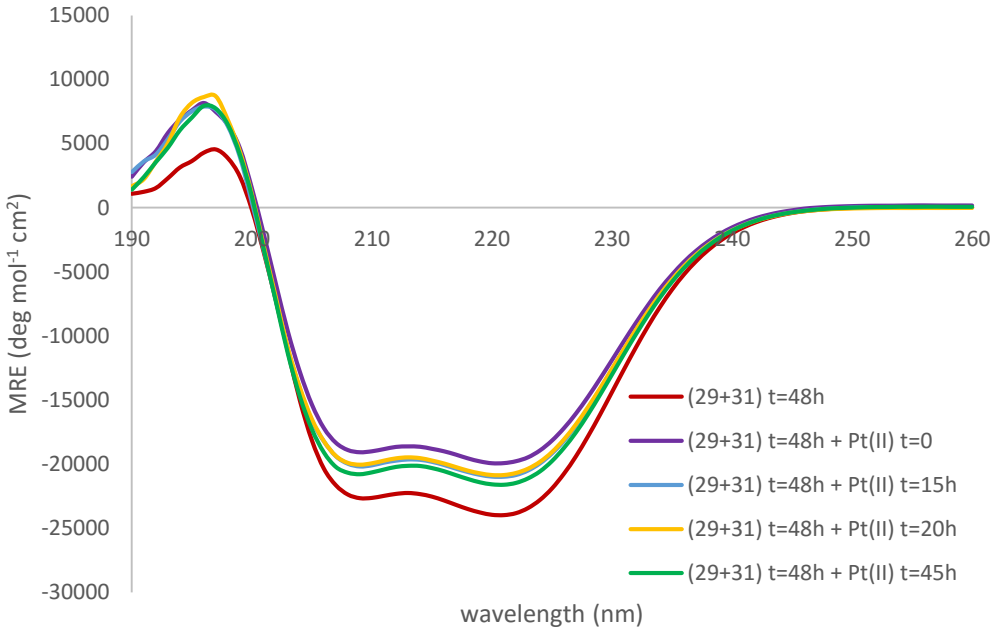

Figure A4.9: CD spectra of 100 µM (**c-BEP**+**c-3PAL10PAL14**) (**29**+**31**) in 10 mM MOPS at pH 8.5 at 21 ˚C after 48 hours, and the result after the addition of the metal complex K_2PtCl_4 at different intervals of time: t=0 (purple line), after 15 hours (blue line), after 20 hours (yellow line) and after 45 hours (green line).

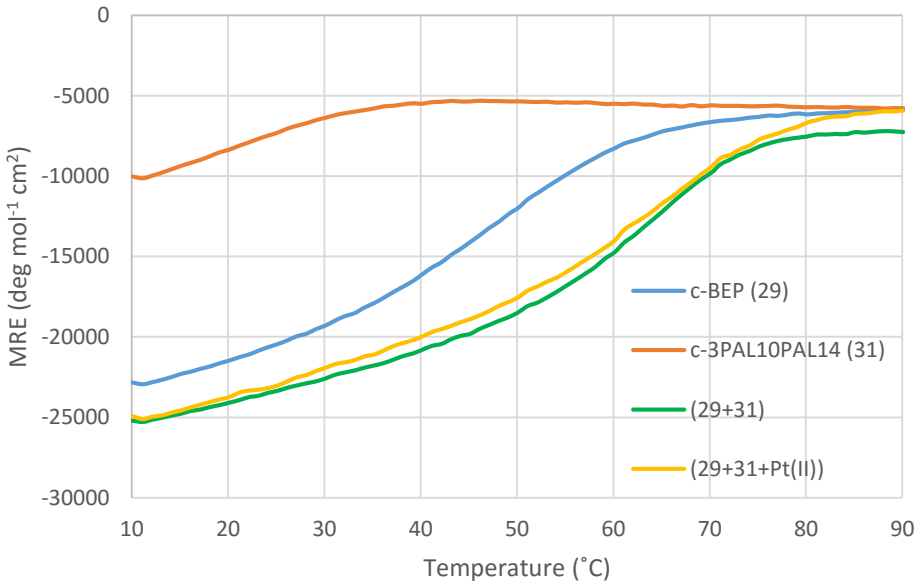

Figure A4.10: Thermal denaturation curves of 100 µM solutions of **c-BEP** (**29**), **c-3PAL10PAL14** (**31**), their mixture (**29**+**31**), and their mixture with the K_2PtCl_4 complex (**29**+**31**+**Pt(II)**) in 10 mM MOPS buffer at pH 8.5. T_M (**29**) = 50.6 ˚C; T_M (**31**) = 29.2 ˚C; T_M (**29**+**31**) = 66.8 ˚C; T_M (**29**+**31**+**Pt(II)**) ~ 65.0 ˚C.

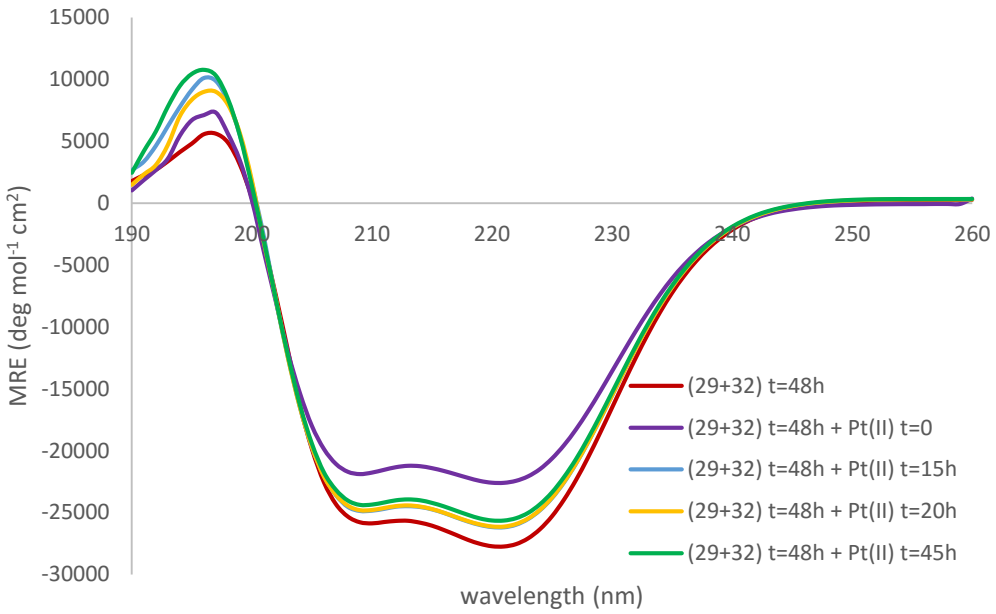

Figure A4.11: CD spectra of 100 µM (**c-BEP+c-3PAL7PAL14**) (**29+32**) in 10 mM MOPS at pH 8.5 at 21 ˚C after 48 hours, and the result after the addition of the metal complex K_2PtCl_4 at different intervals of time: t=0 (purple line), after 15 hours (blue line), after 20 hours (yellow line) and after 45 hours (green line).

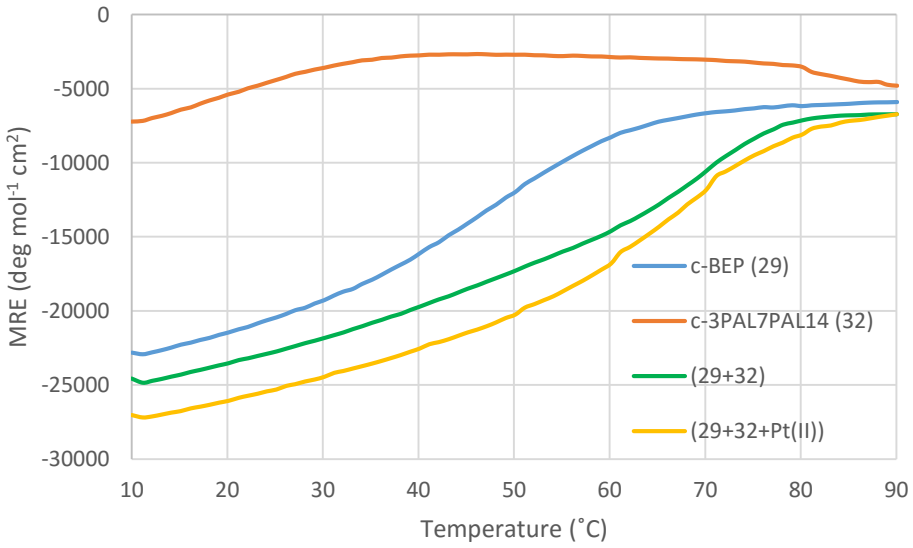

Figure A4.12: Thermal denaturation curves of 100 µM solutions of **c-BEP** (**29**), **c-3PAL7PAL14** (**32**), their mixture (**29+32**), and their mixture with the K_2PtCl_4 complex (**29+32+Pt(II)**) in 10 mM MOPS buffer at pH 8.5. T_M (**29**) = 50.6 ˚C; T_M (**32**) < 25 ˚C; T_M (**29+32**) = 66.8 ˚C; T_M (**29+32+Pt(II)**) = 70.7 ˚C.

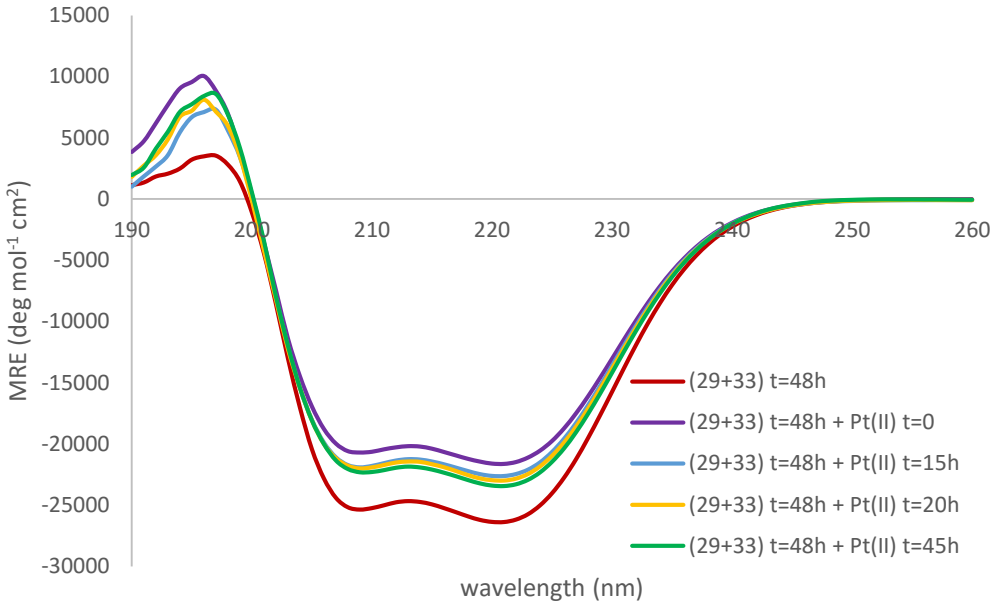

Figure A4.13: CD spectra of 100 µM (**c-BEP+c-4PAL14**) (**29+33**) in 10 mM MOPS at pH 8.5 at 21 ˚C after 48 hours, and the result after the addition of the metal complex K_2PtCl_4 at different intervals of time: t=0 (purple line), after 15 hours (blue line), after 20 hours (yellow line) and after 45 hours (green line).

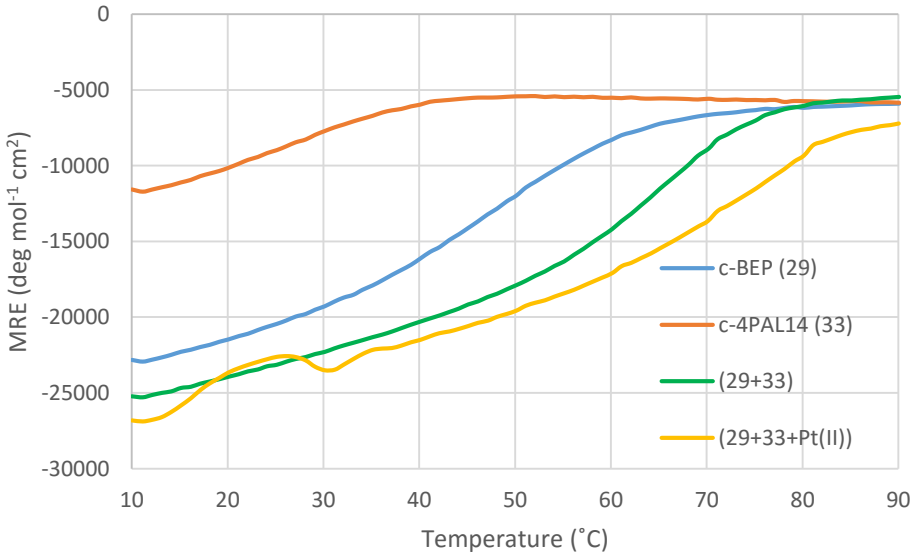

Figure A4.14: Thermal denaturation curves of 100 µM solutions of **c-BEP** (**29**), **c-4PAL14** (**33**), their mixture (**29+33**), and their mixture with the K_2PtCl_4 complex (**29+33+Pt(II)**) in 10 mM MOPS buffer at pH 8.5. T_M (**29**) = 50.6 ˚C; T_M (**33**) = 31.1 ˚C; T_M (**29+33**) = 68.0 ˚C; T_M (**29+33+Pt(II)**) = 68.5 ˚C.

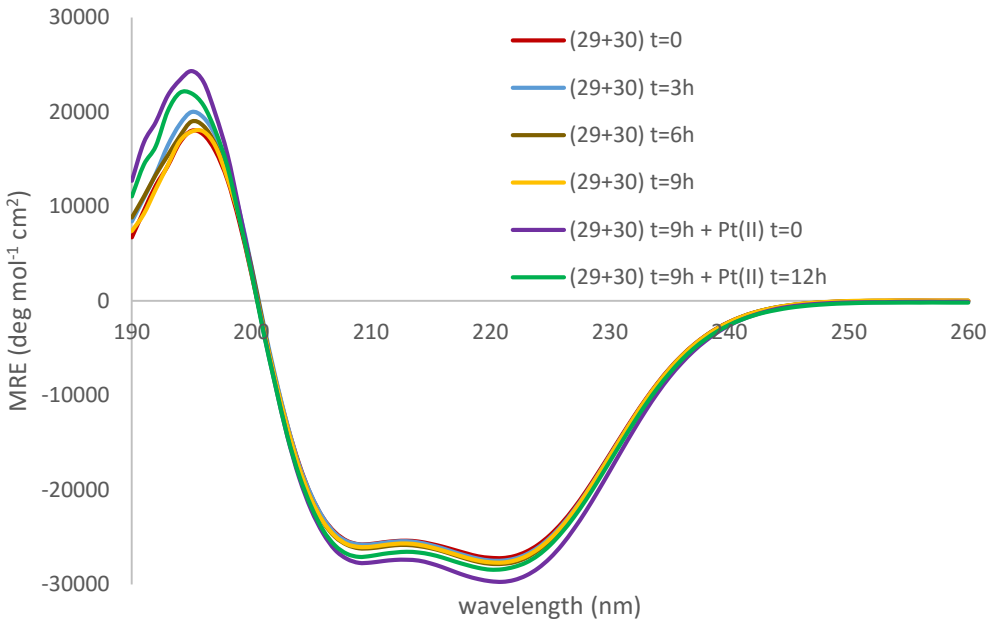

Figure A4.15: CD spectra of 50 µM (**c-BEP+c-3PAL14**) (**29+30**) in 10 mM MOPS at pH 8.5 and at 21 ˚C at different intervals of time for the first 9 hours, and the result after the addition of the metal complex K_2PtCl_4 at the initial time (purple line) and after 12 hours (green line).

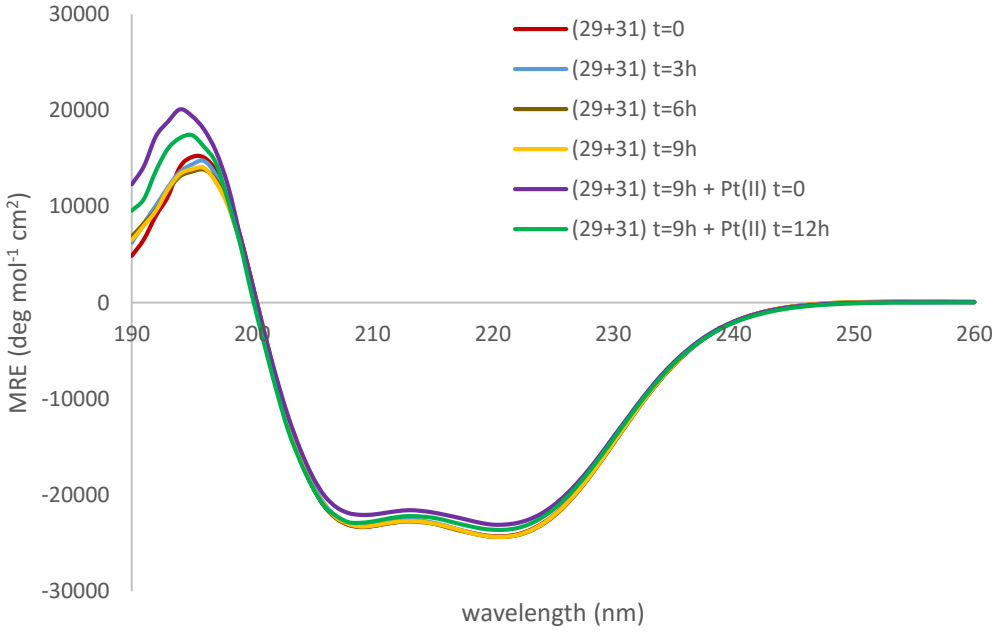

Figure A4.16: CD spectra of 50 µM (**c-BEP+c-3PAL10PAL14**) (**29+31**) in 10 mM MOPS at pH 8.5 at 21 ˚C at different intervals of time for the first 9 hours, and the result after the addition of the metal complex K_2PtCl_4 at the initial time (purple line) and after 12 hours (green line).

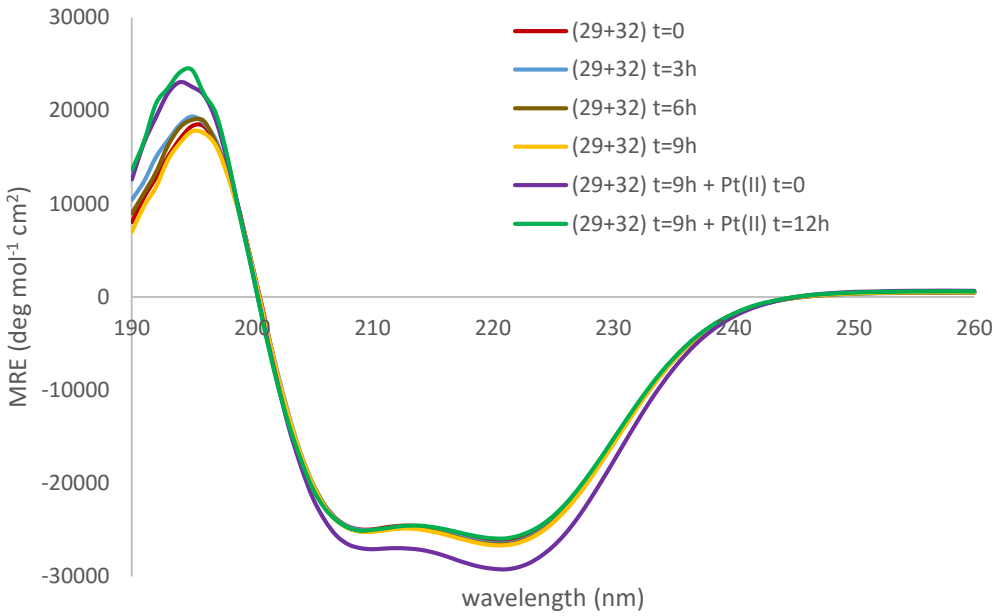

Figure A4.17: CD spectra of 50 µM (**c-BEP+c-3PAL7PAL14**) (**29+32**) in 10 mM MOPS at pH 8.5 and at 21 ˚C at different intervals of time for the first 9 hours, and the result after the addition of the metal complex K_2PtCl_4 at the initial time (purple line) and after 12 hours (green line).

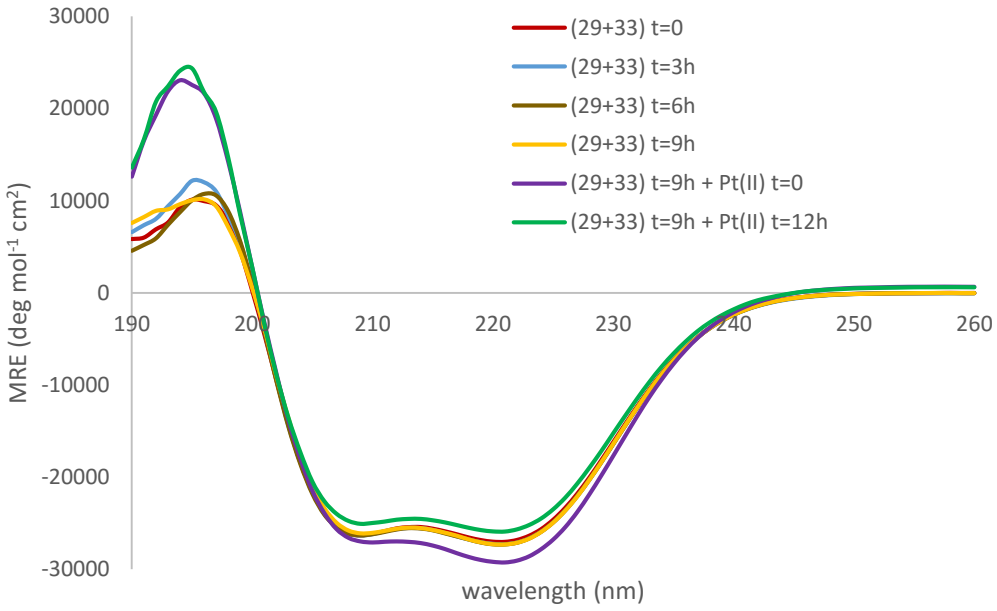

Figure A4.18: CD spectra of 50 µM (**c-BEP+c-4PAL14**) (**29+33**) in 10 mM MOPS at pH 8.5 and at 21 ˚C at different intervals of time for the first 9 hours, and the result after the addition of the metal complex K_2PtCl_4 at the initial time (purple line) and after 12 hours (green line).

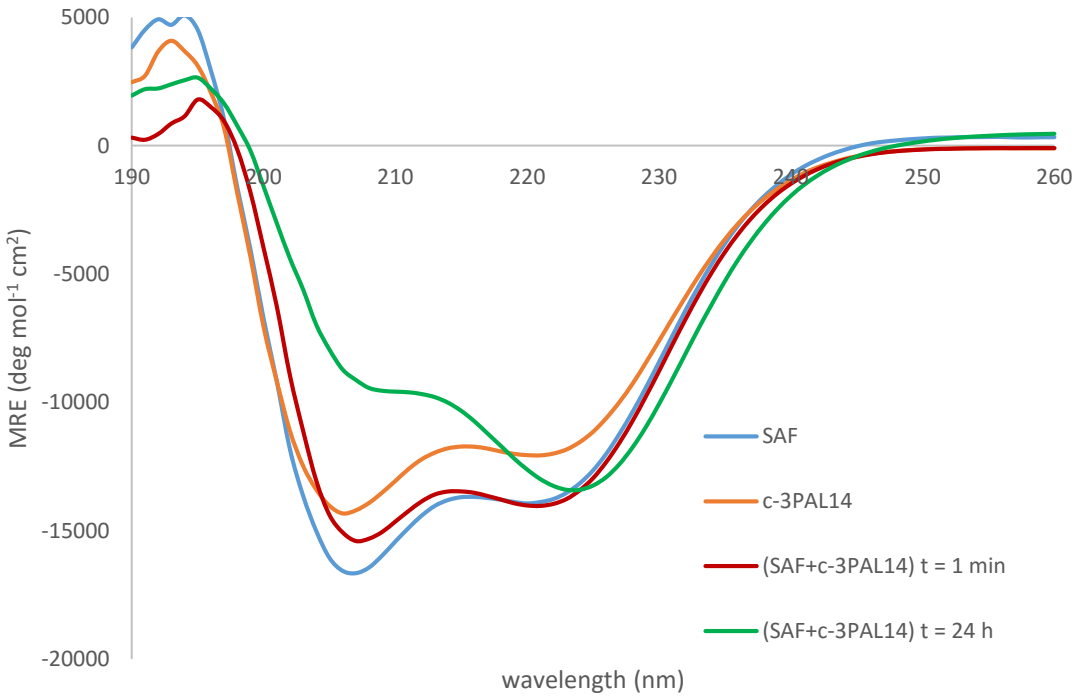

Figure A4.19: CD spectra of 100 µM solutions of **SAF** (**27**), **c-3PAL14** (**30**) and (**SAF+c-3PAL14**) (**27**+**30**) in 10 mM MOPS buffer at pH 8.5 at 21 ˚C. The peptide sequences are shown. **X** = 3-pyridylalanine (3-Pal)

SAF: Ac-KIKALKQKIKALKQEIAALEYENAALEQ-Am
c-3PAL14: Ac-KIAALKQKNAALK**X**EIAALEYEIEALEQ-Am

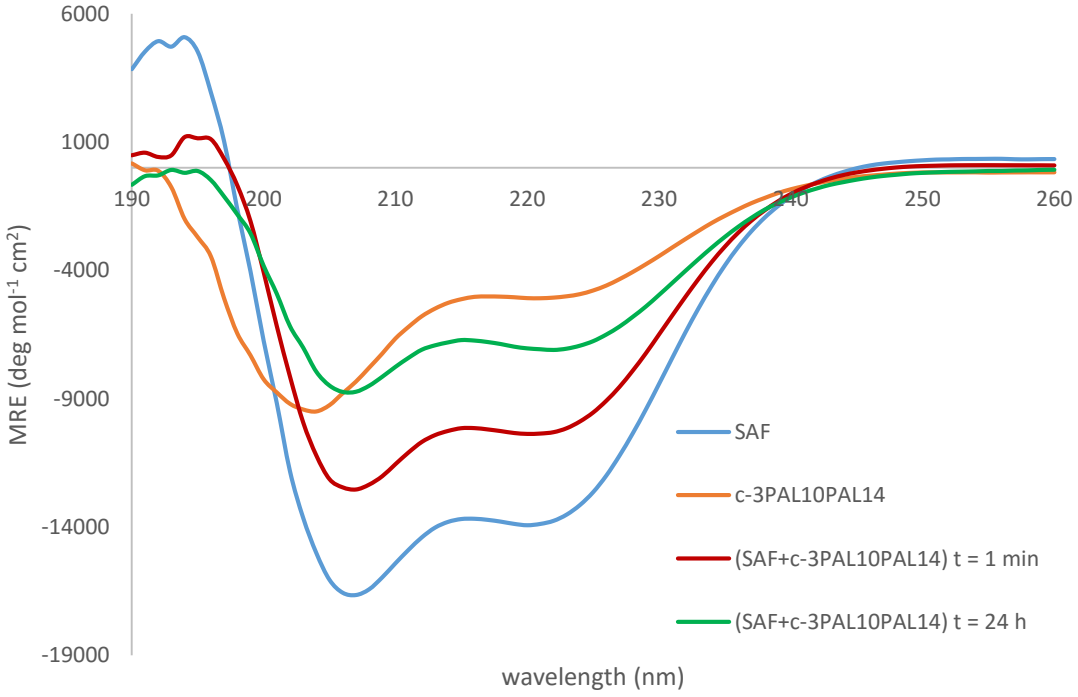

Figure A4.20: CD spectra of 100 µM solutions of **SAF** (**27**), **c-3PAL10PAL14** (**31**) and (**27**+**31**) in 10 mM MOPS buffer at pH 8.5 at 21 ˚C. The peptide sequences are shown. **X** = 3-pyridylalanine (3-Pal)

SAF: Ac-KIKALKQKIKALKQEIAALEYENAALEQ-Am
c-3PAL10PAL14: Ac-KIAALKQKN**X**ALK**X**EIAALEYEIEALEQ-Am

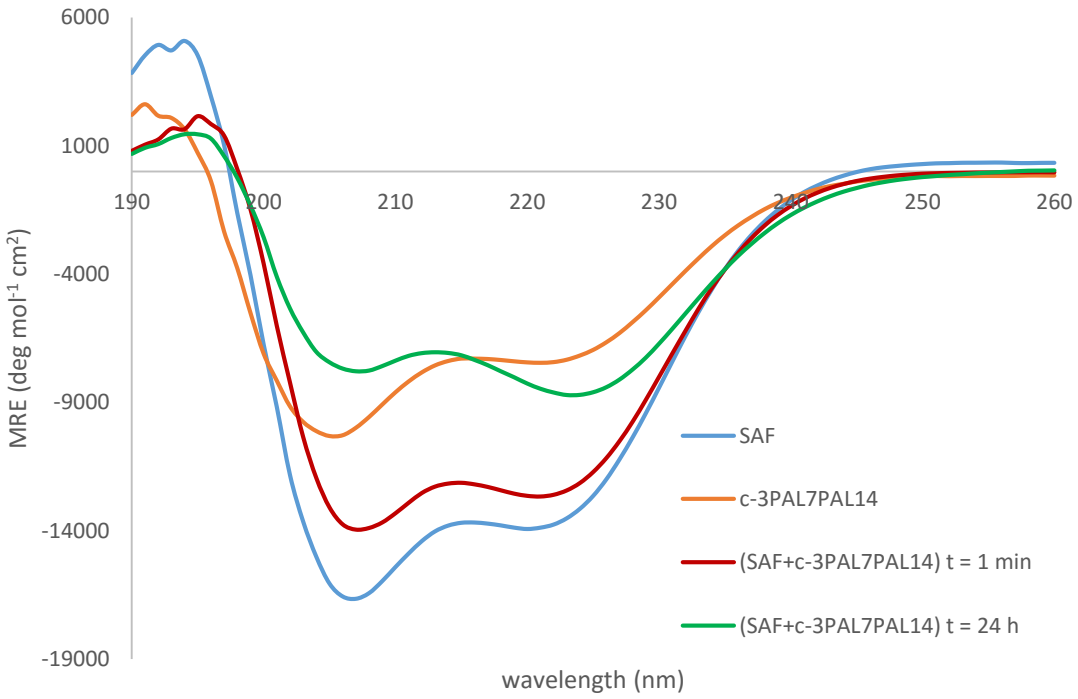

Figure A4.21: CD spectra of 100 µM solutions of **SAF** (**27**), **c-3PAL7PAL14** (**32**) and (**27**+**32**) in 10 mM MOPS buffer at pH 8.5 at 21 ˚C. The peptide sequences are shown. **X** = 3-pyridylalanine (3-Pal)

SAF: Ac-KIKALKQKIKALKQEIAALEYENAALEQ-Am
c-3PAL7PAL14: Ac-KIAALK**X**KN**A**ALK**X**EIAALEYEIEALEQ-Am

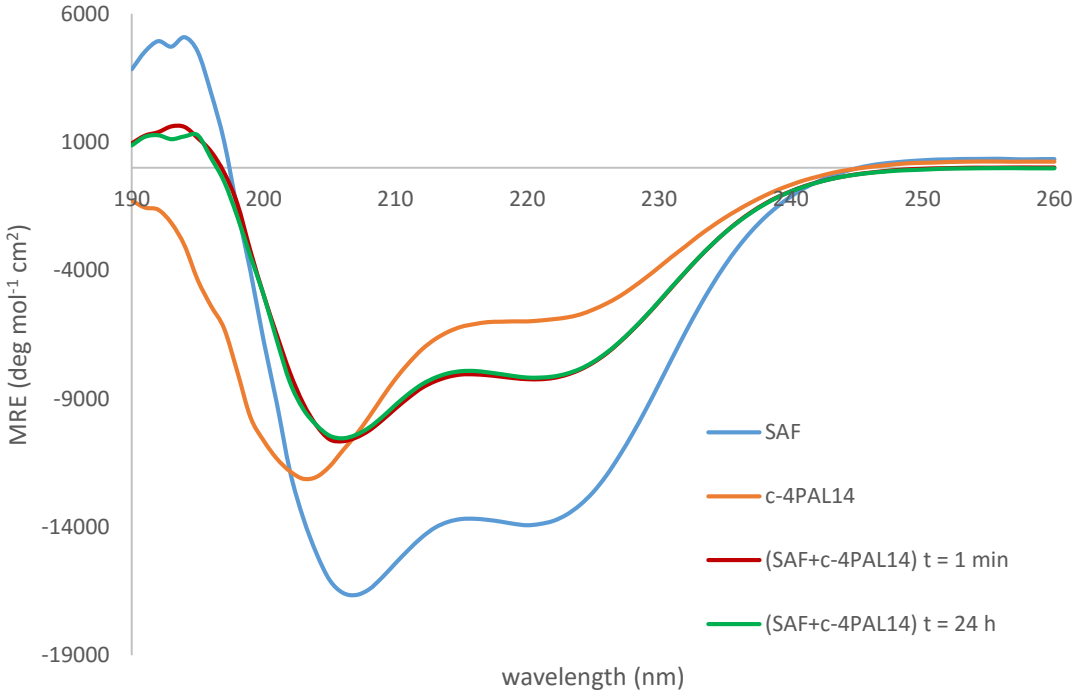

Figure A4.22: CD spectra of 100 µM solutions of **SAF** (**27**), **c-4PAL14** (**33**) and (**SAF+c-4PAL14**) (**27**+**33**) in 10 mM MOPS buffer at pH 8.5 at 21 ˚C. The peptide sequences are shown. **X** = 4-pyridylalanine (4-Pal)

SAF: Ac-KIKALKQKIKALKQEIAALEYENAALEQ-Am
c-4PAL14: Ac-KIAALKQKNAALK**X**EIAALEYEIEALEQ-Am

Chapter 5 – Photoswitching investigations in de novo coiled-coil peptide systems

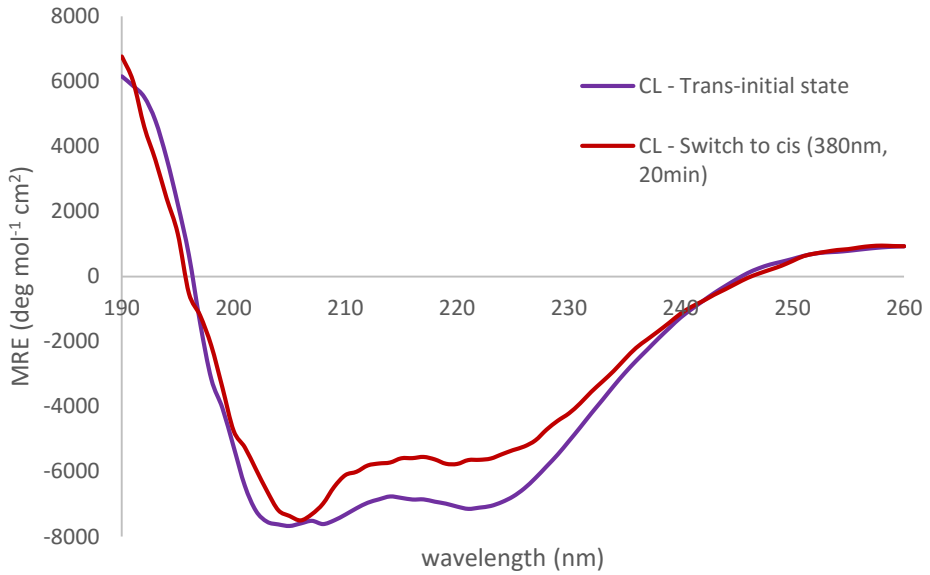

Figure A5.1: Photoisomerization of **CL** (**35**) at an estimated concentration of 25µM in ddH_2O at 21 ˚C. The peptide sequence of **CL** (**35**) is shown. The residues Cys (in red on the sequence) are the binding sites through which the azobenzene **24** is attached:

CL: EIAALEYEN**C**ALEQKIKALK**C**KIKALKQ

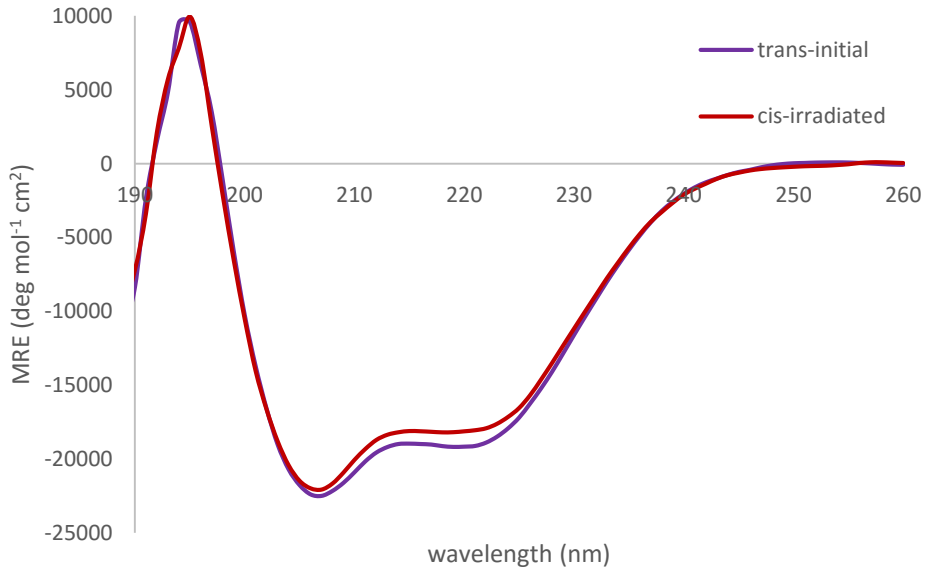

Figure A5.2: Photoisomerization of **c-CL** (**37**) 20µM in PBS at pH 7.4 at 21 ˚C. The peptide sequence (**37**) is shown. The residues Cys (in red on the sequence) are the binding sites through which the azobenzene **24** is attached:

c-**CL**: Ac-EIAALEYEN**C**ALEQKIKALK**C**KIKALKQ-Am

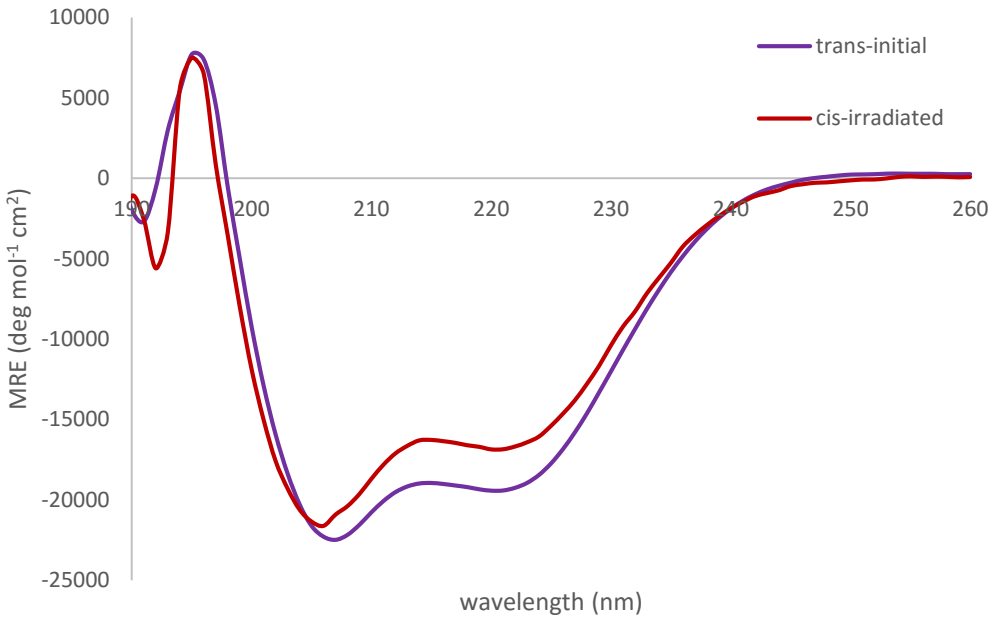

Figure A5.3: Photoisomerization of c-CL (**37**) 50µM in PBS at pH 7.4 at 21 ˚C. The peptide sequence (**37**) is shown. The residues Cys (in red on the sequence) are the binding sites through which the azobenzene **24** is attached:

c-**CL**: Ac-EIAALEYEN**C**ALEQKIKALK**C**KIKALKQ-Am

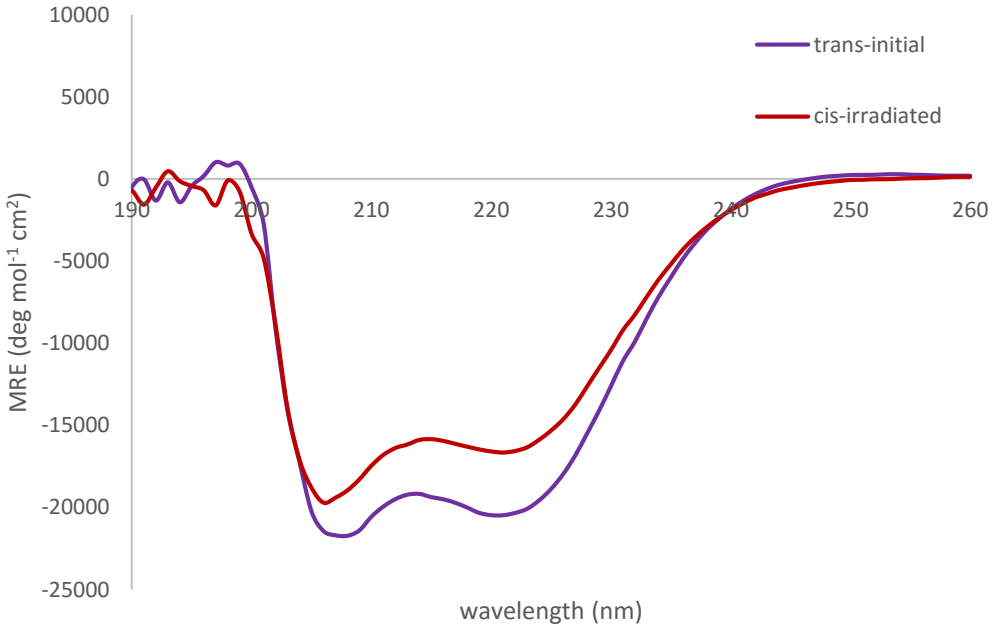

Figure A5.4: Photoisomerization of c-CL (**37**) 200µM in PBS at pH 7.4 at 21 ˚C. The peptide sequence (**37**) is shown. The residues Cys (in red on the sequence) are the binding sites through which the azobenzene **24** is attached:

c-**CL**: Ac-EIAALEYEN**C**ALEQKIKALK**C**KIKALKQ-Am

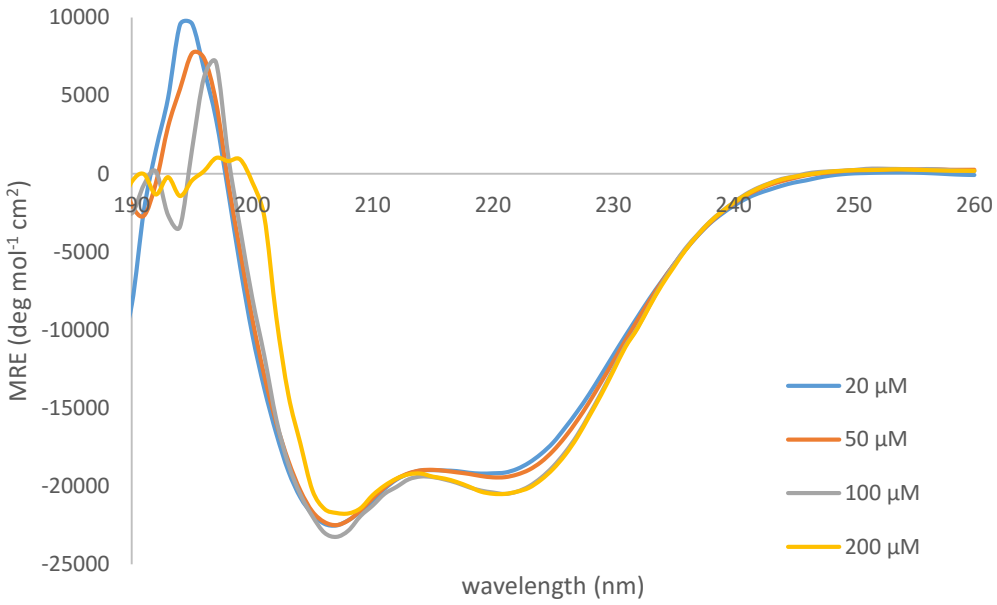

Figure A5.5: CD spectrum of the *trans*-initial conformation of c-CL (**37**) in PBS at pH 7.4 at different concentrations at 21 ˚C. The peptide sequence (**37**) is shown. The residues Cys (in red on the sequence) are the binding sites through which the azobenzene **24** is attached:

c-**CL**: Ac-EIAALEYEN**C**ALEQKIKALK**C**KIKALKQ-Am

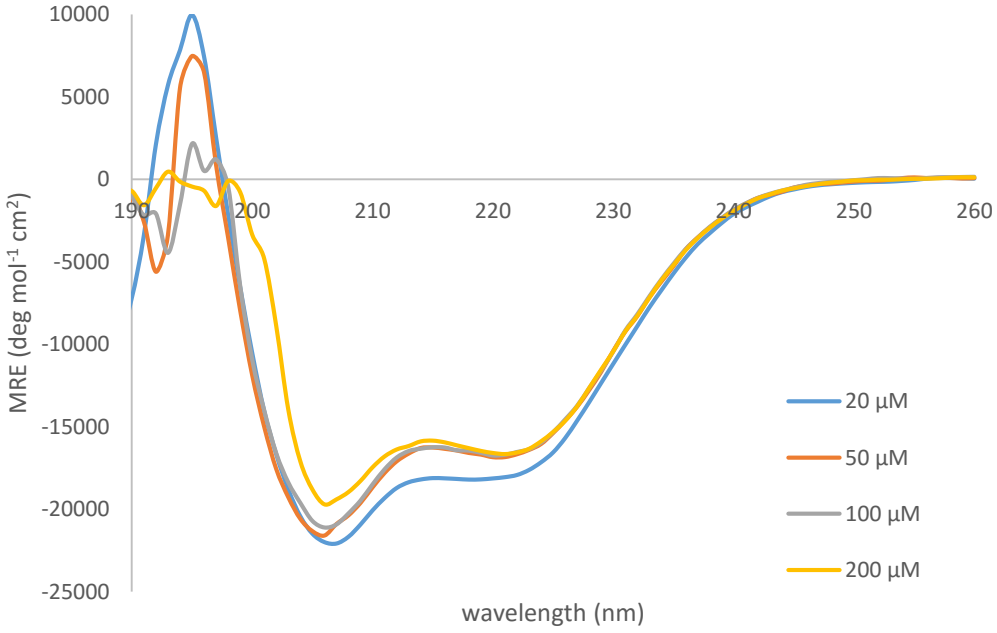

Figure A5.6: CD spectrum of the *cis*-irradiated conformation of c-CL (**37**) in PBS at pH 7.4 at different concentrations at 21 ˚C. The peptide sequence (**37**) is shown. The residues Cys (in red on the sequence) are the binding sites through which the azobenzene **24** is attached:

c-**CL**: Ac-EIAALEYEN**C**ALEQKIKALK**C**KIKALKQ-Am